universität wien

MASTERARBEIT / MASTER'S THESIS

Titel der Masterarbeit / Title of the Master's Thesis

Early Transition Metal Complexes with Bis(phenolate) Type Ligands – Synthesis, Characterisation and Catalytic Studies

verfasst von / submitted by

Olivera Cvetković, BSc

angestrebter akademischer Grad / in partial fulfilment of the requirements for the degree of

Master of Science (MSc)

Wien, 2022 / Vienna 2022

Studienkennzahl lt. Studienblatt / degree programme code as it appears on the student record sheet:	UA 066 862
Studienrichtung lt. Studienblatt / degree programme as it appears on the student record sheet:	Masterstudium Chemie
Betreut von / Supervisor:	Univ.-Prof. Dr. Kai Carsten Hultzsch

Acknowledgements

I would like to take the opportunity and thank people who gave me their support during my master thesis.

First, I want to express my gratitude to Prof. Dr. Kai Carsten Hultzsch for giving me the possibility to perform research in his group and providing me an interesting topic and valuable advice over the course of my work.

Next, I would like to thank the research group at the institute of Chemical Catalysis for a pleasant working atmosphere. In particular, I would like to mention Dr. Mariusz Wolff, who provided me with a lot of helpful advice throughout my work, offered me unreserved support and revised my thesis. I would also like to thank him for the pleasant company in the laboratory.

In addition, I would like to thank the staff of the NMR centre, led by Ass. Prof. Dr. Hanspeter Kählig and particularly the X-Ray centre around Ing. Alexander Prado-Roller who offered excellent assistance in measuring my samples and solving the problems regarding structure analyses.

Lastly, my greatest gratitude goes for my friends and especially my family for the unconditional love and support they have been giving me throughout my studies at the University of Vienna and beyond, during my whole life.

Abstract

Nitrogen containing heterocycles are scaffolds commonly found in natural products, such as alkaloids and valuable pharmaceuticals. Nitrogen containing compounds are also used as building blocks of industrially relevant basic and fine chemicals. An approach to access these indispensable products in a facile and highly atom-economical fashion is the addition of an amine N–H bond across an unsaturated carbon–carbon linkage, the so-called hydroamination.

To investigate the intramolecular hydroamination of aminoalkenes, a class of bis(phenolate) ligands and their respective metal complexes that were to serve as catalysts were prepared. Complexation reactions were performed with early transition metals (yttrium, titanium, zirconium, niobium and tantalum) and three yttrium catalysts were obtained, while the other metals did not yield the desired complexes. Catalysts were tested in the intramolecular hydroamination of aminoalkenes and the reaction progress was monitored using NMR spectroscopy.

Upon optimisation of the reaction conditions, positive results were obtained in the case of catalysts bearing methylenebis(phenolate) ligands, whereas the catalyst bearing a disulfanediylbis(phenolate) ligand, though active, was proven to be inferior, presumably due to the weak coordination of the sulphur atoms to the metal centre, resulting in a partial deactivation of the catalyst.

Zusammenfassung

Stickstoffhaltige Heterocyclen sind Gerüste die häufig in Naturstoffen wie Alkaloiden und wertvollen Pharmazeutika vorkommen. Stickstoffhaltige Verbindungen werden auch als Bausteine industriell relevanter Grund- und Feinchemikalien verwendet. Ein Zugang zu diesen unentbehrlichen Produkten auf eine einfache und höchst atomökonomische Weise ist die Addition einer Amin-N–H-Bindung an eine ungesättigte Kohlenstoff–Kohlenstoff Verknüpfung, die sogenannte Hydroaminierung.

Um die intramolekulare Hydroaminierung einfacher Aminoalkene zu untersuchen, wurde eine Klasse von Bis(phenolat)-Liganden und ihren entsprechenden Metallkomplexen hergestellt, die als Katalysatoren dienen sollten. Komplexierungsreaktionen wurden mit frühen Übergangsmetallen (Yttrium, Titan, Zirconium, Niob und Tantal) durchgeführt und drei Yttrium-Katalysatoren wurden erhalten, wobei die anderen Metalle nicht die gewünschten Komplexe lieferten. Katalysatoren wurden bei der intramolekularen Hydroaminierung von Aminoalkenen untersucht und der Reaktionsverlauf wurde mittels NMR-Spektroskopie verfolgt.

Bei der Optimierung der Reaktionsbedingungen wurden im Fall von Katalysatoren mit Methylenbis(phenolat)-Liganden positive Ergebnisse erhalten, während sich der Katalysator mit einem Disulfanediylbis(phenolat)-Liganden, obwohl aktiv, als unterlegen erwiesen hat, vermutlich aufgrund der schwachen Koordination der Schwefelatome zum Metallzentrum, was zu einer teilweisen Desaktivierung des Katalysators führt.

Abbreviations

Å	Angstrom
BDMA	*N,N*-Dimethyl benzylamine
Cy	Cyclohexyl
d	Doublet
DCM	Dichloromethane
dd	Doublet of doublet
ddd	Doublet of doublet of doublet
ddt	Doublet of doublet of triplet
dH_2O	Deionised water
DMF	*N,N*-Dimethylformamide
dq	Doublet of quartet
dt	Doublet of triplet
ee	Enantiomeric excess
eq, equiv	Equivalent
ESI	Electrospray Ionisation
Et_2O	Diethyl ether
EtOAc	Ethyl acetate
EtOH	Ethanol
h	Hour(s)
hept	Heptane
*i*PrOH	Isopropanol
m	Multiplet
Me	Methyl
MeOH	Methanol
min	Minute(s)
n-BuLi	*n*-Buthyllithium
NBS	N-Bromosuccinimid
NMR	Nuclear Magnetic Resonance
p	Pentet
Ph	Phenyl
ppm	Parts per million
q	Quartet
QTOF	Quadrupole time-of-light
rt	Room temperature
s	Singlet
t	Triplet
t-Bu	*tert*-Butyl
td	Triplet of doublet
tdd	Triplet of doublet of doublet
THF	Tetrahydrofurane
TLC	Thin-layer chromatography
Trt	Trityl

tt	Triplet of triplet
$Y(BDMA)_3$	$[Y(o\text{-}C_6H_4CH_2NMe_2)_3]$
UV	Ultraviolet

Table of contents

1. Introduction

1.1 Amines

Nitrogen-containing scaffolds are substructures of a wide variety of important biologically active compounds, such as alkaloids, amino acids, nucleotides in nucleic acids and vitamins. Their abundance in nature ranges from presence in DNA as building blocks and vitamins and neurotransmitters to support essential processes of living organisms, to opioid and poisonous substances (Figure 1).[1–4]

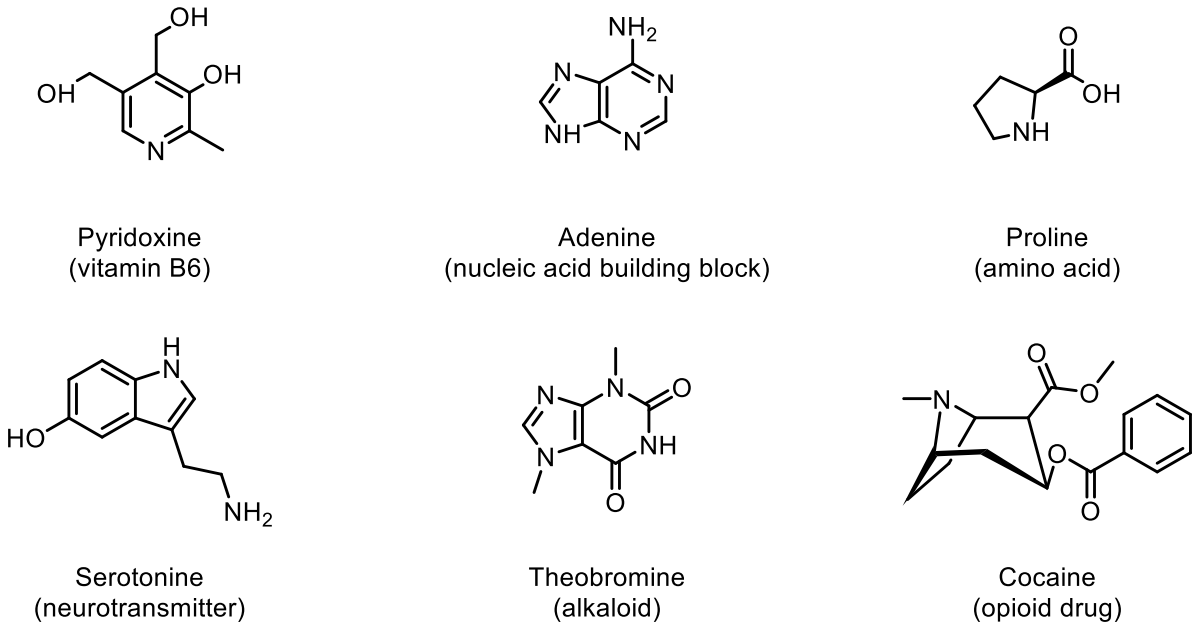

Figure 1. Examples of natural compounds containing nitrogen.[5]

Moreover, nitrogen-containing compounds, for instance amines, enamines and imines have a wide application in pharmaceutical and material sciences, as both fine and bulk chemicals in industry for the manufacture of agricultural chemicals, polymers, food additives, paint and coatings, but also in academic research.[4,6,7] The global amines market, for example, was estimated to grow from USD 14.4 billion turnover in 2016 to USD 29.3 billion by 2025 at an annual rate of 8.3 %.[7,8]

With that in mind, the development of efficient synthetic methods to access nitrogen-containing compounds is of great interest and utmost importance.

Traditional approaches, such as the Curtius rearrangement,[9] the Delépine reaction,[10,11] the Gabriel synthesis[12] or two-step approaches, such as the Mitsunobu[13]

and Staudinger reaction[14,15] and reductive amination reactions,[16] are plagued by the fact that they require employing highly reactive or hazardous chemicals, such as formaldehyde, methyl iodine and hydrazoic acid, either for the reaction itself or for the production of the suitable precursors and that they produce unwanted waste products often in stoichiometric amounts (Scheme 1).

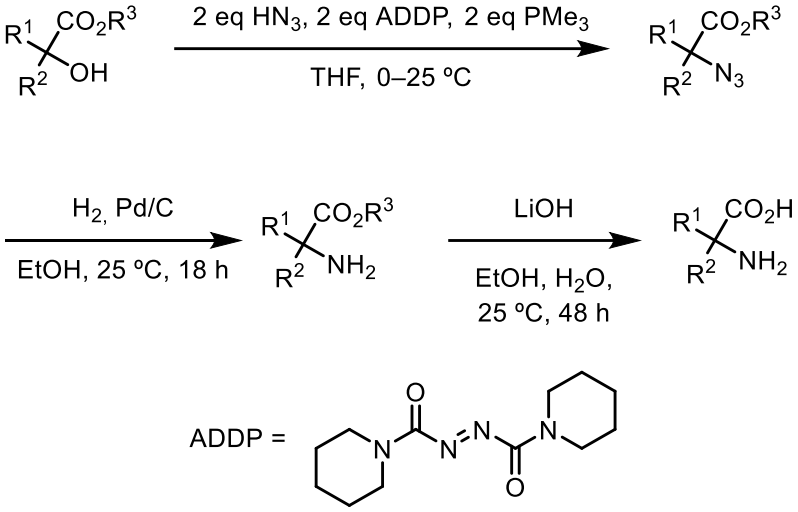

Scheme 1. An example of a three-step Mitsunobu approach for the synthesis of amino acid derivatives.[17]

Since carbon–nitrogen, just like carbon–carbon bond-forming-reactions, count as fundamental transformations in organic chemistry, they are the most useful when performed catalytically, rather than stoichiometrically.[18] Therefore, research efforts have been directed towards finding a suitable pathway in the field of chemical catalysis. One such highly atom-economical approach is the hydroamination reaction. The formation of a new carbon–nitrogen bond is ensured *via* addition of an amine across an unsaturated carbon–carbon bond (Scheme 2).[6,19]

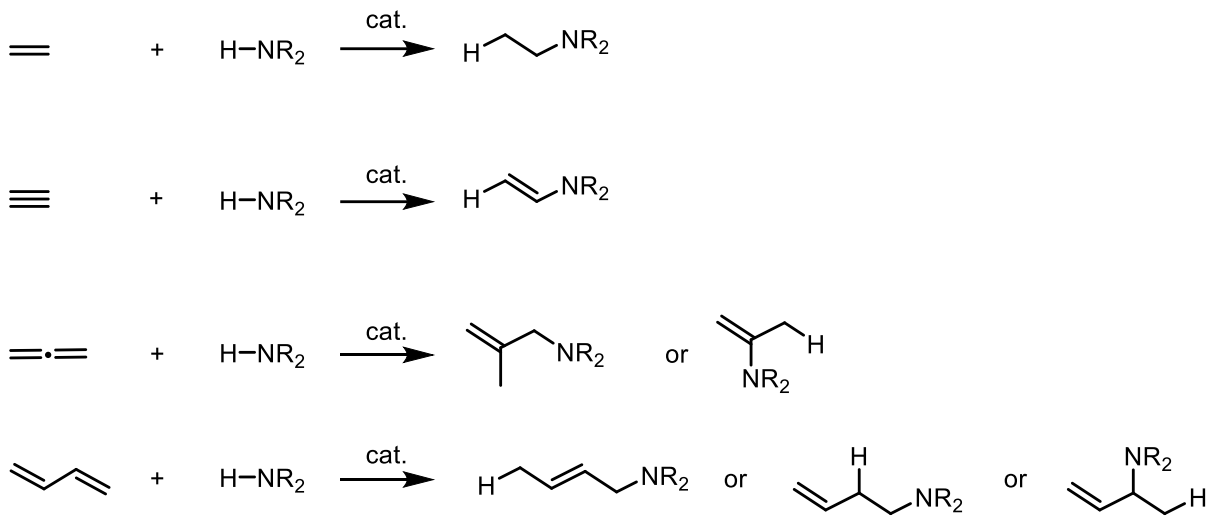

Scheme 2. Hydroamination of alkenes, alkynes, allenes and dienes.[6]

As this work has in its focus early transition metal hydroamination catalysts and their application in intramolecular hydroamination of alkenes, particular attention will be directed towards current advances in those areas in the following sections. To offer an overview on the topic, theoretical background and suitable catalytic systems, including their advantages and drawbacks will be highlighted.

1.2 Hydroamination

Hydroamination offers a pathway to formation of valuable products containing a new carbon–nitrogen bond that have versatile applications, as mentioned previously, in a 100% atom-economical and waste-free fashion, starting from readily available and relatively inexpensive starting materials.[7]

The reaction is nearly thermoneutral (enthalpically favoured, but counterbalanced by negative entropy, especially in the case of intermolecular hydroamination).[20,21] However, it experiences a high reaction barrier due to the electrostatic repulsion between the lone electron pair of the amine nitrogen, that performs a nucleophilic attack, and the π-electrons of the unsaturated C–C bond, which can be overcome by the use of a catalyst. Thus, due to the negative entropy of the reaction, the increase in temperature cannot overcome the reaction barrier, but can rather obstruct it, and shift the equilibrium towards the starting materials.[6,22]

Non-activated C=C bonds were shown to undergo catalytic hydroamination with amines, however, predominantly through intramolecular reactions.[23,24] In these cases, ring-closing is the main driving force to bring the hydroamination reaction to completion.[25,26] The intermolecular hydroamination of non-activated alkenes with simple alkyl amines would be of a great importance, especially in an industrial setting. However, it lacks the aforementioned thermodynamic driving force and, thus, has rarely been reported.[7]

Consequently, depending on the olefinic substrates, the reaction can proceed in an intra- or intermolecular fashion, and depending on the regioselectivity, can lead to a formation of an *exo* or *endo*, and Markovnikov or *anti*-Markovnikov product, respectively (Scheme 3).

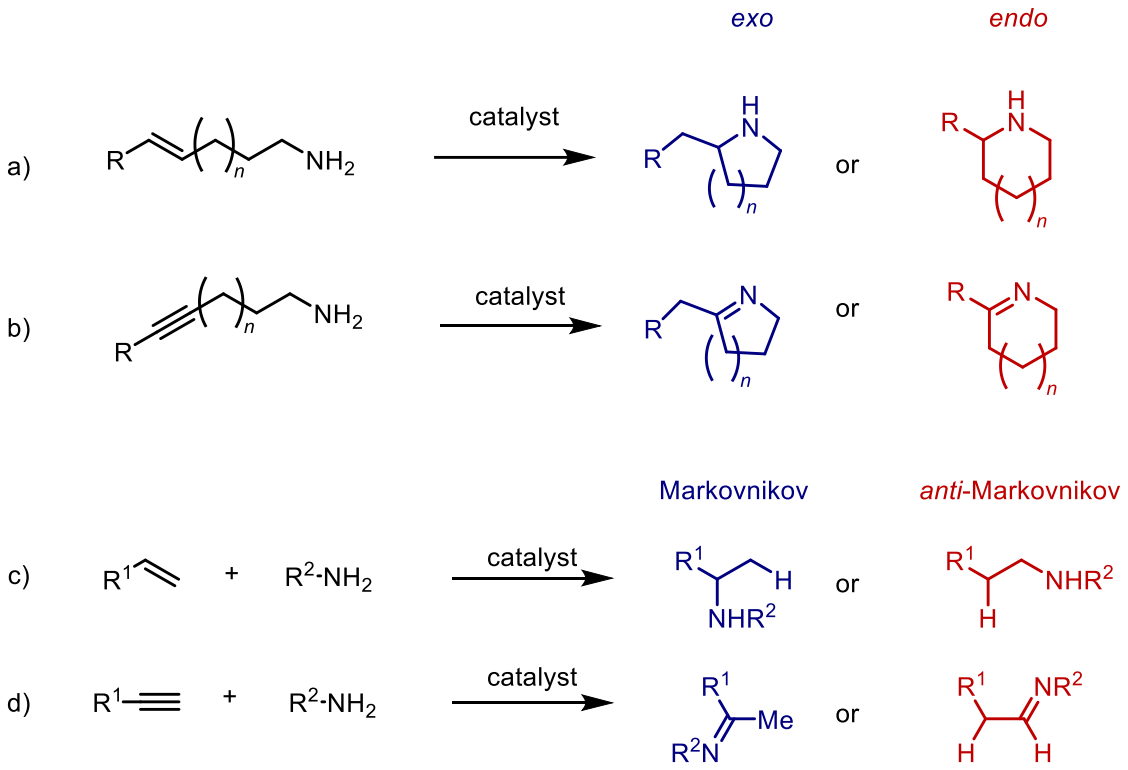

Scheme 3. Overview of different products of the catalytic hydroamination: a) Intramolecular hydroamination of alkenes, b) Intramolecular hydroamination of alkynes, c) Intermolecular hydroamination of alkenes, d) Intermolecular hydroamination of alkynes.[6,22]

The formation of the *endo* and *anti*-Markovnikov product is more rarely observed.[22] It is worth mentioning that the *anti*-Markovnikov addition of amines and ammonia to olefins was, in fact, listed as one of the "Ten Challenges for Catalysis".[27] This is of a particularly great importance in the field of industry, where the search for a method to

achieve the hydroamination of simple non-activated olefins with ammonia is still in progress. One of the obstacles is also the previously mentioned negative entropy of the reaction, which would call for low reaction temperatures and high pressures in an industrial environment.[7] Therefore, over the past three decades, a substantial progress in research has been made and various catalytic systems have been developed.[6]

There is a considerable difference in reactivity, depending on the substrate chosen, which must be taken into account. Due to the lower electron density of carbon–carbon double bond and its lower reactivity, the hydroamination of alkenes is more challenging compared to the hydroamination of alkynes.[6] A way to circumvent the reduced reactivity of the alkenes is the activation of the double bond through neighbouring electron withdrawing groups or featuring ring strain or conjugation.[7,22]

Owing to the great importance of the nitrogen-containing compounds in industry and pharmaceutical sciences, different catalytic systems have been developed.[1,2,6,20,28] When considering reaction mechanisms, it is possible to distinguish between two activation pathways; C–C multiple bond or N–H bond activation, depending on the catalytic system.[22] For instance, alkali and alkaline-earth metals[29] or lanthanides[30] have a tendency to activate the amine by deprotonation. Thus, they form a strongly nucleophilic amido species upon protonolysis of a rare-earth metal amido or alkyl bond of the precatalyst (Scheme 4 a)). The following insertion of the C–C multiple bond into the Ln–N bond is then rendered to be the rate-limiting step. The subsequent protonolysis with a second amine molecule regenerates the amido species and delivers the hydroamination product.

On the other hand, neutral group 4 metal catalysts,[31] also activate the amine to form an imido species (Scheme 4 b)). The mechanism for alkene hydroamination is proposed to be analogous to that of alkyne and allene hydroamination, which were more thoroughly investigated.[28] In the following step, the metal-imido species undergoes the reversible [2+2]-cycloaddition with the alkene moiety to form the azametallacyclobutane, that can be protolytically cleaved to give the hydroamination product and regenerate the metal-imido species. Interesting findings were demonstrated in the case of cationic catalysts,[32] where the proposed mechanism is believed to be similar to the one typical for rare-earth metal catalysts, involving the metal-amido species.

As opposed to amine activation, late transition metals activate the unsaturated C–C bond via coordination, rendering them more susceptible to attack by amine nucleophiles or in the case of electron rich metals, N–H oxidative addition[33] (Scheme 4 c) and d))[22,34]

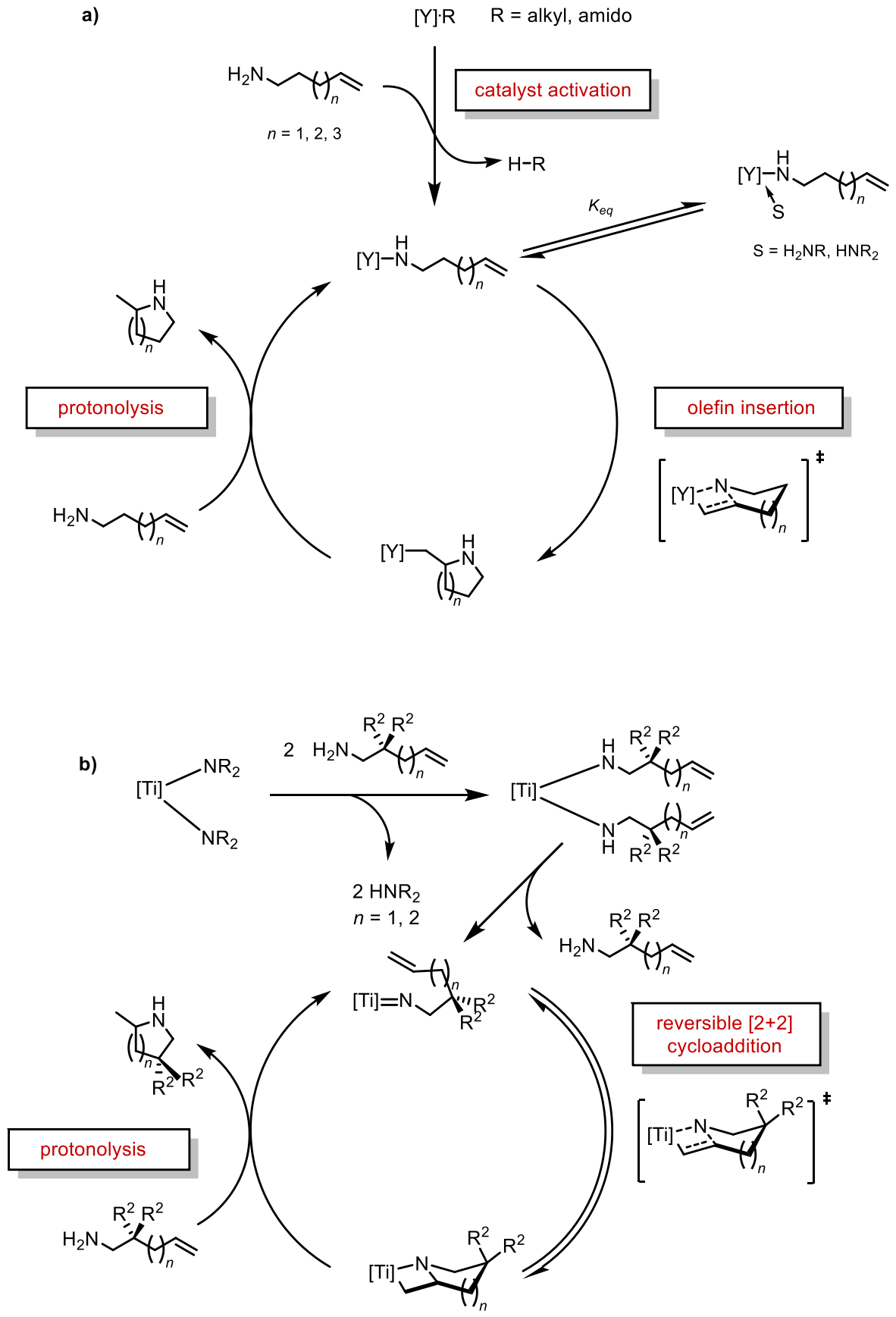
a)
[Y]·R
R = alkyl, amido
catalyst activation
H–R
n = 1, 2, 3
K_{eq}
S = H_2NR, HNR_2
protonolysis
olefin insertion
b)
2 HNR2
n = 1, 2
reversible [2+2] cycloaddition
protonolysis

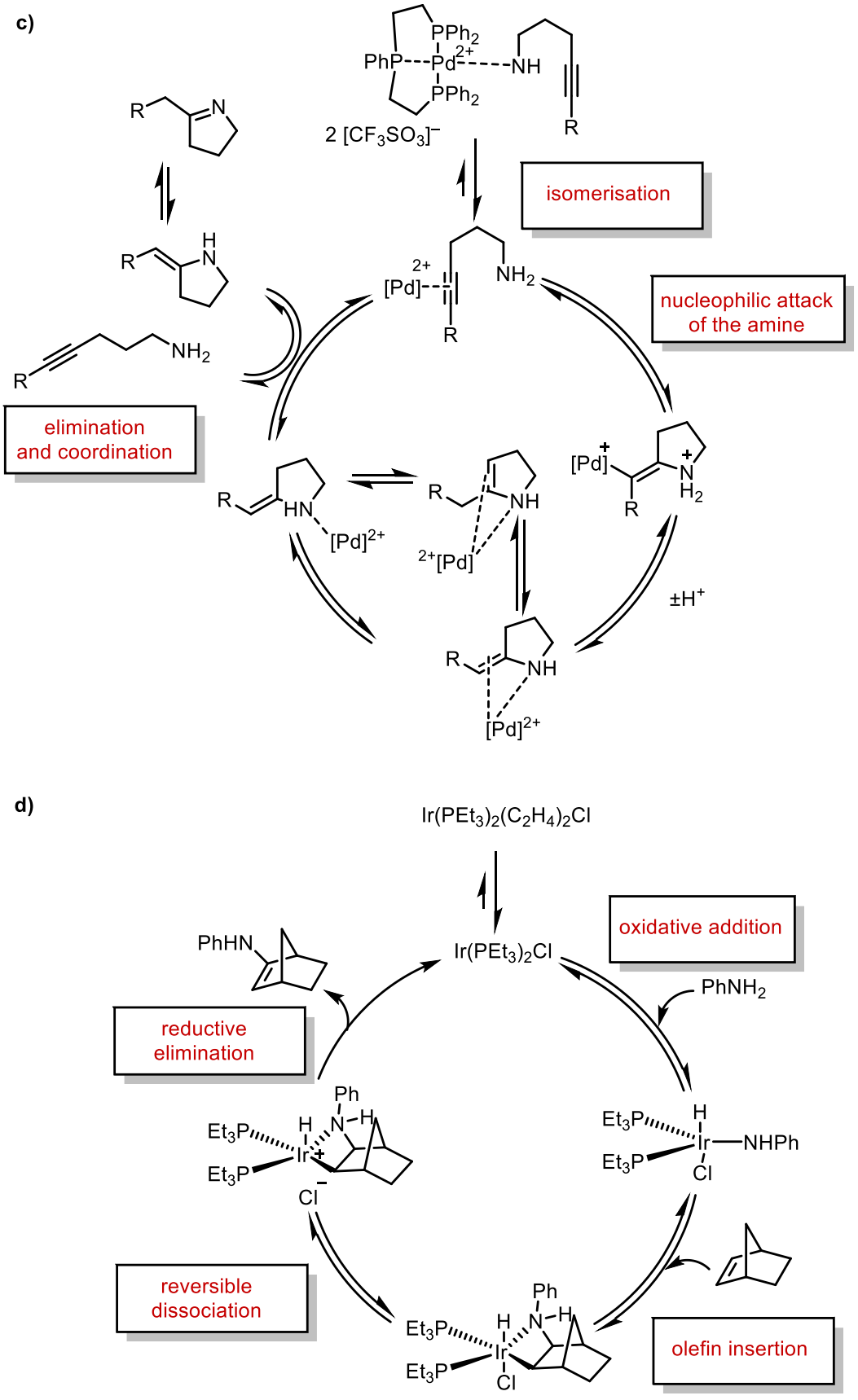

Scheme 4. Different hydroamination mechanisms depending on the catalyst system: a) Lanthanide (Yttrium) catalyst,[6] b) Titanium (Group 4) catalyst,[28] c) Palladium (Late transition metal catalyst),[6] d) Iridium (Electron rich late transition metal catalyst).[28]

As aforementioned, hydroamination reactions were explored thoroughly over the past decades. Here, various examples of different catalytic systems are shown.

Organolanthanide complexes were thoroughly examined by Marks et al. Their research progress is discussed in more detail in the following section. Nonetheless, an interesting example of a successful application of hydroamination/cyclisation in the natural product synthesis was reported by Marks and co-workers in 2003, where two naturally occurring alkaloids, (±)-pinidine and (+)-coniine were obtained in a concise fashion and in high yields and diastereoselectivities using a chiral samarocene catalyst (Scheme 5).[35]

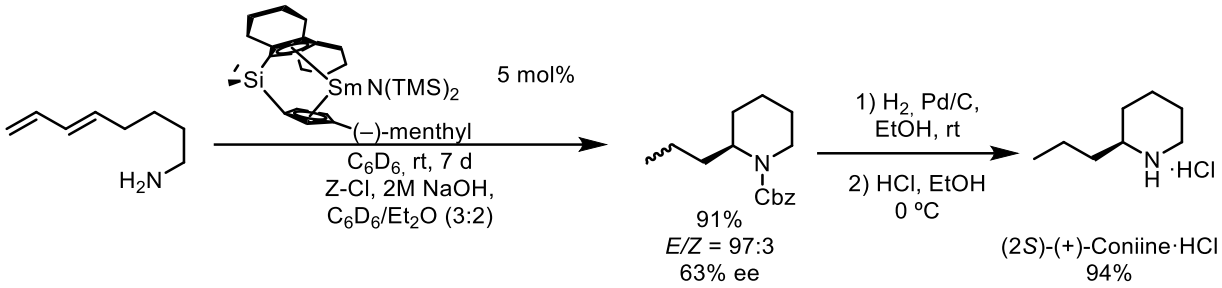

Scheme 5. Synthesis of (+)-Coniine·HCl via enantioselective aminodiene Hydroamination/ Cyclisation.[35]

Base-catalysed hydroamination was established as a very attractive pathway to approach important amines. Chemo- and regioselective hydroamination of myrcene to form diethylgeranylamine showed that the isolated double bonds exhibit significantly lower reactivity compared to the conjugated diene moiety (Scheme 6). This reaction found its industrial application on a multi-ton scale as a part of the Takasago menthol synthesis developed by Noyori.[2,36]

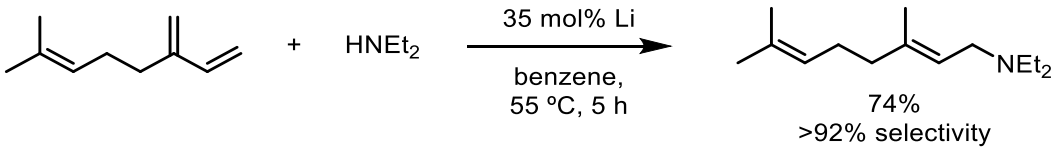

Scheme 6. Formation of diethylgeranylamine from myrcene in Takasago process.[37]

Livinghouse and Lee showed that group 4 metals can readily catalyse the intramolecular hydroamination of aminoalkynes. The metal precursors [$Ti(NMe_2)_4$] and [$Zr(NMe_2)_4$] alone delivered promising results, which could be further improved by

introduction of the novel bis(thiophosphinic) amidate ligands.[38,39] The same commercially available homoleptic metal complexes could serve as catalysts for the intramolecular hydroamination of aminoalkenes activated by *gem*-dialkyl substitution (Scheme 7).[40,41] Compared to rare-earth metal complexes, group 4 metal complexes exhibit a somewhat lower catalytic activity.[28] However, an increase in reactivity was achieved using a zwitterionic zirconium complex, that could lead to the cyclisation of the activated aminoalkene substrates at room temperature (Scheme 8).[42] A chiral variant of this catalyst could also perform the enantioselective hydroamination of aminoalkenes at a temperature as low as –30 ºC, and with reported enantiomeric excess of up to 98% (Scheme 9).[43]

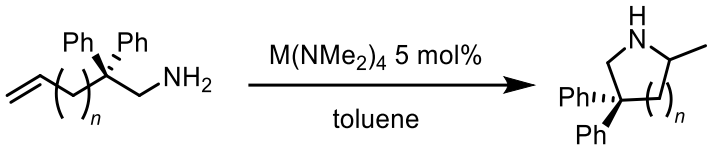

n	M	Temperature	Time	Yield
1	Ti	110 °C	24 h	92%
1	Zr	100 °C	1 h	92%
2	Ti	110 °C	24 h	80%
2	Zr	100 °C	3 h	83%

Scheme 7. Intramolecular hydroamination of activated aminoalkenes catalysed by homoleptic tetraamides of titanium and zirconium.[40,41]

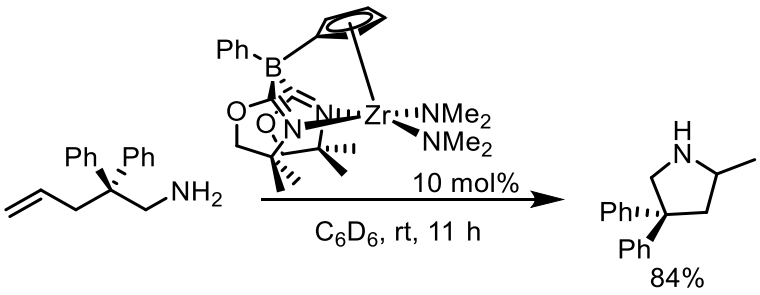

Scheme 8. Intramolecular hydroamination of activated aminoalkenes catalysed by a zwitterionic zirconium cyclopentadienyl-bis(oxazolidinyl)borate complex.[42]

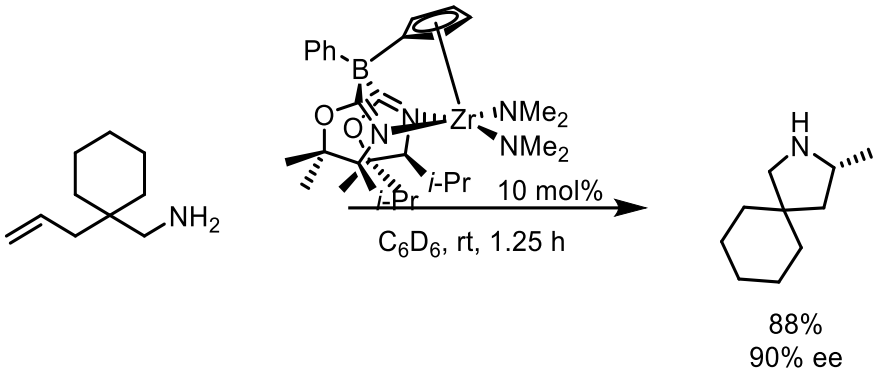

Scheme 9. Enantioselective intramolecular hydroamination of activated aminoalkenes catalysed by a zwitterionic zirconium cyclopentadienyl-bis(oxazolidinyl)borate complex.[43]

Besides, non-metallocene rare-earth metal complexes quickly became the centre of attention, especially through the work of the Hultzsch research group. Various chiral catalysts were designed, which enabled enantioselective inter- and intramolecular hydroamination of alkenes.[28] Some of the examples are presented in the Figure 2. A more detailed look into their development and catalytic performance is discussed in section 1.3.

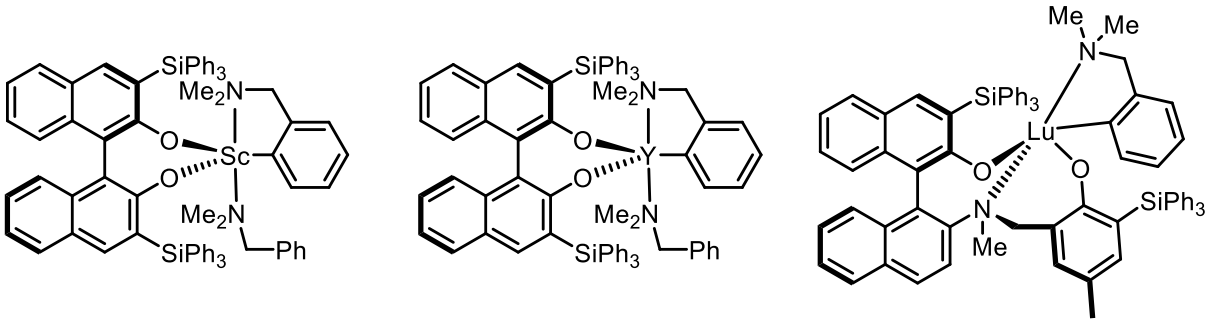

Figure 2. Examples of binaphtholate rare-earth metal complexes by Hultzsch et al.[44–46]

Various late transition metal catalysts have also been employed in hydroamination reactions. In general, it can be stated that they exhibit somewhat larger functional group tolerance as opposed to early transition metals (e.g. group 4 metals), lanthanides or actinides, owing to their lowered affinity to oxygen. Nevertheless, they are also typically less efficient than rare-earth metal catalysts. For instance, Wakatsuki et al. reported in 1999 a ruthenium catalysed intermolecular hydroamination of alkynes with anilines with a catalyst loading as low as 0.1 mol% [$Ru_3(CO)_{12}$] and 0.3 mol% NH_4PF_6.[47] Palladium-catalysed hydroaminations were described as early as 2000 by

Hartwig et al.,[48] where an *in situ* catalyst system was used that consisted of 2 % palladium(II) trifluoracetate, 3 % 1,1'-bis(diphenylphosphanyl) ferrocene, and 20 % trifluoromethane sulfonic acid. However, it required the use of activated substrates, for example substituted vinyl arenes and anilines.

Another interesting example is the cyclisation of aminoalkenes devoid of the activation through the Thorpe-Ingold effect using a rhodium-based catalyst (Scheme 10).[49] As previously mentioned, an advantage of late transition metal catalysts over rare-earth metal complexes is their larger functional group tolerance. This was also demonstrated by Hartwig et al. in 2008 using a rhodium-based catalyst, that successfully performed the intramolecular hydroamination, even in the presence of an unprotected hydroxy group (Scheme 11).[50]

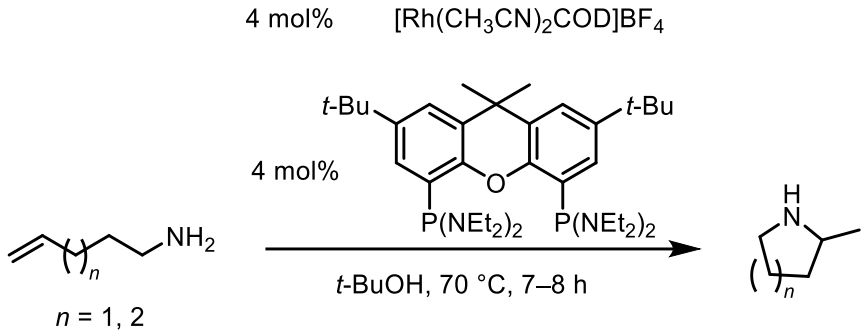

Scheme 10. Hydroamination of unbiased aminoalkenes using a rhodium-based catalyst.[49]

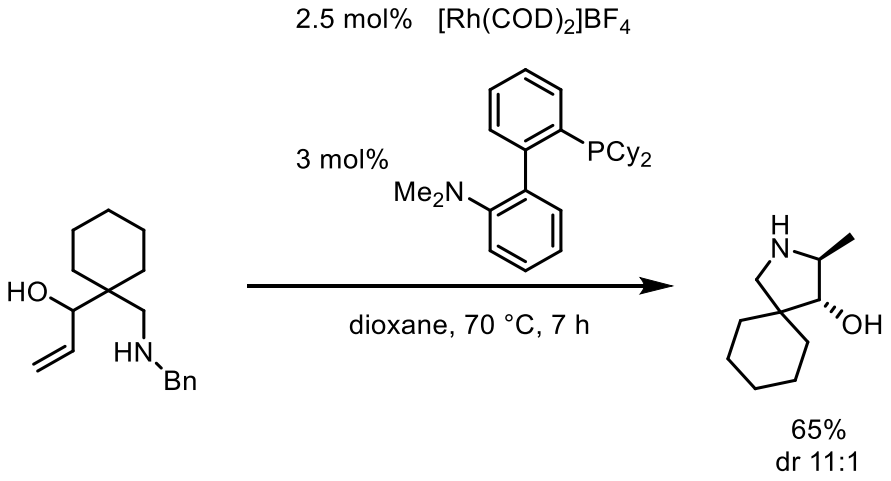

Scheme 11. Intramolecular hydroamination in presence of an unpotected hydroxy group using a rhodium-based catalyst.[50]

1.3 Rare-Earth Metal Catalysed Hydroamination of Alkenes

Early transition and f-element complexes were established as efficient catalysts early on.[22] The reason for it are their highly favourable characteristics, such as very high turnover frequencies and distinct stereoselectivity. This opened the door for the application of rare-earth metal complexes in the total synthesis of various alkaloid and other natural products.[35,51,52]

The first reported catalyst systems were based on lanthanocene complexes developed by Marks.[20] Subsequent ligand development efforts yielded different types of complexes, such as constrained-geometry complexes and post-metallocenes. They were widely employed in the intramolecular hydroamination of aminoalkenes and aminoalkynes.[6]

Marks and Gagné demonstrated the intramolecular hydroamination of aliphatic aminoalkenes catalysed by organolanthanide complexes.[19,24,30,53] Their design showed that these *ansa*-lanthanocene catalysts exhibit increased rates of cyclisation as opposed to the sterically more hindered catalysts. The even greater advantage came subsequently from the sterically more open and less electron-donating constrained-geometry catalysts (Figure 3).[19,54]

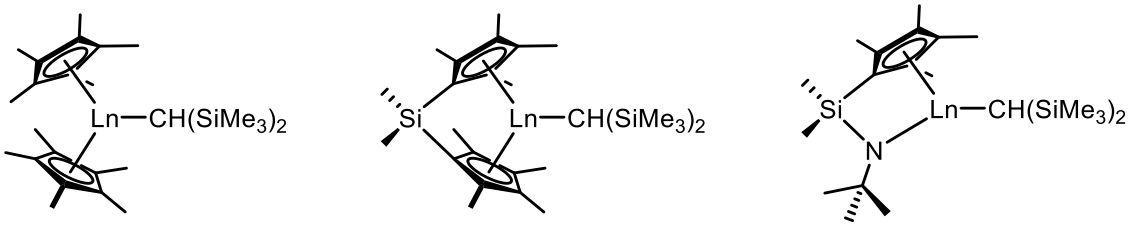

Figure 3. Different rare-earth metallocene complexes varying in steric demand of the ligand framework.[19,54]

Further research led to the development of the first non-metallocene catalysts, that are depicted in Figure 4.[55,56] Due to their lower performance interest shifted towards simple homoleptic rare-earth metal trisamides [Ln(N(SiMe$_3$)$_2$)$_3$] (Ln = La, Y, Nd),[57] that were an improvement in terms of results over the previously reported complexes. Even though they could readily catalyse the cyclisation of aminoalkynes, for aminoalkenes, catalytic activity was only observed in the case of the substrates activated by *gem*-dialkyl effect, such as the substrates used in the catalytic studies in this work.

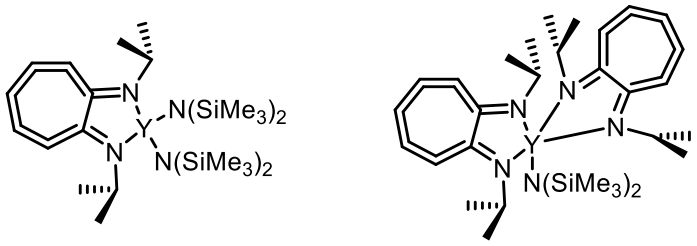

Figure 4. (Aminotroponiminato)yttrium amides as hydroamination catalysts.[55,56]

Intermolecular reactions, however, pose a greater challenge compared to the cyclisation reactions. Therefore, it is no wonder that there are significantly fewer reports on the successful transformations. The most efficient catalysts in this reaction type were shown to be lanthanocene[26] and binaphtholate[45] rare-earth metal complexes. The main difficulty arises from the competition between the weakly binding alkenes and strongly binding amines for the free coordination site on the metal centre, which could only be circumvented using an excess of the olefine substrate. One of the first major breakthroughs in the field was the catalysis with $Me_2Si(C_5Me_4)NdCH(SiMe_3)_2$ reported by Marks (Scheme 12).[26,58]

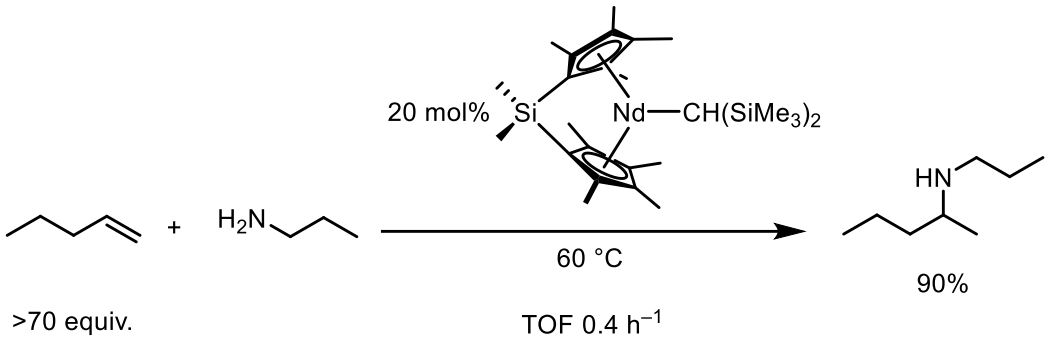

Scheme 12. Intermolecular hydroamination catalysed by neodymium ansa-metallocene catalyst.[26,58]

Enantioselective addition of an amine moiety across C–C double bonds is of a particular interest, since it would allow the stereoselective synthesis of chiral molecules without the use of chiral auxiliaries in stoichiometric amounts, as previously done.[34] Chiral lanthanide complexes were developed for that purpose and have a great asymmetric induction potential.[1] Both metallocene and non-metallocene chiral complexes were prepared for enantioselective hydroamination. Despite the remarkable results obtained with rare-earth metal complexes, their sensitivity towards oxygen and moisture has limited their wide-spread application.[6]

Initial efforts included C_1-symmetric organolanthanide *ansa*-metallocene catalysts bearing (+)-neomenthyl, (–)-menthyl and (–)-phenylmenthyl substituents attached to one of the cyclopentadienyl ligands developed by Marks and co-workers for the enantioselective and diastereoselective intramolecular hydroamination (Scheme 13).[30,53,59] Despite drawbacks of the system that would lead to the epimerisation of the chiral lanthanocene complex during the hydroamination reaction, good enantioselectivities were obtained, with up to 74% ee at low temperatures (Scheme 13).[30,53]

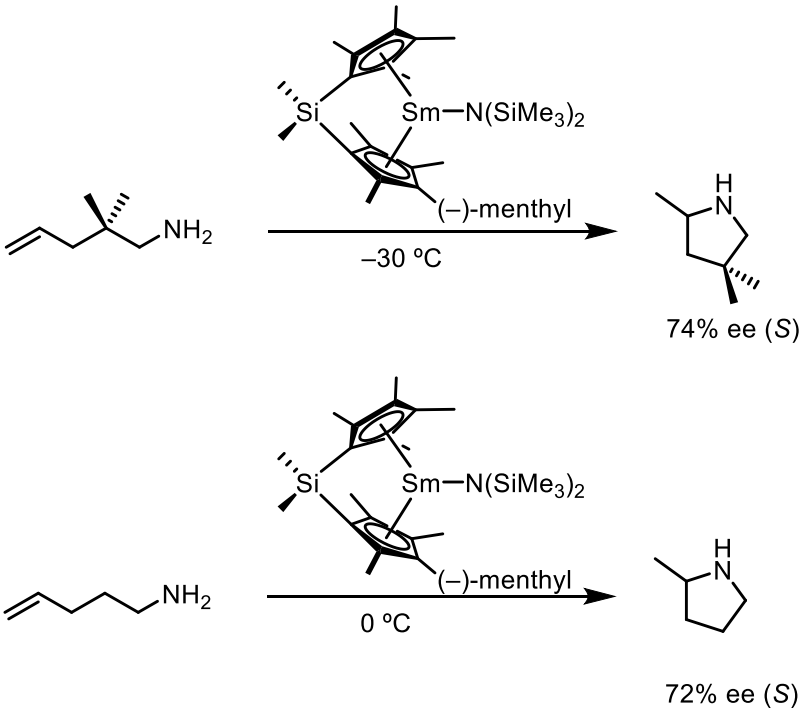

Scheme 13. Intramolecular hydroamination reactions catalysed by samarocene complex.[30,53,59]

Further research efforts led to the development of chiral non-metallocene catalysts, that should be able to retain their configurational integrity, which in return brought great advancements in the area of asymmetric catalysis. One of the first reported examples featured the *in situ* generation of the biaryl diamido precatalysts (Figure 5), which showed unsatisfactory catalytic activity and enantioselectivity. The exchange of the bis(dimethylsilyl)amido ligand for a more basic amido ligand led to the improvement in the catalytic activity (Figure 5).[60]

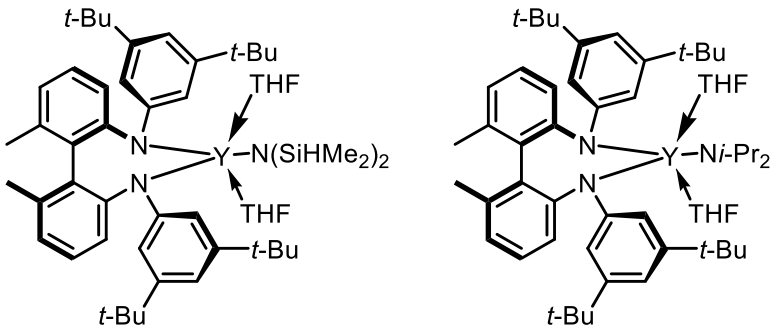

Figure 5. Examples of biaryl diamido rare-earth metal complexes.[60]

It was postulated that the amido ligands can have a great impact on the catalytic performance of a certain metal complex. The less basic ligands, such as bis(dimethylsilyl)amido ligand most likely tend to lead to the reduction in the activity and the more basic ligands are preferred. The effect was explained through the hampered and incomplete initiation in the catalytic cycle (Figure 6).[60] The same observation was made in 2004 by Hultzsch et al. when diamidoamine complexes of yttrium bearing a bis(dimethylsilyl)amido ligand were compared with complexes bearing bis(trimethylsilyl)amido and *ortho*-(dimethylaminomethyl)phenyl ligands in their performance as hydroamination catalysts.[61]

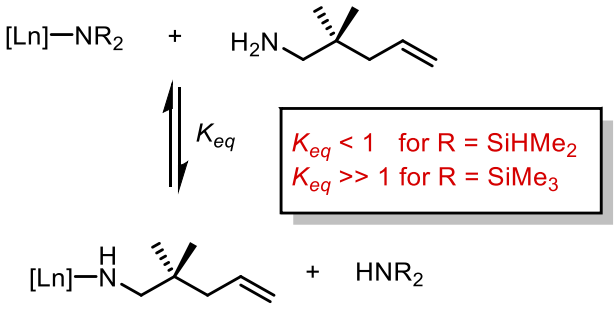

Figure 6. Equilibrium of the catalyst activation.[61]

Subsequently, Hultzsch and co-workers presented rare-earth complexes featuring sterically demanding trisarylsilyl-substituted binaphtholate ligands. They delivered excellent results in both inter- and intramolecular hydroamination using various substrates.

As an example, in 2006 it was reported that the intermolecular hydroamination of vinyl arenes and N-unprotected amines could proceed in *anti*-Markovnikov fashion (Scheme 14).[44]

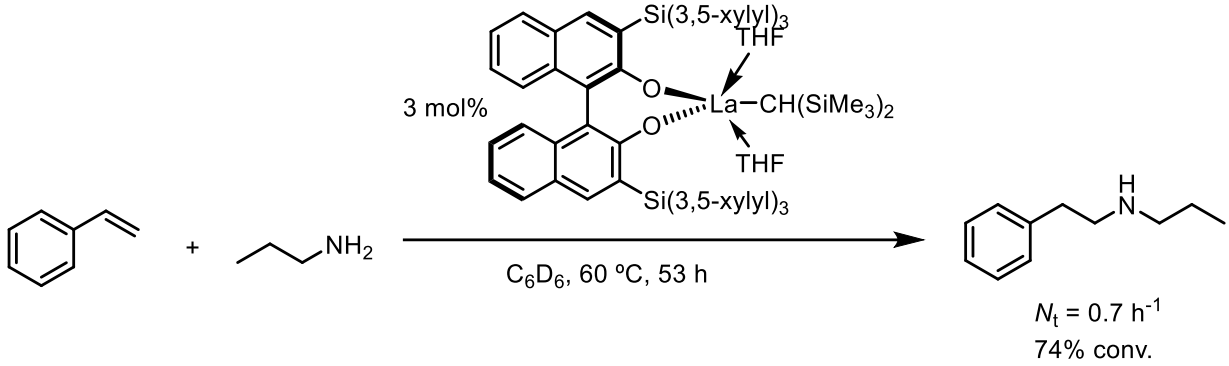

Scheme 14. Anti-Markovnikov hydroamination of vinylarene catalysed by a binaphtholate rare-earth metal complex.[44]

Enantioselectivity as high as 66 % *ee* in asymmetric intermolecular hydroamination was reported in 2010 by Hultzsch et al. by applying similar binaphtholate complexes. A high excess of alkene was applied in order to accelerate the hydroamination[6] and the reaction proceeded with high Markovnikov selectivity, as shown in Scheme 15.[45]

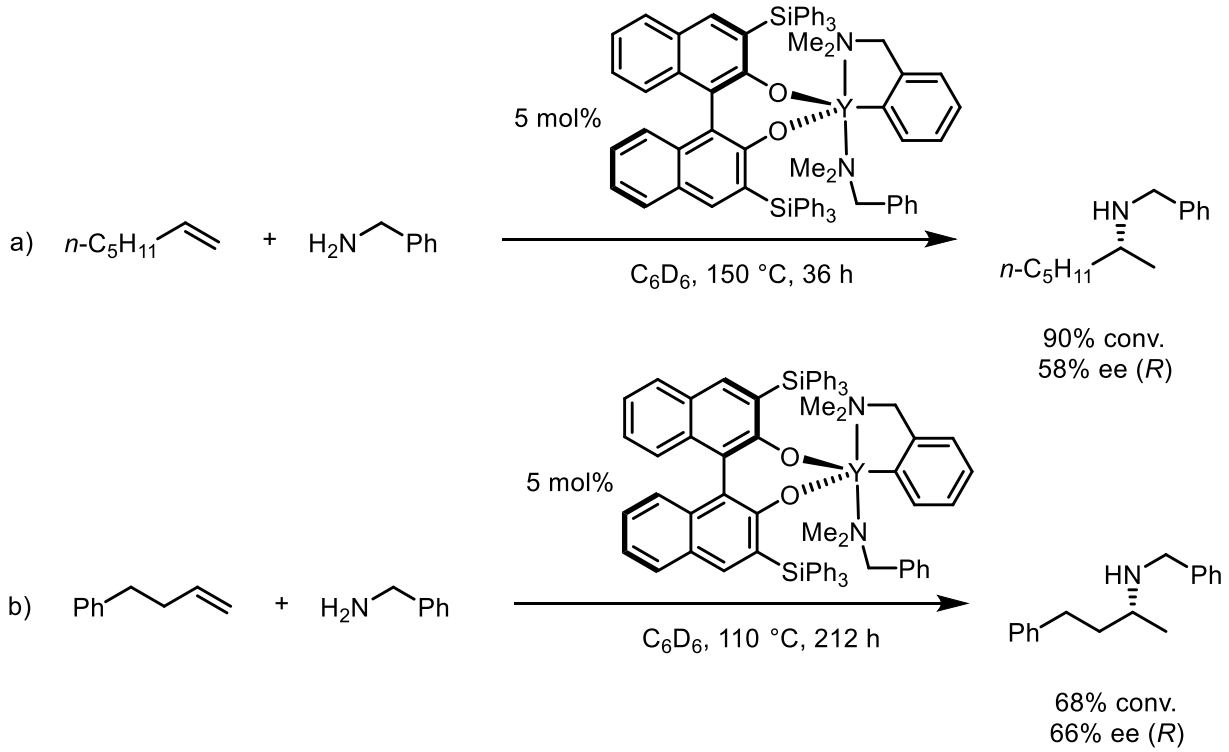

Scheme 15. Asymmetric intermolecular hydroamination of 1-heptene catalysed by a binaphtholate rare-earth metal complex.[45]

Outstanding results were obtained in intramolecular hydroamination of the 1,2-disubstituted olefin activated through Thorpe-Ingold effect.[62] High enantiomeric excess of up to 96 % was reported (Scheme 16).

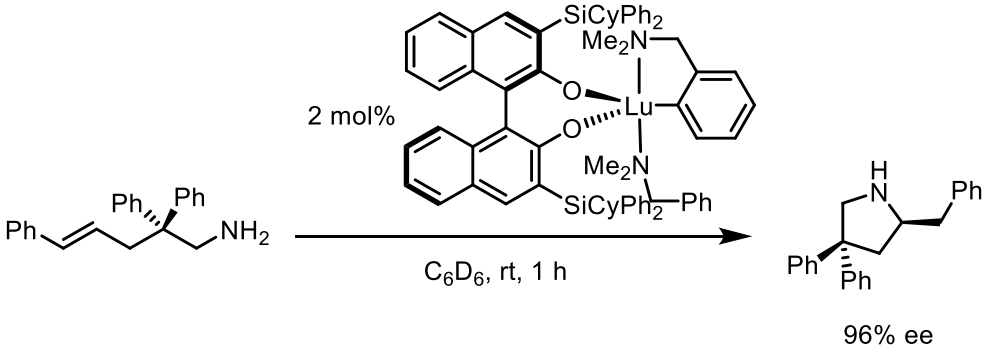

Scheme 16. Asymmetric intramolecular hydroamination of the internal alkene catalysed by a binaphtholate rare-earth metal complex.[62]

2. Scope of work

The aim of this work was to prepare novel bis(phenolate) type ligands with different spacer groups separating the two phenol moieties and their corresponding early transition metal complexes, characterise them *via* NMR spectroscopy and utilise them as catalysts for intramolecular hydroamination of aminoalkenes.

To achieve this, multistep organic syntheses of three different bis(phenolate) type ligands were performed and the obtained ligands were used for the preparation of early-transition metal complexes on an NMR scale. *In situ* obtained and *via* NMR spectroscopy characterised metal complexes were employed in the intramolecular hydroamination of aminoalkenes with ferrocene as an internal standard. The reaction progress was monitored using ^{1}H-NMR spectroscopy.

3. Results and discussion

3.1 Ligand Synthesis

The synthesis of two groups of bis(phenolate) type ligands with different spacer groups between the phenol moieties was envisioned. One group consisted of two ligands (**6** and **7**) containing a CH_2-group separating the phenol moieties and the second group was represented by ligand **9** equipped with a disulphide spacer.

3.1.1 Methylenebis(phenolate) Ligands

A very convenient protocol was developed for the synthesis of methylenebis(phenolate) ligands. It consisted of removal of *tert*-butyl groups of the starting material **1** in the first step, in a way similar to that described in literature by Ojima et al.[63] using $AlCl_3$ in nitromethane to produce 89 % of the desired product **2** after recrystallisation (Scheme 17).

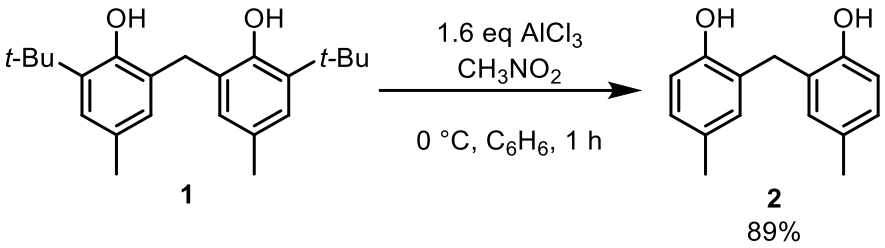

Scheme 17. Synthesis of 2,2'-methylenebis(4-methylphenol) (**2**).

Bisphenol **2** then underwent simple bromination using Br_2[63] to afford the brominated ligand precursor **3** in quantitative yield (Scheme 18), which could be used without further purification, as shown *via* NMR spectroscopy.

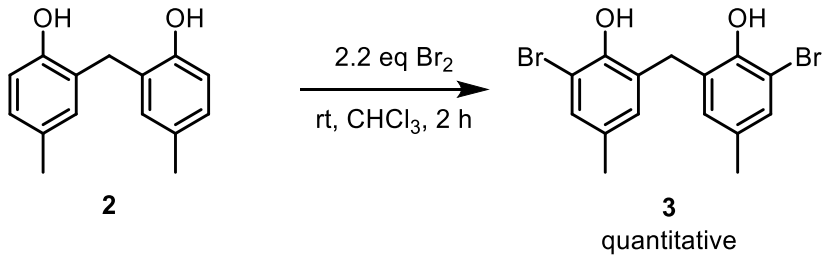

Scheme 18. Synthesis of 6,6'-methylenebis(2-bromo-4-methylphenol) (**3**).

With the ligand precursor in hand, a one-pot silylation/retro-Brook rearrangement reaction could be performed.[64] This step also made the synthetic procedure divergent, as only in this step a suitable silyl-substituent was introduced *via* silylation with the appropriate chlorosilane. Chlorotriphenylsilane is commercially available and was directly employed in the reaction (Scheme 20), whereas chloro(cyclohexyl)diphenylsilane (**5**) was synthesised according to a modified literature protocol (Scheme 19), and was subsequently applied in the synthesis of **7** (Scheme 21).[65]

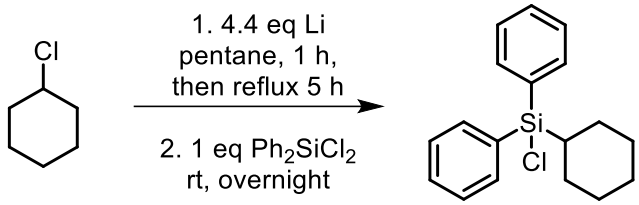

4
2.5 eq

5
60%

Scheme 19. Synthesis of chloro(cyclohexyl)diphenylsilane (**5**).

The obtained ligands were initially purified *via* flash chromatography (Scheme 20 and Scheme 21). Ligand **6** was then freeze-dried from benzene *in vacuo* to remove any minor impurities before being used for complexation reactions in an argon-filled glovebox and was obtained in 83 % yield. Single crystals of high purity, suitable for X-ray diffraction analysis, were grown from ethyl acetate at ambient temperature by slow evaporation (Figure 7). Ligand **7**, on the other hand, could not be obtained as a solid through freeze-drying. Instead, it was also recrystallised from ethyl acetate and dried *in vacuo* before introduction into the glovebox. Isolated yield was somewhat lower, 45 %, and is to be attributed to possible impurities in the corresponding chlorosilane **5** and elaborate isolation process. Single crystals of the ligand were obtained in the same manner as for ligand **6**, by recrystallisation from a small volume of ethyl acetate (Figure 8).

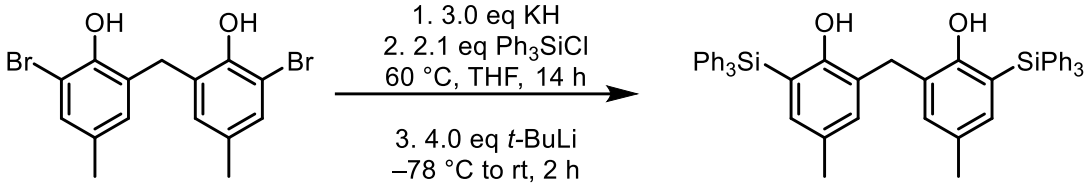

3 **6**
83%

Scheme 20. Synthesis of 6,6'-methylenebis(4-methyl-2-(triphenylsilyl)phenol) (**6**).

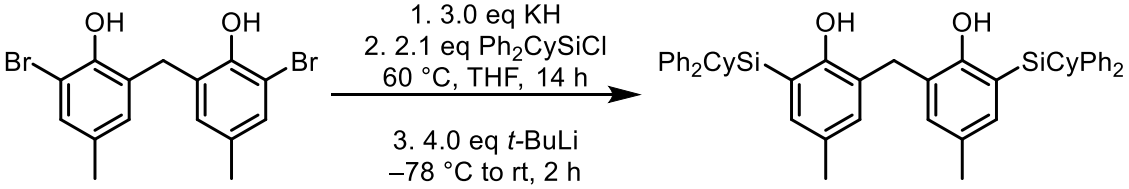

3 **7**
45%

Scheme 21. Synthesis of 6,6'-methylenebis(2-(cyclohexyldiphenylsilyl)-4-methylphenol) (**7**).

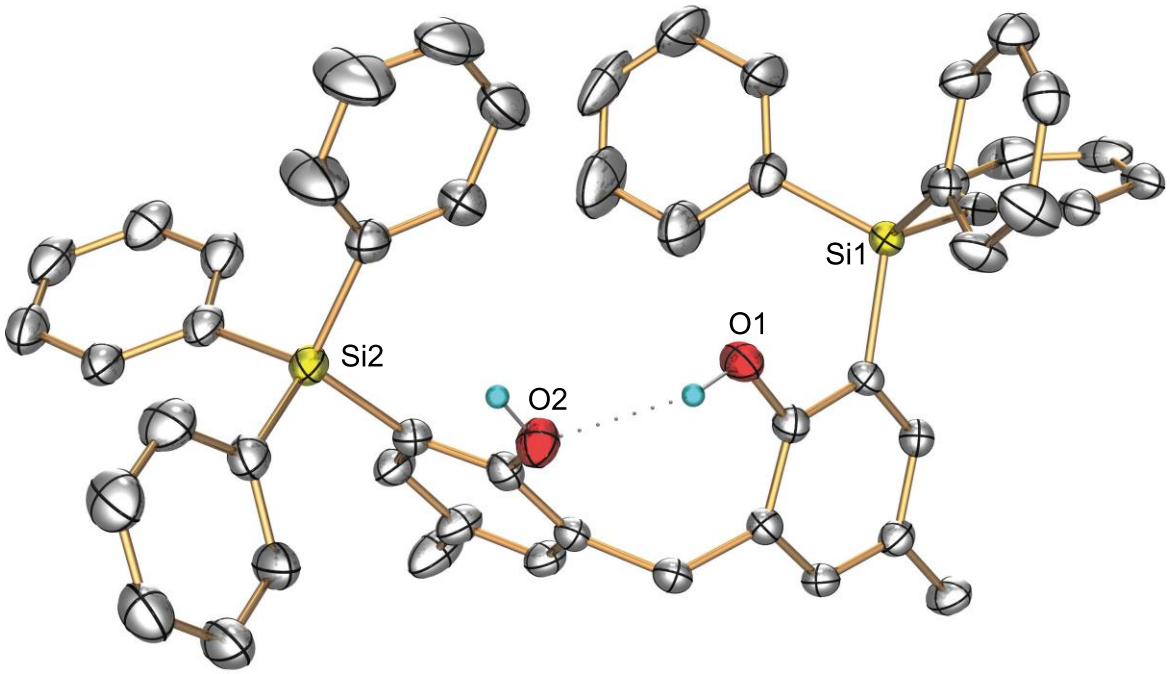

Figure 7. Molecular structure of **6** (hydrogen atoms were omitted for clarity).

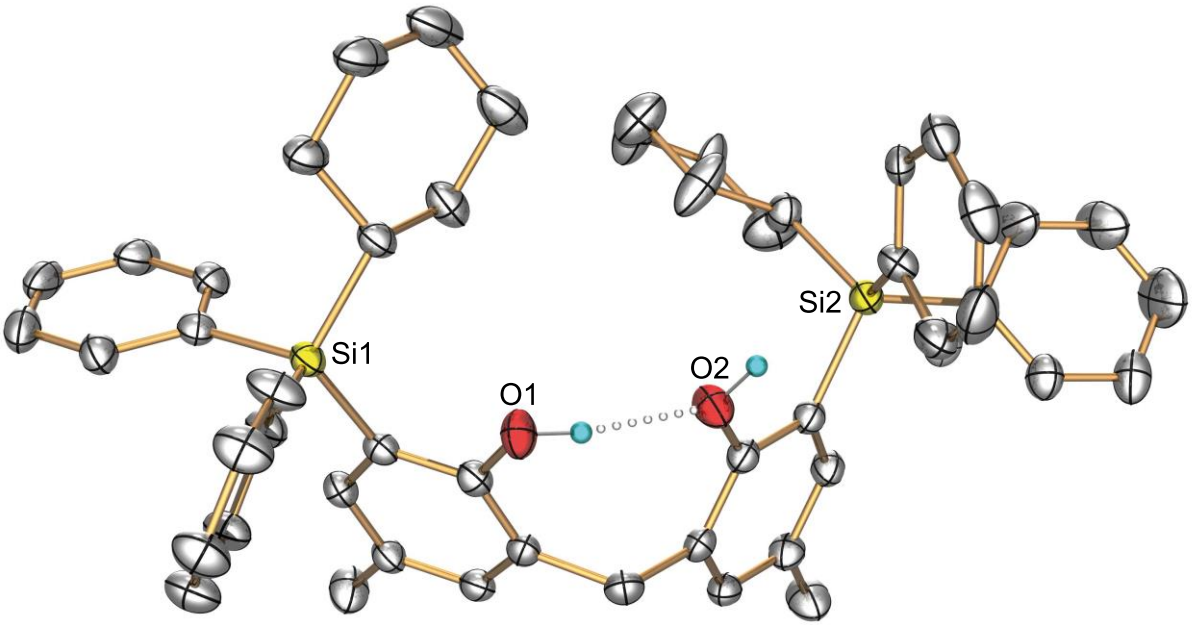

Figure 8. Molecular structure of **7** (hydrogen atoms were omitted for clarity).

Analysis of the molecular structures shown in Figures 7 and 8 reveals that the dihedral angle between benzene rings is 99.98 ° for ligand **6** and 111.08 ° for ligand **7**. The difference in dihedral angles could be explained with slightly increased steric bulk of the cyclohexyl group in the ortho substituent of ligand **7**, as opposed to the phenyl ring of the ligand **6**. The two hydroxyl groups of both ligands form homonuclear hydrogen bonds with one another and, thus it is also possible to compare the hydrogen bond geometries of the two structures. The comparison shows that the O–H bond lies at 0.840 Å for both ligands. O···H bond lengths are 2.146 Å and 2.024 Å for ligands **6** and **7**, respectively and the O–H···O angle lies at 162.14 ° and 161.17 °, respectively. These values lie and within expectations for hydrogen bonds[66] and are mutually almost identical.

3.1.2 Disulfanediylbis(phenolate) Ligand

For the synthesis of 6,6'-disulfanediylbis(4-methyl-2-tritylphenol) (**10**) a two-step synthetic protocol was developed. In the first step, *p*-cresol (**8**) was functionalised with a trityl-substituent in *ortho*-position by performing the reaction in a melt of **8** with 1.3 equiv sodium and TrtCl (Scheme 22).[67,68]

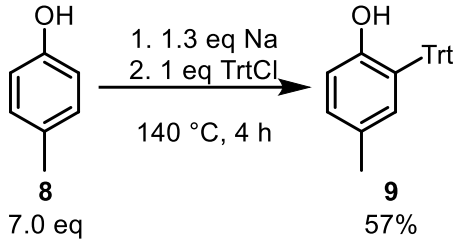

Scheme 22. Synthesis of 6,6'-disulfanediylbis(4-methyl-2-tritylphenol) (**9**).

In the following step (Scheme 23) a disulphide bridge was formed in the reaction of 4-methyl-2-tritylphenol (**9**) and 0.5 equiv S_2Cl_2. The reaction protocol was based on a literature procedure reported by Okuda et al. for the synthesis of 2,2'-dithiobis(6-tert-butyl-4-methylphenol).[69] However, slight modifications in terms of reaction conditions (reaction volume and time) were made. This approach was successful and yielded the desired ligand **10** in 32 % yield after recrystallisation from ethanol followed by freeze-drying.

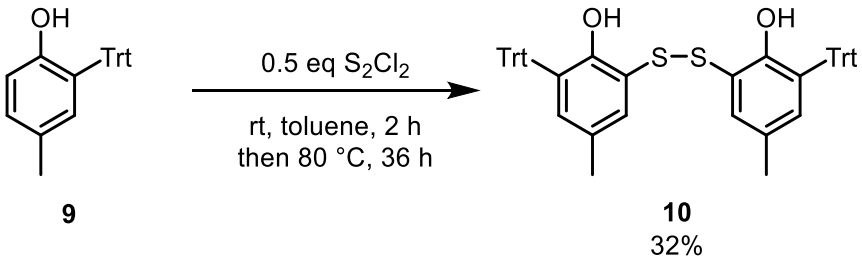

Scheme 23. Synthesis of 6,6'-disulfanediylbis(4-methyl-2-tritylphenol) (**10**).

The ligand was additionally freeze-dried from benzene *in vacuo* before being used for complexation reactions under inert conditions. Unfortunately, no crystal structure of the ligand could be obtained despite repeated efforts. It was observed that the ligand readily crystallises in hexanes. However, no crystallisation conditions could be found to produce the crystals of a shape and size suitable for X-ray measurements.

3.2 Metal Complex Synthesis

Complexation reactions were performed in an argon-filled glovebox under strict inert conditions and the reaction progress was monitored *via* NMR spectroscopy. The initial intention was to produce potentially catalytically active metal complexes that would possess one bis(phenolate) ligand in the coordination sphere of the central atom. Thus, all the reactions were performed in stoichiometric ratio 1:1 if not stated otherwise.

3.2.1 Yttrium Complexes

Initial attempts were made at obtaining yttrium complexes, starting from the precursor [Y(*o*-$C_6H_4CH_2NMe_2)_3$] (**11-Y**) and available bis(phenolate) type ligands, similar to the catalysts previously reported by the Hultzsch group.[44,45,62,70] However, the reaction was not successful (Scheme 24) and led to the mixture of unidentified products.

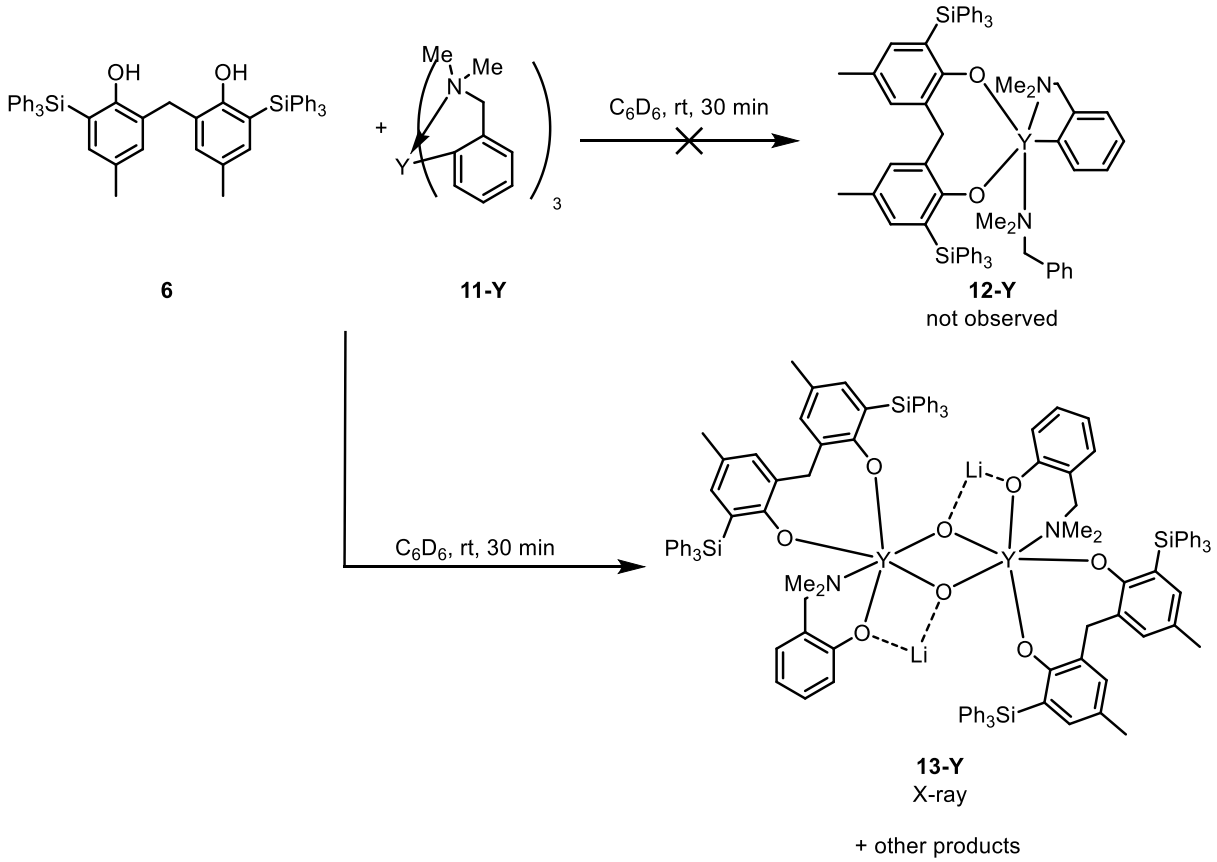

Scheme 24. Attempted complexation of [Y(o-$C_6H_4CH_2NMe_2)_3$] with **6** in C_6D_6 at room temperature and the formation of **13-Y**.

Similar results were obtained in reactions with the remaining two ligands (Scheme 25 and Scheme 26).

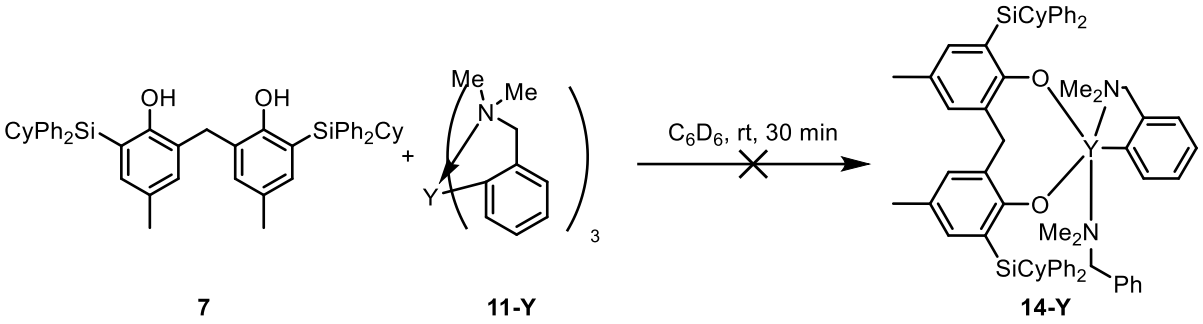

7 **11-Y** **14-Y**

Scheme 25. Attempted complexation of [Y(o-$C_6H_4CH_2NMe_2)_3$] with **7** in C_6D_6 at room temperature.

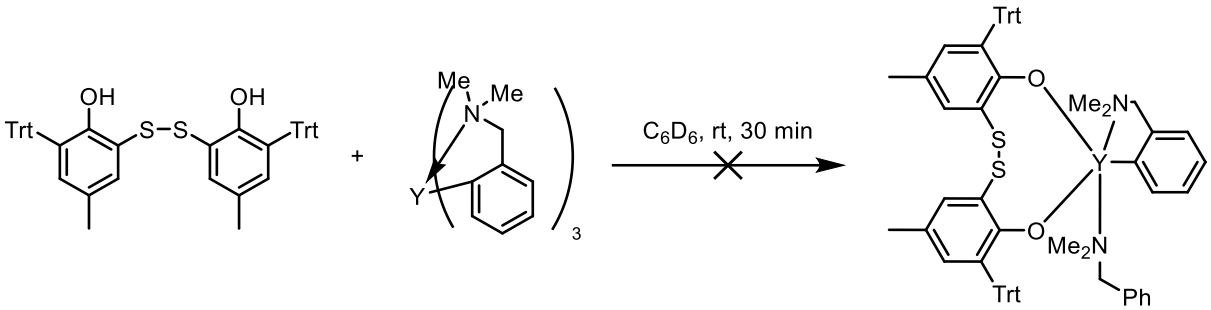

10 **11-Y** **15-Y**

Scheme 26. Attempted complexation of [Y(*o*-$C_6H_4CH_2NMe_2)_3$] with **10** in C_6D_6 at room temperature.

It was presumed that the mixture of products forms due to the reaction temperature and order of addition of the reactants. In order to force the system towards formation of the desired kinetic product **12-Y**, an attempt at performing the reaction at low temperature was made (Scheme 27). The temperature of –20 °C was chosen since it can be achieved inside the glovebox using the aid of the built-in freezer. Even upon slow addition of the ligand solution to the precursor solution, no desired product was obtained.

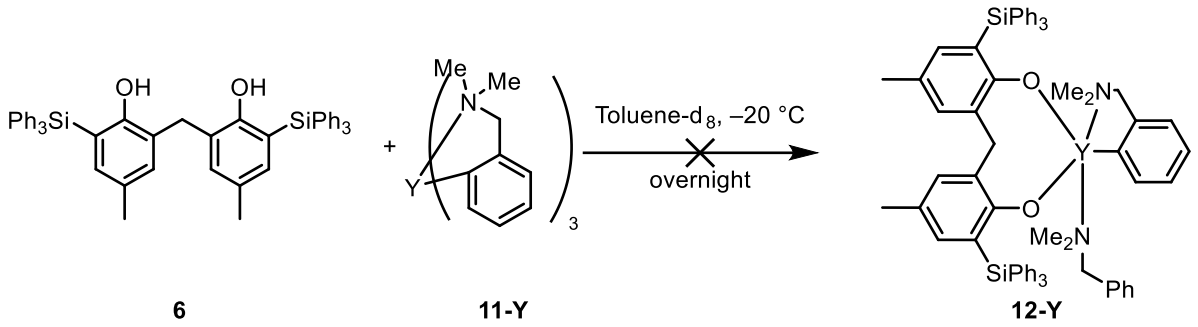

6 **11-Y** **12-Y**

Scheme 27. Attempted complexation of [Y(*o*-$C_6H_4CH_2NMe_2)_3$] with **6** in toluene-d_8 at –20 °C.

However, upon longer stay at room temperature, the solution of the reaction mixture (Scheme 24) produced crystals, some of which could be measured, and the obtained crystal structure showed the formation of the oxo-bridged yttrium species **13-Y** (Figure 9). Presence of the two lithium ions in the structure points towards the complex **13-Y** being formed upon reaction of the complex [LiY(o-$C_6H_4CH_2NMe_2)_4$], rather than [Y(o-$C_6H_4CH_2NMe_2)_3$], which may form during the synthesis of the yttrium precursor **11-Y** in case of a mismatched stoichiometry of starting materials YCl_3 and Li(o-$C_6H_4CH_2NMe_2$). It can be speculated that the species **13-Y** was formed from trace amounts of oxygen in the glovebox or water, e.g. on the glass surface of the reaction vial. Upon closer inspection, it is possible to observe insertion of an oxygen atom into the Y–C_{Ar} bond of the complex, which is an uncommon occurrence and the mechanism for the formation of this species has not yet been fully understood.

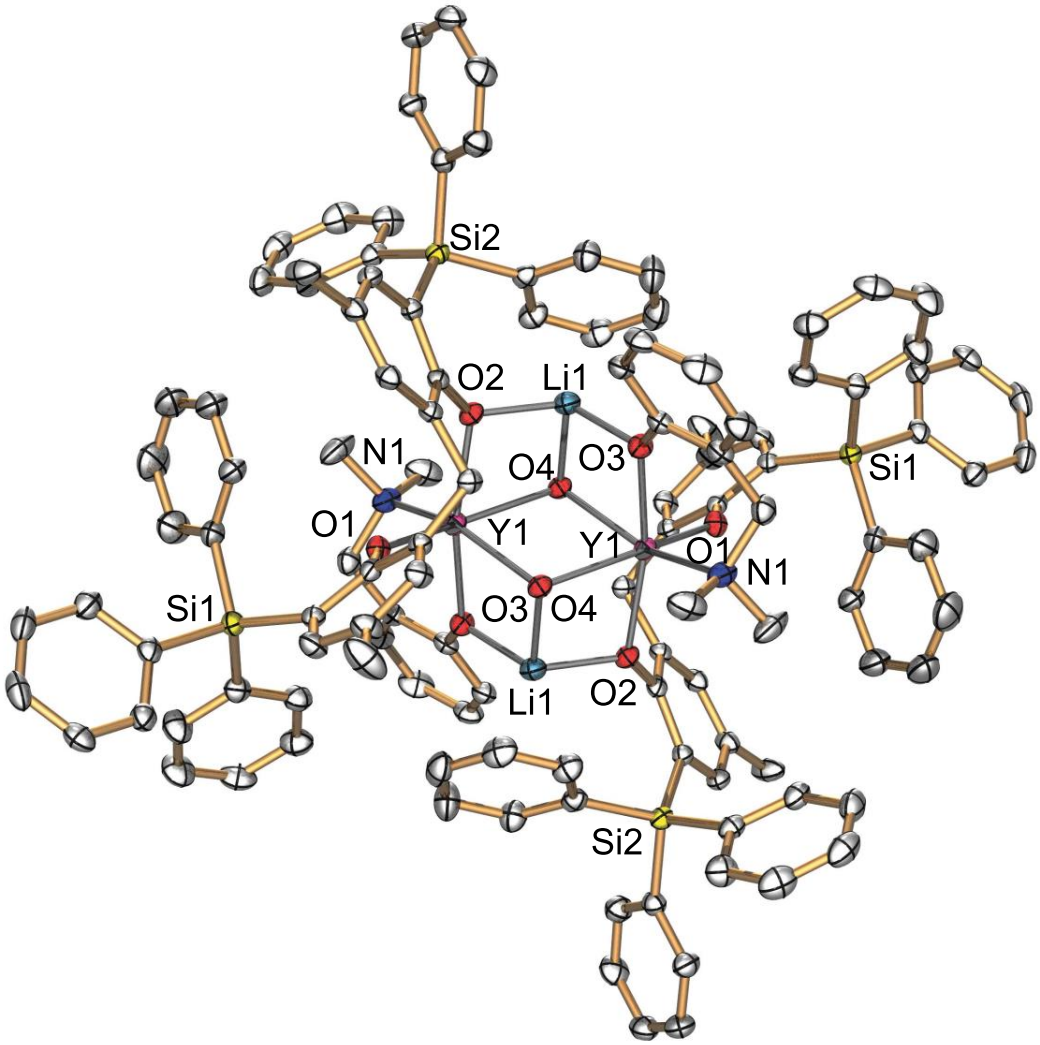

Figure 9. Molecular structure of **13-Y** (solvent molecules and hydrogen atoms were omitted for clarity).

Table 1. Selected bond lengths (Å) and angles (°) in **13-Y**.

	Interatomic distance (Å) / Bond angle (°)
Y1-Y1	3.6819(5)
Y1-O1	2.1217(17)
Y1-O2	2.2644(16)
Y1-O3	2.2525(16)
Y1-O4	2.3159(17)
Y1-O4^{1}	2.2979(17)

Table 1. Selected bond lengths (Å) and angles (°) in **13-Y** - continued

Y1-Li1	3.174(4)
Y1-Li1[1]	3.173(5)
O2-Li1[1]	1.909(5)
O3-Li1	1.936(5)
O4-Li1[1]	1.987(5)
Y1-N1	2.470(2)
Y1-O4-Y1[1]	105.88(7)
O1-Y1-O2	93.37(7)
O1-Y1-O3	100.99(7)
O1-Y1-O4	157.58(7)
O1-Y1-O4[1]	91.13(7)
O2-Y1-O3	165.50(7)
O2-Y1-O4	73.99(6)
O2-Y1-O4[1]	102.29(6)
O3-Y1-O4	91.76(6)
O3-Y1-O4[1]	75.67(6)
O4-Y1-O4[1]	74.12(7)
O1-Y1-N1	103.51(8)
O2-Y1-N1	100.57(7)
O3-Y1-N1	78.12(7)
O4-Y1-N1	97.08(7)

[1]1-X,1-Y,1-Z

Since the yttrium metal in the species **13-Y** possesses an octahedral coordination geometry, it provides an opportunity to determine to which extent the geometry of the said complex deviates from a perfect octahedron. To quantify octahedral distortion, several parameters are used. Important is d_{mean}, which refers to the average

metal–ligand distances in the octahedral sphere. It is followed by parameters ζ, Σ, and Θ, that stand for stretching, angular and torsional distortions, respectively. Additional is the parameter Δ, described as a deviation of metal–ligand distances with respect to the average metal–ligand distance, as shown in Equation (1).[71] Parameters ζ, Σ, and Θ can be calculated according to Equations (2) – (4).[72]

$$\Delta = \frac{1}{6}\sum_{i=1}^{6}\left(\frac{d_i - d_{mean}}{d_{mean}}\right)^2 \quad (1)$$

$$\zeta = \sum_{i=1}^{6}|d_i - d_{mean}| \quad (2)$$

$$\Sigma = \sum_{i=1}^{6}|\phi_i - 90| \quad (3)$$

$$\Theta = \sum_{i=1}^{6}|\theta_i - 60| \quad (4)$$

To obtain the values of the parameters of interest, the software Octahedral Distortion Calculator (OctaDist version 2.6.1) was utilised.[72] As input values for the software, the cartesian coordinates of the central atom and the surrounding six donor atoms were given. The distortion parameters are summarised in Table 2.

Table 2. Computed octahedral distortion parameters for the complex **13-Y**.

Octahedral distortion parameter	Computed values in Å and °
d_{mean}	2.2870 Å
Δ	0.0020
ζ	0.4448 Å
Σ	118.68 °
Θ	337.18 °

As shown in Table 2, geometry of the complex **13-Y** deviates substantially from a perfect octahedron. In the case of a perfect octahedron, the distortion parameters for stretching, angular and torsional distortion, as well as the parameter *Δ*, would have zero values. The computed parameters, however, show that in the case of **13-Y** the stretching, angular and torsional distortion *ζ, Σ* and *Θ* are relatively high, which speaks for a distorted octahedral geometry. For clarity, a visual representation of the octahedron of the complex **13-Y** is given in Figure 10.

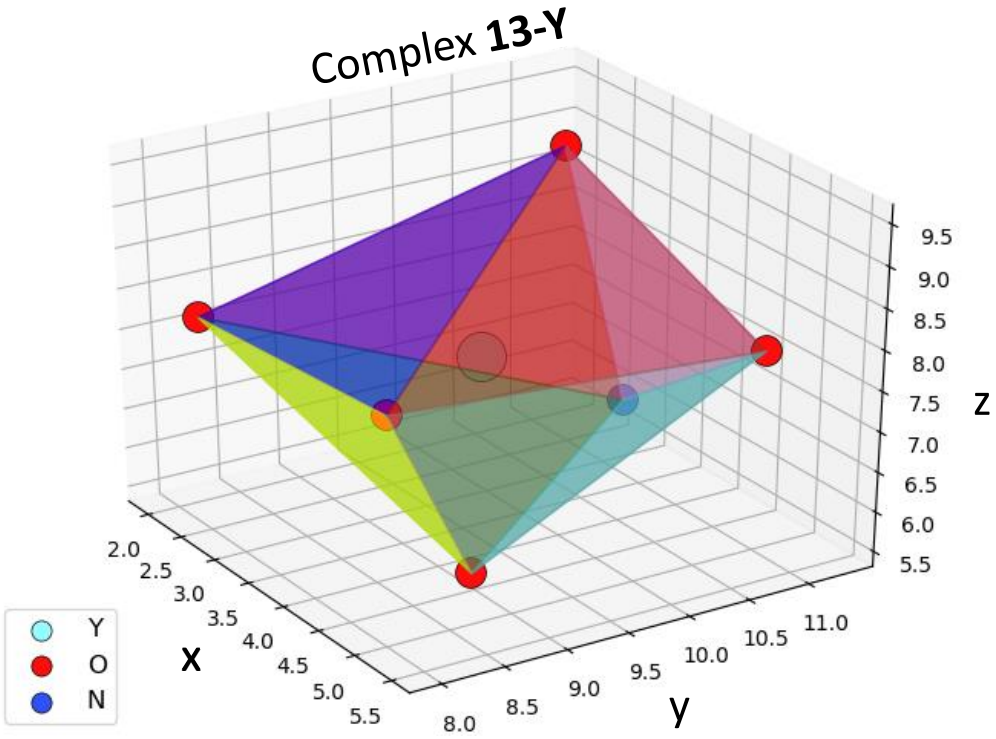

Figure 10. Graphical representation of the octahedron of the complex **13-Y**.

On account of the results shown above, the use of $Y(BDMA)_3$ (**11-Y**) as a metal precursor was abandoned and the alternative precursor $[Y(N(SiHMe_2)_2)_3(THF)_2]$ (**16-Y**) was given precedence. In this case, all three complexation reactions were successful, and the complexes **17-Y**, **18-Y** and **19-Y** could be characterised using NMR spectroscopy (Scheme 28 and Scheme 29).

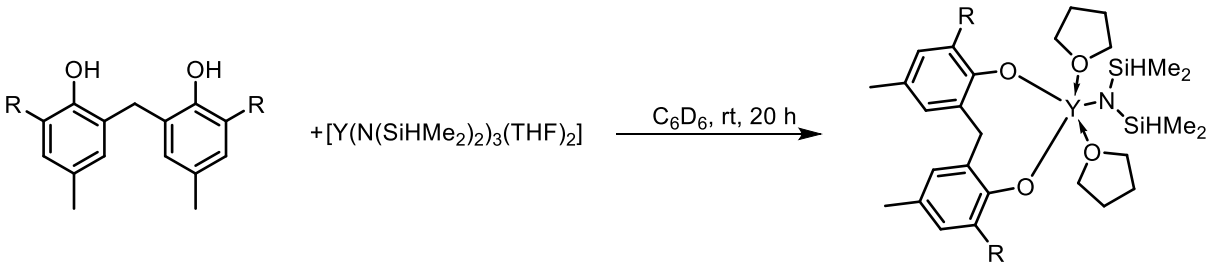

6,7 **16-Y** **17-Y, 18-Y**

6, 17-Y: R= $SiPh_3$ **7, 18-Y:** R=$SiPh_2Cy$

Scheme 28. Synthesis of complexes **17-Y** and **18-Y**.

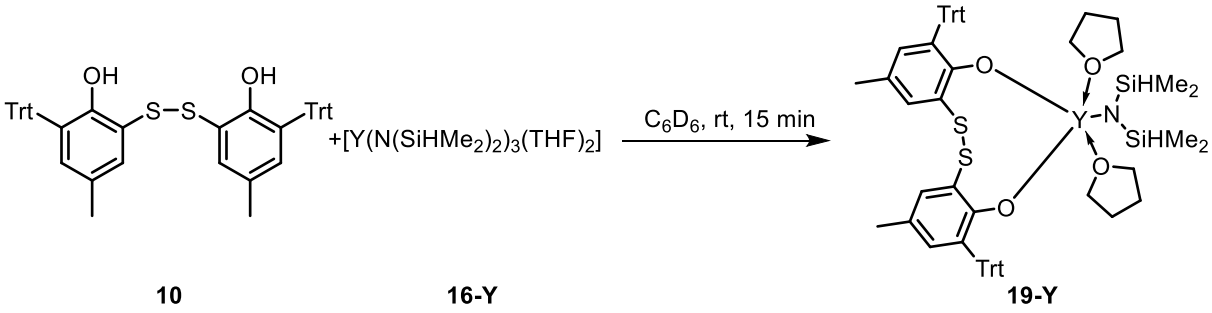

10 **16-Y** **19-Y**

Scheme 29. Synthesis of the complex **19-Y**.

Comparisons of the ^{1}H- and ^{13}C-NMR spectra of the three yttrium complexes **17-Y**, **18-Y** and **19-Y** are depicted in Figures 11 and 12, respectively. Complexation reaction proceeded significantly faster in the case of the complex **19-Y** as opposed to the complexes **17-Y** and **18-Y** (15 min versus 20 h). This observation could be explained with the presence of the disulphide moiety in ligand **10**, which could accelerate the reaction by weakly coordinating to the yttrium atom of the metal precursor and thus bringing the phenol groups of the proligand in close proximity to the metal centre. Upon successful complexation reaction, disappearance of the OH peak of the diol proligand (**6**, **7** and **10**) could be observed in the respective ^{1}H-NMR spectra. At the same time a heptet of the SiH group of the free amine emerged at around 4.72 ppm in ^{1}H-NMR

spectra of all three complexes (▲ in Figure 11). In parallel, methyl-groups of the free amine $HN(SiHMe_2)_2$ could be detected at approximately 0.12 ppm, experiencing a high-field shift compared to the methyl-groups of the amido ligand of the complex (▲ in Figure 11). The same high-field shift could be observed in the corresponding ^{13}C-NMR spectra (▲ in Figure 12). Characteristic peaks of the ligands **6**,**7** and **10** could easily be identified in both ^{1}H- and ^{13}C-NMR spectra (Figure 11 and 12). However, they experienced a slight shift compared to the spectra of the free ligands, which served as a confirmation of the coordination to the metal centre. As shown previously, the SiH signal of the amido ligand is strongly dependent on the nature of the metal centre and the ligands.[73] In the case of the complexes **17-Y** and **18-Y**, this diagnostic peak could be found at 5.00 and 4.66 ppm and 5.23 ppm, respectively (● in Figure 11), whereas in complex **19-Y** it could not be successfully identified.

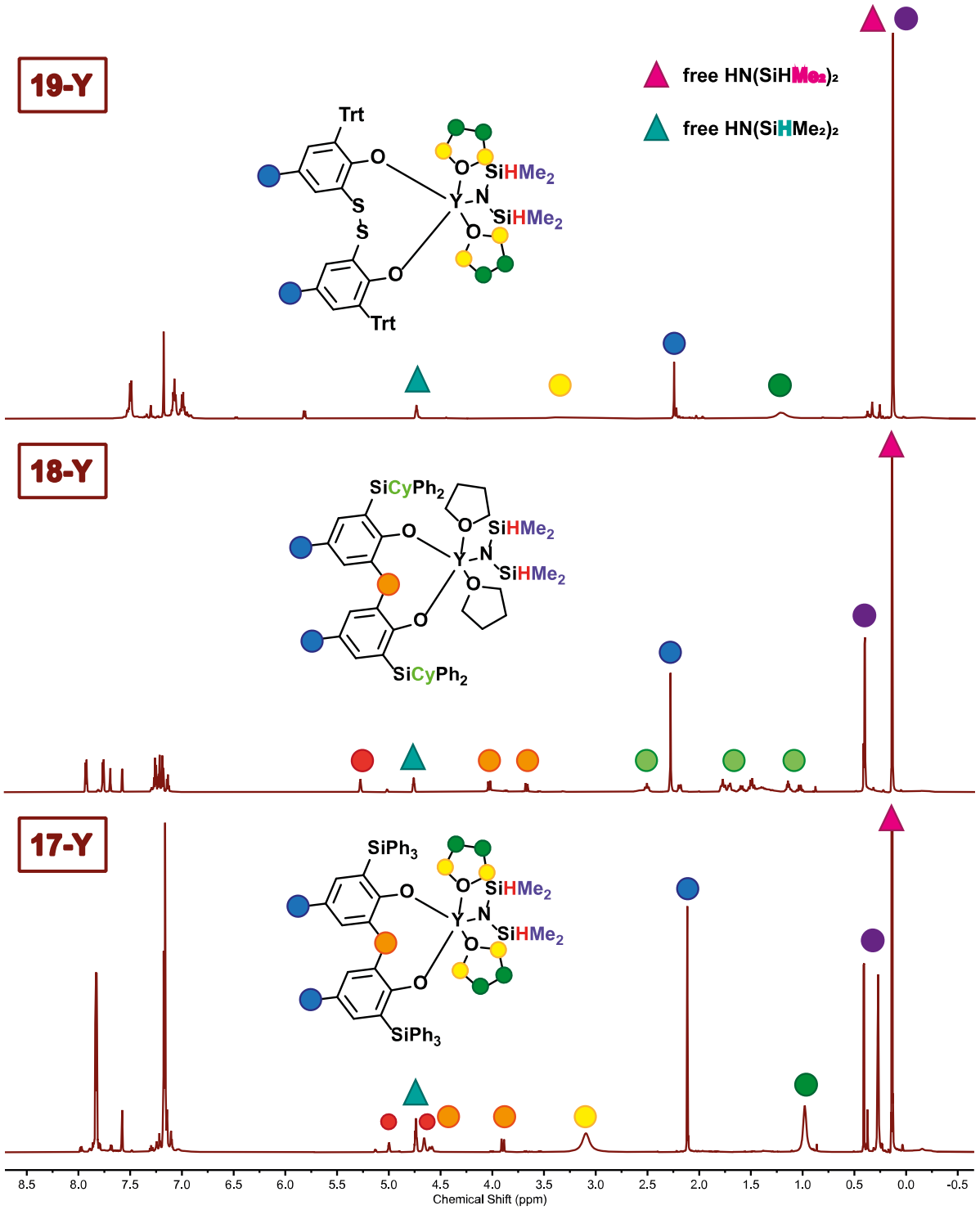

Figure 11. Comparison of ^{1}H-NMR spectra of the complexes **17-Y**, **18-Y** and **19-Y** (diagnostic peaks are colour-coded).

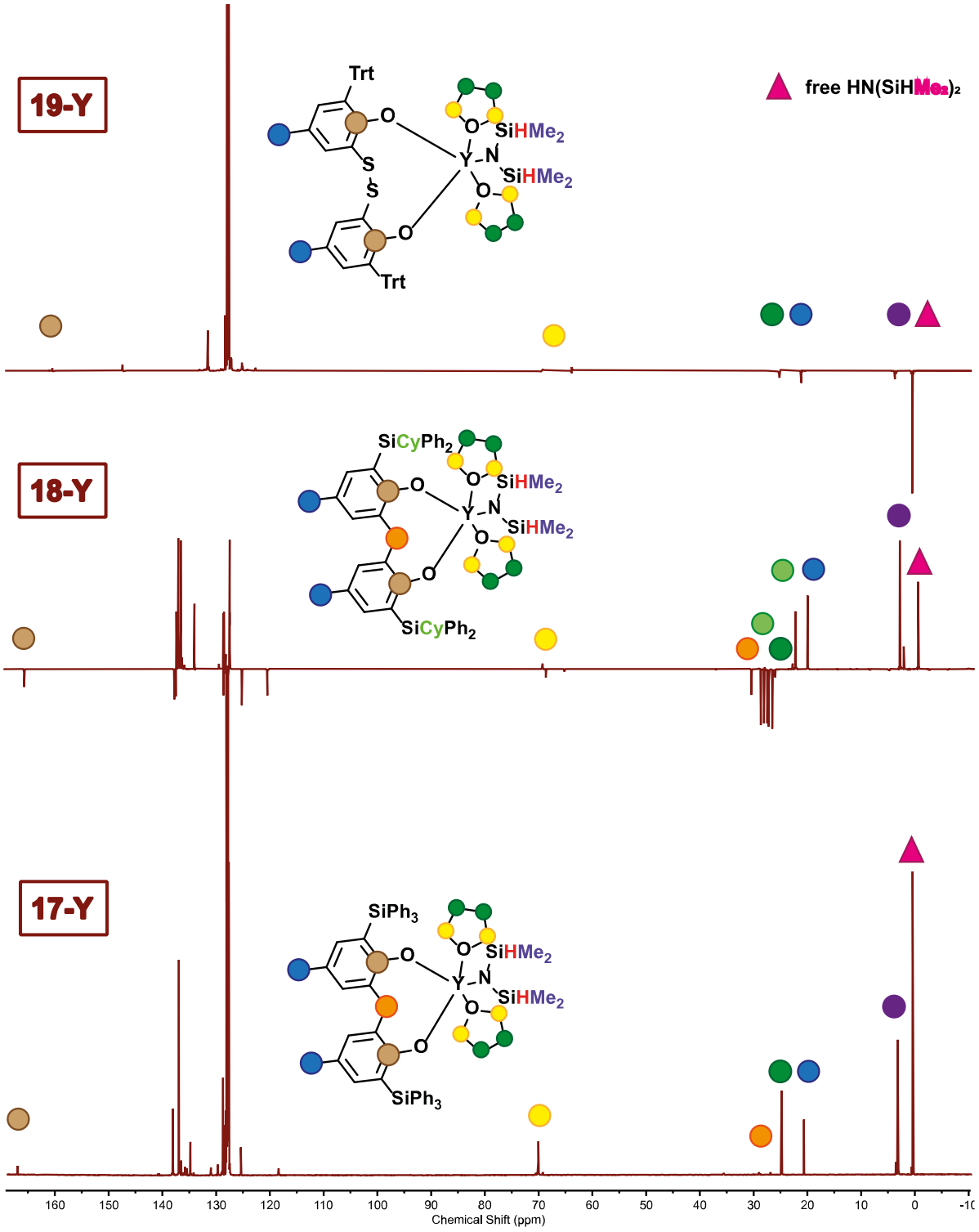

Figure 12. Comparison of ^{13}C-NMR spectra of the complexes **17-Y**, **18-Y** and **19-Y** (diagnostic peaks are colour-coded).

Additionally, different attempts at crystallisation of the said complexes were made, albeit presently without success. It could also be observed that freeze-drying of these complexes *in vacuo* on a Schlenk line, in order to remove the solvent and the free

amine and obtain them in powder form resulted in decomposition of the said complexes, as observed *via* NMR spectroscopy and X-ray measurements in the case of **17-Y** and **19-Y**. When the freeze-dried samples were recrystallised from benzene/hexane mixture, and the crystals subjected to X-ray diffraction analysis, obtained molecular structures showed the ligand decomposition product in the case of **17-Y** and 4-methyl-2-tritylphenol (**9**), precursor of the ligand **10** in the case of **19-Y**.

With the three metal complexes (**17-Y**, **18-Y** and **19-Y**) in hand, catalytic studies were envisioned.

3.2.2 Group 4 Metal Complexes

Attempts to synthesise Group 4 metal complexes were made with both titanium and zirconium precursors. As expected, they exhibited similar behaviour, due to the similarities in their chemical properties. The precursors $[Ti(NMe_2)_4]$ and $[Zr(NMe_2)_4]$ were chosen as they were previously reported to yield desired complexes with bis(phenolate) ligands.[74] It could be observed that a complex mixture of products forms when either of the two metal precursors reacted with 6,6'-methylenebis(4-methyl-2-(triphenylsilyl)phenol) (Scheme 30 and Scheme 33).

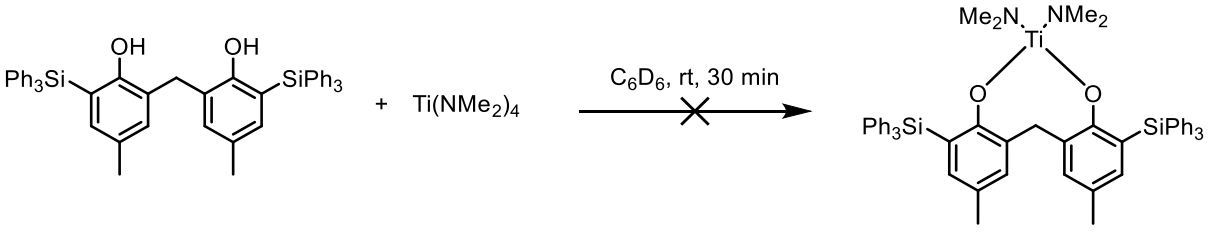

6 **20-Ti** **21-Ti**

Scheme 30. Attempted complexation of $[Ti(NMe_2)_4]$ with **6** in C_6D_6 at room temperature.

However, in another experiment, coordination of two ligand molecules to the metal was achieved at an elevated temperature of 60 °C, though only in the case of titanium (Scheme 31 a) and Table 3, entry 2).

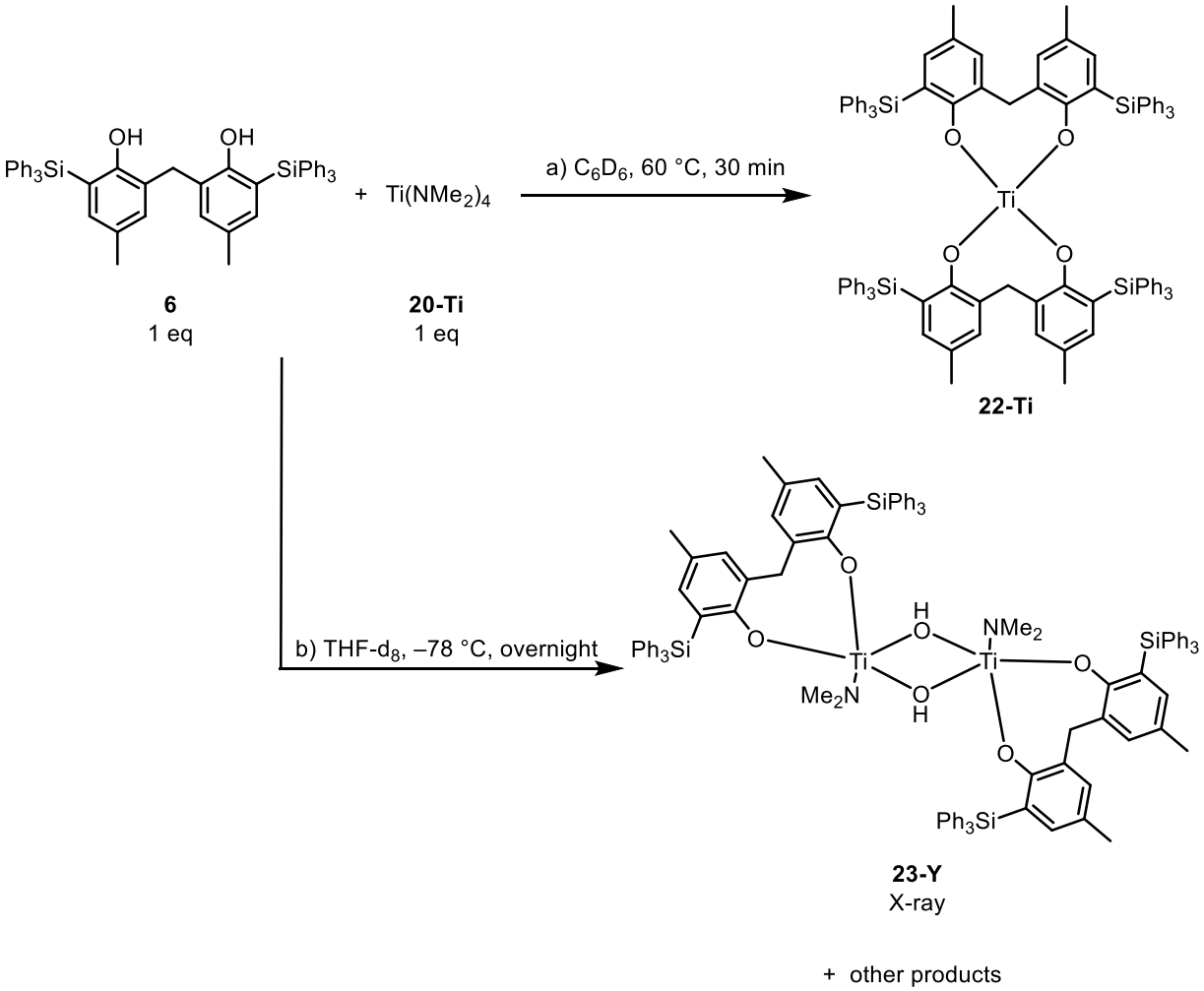

Scheme 31. Synthesis of the complex **22-Ti**.

It can be speculated that this particular reaction could take place due to the exceptionally poor solubility of the ligand batch that was used, which, coupled with the evaporation of the volatile $HNMe_2$ at an elevated temperature (in a closed, but not sealed vial), could lead to the formation of thermodynamically favourable complex **22-Ti**. Interestingly, however, these results could not be repeated when the stoichiometry was altered according to Table 3, entry 6, and the reaction performed at the same temperature using the second ligand batch. Using two equivalents of the metal precursor **20-Ti** also did not yield the desired complex **21-Ti** bearing one bis(phenolate) ligand (Table 3, entry 5).

Table 3. Overview of reaction conditions for the complexation reactions with titanium.

Entry	$Ti(NMe_2)_4$ (eq)	Ligand 6 (eq)	Solvent	Temperature	Reaction time	Reaction product
1	1	1	C_6D_6	rt	30 min	mixture
2	1	1	C_6D_6	60 °C	30 min	**22-Ti**
3	1	1	THF-d_8	–20 °C	overnight	mixture
4	1	1	THF-d_8	–78 °C	overnight	mixture
5	2	1	C_6D_6	rt	30 min	mixture
6	1	2	C_6D_6	60 °C	30 min	mixture

Correspondingly to the complexations with $Y(BDMA)_3$ (**11-Y**), attempts at forcing the system towards the formation of the desired kinetic product **21-Ti** were made. Analogous to the reaction shown in Scheme 27, the reaction with $[Ti(NMe_2)_4]$ (**20-Ti**) was performed in the glovebox using the same reaction setup, at –20 °C (Table 3, entry 3), but without any success.

Subsequently, similar to the procedure reported by Takashima and coworkers,[75] the reaction was performed at –78 °C on the Schlenk line (Scheme 31 b) and Table 3, entry 4). In this case, a mixture of products was obtained as well. However, storing the sample at low temperature in the freezer, allowed a crystal formation. The X-ray measurements revealed that an oxo-bridged **23-Ti** species was formed (Scheme 31 b) and Figure 13).

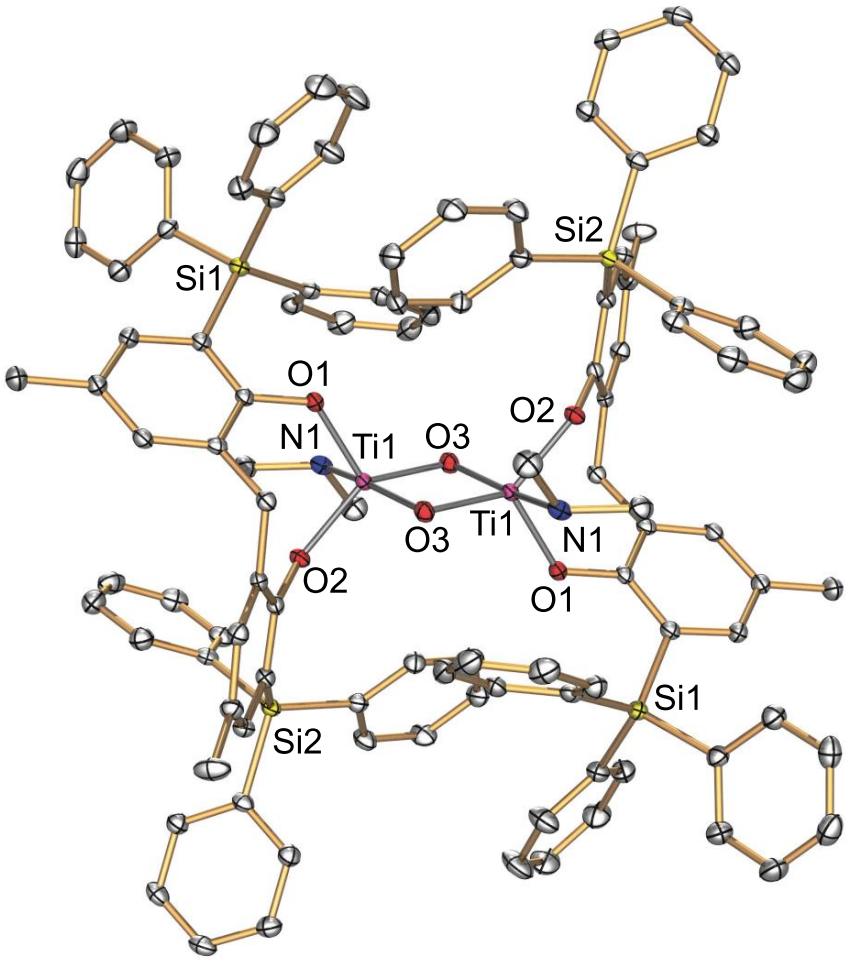

Figure 13. Molecular structure of **23-Ti** (solvent molecules and hydrogen atoms were omitted for clarity)

Table 4. Selected bond lengths (Å) and angles (°) in **23-Ti**.

	Interatomic distance (Å) / Bond angle (°)
Ti1-Ti1[1]	2.7930(5)
Ti1-O1	1.8462(10)
Ti1-O2	1.8720(10)
Ti1-O3	1.8463(11)
Ti1-O3[1]	1.8570(11)
Ti1-N1	2.2471(13)
Ti1-O3-Ti1[1]	97.91(5)

Table 4. Selected bond lengths (Å) and angles (°) in **23-Ti** - continued

O1-Ti1-O2	107.05(5)
O1-Ti1-O3	107.07(5)
O1-Ti1-O3[1]	115.23(5)
O2-Ti1-O3	97.85(4)
O2-Ti1-O3[1]	135.79(4)
O3-Ti1-O3[1]	82.09(5)
O1-Ti1-N1	90.83(5)
O2-Ti1-N1	84.25(4)
O3-Ti1-N1	160.30(5)
O3[1]-Ti1-N1	82.85(5)

[1]1-X,1-Y,1-Z

It was presumed that the species formed due to the reaction having been performed outside of the glovebox, since even traces of oxygen or water can suffice for its formation. This also confirms that the reaction is extremely sensitive to air.

Since the reactions with 6,6'-disulfanediylbis(4-methyl-2-tritylphenol) (**10**) did not produce the desired results either (Scheme 32), no further attempts to obtain titanium complexes were made.

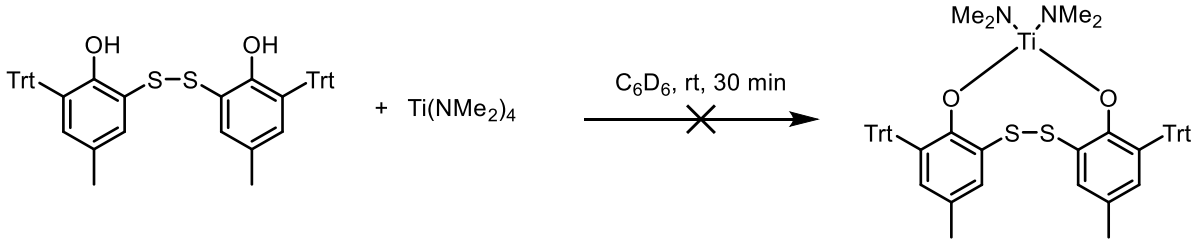

10 **20-Ti** **24-Ti**

Scheme 32. Attempted complexation of $[Ti(NMe_2)_4]$ with **10** in C_6D_6 at room temperature.

Complexation trials using the zirconium precursor $[Zr(NMe_2)_4]$ (**25-Zr**) were performed in parallel to the experiments with titanium and showed almost identical results (Scheme 33 and Scheme 34).

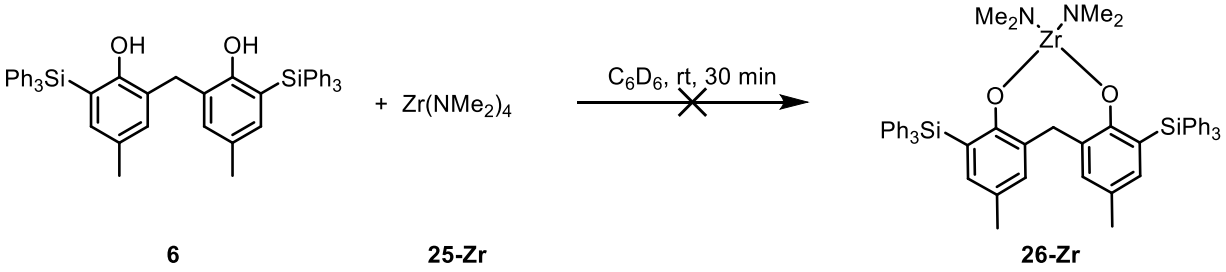

6 **25-Zr** **26-Zr**

Scheme 33. Attempted complexation of [$Zr(NMe_2)_4$] with **6** in C_6D_6 at room temperature.

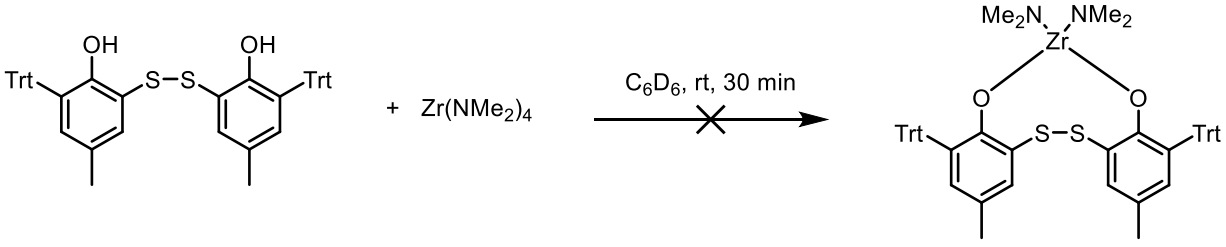

10 **25-Zr** **27-Zr**

Scheme 34. Attempted complexation of [$Zr(NMe_2)_4$] with 10 in C_6D_6 at room temperature.

An interesting deviation was observed when the complexation reaction of **6** with **25-Zr** was performed at 60 °C, leading to a mixture of products with identical ^{1}H- and ^{13}C-NMR spectra to the reaction at room temperature (Scheme 33), while the analogous reaction with titanium delivered the disubstituted complex **22-Ti** (Scheme 30).

Because the complexation attempts with Group 4 metals were of little success, no further attempts were made.

3.2.3 Group 5 Metal Complexes

The final attempts in the quest for suitable metal complexes to serve as hydroamination or hydroaminoalkylation catalysts were directed at the Group 5 metals. Initial trials were made only with 6,6'-methylenebis(4-methyl-2-(triphenylsilyl)phenol) (**6**) and the suitable metal precursors [$Nb(NMe_2)_5$] (**28-Nb**) and [$Ta(NMe_2)_5$] (**30-Ta**). Upon complexation reaction, it was determined that in both cases a mixture of products was formed and therefore, no further ligands were tested, since it has been established previously that ligands **7** and **10** demonstrated similar behaviour when brought in reaction with early transition metal precursors. Regardless, crystals were obtained in both cases. X-ray measurements showed that only the desired monosubstituted complex **29-Nb** (Scheme 35), respectively **31-Ta** (Scheme 36), crystallised.

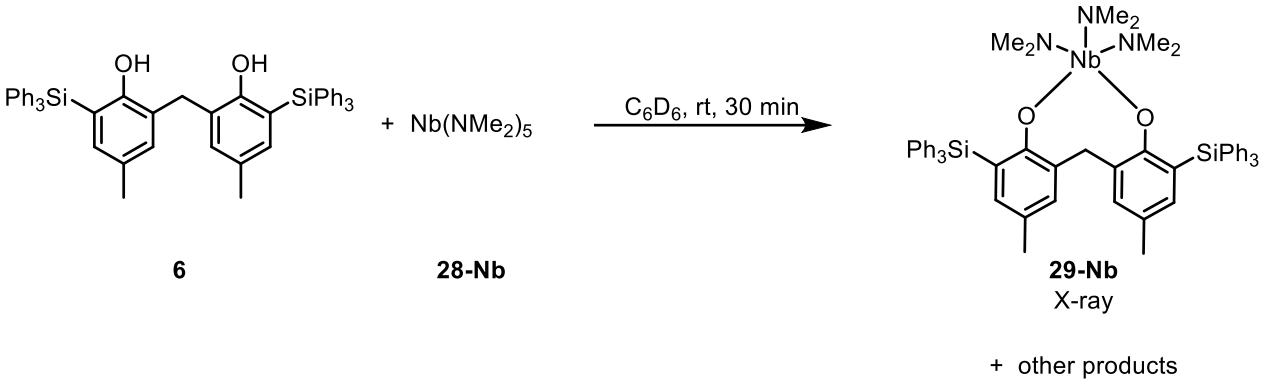

Scheme 35. Synthesis of the complex **29-Nb**.

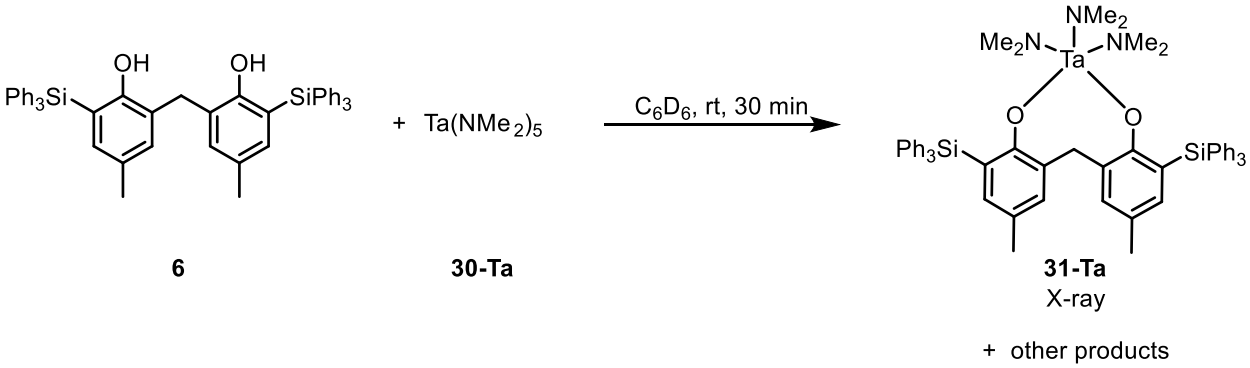

Scheme 36. Synthesis of the complex **31-Ta**.

This allowed to make a comparison between the geometry of the obtained complexes and the published Group 5 bis(phenolate) complexes.[64,76–80] The data is summarised in Table 5. As shown in Table 5, M–O and M–N bond lengths seem to lie in a similar

range compared to the previously published structures. O–M–O angles of the complexes **29-Nb** and **31-Ta** are mutually similar and somewhat smaller compared to their counterparts **32-Nb** and **33-Ta**. On the other hand, M–O–C(Ar) angles are significantly greater compared to **32-Nb** and **33-Ta** which lies within expectations, since the CH_2-group of the methylene bridge of the corresponding ligand offers greater flexibility compared to the more rigid binaphtholate ligand. Larger differences between the two niobium, and the two tantalum complexes can also be found when other valence angles of the coordination centre (L–M–L') are subjected to analysis, as shown in Table 5.

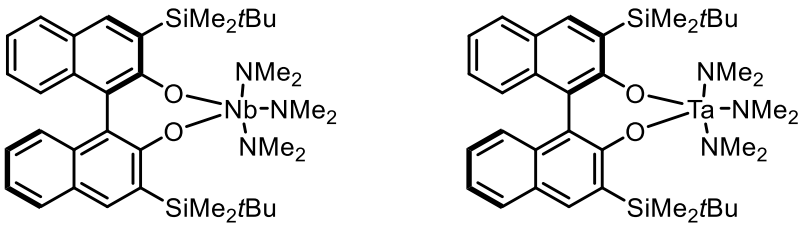

38-Nb **39-Ta**

Scheme 37. Structures of complexes **32-Nb** and **33-Ta**.[64,76]

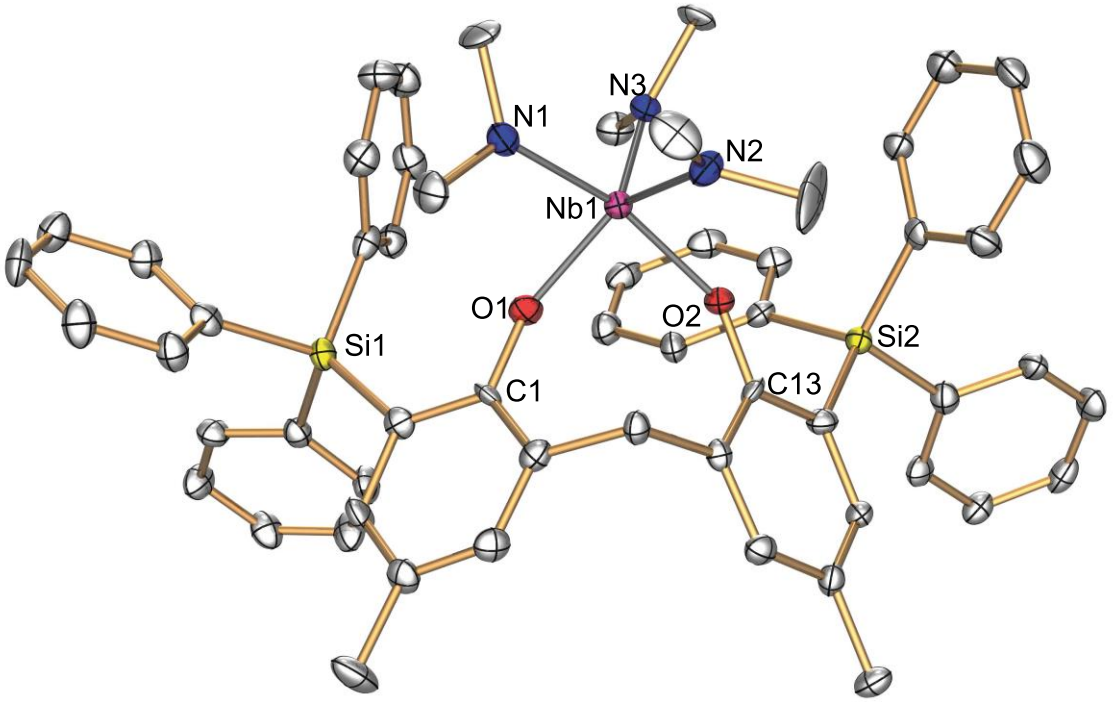

Figure 14. Molecular structure of **29-Nb** (solvent molecules and hydrogen atoms were omitted for clarity).

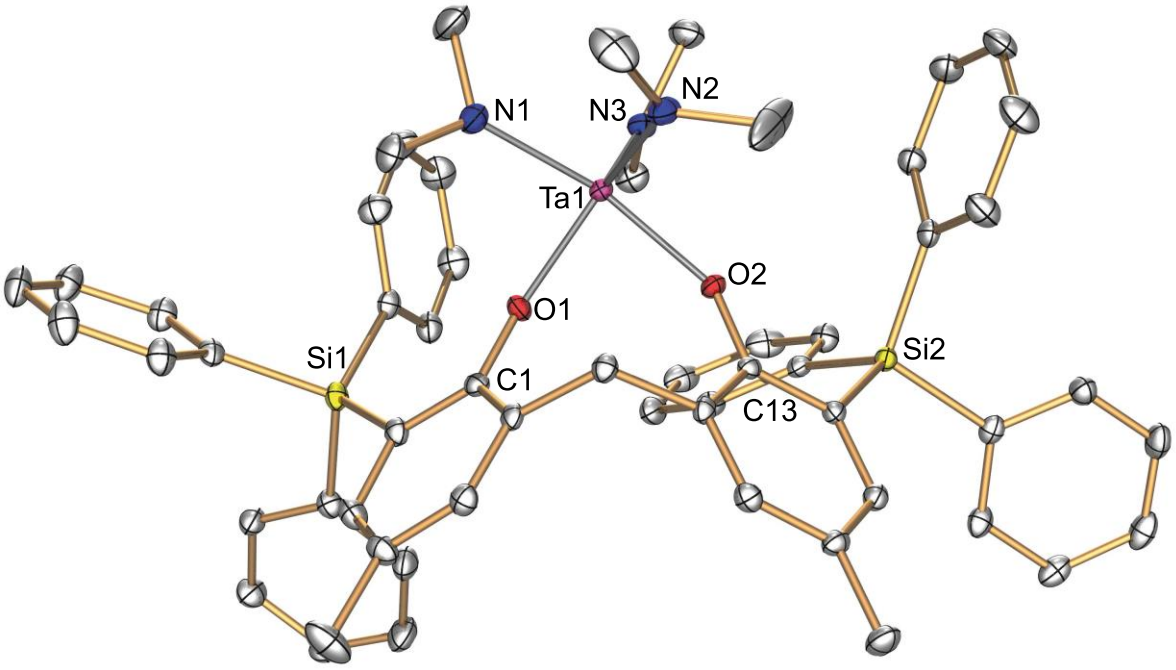

Figure 15. Molecular structure of **31-Ta** (solvent molecules and hydrogen atoms were omitted for clarity).

Table 5. Selected bond lengths (Å) and angles (°) in **29-Nb** and **31-Ta** compared to **32-Nb** and **33-Ta**.

	29-Nb	32-Nb[64,76]	31-Ta	33-Ta[64,76]
M-N1	2.006(4)	1.9528(13)	2.0023(18)	1.9591(15)
M-N2	1.999(4)	1.9351(12)	1.9866(18)	1.9354(15)
M-N3	1.938(4)	2.0380(12)	1.9397(18)	2.0303(14)
M-O1	1.996(3)	2.0916(9)	1.9711(14)	2.0763(12)
M-O2	2.030(3)	1.9594(9)	2.0150(13)	1.9478(11)
O1-M-O2	84.09(11)	85.43(4)	84.28(6)	85.10(5)
O1-M-N1	85.90(13)	84.88(4)	85.32(7)	84.75(5)
O1-M-N2	136.38(14)	96.27(5)	136.25(7)	96.09(5)
O1-M-N3	119.83(13)	172.32(5)	119.32(7)	172.27(5)
O2-M-N1	164.05(13)	125.79(5)	163.51(7)	125.36(6)
O2-M-N2	89.61(13)	114.08(5)	89.44(7)	114.80(6)
O2-M-N3	96.89(13)	97.77(4)	96.78(6)	97.46(5)
N1-M-N2	89.09(15)	119.95(6)	89.26(8)	119.61(6)
N1-M-N3	98.86(15)	87.60(5)	99.46(7)	87.83(6)
N2-M-N3	103.76(15)	88.82(5)	104.40(8)	89.48(6)
M-O1-C(Ar)	143.2(3)	112.89(5)	143.96(13)	113.61(9)
M-O2-C(Ar)	143.4(3)	135.92(13)	143.95(13)	136.58(11)

Given the fact that **29-Nb**, **31-Ta**, **32-Nb**, **33-Ta** are pentacoordinated complexes, it would be possible to speculate whether the Group 5 metal complexes in question adopt a trigonal bipyramidal or square pyramidal geometry. This can be achieved by introducing a structural index parameter τ, described by Addison et al.[81] The parameter τ shows a level of trigonality of a pentacoordinate structure and is defined as shown in Equation (5), where $\beta>\alpha$ and α and β represent the two greatest angles of the coordination centre.

$$\tau = \frac{(\beta - \alpha)}{60} \quad (5)$$

Consequently, two extreme values of τ are associated with the two opposing geometries for the pentacoordinated complexes. Values of τ close to 0 refer to square pyramidal geometry, and the values of τ close to 1 imply that the structure has geometry similar to trigonal bipyramidal.

Angles α and β were selected from Table 5 and were used to calculate the degree of trigonality τ, according to Equation (5). Results are summarised in Table 6. Interestingly, both complexes **32-Nb** and **33-Ta** featuring binaphtholate ligands[64,76] seem to have a geometry closer to trigonal bipyramidal. On the other hand, newly synthesised Group 5 metal complexes **29-Nb** and **31-Ta** are more ambiguous in that respect, since the corresponding τ values lie close to 0.5, leaning slightly towards square pyramidal geometry. However, it is clear that the complexes bearing methylenebis(phenolate) ligands differ in geometry compared to their binaphtholate-ligand-containing counterparts. Thus, the aforementioned difference in angles of the coordination centre (Table 5) of the corresponding complexes is mirrored in the difference in their levels of trigonality.

Table 6. Overview of angles α and β and the calculated τ values of the pentacoordinated complexes **29-Nb**, **31-Ta**, **32-Nb** and **33-Ta**.

	α (°)	β (°)	τ
29-Nb	136.38(14)	164.05(13)	0.46
32-Nb[64,76]	125.79(5)	172.32(5)	0.78
31-Ta	136.25(7)	163.51(7)	0.45
33-Ta[64,76]	125.36(6)	172.27(5)	0.78

3.3 Catalytic Studies

Investigations in the catalytic intramolecular hydroamination were performed by screening three aminoalkene substrates and testing three yttrium metal complexes (**17-Y**, **18-Y** and **19-Y**) that were obtained as described in section 3.2.1.

3.3.1 Suitable Catalytic Systems

First, all three potential catalysts were tested for their activity with 2,2-diphenylpent-4-en-1-amine (**34**). It is worth mentioning that the three substrates were chosen for their increased propensity to undergo intramolecular hydroamination, since the cyclisation products would be thermodynamically favourable 5- and 6-membered rings. Moreover, the 2,2 substitution pattern present in each substrate caused activation of the substrates through the Thorpe-Ingold effect and facilitation of the cyclisation product formation.[22]

Since the synthesised complexes showed high sensitivity towards moisture and oxygen, the catalytic reactions were performed under strict inert conditions in an argon-filled glovebox. In order to allow the monitoring of the reaction progress, all reactions were performed in deuterated solvents on an NMR-scale and in an appropriate screw-cap NMR tube. It is also important to emphasise that deuterated solvents were additionally dried as described in section 5.1.

Initial reaction conditions were chosen akin to the already established protocol in the Hultzsch research group.[46,62] It consisted of performing the reaction starting from 2 mol% catalyst loading at room temperature using C_6D_6 as solvent. The initial tests are shown in Table 7, entries 1–3. It was observed that all three catalysts showed activity in the intramolecular hydroamination reaction. However, only complex **17-Y** showed satisfactory results with full conversion of the substrate to the product within 25 h. Interestingly, complex **18-Y**, having a similar structure, differing only in the substituents on the phenol rings of the ligand was expected to perform in the same manner. Nevertheless, this was not the case, and identical results were observed even upon repetition of the catalytic tests.

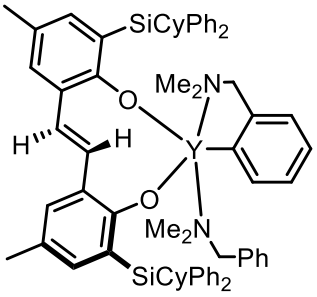

36-Y

Figure 16. Structure of the complex **36-Y**

Table 7. Intramolecular hydroamination of 2,2-diphenylpent-4-en-1-amine (**34**).

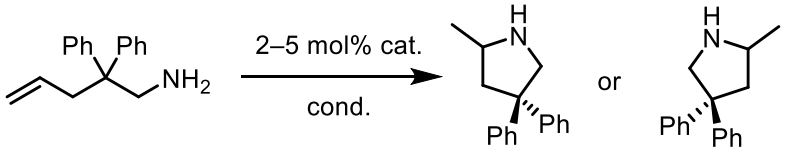

34 **35**

Entry	Catalyst	Cat. Loading	Solvent	Temperature	Reaction time	Conversion [a]
1	**17-Y**	2 mol%	C_6D_6	rt	25 h	Quant.
2	**18-Y**	2 mol%	C_6D_6	rt	96 h	34 %
3	**19-Y**	2 mol%	C_6D_6	rt	96 h	24 %
4	**17-Y**	5 mol%	toluene-d_8	100 °C	<10 min	Quant.
5	**17-Y**	5 mol%	C_6D_6	100 °C	<10 min	Quant.
6	**18-Y**	5 mol%	toluene-d_8	100 °C	30 min	Quant.
7	**19-Y**	5 mol%	toluene-d_8	100 °C	<10 min	55 %
9	**36-Y**	5 mol%	C_6D_6	rt	5 min	Quant.

[a]Conversion was determined using ^{1}H-NMR spectroscopy

The results pointed towards the need to alter the reaction conditions in order to obtain more desirable conversions. The overall lower activity of the complexes bearing a $N(SiHMe_2)_2$ ligand can also be explained with their lower basicity as discussed in section 1.3.[60,61] The estimated p*K*a value of the conjugated acid tetramethyldisilazane

$HN(SiHMe_2)_2$ lies at 22.8.[73] As a result, the corresponding amido ligand is less basic and hampers the precatalyst activation in the first step of the catalytic cycle, as shown in Scheme 4 a) and Figure 6.

This observation resulted in increasing the catalyst loading from 2 mol% to 5 mol% and increasing the reaction temperature to 100 °C. The corresponding solvent was changed to toluene-d_8 accordingly, due to its higher boiling point. Under these conditions, the reaction could be brought to completion within minutes using **17-Y** and **18-Y** (Table 7, entries 4 and 6). With **19-Y**, the reaction was stopped at 55 % conversion (Table 7, entry 7). This was attributed to the lability of the disulphide bridge of the corresponding ligand, that possibly cannot withstand the temperature of 100 °C, but remains relatively stable at temperatures up to 80 °C.

To demonstrate that the solvent was exhibiting no influence on the reaction outcome and catalyst performance, the same reaction conditions were applied on the system with C_6D_6 as a solvent and obtained reproducible results (Table 7, entry 5). For comparison, the known catalyst **36-Y**[82] (Figure 16) was tested alongside and its performance is listed in Table 7, entry 9.

Substrate **37** was tested next, being slightly less activated compared to substrate **34**. At room temperature the reaction did not proceed in a satisfactory manner with any of the tested catalysts (Table 8, entry 1–3). This being a very peculiar result, we decided to test the substrate itself with an already proven active catalyst **36-Y**. This has shown that the substrate **37**, though appearing to be pure in the NMR spectra, was not of a sufficient purity and had to be handled additionally. This caused introduction of an additional preparation step which consisted of drying of the substrate stock solution over CaH_2 overnight, as described in section 5.5.1.

Table 8. Intramolecular hydroamination of (1-allylcyclohexyl)methanamine (**37**).

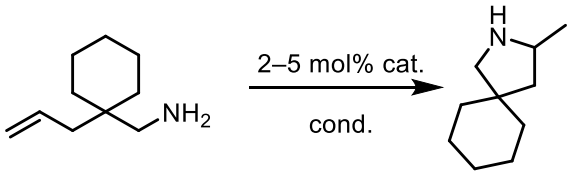

37 **38**

Entry	Catalyst	Cat. Loading	Solvent	Temperature	Reaction time	Conversion [a]
1	**17-Y**	2 mol%	C_6D_6	rt	72 h	13 %
2	**18-Y**	2 mol%	C_6D_6	rt	72 h	13 %
3	**19-Y**	2 mol%	C_6D_6	rt	72 h	0 %
Drying over CaH_2						
4	**17-Y**	5 mol%	C_6D_6	60 °C	72 h	26 %
5	**18-Y**	5 mol%	C_6D_6	60 °C	22 h	6 %
6	**19-Y**	5 mol%	C_6D_6	60 °C	72 h	5 %
7	**17-Y**	5 mol%	toluene-d_8	100 °C	<30 min	Quant.
8	**17-Y**	5 mol%	C_6D_6	100 °C	<30 min	Quant.
9	**18-Y**	5 mol%	toluene-d_8	100 °C	<30 min	Quant.
10	**19-Y**	5 mol%	toluene-d_8	100 °C	72 h	8 %
11	**36-Y**	5 mol%	C_6D_6	rt	10 min	Quant.

[a]Conversion was determined using ^{1}H-NMR spectroscopy

After this step, it was proven that substrate is active by performing another test reaction with catalyst **36-Y** (Table 8, entry 11). Following tests with catalysts **17-Y**, **18-Y** and **19-Y** with higher catalyst loading and elevated temperature showed somewhat improved, but still not satisfactory results (Table 8, entry 4–6). For that reason, the optimised reaction conditions from the previous catalytic test (Table 7) were applied.

As shown in Table 8, entries 7–9, the conversion increased to quantitative in less than 30 min reaction time, with both catalysts **17-Y** and **18-Y**. As expected, the elevated temperature did not suit **19-Y** (Table 8, entry 10), which exhibited poor performance with only 8 % conversion. Catalyst **36-Y**, on the other hand, showed high activity under mild conditions (Table 8, entry 11).

The final substrate **39** was also the least active out of the three test substrates, since being subjected to intramolecular hydroamination would result in the formation of a kinetically slightly less favourable 6-membered ring. With that in mind, and in accordance to the previous observations,[46,62] the reaction was performed at elevated temperature, starting at 60 °C.

Table 9. Intramolecular hydroamination of 2,2-diphenylhex-5-en-1-amine (**39**).

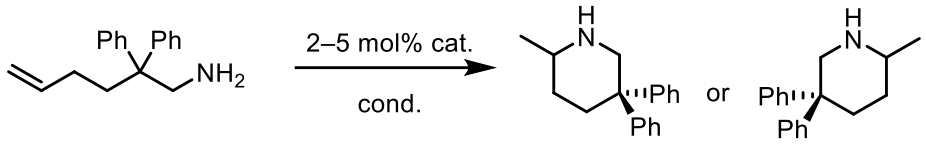

39 **40**

Entry	Catalyst	Cat. Loading	Solvent	Temperature	Reaction time	Conversion [a]
1	**17-Y**	2 mol%	C_6D_6	60 °C	20 h	3 %
2	**17-Y**	5 mol%	C_6D_6	60 °C	24 h	6 %
3	**18-Y**	2 mol%	C_6D_6	60 °C	20 h	2 %
4	**19-Y**	2 mol%	C_6D_6	60 °C	20 h	28 %
Drying over CaH_2						
5	**17-Y**	5 mol%	C_6D_6	60 °C	48 h	32 %
6	**18-Y**	5 mol%	C_6D_6	60 °C	48 h	25 %
7	**19-Y**	5 mol%	C_6D_6	60 °C	48 h	7 %
Drying over CaH_2						
8	**17-Y**	5 mol%	toluene-d_8	100 °C	22 h	39 %
9	**18-Y**	5 mol%	toluene-d_8	100 °C	22 h	35 %
10	**19-Y**	5 mol%	toluene-d_8	100 °C	96 h	21 %
11	**36-Y**	5 mol%	C_6D_6	60 °C	1 h	3 %
12[b]	**36-Y**	5 mol%	C_6D_6	60 °C	1 h	Quant.

[a]Conversion was determined using ^{1}H-NMR spectroscopy

[b]Result were reported previously by the Hultzsch group[82] using a pure batch of substrate

Initial tests yielded rather poor results (Table 9, entries 1–4), and called for another test of the substrate itself. This showed that substrate **39** had to be purified additionally, as **36-Y** also could not lead the substrate to full conversion. A drying step with CaH_2 was performed and the reactions repeated, this time with a slightly improved conversion (Table 9, entries 5–7). Repeated testing with **36-Y** showed that substrate

39 was still not of a satisfactory quality. Therefore, the drying step was repeated. Finally, the optimised conditions from the previous two catalytic studies were applied and this brought a modest improvement in terms of conversion after prolonged reaction time (Table 9, entries 8–10). Once again, the benchmark catalyst **36-Y** also showed incomplete conversion (Table 9, entry 11), which led us to believe that substrate **39** still contained some impurities and must be synthesised and tested again. Due to time constraints, the additional substrate synthesis was delayed.

3.3.2 Spectroscopic Analysis

The reactions were monitored *via* ^{1}H-NMR spectroscopy. For that reason, an internal standard was introduced into each sample. As an appropriate internal standard, ferrocene was chosen. It shows a singlet in both ^{1}H- and ^{13}C-NMR spectra and it does not overlap with any of the substrate or product peaks, which was very convenient for the result analysis. The conversion was therefore determined from ^{1}H-NMR spectra, as a function of the decrease of the olefinic peak area relative to the peak area of ferrocene (Scheme 41). In each catalytic experiment, both olefinic peaks were integrated and the conversion determined. As the final value, an average of the two values was taken. For that reason, NMR spectra before, during and after a catalytic experiment had to be acquired.

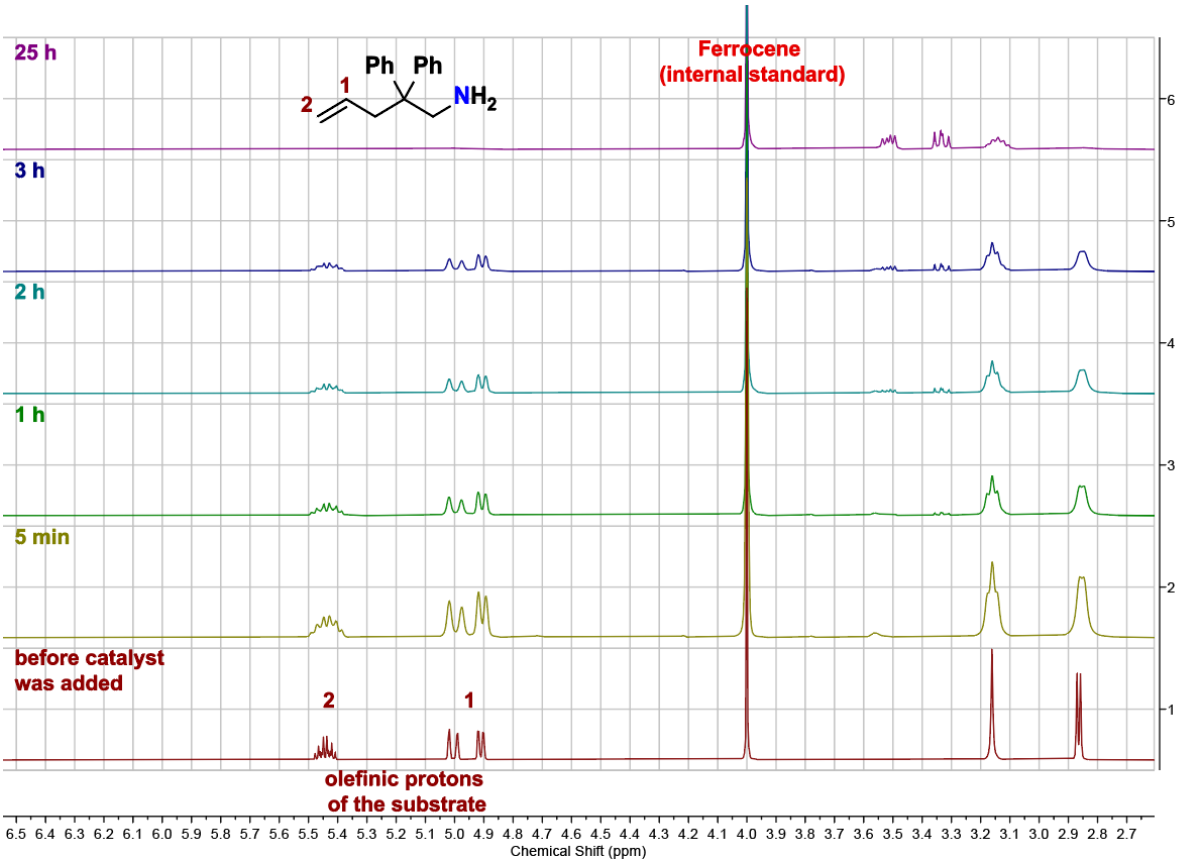

Scheme 38. Monitoring of the intramolecular hydroamination of aminoalkenes via ^{1}H-NMR spectroscopy.

4. Conclusion and outlook

In this work three different bis(phenolate) ligands, 6,6'-methylenebis (4-methyl-2-(triphenylsilyl)phenol) (**6**) ,6,6'-methylenebis(2-(cyclohexyldiphenylsilyl)-4-methylphenol) (**7**) and 6,6'-disulfanediylbis(4-methyl-2-tritylphenol) (**10**) were synthesised and complexation to different early transition metal precursors [Y(*o*-$C_6H_4CH_2NMe_2)_3$], [$Y(N(SiHMe_2)_2)_3(THF)_2$], [$Ti(NMe_2)_4$], [$Zr(NMe_2)_4$], [$Nb(NMe_2)_5$] and [$Ta(NMe_2)_5$] were attempted. In addition to that, catalytic intramolecular hydroamination of 2,2-disubstituted aminoalkenes (2,2-diphenylpent-4-en-1-amine (**34**), (1-allylcyclohexyl)methanamine (**37**) and 2,2-diphenylhex-5-en-1-amine (**39**)) with prepared metal complexes **17-Y**, **18-Y** and **19-Y** was investigated.

The ligand synthesis was designed to yield the desired bis(phenolate) compounds in few steps starting from simple, inexpensive and commercially available chemicals. In the case of the synthesis of methylenebis(phenolate) ligands, high yields were achieved in all steps, allowing a synthetic divergence in the last step, which made the synthesis very efficient. The synthesis of the disulfanediylbis(phenolate) ligand **10** suffered from somewhat lower yields in the corresponding steps. However, the ligand synthesis could be performed successfully in only two steps, which posed a significant advantage of the synthetic protocol.

The complexation reactions were proven to pose a challenge regarding the chosen ligands and were the key part of this work. One of the challenges being the sensitivity of the metal precursors and products to oxygen and moisture, complexation reactions had to be performed under strict inert conditions. Despite the efforts, desired metal complexes with [Y(*o*-$C_6H_4CH_2NMe_2)_3$] as a precursor could not be successfully obtained. Similar results were acquired when complexation with precursors [$Ti(NMe_2)_4$] and [$Zr(NMe_2)_4$] was attempted, regardless of the reaction conditions. We attribute the experienced difficulties to the nature of the ligands used, which, on one hand have a significant steric bulk depicted in the sterically demanding silyl substituents, but at the same time offer a certain level of flexibility, through presence of the CH_2-group of the methylene(bis)phenolate ligand or the disulphide moiety of the disulfanediylbis(phenolate) ligand.

Despite the challenges, it was possible to successfully synthesise and characterise *via* NMR spectroscopy complexes **17-Y**, **18-Y** and **19-Y** of [$Y(N(SiHMe_2)_2)_3(THF)_2$]

as a metal precursor and the three synthesised ligands. Moreover, though the complexation attempts with niobium and tantalum metal precursors yielded product mixtures, it was possible to crystallise and characterise the desired corresponding monosubstituted complexes **29-Nb** and **31-Ta** with 6,6'-methylenebis(4-methyl-2-(triphenylsilyl)phenol) (**6**) by single crystal X-ray diffraction analysis, which was an important finding and allowed a comparison between the said complexes and the other previously published members of the bis(phenolate) complex family.

The successfully obtained yttrium complexes (**17-Y**, **18-Y** and **19-Y**) could be subsequently employed as catalysts in the catalytic intramolecular hydroamination of aminoalkenes. It was also possible to prove their activity in the said reaction and optimise the reaction conditions, so as to obtain quantitative conversions in the cases of yttrium complexes **17-Y** and **18-Y**. On the other hand, catalyst **19-Y** exhibited inferior performance, which was in line with our expectations due to the weak coordination ability of the disulphide bridge and the overall lability of the disulphide bridge at elevated temperatures over 80 °C. Upon comparison of the catalyst performance with other catalysts with bis(phenolate) ligands,[44–46,62] it was possible to observe that newly synthesised catalysts required somewhat harsher reaction conditions in order to bring the reaction to completion. This also stands in line with the expectations, due to the lower basicity of the bis(dimethylsilyl)amido ligand compared to dimethylbenzylamido ligand in the case of the aforementioned complexes, which in return accounts for a slower rate of the hydroamination reaction.

Further challenges in this topic will be efforts to understand the complexation process and attempt to find suitable conditions to successfully perform the complexation between the ligands **6**, **7** and **10** and other early transition metal precursors, e.g. $[Y(N(SiMe_3)_2)_3]$, $TiCl_4$, $[Ti(OMe)_4]$, $ZrCl_4$, $[Zr(OEt)_4]$ etc. Another possibility would be to embark on a search for a new multistep synthetic procedure to produce desired complexes starting from another metal precursor that would show greater compatibility with the produced ligands. However, it would be important to also carefully weigh out the cost in terms of number and complexity of steps needed for these endeavours.

As for the presently successfully prepared complexes, it would be of utmost importance to obtain their crystal structures, which would offer greater insight into their exact geometry, especially in the case of the alleged weak coordination of disulphide bridge

moiety of the 6,6'-disulfanediylbis(4-methyl-2-tritylphenol) ligand to the metal centre, which impairs its catalytic activity.

Moreover, another interesting possibility would be to expand this family of ligands, introducing new sterically demanding substituents and characterising the ligands in order to expand knowledge on this class of chemical compounds.

In terms of the catalytic studies, an important aspect would be to perform further investigations in catalytic reactions and expand the substrate scope.

5. Experimental section

5.1 General

Unless stated otherwise all reactions were performed under inert conditions, either using standard Schlenk techniques under argon in flame-dried glassware or in an argon-filled MBraun® UNIlab pro glovebox. Solvents were distilled before use unless stated otherwise. THF, toluene and benzene were distilled from sodium benzophenone ketyl. All reagents were used as received from commercial suppliers unless otherwise stated.

Glassware was cleaned by submerging in a base bath (KOH solution in isopropanol) overnight. Followed by thorough rinse with water, it was submerged in an acid bath (diluted aqueous HCl solution) for another day, rinsed with water and washed in a laboratory dishwasher. Glassware was then rinsed with ethyl acetate and placed in a drying oven at 120 °C overnight.

Vials and vial caps were discarded after single use. NMR tubes were rinsed thoroughly with acetone and subsequently washed by sonication for at least 15 min using different solvents (acetone, DCM, ethyl acetate, methanol, ethanol) in succession and placed in a drying oven at 120 °C overnight.

Reaction progress was monitored using TLC on aluminium sheets coated with silica gel 60 with 0.2 mm thickness (Pre-coated TLC-sheets ALUGRAM® Xtra SIL G/UV254). Visualisation was achieved by UV light (254 nm and 363 nm). Column chromatography was performed using silica gel 60 (230-400 Mesh, MERCK AND CO.) and Biotage® SP4 and Isolera Flash Systems.

All ^{1}H-NMR and ^{13}C-NMR spectra were recorded on BRUKER BIOSPIN AV NEO 400, AV NEO 500, AV NEO 600, AV III 600 and AV III HD 700 instruments. Thereby the proton NMR spectra were measured at 400.27 MHz, 500.32 MHz, 600.18 MHz, 600.25 MHz and 700.40 MHz respectively, and the carbon NMR spectra at 100.65 MHz, 125.81 MHz, 150.92 MHz, 150.93 MHz and 176.12 MHz, respectively. Deuterated chloroform, benzene, toluene and THF were used as solvents. Chemical shifts (δ) were given in “parts per million” (ppm), referenced to the peak of TMS (δ = 0.00 ppm), using the solvent as internal standard (^{1}H: δ($CDCl_3$) = 7.26 ppm; δ(C_6D_6) = 7.16 ppm; δ(C_7D_8) = 2.08, 6.97, 7.01, 7.09 ppm; δ(C_4D_8O) = 1.72, 3.58 ppm;

^{13}C: δ($CDCl_3$) = 77.16 ppm; δ(C_6D_6) = 128.06 ppm; δ(C_7D_8) = 20.43, 125.13, 127.96, 128.87, 137.48 ppm; δ(C_4D_8O) = 25.31; 67.21 ppm). Coupling constants (J) were given in Hz. Spectroscopy splitting patterns were designated as singlet (s), doublet (d), triplet (t), quartet (q), pentet (p) multiplet (m) or combinations of that. Mass spectra were obtained using a BRUKER QTOF maXis spectrometer with ESI and the main signals were given in m/z units. Single-crystal X-ray Diffraction measurements were performed at the Centre for X-ray Structure Analysis of the University of Vienna on a Bruker D8 dual source instrument.

The following computer programs were used: MNova 14.2 from Mestrelab Research S.L., Olex2 1.5-alpha from OlexSys Ltd., ORTEP-3 2013.1 from L.J. Farrugia, University of Glasgow,[83] POV-Ray 3.7.0 from Persistence of Vision Raytracer Pty. Ltd., ChemDraw 20.1 from PerkinElmer and OctaDist 2.6.1 from Rangsiman Ketkaew et al.[72]

5.2 Synthesis of Ligands

5.2.1 Synthesis of 2,2'-methylenebis(4-methylphenol) (**2**)[63]

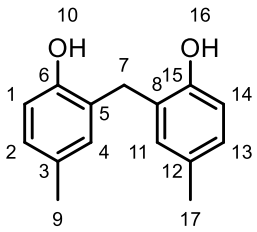

To a solution of 6,6'-methylenebis(2-(tert-butyl)-4-methylphenol) (6.81 g, 20.0 mmol, 1.0 equiv) in C_6H_6 (100 mL) in flame-dried Schlenk flask, cooled in an ice bath, a mixture of $AlCl_3$ (4.27 g, 32.0 mmol, 1.6 equiv) in 20 mL C_6H_6 and nitromethane (39.9 g, 35 mL, d = 1.14 g/mL, 65.3 mmol, 3.3 equiv) was added dropwise over 45 min under argon *via* cannula. The resulting reaction mixture was then stirred at 0 °C for another 1 h and then brought slowly to room temperature before quenching. The reaction was then quenched by addition of water. The layers were separated, and the aqueous layer was extracted with Et_2O (3×20 mL). Subsequently, the combined organic layers were washed with brine (50 mL) and dried over $MgSO_4$. The solution was concentrated under reduced pressure using rotary evaporator to give the crude product as a brown oil, which was then recrystallised from hexane/DCM (2:1) mixture to afford the pure product as a brown solid (4.06 g, 17.8 mmol, 89 %).

^{1}H NMR (600 MHz, $CDCl_3$): δ = 7.07 (s, 2H, H-4, H-11), 6.89 (dd, *J* = 8.1, 2.2 Hz, 2H, H-2, H-13), 6.71 (d, *J* = 8.1 Hz, 2H, H-1, H-14), 6,54 (s, 1H, OH), 6.42 (s, 1H, OH), 3.85 (s, 2H, H-7), 2.26 (s, 6H, H-9, H-17) ppm.

^{13}C NMR (151 MHz, $CDCl_3$): δ = 150.4 (C-6, C-15), 131.4 (C-4, C-11), 130.8 (C-3, C-12), 128.6 (C-2, C13), 126.7 (C-5, C-8), 115.9 (C-1, C-14), 31.0 (C-7), 20.7 (C-9, C-17) ppm.

HRMS (ESI): Calc. for $C_{15}H_{16}O_2Na$ 251.1092, found 251.1044 $[MNa]^+$.

The NMR spectroscopic data is in agreement with the literature.[84,85]

5.2.2 Synthesis of 6,6'-methylenebis(2-bromo-4-methylphenol) (**3**)

5.2.2.1 Synthesis using NBS[86]

To a solution of 2,2'-methylenebis(4-methylphenol) (**2**) (520 mg, 2.3 mmol, 1.0 equiv) in DMF (3 mL) in a Schlenk flask, a solution of NBS (818 mg, 4.6 mmol, 2.0 equiv) in DMF (10 mL) was added dropwise via cannula. The resulting yellow reaction mixture was stirred for 24 h at room temperature. Afterwards, it was poured into H_2O (100 mL). The aqueous solution was then extracted with 5 % benzene/hexane (3×50 mL). The combined organic extracts were then washed with H_2O (50 mL) and brine (50 mL). After drying over $MgSO_4$, the solvent was removed under reduced pressure to afford a yellow solid (0.291 g, 0.7 mmol, 32 %). The product was not purified further.

5.2.2.2 Synthesis using Bromine[63]

The reaction was performed under inert conditions using standard Schlenk techniques. To a solution of 2,2'-methylenebis(4-methylphenol) (**2**) (1.5 g, 6.6 mmol, 1.0 equiv) in $CHCl_3$ (50 mL) was added Br_2 (2.32 g, 0.7 mL, d = 3.119 g/mL, 2.2 equiv) in $CHCl_3$ (10 mL) dropwise via cannula at room temperature over the course of 30 min. The orange reaction mixture was stirred further for 2 h. It was then quenched by the addition of saturated $Na_2S_2O_3$ solution (50 mL). The phases were separated, and the aqueous layer was extracted with Et_2O (3×20 mL). The combined organic layers were washed with dH_2O (25 mL) and brine (25 ml) and dried over $MgSO_4$. The organic solution was concentrated under reduced pressure to afford 6,6'-methylenebis(2-bromo-4-

methylphenol) as an off-white solid (2.52 g, 6.5 mmol, 99 %). The product was used in subsequent steps without further purification.

The sample for the X-ray measurement was obtained by recrystallisation from pentane/DCM mixture (2:1).

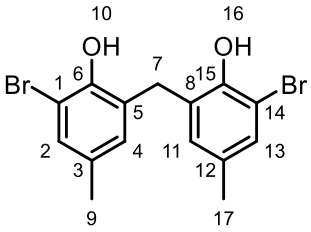

^{1}H NMR (600 MHz, $CDCl_3$): δ = 7.16 (d, *J* = 2.1 Hz, 2H, H-4, H-11), 6.91 (d, *J* = 2.1 Hz, 2H, H-2, H-13), 5.94 (s, 2H, OH), 3.95 (s, 2H, H-7), 2.23 (s, 6H, H-9, H-17) ppm.

^{13}C NMR (151 MHz, $CDCl_3$): δ = 147.7 (C-6, C-15), 131.5 (C-3, C-12), 130.9 (C-4, C-11), 130.8 (C-2, C-13), 127.3 (C-5, C-8), 110.4 (C-1, C-14), 31.5 (C-7), 20.5 (C-9, C-17) ppm.

HRMS (ESI): Calc. for $C_{15}H_{14}Br_2O_2Na$ 408.9192, found 408.9233 $[MNa]^+$.

After performing the synthesis of 6,6'-methylenebis(2-bromo-4-methylphenol) (**3**) using both previously described methods, it was possible to conclude that the method using elemental bromine delivered better results than the bromination with NBS. Not only was the isolated yield substantially higher using the former method, but the purity of the isolated product was improved as well. As shown in Supplementary Information (Supp. 3), the ^{1}H-NMR spectrum of the NBS-brominated ligand precursor (**3**) shows traces of water (δ = 1.54 ppm), that could not be removed even after prolonged drying on the Schlenk line. Therefore, the other method was preferred for the synthesis of the compound **3**.

5.2.3 Synthesis of 6,6'-methylenebis(4-methyl-2-(triphenylsilyl)phenol) (**6**)[64]

All glassware needed for the reaction was stored in an oven overnight. On the next day, 6,6'-methylenebis(2-bromo-4-methylphenol) (500 mg, 1.3 mmol, 1.0 equiv) was dissolved in dry THF (25 mL) in a dry Schlenk flask under argon. The solution was then charged with KH (156 mg, 3.9 mmol, 3.0 equiv) and the mixture was stirred vigorously for about 30 minutes at room temperature. To the resultant blue mixture was added chlorotriphenylsilane (800 mg, 2.7 mmol, 2.1 equiv). After the installation of the condenser, the reaction mixture was heated overnight (>14 h) at 60 °C in a sealed

system under argon. On the next day, the orange reaction mixture was cooled to –78 °C and *t*-BuLi (0.33 g, 1.7 M in hexanes, 3.1 mL, 5.2 mmol, 4.0 equiv) was carefully drawn from the bottle and added to the reaction mixture dropwise. The resulting mixture was stirred at that temperature for about 30 min and the temperature was then gradually raised to 0 °C over 1.5 h using an ice bath. Once at room temperature, the reaction was quenched using saturated a NH_4Cl solution (10 mL). THF was then evaporated under reduced pressure and formed aqueous sludge was extracted with Et_2O (2×25 mL) and the organic phases were combined. The organic phase was then washed with H_2O (10 mL) and brine (10 mL), dried over anhydrous $MgSO_4$ and filtered. After removal of the solvent under reduced pressure, the crude product was purified *via* flash column chromatography (silica, 10-40 % EtOAc in heptane). The obtained 6,6'-methylenebis(4-methyl-2-(triphenylsilyl)phenol) (**6**) was freeze dried from benzene on the Schlenk line before further use in the argon filled glovebox. The product was obtained as a fine off-white powder (0.804 g, 1.08 mmol, 83 %).

The sample for the X-ray measurement was obtained by recrystallisation from EtOAc.

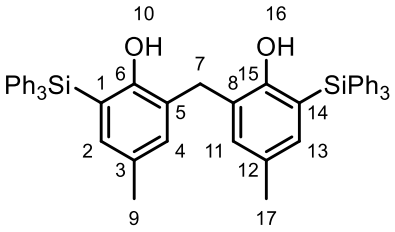

^{1}H NMR (600 MHz, C_6D_6): δ = 7.73 (dt, *J* = 6.7, 1.5 Hz, 12H, aryl-H), 7.71 – 7.69 (m, 2H, aryl-H), 7.65 (dd, *J* = 7.8, 1.7 Hz, 1H, aryl-H), 7.19 (dq, *J* = 4.8, 2.3 Hz, 4H, aryl-H), 7.12 – 7.11 (m, 11H, aryl-H), 7.10 (d, *J* = 2.3 Hz, 2H, H-4, H-11), 7.07 (d, *J* = 2.3 Hz, 2H, H-2, H-13), 5.98 (s, 2H, OH), 3.78 (s, 2H, H-7), 1.95 (s, 6H, H9, H-17) ppm.

^{13}C NMR (151 MHz, C_6D_6): δ = 157.0 (C-6, C-15), 137.4, 136.8, 135.7, 134.7 (aryl-C), 130.5 (C-3, C-12), 130.0, 128.5, 127.3 (C-5, C-8), 120.0 (C-1, C-14), 31.2 (C-7), 20.6 (C-9, C-17) ppm.

HRMS (ESI): Calc. for $C_{51}H_{44}O_2Si_2Na$ 767.2792, found 767.2771 $[MNa]^+$.

5.2.4 Synthesis of chloro(cyclohexyl)diphenylsilane (**5**)[65]

To a suspension of cut lithium wire (1.60 g, 226.0 mmol, 4.4 equiv) in dry pentane (150 mL) was added slowly chlorocyclohexane (15.42 g, 15.40 mL, d = 1 g/mL, 127.5 mmol, 2.5 equiv) *via* syringe pump over a period of 1 h while gently heating. The

resulting reaction mixture was heated to reflux for 5 h. The violet mixture was cooled down in an ice bath and a solution of diphenyldichlorosilane (13.31 g, 11.0 mL, d = 1.2 g/mL, 51.0 mmol, 1.0 equiv) in pentane (10 mL) was added dropwise *via* cannula. The resulting mixture was then allowed to warm to room temperature and was stirred overnight. Precipitated lithium chloride salt and excessive lithium were filtered off under inert conditions using a glass-fiber filter cannula. The filtrate was treated with ice cold 2M HCl solution (30 mL) to quench the excess cyclohexyllithium. The organic layer was separated, dried over anhydrous $MgSO_4$ and concentrated to give a cloudy light-yellow oil. The crude product was therefore filtered one more time in the same manner and it was further purified by vacuum distillation (120–145 °C at 0.1 mbar), giving the product as a colourless oil (9.22 g, 30.6 mmol, 60 %).

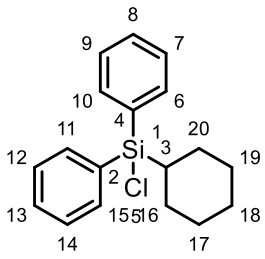

^{1}H NMR (700 MHz, $CDCl_3$): δ = 7.80 – 7.78 (m, 1H, aryl-H), 7.69 (dt, *J* = 6.8, 1.5 Hz, 2H, aryl-H), 7.62 (dt, *J* = 6.6, 1.6 Hz, 1H, aryl-H), 7.57 – 7.54 (m, 1H, aryl-H), 7.50 – 7.46 (m, 2H, aryl-H), 7.45 – 7.39 (m, 3H, aryl-H), 1.79 – 1.74 (m, 3H, Cy), 1.70 (tdd, *J* = 12.9, 3.3, 1.7 Hz, 2H, Cy),1.39 – 1.27 (m, 3H, Cy), 1.24 (qt, J = 12.4, 3.5 Hz, 2H, Cy), 1.19 – 1.10 (m, 1H, Cy) ppm.

^{13}C NMR (176 MHz, $CDCl_3$): δ = 134.8 (aryl-H), 133.0 (C-2, C-4), 130.5 (aryl-H), 128.1 (aryl-H), 30.3 (Cy), 28.5 (Cy), 28.0 (Cy), 27.8 (Cy), 27.1 (Cy), 26.8 (C-3) ppm.

The spectroscopic data is in agreement with the literature.[87]

5.2.5 Synthesis of 6,6'-methylenebis(2-(cyclohexyldiphenylsilyl)-4-methylphenol) (**7**)[64]

All glassware needed for the reaction was stored in an oven overnight. On the next day, 6,6'-methylenebis(2-bromo-4-methylphenol) (500 mg, 1.3 mmol, 1.0 equiv) was dissolved in dry THF (25 mL) in a dry Schlenk flask under argon. The solution was then charged with KH (158 mg, 3.9 mmol, 3.0 equiv) and the mixture was stirred vigorously for about 30 minutes at room temperature. To the resultant mixture was added chloro(cyclohexyl)diphenylsilane (0.814 g, 2.7 mmol, 2.1 equiv). After the installation of the condenser, the reaction mixture was heated overnight (>14 h) at

60 °C in a sealed system under argon. On the next day, the reaction mixture was cooled to –78 °C using dry ice/acetone mixture and *t*-BuLi (0.33 g, 1.7 M in hexanes, 3.1 mL, 5.2 mmol, 4.0 equiv) was carefully drawn from the bottle and added to the reaction mixture dropwise. The resulting mixture was stirred at that temperature for about 30 min and the temperature was then gradually raised to 0 °C over 1.5 h using an ice bath. Once at room temperature, the reaction was quenched using saturated NH_4Cl solution (10 mL). THF was then evaporated under reduced pressure, the formed aqueous sludge was extracted with Et_2O (2×25 mL) and the organic phases were combined. The organic phase was then washed with H_2O (10 mL) and brine (10 mL), dried over anhydrous $MgSO_4$ and filtered. After removal of the solvent under reduced pressure, the crude product was purified *via* flash column chromatography (silica, 10-40 % EtOAc in heptane), which afforded a colourless oil. The product was recrystallised from EtOAc before further use and was obtained as a fine white powder (0.440 g, 0.58 mmol, 45 %).

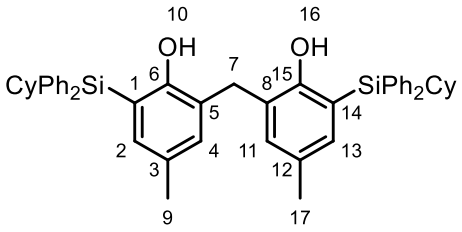

^{1}H NMR (600 MHz, C_6D_6): δ = 7.79 – 7.66 (m, 9H, aryl-H), 7.65 – 7.55 (m, 1H, aryl-H), 7.34 – 7.26 (m, 2H, aryl-H), 7.20 – 7.16 (m, 10H, aryl-H), 7.00 (d, *J* = 2.3 Hz, 2H, H-2, H-13), 5.97 (s, 2H, OH), 3.69 (s, 2H, H-7), 2.04 (s, 6H, H-9, H-17), 1.82 (tt, *J* = 12.5, 2.8 Hz, 3H, Cy), 1.66 (tdd, *J* = 17.8, 9.1, 5.5 Hz, 7H, Cy), 1.45 – 1.24 (m, 9H, Cy), 1.10 (dddd, *J* = 16.4, 12.8, 8.1, 3.5 Hz, 3H, Cy) ppm.

^{13}C NMR (151 MHz, C_6D_6): δ = 157.0 (C-6, C-15), 136.6, 136.4, 135.0 (aryl-C), 133.9, 130.2, 129.8, 128.45, 126.8 (C-5, C-8), 120.1 (C-1, C-14), 31.3 (C-7), 28.8 (Cy), 28.6 (Cy), 27.2 (Cy), 24.7 (Cy), 20.7 (C-9, C-17) ppm.

HRMS (ESI): Calc. for $C_{51}H_{56}O_2Si_2Na$ 779.3692, found 779.3698 $[MNa]^+$.

5.2.6 Synthesis of 4-methyl-2-tritylphenol (**9**)[67,68]

p-Cresol (35 g, 324 mmol, 7 equiv) was heated in a Schlenk flask to 100 °C under argon. Metallic sodium (1.4 g, 61 mmol, 1.3 equiv) was added slowly under vigorous stirring to afford a cresolate melt. The reaction mixture was then charged with triphenylchloromethane (13 g, 47 mmol, 1.0 equiv) and the mixture was stirred at

140 °C for 4 h. The reaction mixture was then cooled down and left overnight at room temperature. On the next day, the liquid reaction mixture was treated with 7 % aq. NaOH (200 mL) and Et_2O (400 mL). The layers were separated, and the organic phase was washed with 7 % NaOH (5×50 mL), water (100 mL) and brine (50 mL). After drying over $MgSO_4$ and filtration, the solvent was removed under reduced pressure. The crude product was obtained as a brown solid. The product was then recrystallised from ethanol in the refrigerator which afforded 4-methyl-2-tritylphenol as a light brown solid (9.4 g, 27 mmol, 57 %).

A sample for the X-ray measurement was obtained by recrystallisation from a MeOH/DCM (1:1) mixture.

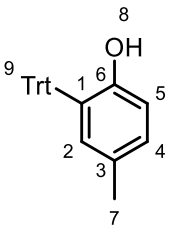

^{1}H NMR (600 MHz, $CDCl_3$): δ = 7.28 – 7.13 (m, 15H, Trt), 7.00 (dd, *J* = 8.0, 2.1 Hz, 1H, H-2), 6.82 (d, *J* = 2.2 Hz, 1H, H-4), 6.70 (d, *J* = 8.0 Hz, 1H, H-5), 4.28 (s, 1H, OH), 2.15 (s, 3H, H-7) ppm.

^{13}C NMR (151 MHz, $CDCl_3$): δ = 152.4 (C-6), 144.4 (3C, Trt), 133.0 (C-3), 131.15, 131.10, 129.6 (C-1), 129.4, 128.1, 126.9, 118.0 (C-5), 62.8 (CPh_3), 21.1 (C-7) ppm.

HRMS (ESI): Calc. for $C_{26}H_{22}ONa$ 373.1592, found 373.1563 $[MNa]^+$.

The NMR spectroscopic data is in agreement with the literature.[67,68]

5.2.7 Synthesis of 6,6'-disulfanediylbis(4-methyl-2-tritylphenol)(**10**)[69]

In a flame-dried Schlenk flask was placed a solution of 4-methyl-2-tritylphenol (1.0 g, 2.8 mmol, 1.0 equiv) in toluene (15 mL). A solution of disulphur dichloride (0.19 g, 0.11 mL, d=1.69 g/mL, 1.4 mmol, 0.5 equiv) in toluene (10 mL) was added dropwise over a period of 3 h at room temperature. The resulting reaction mixture was then heated to 80 °C and stirred at that temperature overnight. On the next day the mixture was cooled to room temperature and the solvent was then evaporated under reduced pressure to afford a brown crude product, which was dissolved in hot ethanol (100 mL) and recrystallised. The purified product was freeze dried from benzene on a Schlenk line before further use. The product was obtained as a grey solid (0.695 mg, 0.9 mmol, 32 %).

^{1}H NMR (600 MHz, C_6D_6): δ = 7.35 (dd, *J* = 8.4, 1.4 Hz, 11H, aryl-H), 7.25 – 7.21 (m, 1H, aryl-H), 7.19 (d, *J* = 2.3 Hz, 2H, aryl-H), 7.13 – 7.10 (m, 1H, aryl-H), 7.10 – 7.04 (m, 2H, aryl-H), 7.02 (t, *J* = 7.4 Hz, 7H, aryl-H), 6.99 – 6.95 (m, 6H, aryl-H), 6.91 (dd, *J* = 8.1, 2.3 Hz, 2H, H-4, H-13), 6.87 (d, *J* = 8.0 Hz, 2H, H-2, H-15), 4.53 (s, 2H, OH), 2.05 (s, 6H, H-7, H-20) ppm.

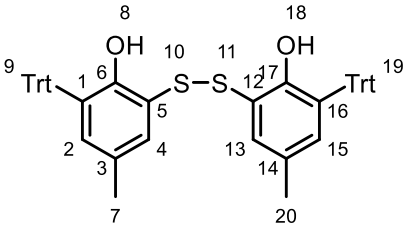

^{13}C NMR (151 MHz, C_6D_6): δ = 153.4 (C-6, C-17), 145.0, 133.5, 131.4, 131.4, 130.0, 129.3, 128.6, 128.3, 128.2, 126.9 (C-5, C-12), 118.6 (Trt), 21.0 (C-7, C-20) ppm.

HRMS (ESI): Calc. for $C_{52}H_{42}O_2S_2Na$ 785.2492, found 785.2515 $[MNa]^+$.

5.3 Synthesis of Metal Complexes

5.3.1 General procedure for complexation reactions on NMR scale (GP1)

Inside the argon filled glovebox, 0.06 mmol of the corresponding diol proligand and the appropriate metal precursor were weighed in two separate vials. Subsequently, dry deuterated benzene (500 µL), respectively, was taken with a microsyringe and added to each vial and shaken well. Once contents of the vials were dissolved in benzene, the precursor stock solution was taken with a microsyringe and transferred quantitatively into the vial containing the proligand solution (or suspension). The mixture was kept at ambient temperature to allow the reaction to take place. Subsequently, it was transferred to an NMR tube equipped with a screw cap, sealed with a Teflon band and taken out of the glovebox. After the acquisition of both ^{1}H-and ^{13}C-NMR spectra was completed and thus the reaction completion confirmed, the sample was returned to the glovebox and stored in the freezer at –20 °C until further use.

The yttrium precursor $[Y(N(SiHMe_2)_2)_3(THF)_2]$ was synthesised according to the previously published protocol[88] by former group members and was directly used in complexation reactions.

5.3.2 Synthesis of Yttrium Complexes

*5.3.2.1 Synthesis of [Y(o-$C_6H_4CH_2NMe_2)_3$] precursor (**11-Y**)[89,90]*

YCl_3 (994 mg, 5.1 mmol, 1.0 equiv) was weighed in the glovebox in a Schlenk flask. Subsequently, it was suspended in dry THF (5 mL). The resulting suspension was stirred for 1 h at 50 °C. THF was then removed *in vacuo* on the Schlenk line. In the glovebox, LiBDMA (2.176 g, 5.3 mmol, 1.0 equiv) was then added. To the flask containing the mixture dry Et_2O (50 mL) was added. The resulting mixture was stirred for additional 18 h. The solvent was then removed *in vacuo*. The residue was first washed with Et_2O (10 mL + 5 mL) and subsequently extracted with dry toluene (40 + 15 mL) under inert conditions *via* cannula. The solvent was then evaporated in vacuo to afford the final product. $Y(BDMA)_3$ (**11-Y**) precursor was obtained as orange-brown powder (0.742 g, 1.5 mmol, 29 %).

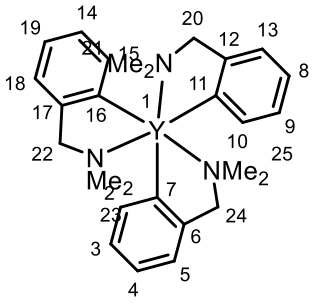

^{1}H NMR (600 MHz, C_6D_6): δ = 8.21 (d, *J* = 6.8 Hz, 3H, H-2, H-10, H-15), 7.35 (td, *J* = 7.1, 1.1 Hz, 3H), 7.25 (td, *J* = 7.4, 1.5 Hz, 3H), 6.97 (d, *J* = 7.4 Hz, 3H, H-5, H-13, H-18), 3.45 (s, 6H, H-20, H-22, H-24), 2.15 (s, 18H, NMe_2) ppm.

^{13}C NMR (151 MHz, C_6D_6): δ = 186.9 (d, *J* = 43.5 Hz, C-7, C-11, C-16), 146.8, 138.7, 125.8, 125.3, 124.8, 69.8 (C-20, C-22, C-24), 45.9 (Me) ppm.

The spectroscopic data is in agreement with the literature.[89]

5.3.2.2 Attempted complexation of $Y(BDMA)_3$ with 6,6'-methylenebis(4-methyl-2-(triphenylsilyl)phenol) at room temperature

Reaction was performed according to the general procedure (GP1). A solution of $Y(BDMA)_3$ (29.5 mg, 0.06 mmol, 1.0 equiv) in C_6D_6 (500 µL) was added to the suspension of the diol proligand **6** (44.7 mg, 0.06 mmol, 1.0 equiv) in C_6D_6 (500 µL) and left to react over a period of 30 min to afford a yellow-orange solution containing an unidentifiable mixture of products.

5.3.2.3 Attempted complexation of $Y(BDMA)_3$ with 6,6'-methylenebis(4-methyl-2-(triphenylsilyl)phenol) at –20 °C

Complexation diverted from the general procedure (GP1). In the glovebox, stock solutions of $Y(BDMA)_3$ (29.5 mg, 0.06 mmol, 1.0 equiv) in toluene-d_8 (500 µL) and diol proligand **6** (44.7 mg, 0.06 mmol, 1.0 equiv) in toluene-d_8 (500 µL) were prepared and stored in the freezer at –20 °C overnight together with an aluminium block. On the following day, the ligand solution was added dropwise under stirring to the solution of the precursor that was placed in the chilled aluminium block. The reaction mixture was left in the freezer overnight. Obtained was an orange solution containing an unidentifiable mixture of products.

5.3.2.4 Attempted complexation of $Y(BDMA)_3$ with 6,6'-disulfanediylbis(4-methyl-2-tritylphenol)

The reaction was performed according to the general procedure (GP1). To a solution of $Y(BDMA)_3$ (29.5 mg, 0.06 mmol, 1.0 equiv) in C_6D_6 (500 µL) was added the solution of the diol proligand **10** (45.8 mg, 0.06 mmol, 1.0 equiv) in C_6D_6 (500 µL) and left to react over a period of 30 min to afford an orange solution containing an unidentifiable mixture of products.

5.3.2.5 Attempted complexation of $Y(BDMA)_3$ with 6,6'-methylenebis(2-(cyclohexyldiphenylsilyl)-4-methylphenol)

The reaction was performed according to the general procedure (GP1). To a solution of $Y(BDMA)_3$ (29.5 mg, 0.06 mmol, 1.0 equiv) in C_6D_6 (500 µL) was added the solution of the diol proligand **7** (45.4 mg, 0.06 mmol, 1.0 equiv) in C_6D_6 (500 µL) and left to react over a period of 30 min to afford a yellow solution containing an unidentifiable mixture of products.

*5.3.2.6 Complexation of $[Y(N(SiHMe_2)_2)_3(THF)_2]$ with 6,6'-methylenebis(4-methyl-2-(triphenylsilyl)phenol) (**17-Y**)*

The reaction was performed according to the general procedure (GP1). A solution of $[Y(N(SiHMe_2)_2)_3(THF)_2]$ (37.8 mg, 0.06 mmol, 1.0 equiv) in C_6D_6 (500 µL) was added

to the suspension of the diol proligand **6** (44.7 mg, 0.06 mmol, 1.0 equiv) in C_6D_6 (500 µL) and left to react over a period of 20 h to afford a yellow solution containing the desired complex **17-Y**. Initial attempt at isolation of the complex by freeze drying on the Schlenk line led to decomposition of the complex. Therefore, the complex was not isolated, but the solution was stored in the glovebox freezer at –20 °C until further use.

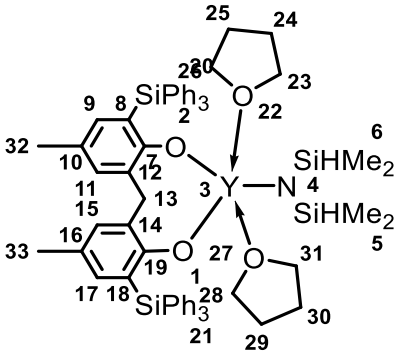

^{1}H NMR (600 MHz, C_6D_6): δ = 7.98 (dq, *J* = 7.3, 1.4 Hz, 1H, aryl-H), 7.86 – 7.80 (m, 15H, aryl-H), 7.70 – 7.67 (m, 1H, aryl-H), 7.58 (d, *J* = 2.4 Hz, 2H, aryl-H), 7.31 – 7.20 (m, 1H, aryl-H), 7.19 – 7.17 (m, 10H, aryl-H), 7.16 – 7.14 (m, 3H, aryl-H), 7.10 (dd, *J* = 5.0, 1.9 Hz, 1H, aryl-H), 5.00 (p, *J* = 3.0 Hz, 1H, SiH), 4.75 – 4.72 (m, 4H, free $HN(SiHMe_2)_2$), 4.66 (s, 1H, SiH), 4.59 (d, *J* = 14.2 Hz, 1H, H-13), 3.90 (d, *J* = 14.2 Hz, 1H, H-13), 3.09 (s, 8H, THF), 2.12 (s, 6H, H-32, H-33), 0.98 (s, 8H, THF), 0.43 – 0.36 (m, 6H, $SiMe_2$), 0.27 (d, *J* = 3.0 Hz, 6H, $SiMe_2$), 0.14 (d, *J* = 3.1 Hz, 24H, free $HN(SiHMe_2)_2$) ppm.

^{13}C NMR (151 MHz, C_6D_6): δ = 167.2 (C7, C-14), 138.2, 137.1, 135.0, 129.9, 128.9, 128.6, 127.8, 128.4, 125.6 (aryl-C), 70.3 (THF), 35.7 (C-13), 25.0 (THF), 20.8 (C-32, C-33), 3.4 ($SiMe_2$), 3.3 ($SiMe_2$), 0.6 (free $HN(SiHMe_2)_2$) ppm.

*5.3.2.7 Complexation of $[Y(N(SiHMe_2)_2)_3(THF)_2]$ with 6,6'-methylenebis(2-(cyclohexyldiphenylsilyl)-4-methylphenol) (**18-Y**)*

The reaction was performed according to the general procedure (GP1). To a solution of $[Y(N(SiHMe_2)_2)_3(THF)_2]$ (37.8 mg, 0.06 mmol, 1.0 equiv) in C_6D_6 (500 µL) was added the solution of the diol proligand **7** (45.4 mg, 0.06 mmol, 1.0 equiv) in C_6D_6 (500 µL) and left to react over a period of 20 h to afford a bright yellow solution containing the desired complex **18-Y**. The complex was not isolated but was stored in the glovebox freezer at –20 °C until further use.

^{1}H NMR (700 MHz, C_6D_6): δ = 7.89 – 7.85 (m, 4H, aryl-H), 7.72 – 7.68 (m, 4H, aryl-H), 7.64 (d, *J* = 2.4 Hz, 2H, aryl-H), 7.52 (d, *J* = 2.4 Hz, 2H, aryl-H), 7.22 – 7.19 (m, 4H, aryl-H), 7.19 – 7.16 (m, 2H, aryl-H), 7.13 (t, *J* = 7.2 Hz, 4H, aryl-H), 7.10 – 7.06 (m, 2H, aryl-H), 5.23 (hept, *J* = 2.9 Hz, 2H, SiH), 4.74 – 4.69 (m, *J* = 3.1 Hz, 4H, free $HN(SiHMe_2)_2$), 3.99 (d, *J* = 14.3 Hz, 1H, H-13), 3.63 (d, *J* = 14.4 Hz, 1H, H-13), 2.47 (tt, *J* = 12.3, 2.7 Hz, 2H, Cy), 2.25 (s, 6H, H-32, H-33), 2.16 (d, *J* = 13.5 Hz, 2H, Cy), 1.79 – 1.71 (m, 4H, Cy), 1.68 (dt, *J* = 12.7, 3.3 Hz, 2H, Cy), 1.57 (pt, *J* = 12.7, 3.2 Hz, 2H, Cy), 1.52 – 1.43 (m, 4H, Cy), 1.40 – 1.22 (m, 1H, Cy), 1.15 – 1.07 (m, 3H, Cy), 1.00 (qd, *J* = 13.1, 3.4 Hz, 2H, Cy), 0.39 – 0.35 (m, 12H, H-5, H-6), 0.11 (d, *J* = 3.2 Hz, 24H, free $HN(SiHMe_2)_2$) ppm.

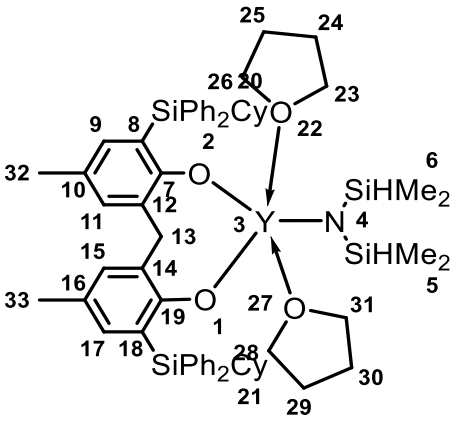

^{13}C NMR (176 MHz, C_6D_6): δ = 165.5 (C7, C-14), 137.8, 137.54, 137.45, 137.1, 136.7, 134.1, 129.7, 129.6, 128.79, 128.77, 128.66, 127.68, 127.61, 125.4, 120.7 (aryl-C), 69.3 (THF), 31.4 (C-13), 29.6 (Cy), 29.1 (Cy), 28.4 (Cy), 28.2 (Cy), 27.5 (THF), 23.2 (Cy-CH), 21.0 (C-32, C-33), 4.0 ($SiMe_2$), 3.3 ($SiMe_2$), 0.6 (free $HN(SiHMe_2)_2$) ppm.

*5.3.2.8 Complexation of $[Y(N(SiHMe_2)_2)_3(THF)_2]$ with 6,6'-disulfanediylbis(4-methyl-2-tritylphenol) (**19-Y**)*

The reaction was performed according to the general procedure (GP1). To a solution of $[Y(N(SiHMe_2)_2)_3(THF)_2]$ (37.8 mg, 0.06 mmol, 1.0 equiv) in C_6D_6 (500 µL) was added the solution of the diol proligand **10** (45.8 mg, 0.06 mmol, 1.0 equiv) in C_6D_6 (500 µL) and left to react over a period of 15 min to afford a light orange solution containing the desired complex **19-Y**. An initial attempt at isolation of the complex by freeze drying on the Schlenk line led to decomposition of the complex. Therefore, the complex was not isolated, but the solution was stored in the glovebox freezer at –20 °C until further use.

^{1}H NMR (600 MHz, C_6D_6): δ = 7.48 (d, *J* = 7.9 Hz, 10H, aryl-H), 7.28 (d, *J* = 2.3 Hz, 2H, aryl-H), 7.06 (t, *J* = 7.8 Hz, 13H, aryl-H), 6.99 – 6.96 (m, 7H, aryl-H), 5.80 (d, *J* = 7.9 Hz, 2H, aryl-H), 4.72 (hept, *J* = 3.0 Hz, 4H, free $HN(SiHMe_2)_2$), 3.29 (s, 8H, THF), 2.23 (s, 6H, H-23, H-24), 1.19 (s, 8H, THF), 0.12 (d, *J* = 3.1 Hz, 36H, H-3, H-4, free $HN(SiHMe_2)_2$) ppm.

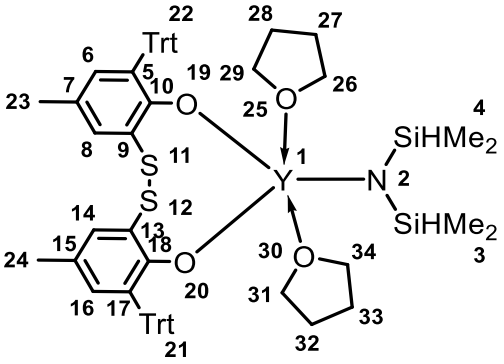

^{13}C NMR (151 MHz, C_6D_6): δ = 160.7 (C-10, C-18), 147.7, 131.8, 128.6, 127.5, 127.4, 125.4, 125.3, 122.9 (aryl-C), 64.0 (THF), 25.34 (THF), 21.3 (C-23, C-24), 3.8 (C-3, C-4), 0.7 (free $HN(SiHMe_2)_2$) ppm.

5.3.3 Synthesis of Titanium and Zirconium Complexes

5.3.3.1 Attempted complexation of $[Ti(NMe_2)_4]$ with 6,6'-methylenebis(4-methyl-2-(triphenylsilyl)phenol)

The reaction was performed according to the general procedure (GP1). A solution of $[Ti(NMe_2)_4]$ (13.5 mg, 0.06 mmol, 1.0 equiv) in C_6D_6 (500 µL) was added to the suspension of the diol proligand **6** (44.7 mg, 0.06 mmol, 1.0 equiv) in C_6D_6 (500 µL) and left to react over a period of 30 min to afford a bright orange solution containing an unidentifiable mixture of products.

*5.3.3.2 Complexation of $[Ti(NMe_2)_4]$ with 6,6'-methylenebis(4-methyl-2-(triphenylsilyl)phenol) at 60 °C (**22-Ti**)*

The reaction was performed according to the general procedure (GP1). Solution of $[Ti(NMe_2)_4]$ (13.5 mg, 0.06 mmol, 1.0 equiv) in C_6D_6 (500 µL) was added to the suspension of the diol proligand **6** (44.7 mg, 0.06 mmol, 1.0 equiv) in C_6D_6 (500 µL) to afford a milky orange suspension, which was subsequently heated to 60 °C in the glovebox for 30 min. A clear orange solution containing complex **22-Ti** was obtained. However, the synthesis could not be reproduced under the same conditions, which is to be attributed to a different batch of the diol proligand **6**, that was of a higher purity than the initially used one, and of a slightly better solubility.

^{1}H NMR (600 MHz, C_6D_6): δ = 7.80 – 7.73 (m, 24H, aryl-H), 7.22 – 7.19 (m, 24H, aryl-H), 7.15 – 7.08 (m, 22H, aryl-H), 3.89 (s, 4H, H-7, H-27), 2.01 (s, 12H, H-15, H-16, H-35, H-36) ppm.

^{13}C NMR (151 MHz, C_6D_6): δ 158.9 (C-6, C-13, C-26, C-33), 137.6, 136.9, 135.8, 134.5, 129.6, 129.4, 128.6, 128.2, 120.4 (aryl-C), 32.7 (C-7, C-27), 20.7 (C-15, C-16, C-35, C-36) ppm.

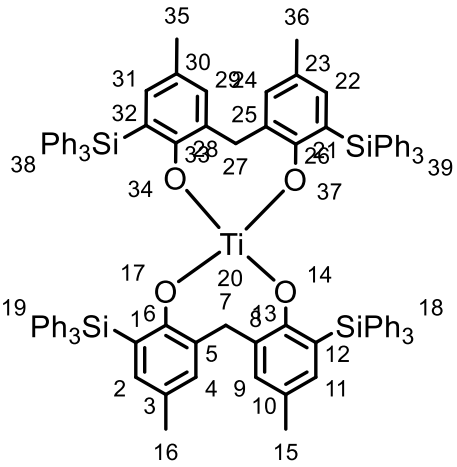

5.3.3.3 Attempted complexation of [Ti(NMe$_2$)$_4$] with 6,6'-methylenebis(4-methyl-2-(triphenylsilyl)phenol) at –20 °C

The complexation diverted from the general procedure (GP1). In the glovebox, stock solutions of [Ti(NMe$_2$)$_4$] (13.5 mg, 0.06 mmol, 1.0 equiv) in THF-d$_8$ (500 µL) and diol proligand **6** (44.7 mg, 0.06 mmol, 1.0 equiv) in THF-d$_8$ (500 µL) were prepared and stored in the freezer at –20 °C overnight together with an aluminium block. On the following day, the ligand solution was added dropwise under stirring to the solution of the Ti-precursor that was placed in the chilled aluminium block. The reaction mixture was left in the freezer overnight. An orange solution containing an unidentifiable mixture of products was obtained.

5.3.3.4 Attempted complexation of [Ti(NMe$_2$)$_4$] with 6,6'-methylenebis(4-methyl-2-(triphenylsilyl)phenol) at –78 °C[75]

The complexation procedure diverted from the general procedure (GP1). In the glovebox, stock solutions of [Ti(NMe$_2$)$_4$] (13.5 mg, 0.06 mmol, 1.0 equiv) in THF-d$_8$ (500 µL) and diol proligand **6** (44.7 mg, 0.06 mmol, 1.0 eq) in THF-d$_8$ (500 µL) were prepared in separate Schlenk flasks. They were then taken out of the glovebox and, on the Schlenk line, under inert atmosphere and stirring, a solution of the Ti-precursor was cooled down to –78 °C. The solution of the diol proligand was added dropwise to a solution of the Ti-precursor *via* cannula over the course of 1 h. The reaction mixture

was left stirring in the dry ice/acetone mixture overnight. On the following day, an orange solution containing an unidentifiable mixture of products was obtained.

5.3.3.5 Attempted complexation of [Ti(NMe$_2$)$_4$] with 6,6'-methylenebis(4-methyl-2-(triphenylsilyl)phenol) in ratio 2:1 at room temperature

The reaction was performed according to the general procedure (GP1), nonetheless in the ratio 2:1 (precursor : ligand). A solution of [Ti(NMe$_2$)$_4$] (13.5 mg, 0.06 mmol, 2.0 equiv) in C_6D_6 (500 µL) was added to the suspension of the diol proligand **6** (22.3 mg, 0.03 mmol, 1.0 equiv) in C_6D_6 (500 µL) and left to react over a period of 30 min at room temperature to afford an orange solution containing an unidentifiable mixture of products.

The obtained NMR spectra are identical to the NMR spectra obtained in section 5.3.3.1.

5.3.3.6 Attempted complexation of [Ti(NMe$_2$)$_4$] with 6,6'-methylenebis(4-methyl-2-(triphenylsilyl)phenol) in ratio 1:2 at 60 °C

The reaction was performed according to the general procedure (GP1), nonetheless in the ratio 1:2 (precursor : ligand). A solution of [Ti(NMe$_2$)$_4$] (6.7 mg, 0.03 mmol, 1.0 equiv) in C_6D_6 (500 µL) was added to the suspension of the diol proligand **6** (44.7 mg, 0.06 mmol, 2.0 equiv) in C_6D_6 (500 µL) and left to react over a period of 30 min at 60 °C to afford an orange solution containing an unidentifiable mixture of products.

The obtained NMR spectra are identical to the NMR spectra obtained in section 5.3.3.1.

5.3.3.7 Attempted complexation of [Ti(NMe$_2$)$_4$] with 6,6'-disulfanediylbis(4-methyl-2-tritylphenol) at room temperature

The reaction was performed according to the general procedure (GP1). A solution of [Ti(NMe$_2$)$_4$] (13.5 mg, 0.06 mmol, 1.0 equiv) in C_6D_6 (500 µL) was added to the solution of the diol proligand **10** (45.8 mg, 0.06 mmol, 1.0 equiv) in C_6D_6 (500 µL) and left to react over a period of 30 min at room temperature to afford a dark brown solution containing an unidentifiable mixture of products.

5.3.3.8 Attempted complexation of [Zr(NMe$_2$)$_4$] with 6,6'-methylenebis(4-methyl-2-(triphenylsilyl)phenol) at room temperature

The reaction was performed according to the general procedure (GP1). A solution of [Zr(NMe$_2$)$_4$] (16.0 mg, 0.06 mmol, 1.0 equiv) in C_6D_6 (500 µL) was added to the solution of the diol proligand **6** (44.7 mg, 0.06 mmol, 1.0 equiv) in C_6D_6 (500 µL) and left to react over a period of 30 min at room temperature to afford a pale yellow solution containing an unidentifiable mixture of products.

5.3.3.9 Attempted complexation of [Zr(NMe$_2$)$_4$] with 6,6'-methylenebis(4-methyl-2-(triphenylsilyl)phenol) at 60 °C

The reaction was performed according to the general procedure (GP1). A solution of [Zr(NMe$_2$)$_4$] (16.0 mg, 0.06 mmol, 1.0 equiv) in C_6D_6 (500 µL) was added to the suspension of the diol proligand **6** (44.7 mg, 0.06 mmol, 1.0 equiv) in C_6D_6 (500 µL) to afford a milky orange suspension, which was then heated to 60 °C in the glovebox for 30 min. A clear pale yellow solution containing an unidentifiable mixture of products was obtained.

The obtained NMR spectra are identical to the NMR spectra obtained in section 5.3.3.8

5.3.3.10 Attempted complexation of [Zr(NMe$_2$)$_4$] with 6,6'-disulfanediylbis(4-methyl-2-tritylphenol) at room temperature

The reaction was performed according to the general procedure (GP1). A solution of [Zr(NMe$_2$)$_4$] (16.0 mg, 0.06 mmol, 1.0 equiv) in C_6D_6 (500 µL) was added to the solution of the diol proligand **10** (45.8 mg, 0.06 mmol, 1.0 equiv) in C_6D_6 (500 µL) and left to react over a period of 30 min at room temperature to afford a bright yellow solution containing an unidentifiable mixture of products.

5.3.4 Synthesis of Niobium and Tantalum Complexes

*5.3.4.1 Complexation of [Nb(NMe$_2$)$_5$] with 6,6'-methylenebis(4-methyl-2-(triphenylsilyl)phenol) (**29-Nb**)*

The reaction was performed according to the general procedure (GP1). A solution of [Nb(NMe$_2$)$_5$] (18.8 mg, 0.06 mmol, 1.0 equiv) in C_6D_6 (500 µL) was added to the solution of the diol proligand **6** (44.7 mg, 0.06 mmol, 1.0 equiv) in C_6D_6 (500 µL) and left to react over a period of 30 min at room temperature to afford a brown solution containing a mixture of products, one of which is complex **29-Nb** (determined by X-ray crystallography). Crystals for X-ray measurements were obtained after thawing the above-mentioned brown solution after a prolonged stay at –20 °C in the glovebox freezer.

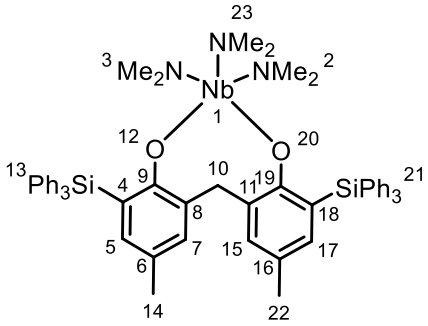

^{1}H NMR (600 MHz, C_6D_6) δ = 7.92 (s), 7.85 – 7.77 (m), 7.75 – 7.71 (m), 7.54 (dt, *J* = 6.7, 1.5 Hz), 7.29 – 7.24 (m), 7.23 – 7.19 (m), 7.17 (q, *J* = 1.1 Hz), 7.15 (t, *J* = 1.4 Hz), 3.77 – 3.67 (m), 3.16 (s), 2.83 – 2.54 (m), 2.26 (d, *J* = 6.4 Hz), 2.11 – 2.07 (m) ppm.

^{13}C NMR (151 MHz, C_6D_6) δ = 166.8 (C-9, C-19), 138.1, 137.2, 136.9, 135.8, 133.9, 130.6, 129.9, 129.1, 128.6, 128.0, 121.0 (aryl-C), 47.3 (free HNMe$_2$), 39.0 (NMe$_2$), 37.8 (C-10), 20.7 (C-14, C-22) ppm.

*5.3.4.2 Complexation of [Ta(NMe$_2$)$_5$] with 6,6'-methylenebis(4-methyl-2-(triphenylsilyl)phenol) (**31-Ta**)*

The reaction was performed according to the general procedure (GP1). Solution of [Ta(NMe$_2$)$_5$] (24.0 mg, 0.06 mmol, 1.0 equiv) in C_6D_6 (500 µL) was added to the solution of the diol proligand (number) (44.7 mg, 0.06 mmol, 1.0 eq) in C_6D_6 (500 µL) and left to react over a period of 30 min at room temperature to afford a yellow solution containing a mixture of products, one of which is complex **31-Ta** (determined by X-ray crystallography). Crystals for X-ray measurements were obtained after thawing the above-mentioned yellow solution after a prolonged stay at –20 °C in the glovebox freezer.

^{1}H NMR (600 MHz, C_6D_6) δ = 7.91 – 7.89 (m), 7.85 – 7.83 (m), 7.80 – 7.77 (m), 7.74 – 7.71 (m), 7.31 – 7.27 (m), 7.26 – 7.18 (m), 7.17 (t, *J* = 1.0 Hz), 7.15 (d, *J* = 1.4 Hz), 3.83 (s), 3.26 (s), 2.98 – 2.74 (m), 2.26 (d, *J* = 6.4 Hz), 2.08 (s) ppm.

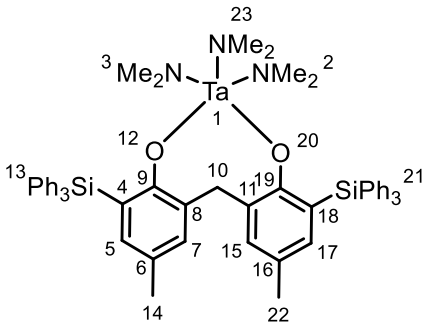

^{13}C NMR (151 MHz, C_6D_6) δ = 166.0 (C-9, C-19), 138.0, 136.9, 136.3, 135.5, 133.4, 130.0, 128.3, 128.1, 121.7 (aryl-C), 46.0 (free $HNMe_2$), 38.7 ($HNMe_2$), 37.7 (C-10), 20.4 (C-14, C-22) ppm.

5.4 X-ray Analysis

The X-ray intensity data was measured on Bruker D8 Venture diffractometer equipped with multilayer monochromator, Mo K/α INCOATEC micro focus sealed tube and Oxford cooling system. The structure was solved by *Direct Methods*. Non-hydrogen atoms were refined with *anisotropic displacement parameters*. Hydrogen atoms were inserted at calculated positions and refined with riding model. The following software was used: *Bruker SAINT software package* (Bruker SAINT v8.38B Copyright © 2005-2019 Bruker AXS) using a narrow-frame algorithm for frame integration, *SADABS* (Sheldrick, G. M. (1996) SADABS, University of Göttingen, Germany) for absorption correction, *OLEX2*[91] for structure solution, refinement, molecular diagrams and graphical user-interface, *Shelxle*[92] for refinement and graphical user-interface *SHELXS-2015* (Sheldrick, G. M. (2015) SHELXS v2016/4, University of Göttingen, Germany) for structure solution, *SHELXL-2015* (Sheldrick, G. M. (2015) SHELXL v2016/4, University of Göttingen, Germany) for refinement, *Platon*[93] for symmetry check.

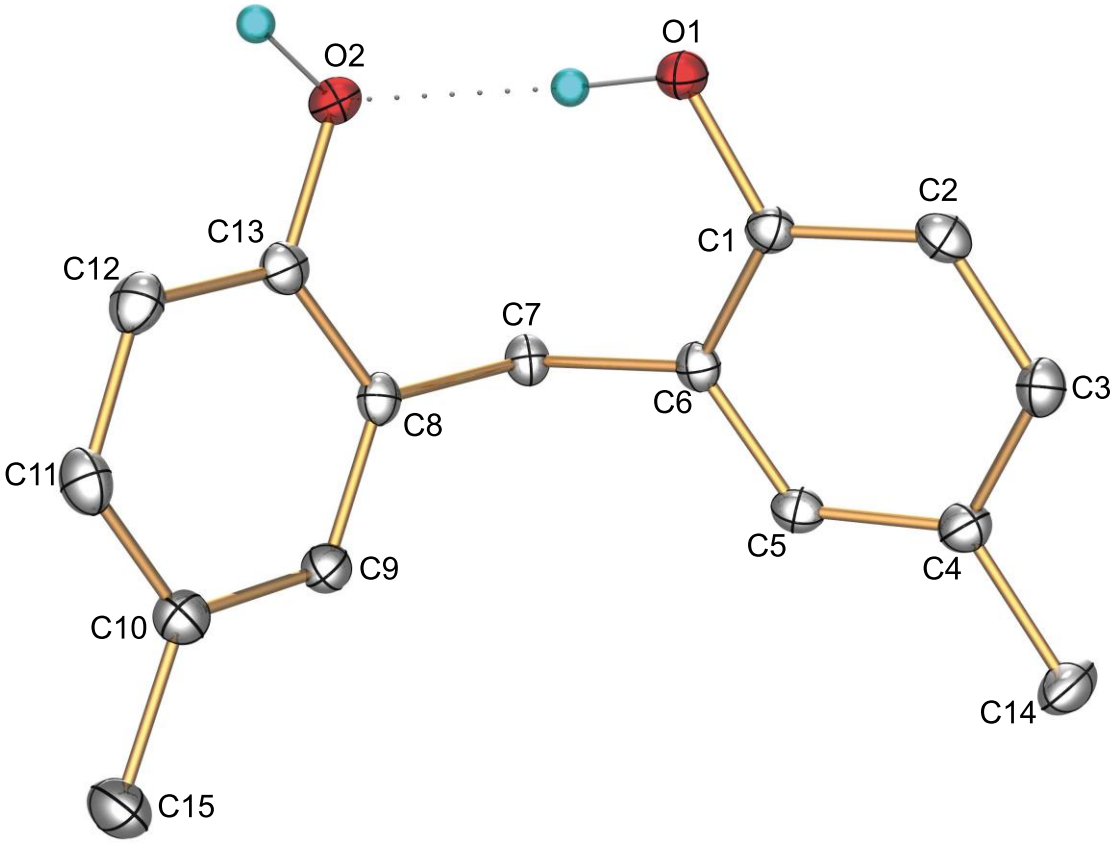

Figure 17. Molecular Structure of 2,2'-methylenebis(4-methylphenol) (**1**) (hydrogen atoms were omitted for clarity).

Table 10. Crystallographic data for 2,2'-methylenebis(4-methylphenol) (**1**).

Parameter	Value
Empirical formula	$C_{15}H_{16}O_2$
Formula weight	228.28
Temperature	100.0 K
Crystal system	Orthorhombic
Space group	$P2_12_12_1$
Unit cell dimensions	*a* = 8.0172(5) Å, α = 90 ° b = 10.6070(10) Å, β = 90 ° c = 14.4835(7) Å, γ = 90 °
Volume	1231.65(15) $Å^3$
Z	4
Density (calculated)	1.231 g/cm^3
Absorption coefficient μ	0.080 mm^{-1}
F(000)	488.0
Crystal size	0.1 × 0.1 × 0.05 mm^3
Radiation	MoKα (λ = 0.71073)
2Θ range for data collection	4.76 to 60.088 °
Index ranges	–10 ≤ h ≤ 11, –14 ≤ k ≤ 14, –20 ≤ l ≤ 18
Reflections collected	11016
Independent reflections	3418 [R_{int} = 0.0621, R_{sigma} = 0.0588]
Data / restraints / parameters	3418/0/164
Goodness-of-fit on F^2	1.039
Final R indices [I>2σ (I)]	R_1 = 0.0437, wR_2 = 0.1017
Final R indices [all data]	R_1 = 0.0546, wR_2 = 0.1115
Largest diff. peak and hole	0.24/–0.29 $eÅ^{-3}$
Absolute structure parameter	–0.9(8)

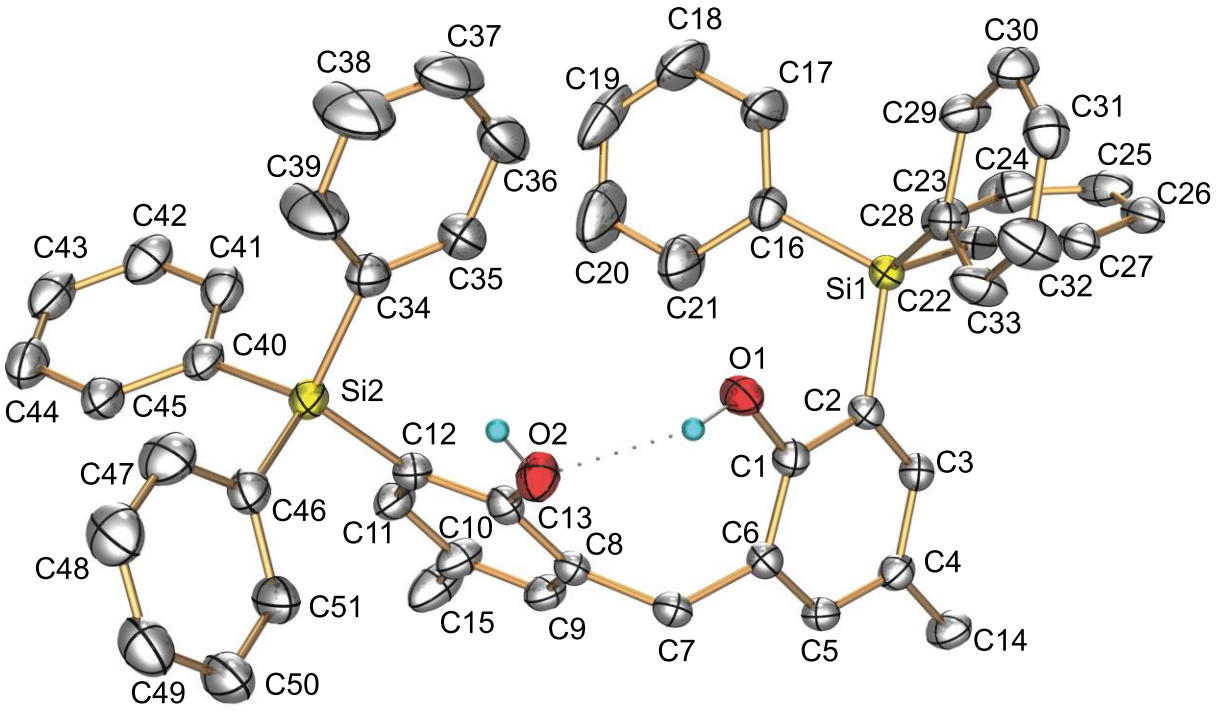

Figure 18. Molecular Structure of 6,6'-methylenebis(4-methyl-2-(triphenylsilyl)phenol) (**6**) (hydrogen atoms were omitted for clarity).

Table 11. Crystallographic data for 6,6'-methylenebis(4-methyl-2-(triphenylsilyl)phenol) (**6**).

Parameter	Value
Empirical formula	$C_{51}H_{44}O_2Si_2$
Formula weight	745.04
Temperature	100.0 K
Crystal system	Triclinic
Space group	P-1
Unit cell dimensions	*a* = 9.4864(8) Å, α = 79.762 ° b = 9.7347(7) Å, β = 87.043 ° c = 23.6097(16) Å, γ = 68.480 °
Volume	1995.8(3) $Å^3$
Z	2
Density (calculated)	1.240 g/cm^3
Absorption coefficient μ	0.130 mm^{-1}
F(000)	788.0
Crystal size	0.303 × 0.137 × 0.069 mm^3
Radiation	MoKα (λ = 0.71073)
2Θ range for data collection	4.566 to 60.116 °
Index ranges	–13 ≤ h ≤ 13, –13 ≤ k ≤ 13, –33 ≤ l ≤ 33
Reflections collected	49858
Independent reflections	11670 [R_{int} = 0.0775, R_{sigma} = 0.0695]
Data / restraints / parameters	11670/0/506
Goodness-of-fit on F^2	1.029
Final R indices [I>2σ (I)]	R_1 = 0.0665, wR_2 = 0.1346
Final R indices [all data]	R_1 = 0.1163, wR_2 = 0.1611
Largest diff. peak and hole	0.65/–0.39 $eÅ^{-3}$

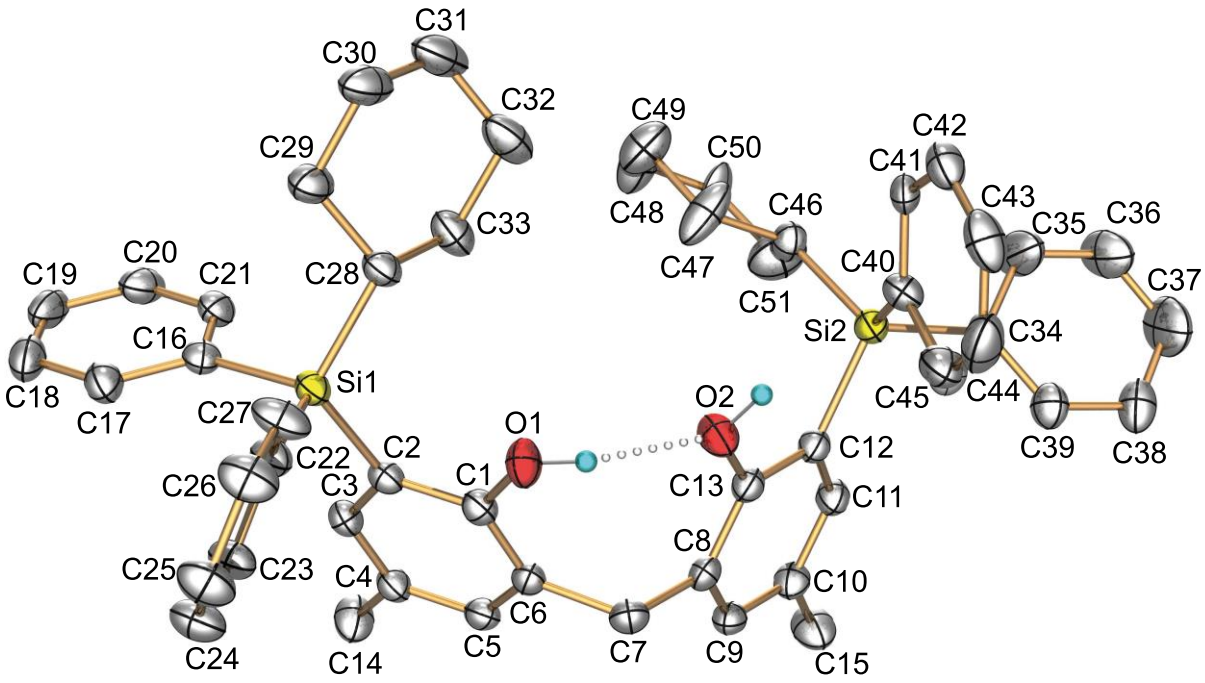

Figure 19. Molecular Structure of 6,6'-methylenebis(2-(cyclohexyldiphenylsilyl)-4-methylphenol) (**7**) (hydrogen atoms were omitted for clarity).

Table 12. Crystallographic data for 6,6'-methylenebis(2-(cyclohexyldiphenylsilyl)-4-methylphenol) (**7**).

Parameter	Value
Empirical formula	$C_{51}H_{56}O_2Si_2$
Formula weight	757.13
Temperature	100.0 K
Crystal system	Monoclinic
Space group	$P2_1/n$
Unit cell dimensions	*a* = 10.2760(4) Å, α = 90 ° b = 27.1685(10) Å, β = 96.6246(13) ° c = 15.1170(5) Å, γ = 90 °
Volume	4192.3(3) $Å^3$
Z	4
Density (calculated)	1.200 g/cm^3
Absorption coefficient μ	0.125 mm^{-1}
F(000)	1624.0
Crystal size	0.09 × 0.08 × 0.05 mm^3
Radiation	MoKα (λ = 0.71073)
2Θ range for data collection	4.262 to 60.154 °
Index ranges	–14 ≤ h ≤ 14, –38 ≤ k ≤ 38, –21 ≤ l ≤21
Reflections collected	67451
Independent reflections	12087 [R_{int} = 0.1348, R_{sigma} = 0.0953]
Data / restraints / parameters	12087/12/566
Goodness-of-fit on F^2	1.086
Final R indices [I>2σ (I)]	R_1 = 0.0764, wR_2 = 0.1361
Final R indices [all data]	R_1 = 0.1523, wR_2 = 0.1639
Largest diff. peak and hole	0.36/–0,41 $eÅ^{-3}$

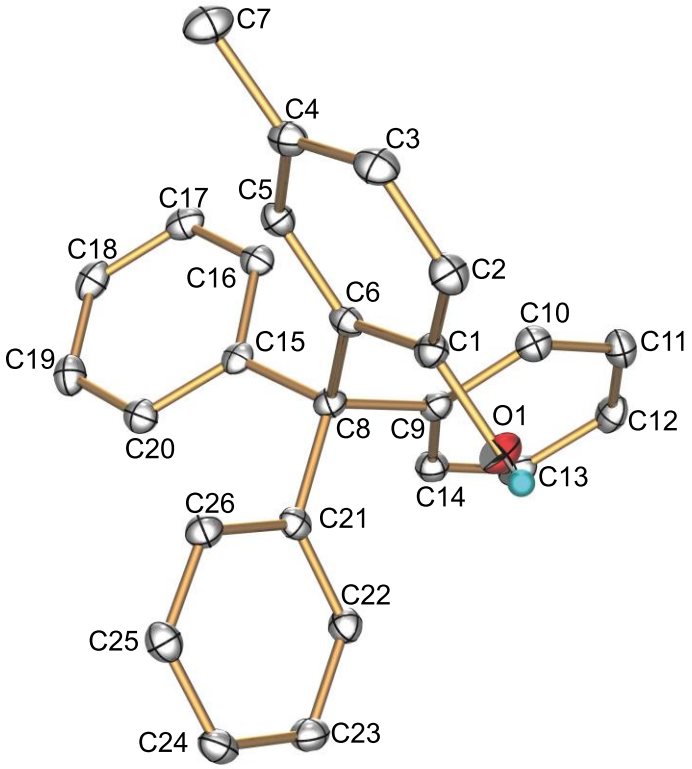

Figure 20. Molecular Structure of 4-methyl-2-tritylphenol (**9**) (solvent molecules and hydrogen atoms were omitted for clarity).

Table 13. Crystalographic data for 4-methyl-2-tritylphenol (**9**).

Parameter	Value
Empirical formula	$C_{27}H_{26}O_2$
Formula weight	382.48
Crystal system	Triclinic
Space group	P-1
Unit cell dimensions	*a* = 9.2603(8) Å, α = 106.902(3) ° b = 10.7016(8) Å, β = 92.544(5) ° c = 11.0787(13) Å, γ = 98.689(4) °
Volume	1033.89(17) $Å^3$
Z	2
Density (calculated)	1.229 g/cm^3
Absorption coefficient μ	0.076 mm^{-1}
F(000)	408.0
Crystal size	0.12 × 0.1 × 0.05 mm^3
Radiation	MoKα (λ = 0.71073)
2Θ range for data collection	4.47 to 50.698 °
Index ranges	–11 ≤ h ≤ 11, –12 ≤ k ≤ 12, –13 ≤ l ≤ 13
Reflections collected	18671
Independent reflections	3767 [R_{int} = 0.0474, R_{sigma} = 0.0347]
Data / restraints / parameters	3767/0/266
Goodness-of-fit on F^2	1.038
Final R indices [I>2σ (I)]	R_1 = 0.0365, wR_2 = 0.869
Final R indices [all data]	R_1 = 0.0441, wR_2 = 0.0925
Largest diff. peak and hole	0.25/–0.21 $eÅ^{-3}$

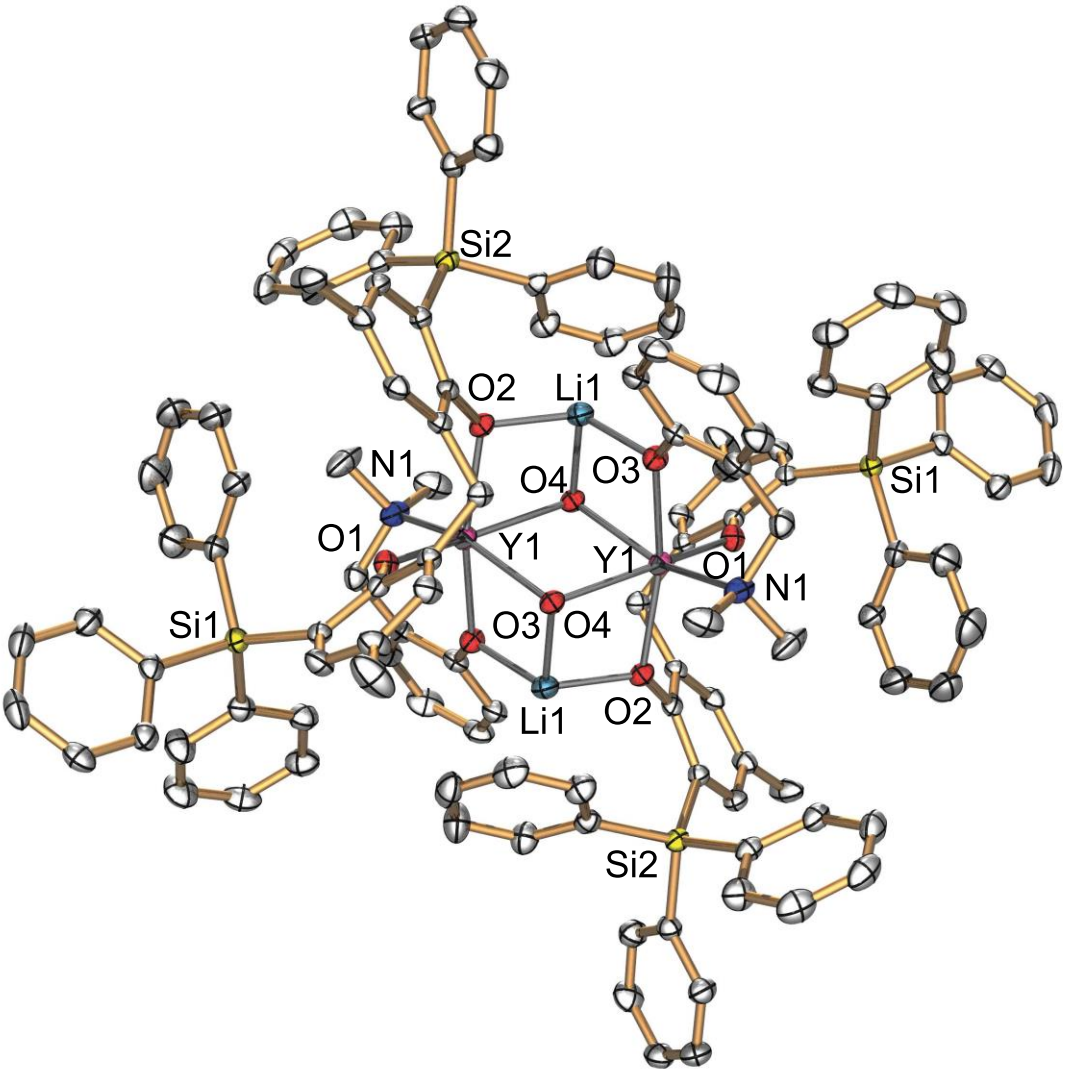

Figure 21. Molecular Structure of **13-Y** (solvent molecules and hydrogen atoms were omitted for clarity).

Table 14. Crystallographic data for **13-Y**.

Parameter	Value
Empirical formula	$C_{126}H_{114}Li_{1.98}N_2O_8Si_4Y_2$
Formula weight	2088.07
Temperature	125.00 K
Crystal system	Monoclinic
Space group	$P2_1/n$
Unit cell dimensions	*a* = 17.9228(5) Å, α = 90 ° b = 18.7188(4) Å, β = 114.3280(10) ° c =17.9246(4) Å, γ = 90°
Volume	5479.6(2) $Å^3$
Z	2
Density (calculated)	1.266 g/cm^3
Absorption coefficient μ	1.156 mm^{-1}
F(000)	2176.0
Crystal size	0.131 × 0.072 × 0.031 mm^3
Radiation	MoKα (λ = 0.71073)
2Θ range for data collection	4.722 to 60.442 °
Index ranges	–25 ≤ h ≤ 17, –24 ≤ k ≤ 26, –23 ≤ l ≤ 25
Reflections collected	38682
Independent reflections	15832 [R_{int} = 0.0755, R_{sigma} = 0.1289]
Data / restraints / parameters	15832/0/648
Goodness-of-fit on F^2	0.941
Final R indices [I>2σ (I)]	R_1 = 0.0504, wR_2 = 0.1116
Final R indices [all data]	R_1 = 0.1126, wR_2 = 0.1269
Largest diff. peak and hole	0.54/–0.75 $eÅ^{-3}$

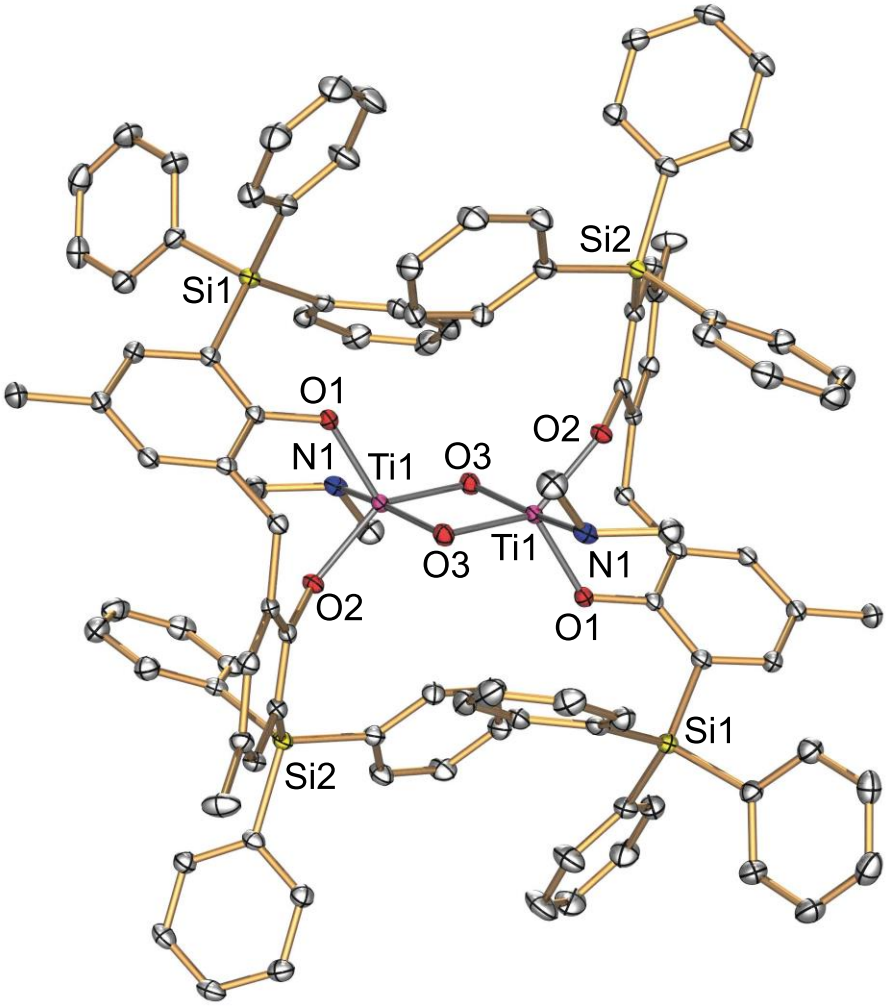

Figure 22. Molecular Structure of **23-Ti** (solvent molecules and hydrogen atoms were omitted for clarity).

Table 15. Crystallographic data for **23-Ti**.

Parameter	Value
Empirical formula	$C_{122}H_{130}N_2O_{10}Si_4Ti_2$
Formula weight	1992.43
Temperature	100.0 K
Crystal system	Triclinic
Space group	P-1
Unit cell dimensions	*a* = 13.1313(5) Å, α = 102.189(4) ° b = 13.8973(5) Å, β = 113.890(2) ° c = 16.0742(11) Å, γ = 94.062(3) °
Volume	2581.2(2) $Å^3$
Z	1
Density (calculated)	1.282 g/cm^3
Absorption coefficient μ	0.264 mm^{-1}
F(000)	1056.0
Crystal size	0.19 × 0.14 × 0.131 mm^3
Radiation	MoKα (λ = 0.71073)
2Θ range for data collection	4.18 to 60.272 °
Index ranges	–18 ≤ h ≤ 18, –19 ≤ k ≤ 19, –22 ≤ l ≤ 22
Reflections collected	85274
Independent reflections	15145 [R_{int} = 0.0600, R_{sigma} = 0.0472]
Data / restraints / parameters	15145/1/641
Goodness-of-fit on F^2	1.066
Final R indices [I>2σ (I)]	R_1 = 0.0418, wR_2 = 0.1020
Final R indices [all data]	R_1 = 0.0691, wR_2 = 0.1103
Largest diff. peak and hole	0.54/–0.45 $eÅ^{-3}$

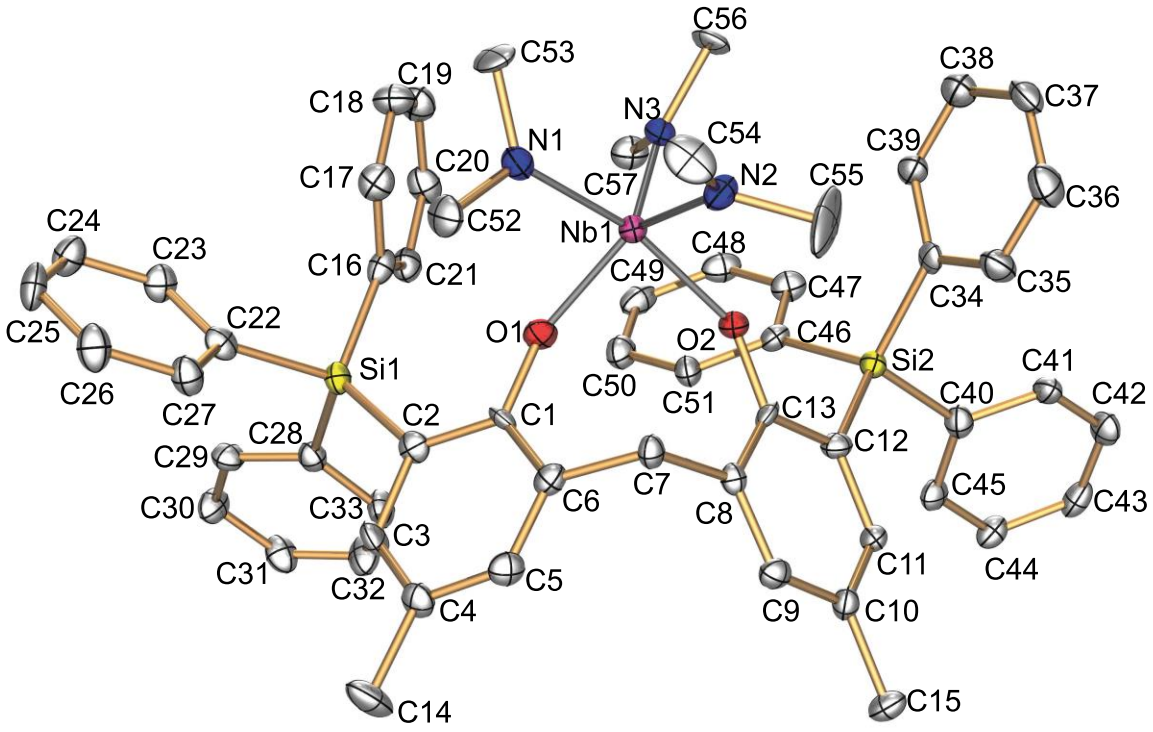

Figure 23. Molecular Structure of **29-Nb** (solvent molecules and hydrogen atoms were omitted for clarity).

Table 16. Crystallographic data for **29-Nb**.

Parameter	Value
Empirical formula	$C_{69}H_{72}N_3NbO_2Si_2$
Formula weight	1124.38
Temperature	100.0 K
Crystal system	Monoclinic
Space group	$P2_1/n$
Unit cell dimensions	*a* = 11.7857(2) Å, α = 90 ° b = 26.3939(5) Å, β = 99.505(2) ° c = 21.4503(5) Å, γ = 90°
Volume	6581.0(2) $Å^3$
Z	4
Density (calculated)	1.135 g/cm^3
Absorption coefficient μ	2.165 mm^{-1}
F(000)	2368.0
Crystal size	0.1 × 0.08 × 0.05 mm^3
Radiation	CuKα (λ = 1.54186)
2Θ range for data collection	5.354 to 137.094 °
Index ranges	–8 ≤ h ≤ 14, –31 ≤ k ≤ 25, –25 ≤ l ≤ 18
Reflections collected	39565
Independent reflections	11968 [R_{int} = 0.0538, R_{sigma} = 0.0564]
Data / restraints / parameters	11968/0/702
Goodness-of-fit on F^2	1.065
Final R indices [I>2σ (I)]	R_1 = 0.0559, wR_2 = 0.1311
Final R indices [all data]	R_1 = 0.0811, wR_2 = 0.1537
Largest diff. peak and hole	0.61/–1.10 $eÅ^{-3}$

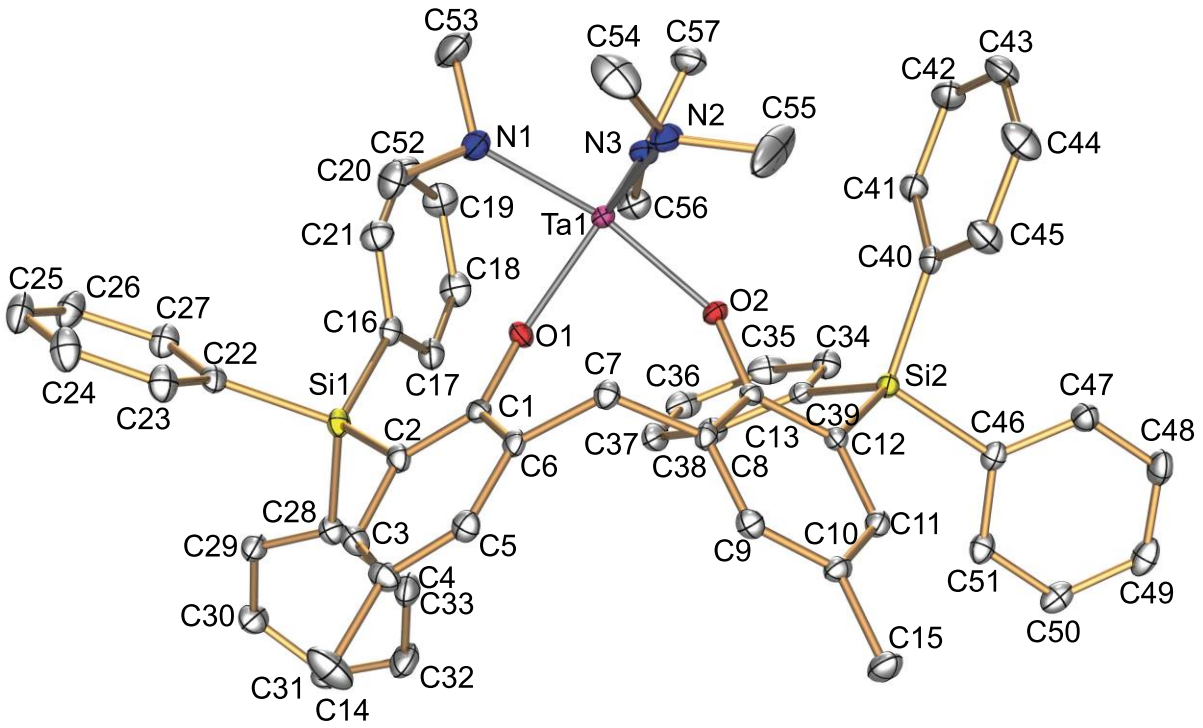

Figure 24. Molecular Structure of **31-Ta** (solvent molecules and hydrogen atoms were omitted for clarity).

Table 17. Crystallographic data for **31-Ta**.

Parameter	Value
Empirical formula	$C_{76.5}H_{79.5}N_3O_2Si_2Ta$
Formula weight	1310.06
Temperature	100.0 K
Crystal system	Monoclinic
Space group	$P2_1/n$
Unit cell dimensions	*a* = 11.7954(2) Å, α = 90 ° b = 26.3802(5) Å, β = 99.4300(10) ° c = 21.4432(7) Å, γ = 90 °
Volume	6582.2(3) Å^3
Z	4
Density (calculated)	1.322 g/cm^3
Absorption coefficient μ	1.755 mm^{-1}
F(000)	2706.0
Crystal size	0.161 × 0.078 × 0.047 mm^3
Radiation	MoKα (λ = 0.71073)
2Θ range for data collection	3.638 to 56.564 °
Index ranges	–15 ≤ h ≤ 15, –35 ≤ k ≤ 35, –28 ≤ l ≤ 28
Reflections collected	178449
Independent reflections	16339 [R_{int} = 0.0579, R_{sigma} = 0.0297]
Data / restraints / parameters	16339/936/946
Goodness-of-fit on F^2	1.072
Final R indices [I>2σ (I)]	R_1 = 0.0242, wR_2 = 0.0580
Final R indices [all data]	R_1 = 0.0346, wR_2 = 0.0600
Largest diff. peak and hole	0.73/–1.04 eÅ^{-3}

5.5 Catalytic studies

5.5.1 General procedure for catalytic intramolecular hydroamination reactions (GP2)

In the glovebox, a screw cap NMR tube was charged with 500 µL of the appropriate deuterated solvent (C_6D_6 or toluene-d_8) and 80 µL of the 0.75M solution of the appropriate aminoalkane in C_6D_6. Next, 1–4 mg ferrocene was added, and the NMR tube was closed, sealed with Teflon band, taken out of the glovebox and ^{1}H and ^{13}C NMR spectra of the sample were measured. Subsequently, inside the glovebox, 20–50 µL of the 0.06M solution of the appropriate catalyst in C_6D_6 was added to achieve 2–5 mol% catalyst loading, and the NMR tube was taken out of the glovebox and placed in an oil bath or kept at room temperature. The reaction progress was monitored by using ^{1}H-NMR spectroscopy, whereas the conversion was measured as a function of a decrease of olefinic peak area relative to the ferrocene internal standard.

Substrates, 2,2-diphenylpent-4-en-1-amine,[94] (1-allylcyclohexyl)methanamine,[95] 2,2-diphenylhex-5-en-1-amine[94] were synthesised previously by former group members according to literature procedures. The substrate stock solutions were prepared in the following way: 125 µL of (1-allylcyclohexyl)methanamine (0.115 g, 0.750 mmol) was taken in a screw cap vial and 875 µL of C_6D_6 was added. 2,2-diphenylpent-4-en-1-amine (0.356 g, 1.50 mmol) and 2,2-diphenylhex-5-en-1-amine (0.377 g, 1.50 mmol), were weighed in a 2.0 mL graduation flask and filled with C_6D_6. In the case of (1-allylcyclohexyl)methanamine and 2,2-diphenylhex-5-en-1-amine, it was resorted to additional purification of the stock solutions as stated in Table 19 and Table 20. The stock solutions were thus additionally dried over CaH_2 overnight, filtered and stored in the freezer inside the glovebox over 4 Å molecular sieves. Prior to each catalytic experiment, the appropriate stock solution was taken out from the freezer and was allowed to reach room temperature. Catalyst stock solutions were prepared as described in the general procedure (GP1) and stored in the freezer. Similarly, prior to each catalytic experiment, the appropriate catalyst stock solution was taken out of the freezer and allowed to reach room temperature.

5.5.2 Screening of reaction conditions

Samples for catalytic experiments were prepared according to the general procedure (GP2). Varied was the solvent, reaction temperature and catalyst loading. Moreover, upon realisation that varying the reaction conditions does not affect the conversion, additional drying step in the substrate preparation was introduced. It consisted of drying the stock solutions of substrates over CaH_2, followed by filtering of the drying agent as described in the general procedure (GP2).

More detailed information, including the comparison with other active catalysts are listed in section 3.3.1.

Table 18. Reaction conditions for intramolecular hydroamination of 2,2-diphenylpent-4-en-1-amine (**34**).

Entry	Catalyst	Cat. Loading	Solvent	Temperature	Reaction time	Conversion [a]
1	**17-Y**	2 mol%	C_6D_6	rt	25 h	Quant.
2	**17-Y**	5 mol%	toluene-d_8	100 °C	<10 min	Quant.
3	**17-Y**	5 mol%	C_6D_6	100 °C	<10 min	Quant.
4	**18-Y**	2 mol%	C_6D_6	rt	96 h	34 %
5	**18-Y**	5 mol%	toluene-d_8	100 °C	30 min	Quant.
6	**19-Y**	2 mol%	C_6D_6	rt	96 h	24 %
7	**19-Y**	5 mol%	toluene-d_8	100 °C	<10 min	55 %

[a]Conversion was determined using ^{1}H-NMR spectroscopy

Table 19. Reaction conditions for intramolecular hydroamination of 2,2-diphenylhex-5-en-1-amine (**39**).

Entry	Catalyst	Cat. Loading	Solvent	Temperature	Reaction time	Conversion [a]
1	**17-Y**	2 mol%	C_6D_6	60 °C	20 h	3 %
2	**17-Y**	5 mol%	C_6D_6	60 °C	24 h	6 %
3	**18-Y**	2 mol%	C_6D_6	60 °C	20 h	2 %
4	**19-Y**	2 mol%	C_6D_6	60 °C	20 h	28 %
Drying over CaH_2						
5	**17-Y**	5 mol%	C_6D_6	60 °C	48 h	32 %
6	**18-Y**	5 mol%	C_6D_6	60 °C	48 h	25 %
7	**19-Y**	5 mol%	C_6D_6	60 °C	48 h	7 %
Drying over CaH_2						
8	**17-Y**	5 mol%	toluene-d_8	100 °C	22 h	39 %
9	**18-Y**	5 mol%	toluene-d_8	100 °C	22 h	35 %
10	**19-Y**	5 mol%	toluene-d_8	100 °C	96 h	21 %

[a]Conversion was determined using ^{1}H-NMR spectroscopy

Table 20. Reaction conditions for intramolecular hydroamination of (1-allylcyclohexyl)methanamine (**37**).

Entry	Catalyst	Cat. Loading	Solvent	Temperature	Reaction time	Conversion [a]
1	**17-Y**	2 mol%	C_6D_6	rt	72 h	13 %
2	**18-Y**	2 mol%	C_6D_6	rt	72 h	13 %
3	**19-Y**	2 mol%	C_6D_6	rt	72 h	0 %
Drying over CaH_2						
4	**17-Y**	5 mol%	C_6D_6	60 °C	72 h	26 %
5	**18-Y**	5 mol%	C_6D_6	60 °C	22 h	6 %
6	**19-Y**	5 mol%	C_6D_6	60 °C	72 h	5 %
7	**17-Y**	5 mol%	toluene-d_8	100 °C	<30 min	Quant.
8	**17-Y**	5 mol%	C_6D_6	100 °C	<30 min	Quant.
9	**18-Y**	5 mol%	toluene-d_8	100 °C	<30 min	Quant.
10	**19-Y**	5 mol%	toluene-d_8	100 °C	72 h	8 %

[a]Conversion was determined using ^{1}H-NMR spectroscopy

5.5.3 Intramolecular Hydroamination of 2,2-diphenylpent-4-en-1-amine

*2,2-Diphenylpent-4-en-1-amine (**34**)*

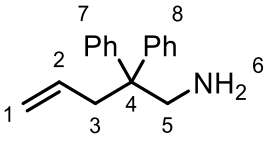

^{1}H NMR (400 MHz, Tol-d_8): δ = 7.11 – 6.98 (m, 10H, aryl-H), 5.40 (ddt, *J* = 17.2, 10.1, 7.1 Hz, 1H, H-2), 5.04 – 4.86 (m, 2H, H-1), 3.14 (s, 2H, H-5), 2.84 (dt, J = 7.1, 1.3 Hz, 2H, H-3), 0.32 (s, 2H, NH_2) ppm.

^{13}C NMR (101 MHz, Tol-d_8): δ = 147.5, 135.8, 129.0, 128.6, 126.5, 117.8, 51.9, 49.1 (C-5), 41.6 (C-3) ppm.

The NMR spectroscopic data is in agreement with the literature.[96]

*2-Methyl-4,4-diphenylpyrrolidine (**35**)*

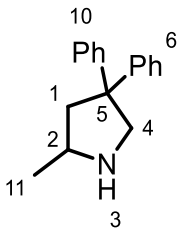

^{1}H NMR (400 MHz, Tol-d_8): δ = 7.21 – 7.10 (m, 4H, aryl-H), 7.08 – 7.05 (m, 3H, aryl-H), 7.04 – 6.96 (m, 3H, aryl-H), 3.48 (dd, *J* = 11.1, 5.9 Hz, 1H, H-4), 3.35 – 3.26 (m, 1H, H-4), 3.13 (s, 1H, H-2), 2.37 (dd, *J* = 12.4, 6.4 Hz, 1H, H-1), 1.79 (dd, *J* = 12.4, 9.2 Hz, 1H, H-1), 1.24 (s, 1H, NH), 1.02 (d, *J* = 6.3 Hz, 3H, H-11) ppm.

^{13}C NMR (101 MHz, Tol-d_8): δ = 149.2, 148.6, 129.6, 128.8, 127.94, 127.87, 126.42, 126.37, 59.1 (C-4), 57.7 (C-2), 53.6 (C-1), 48.0 (C-5), 22.9 (C-11) ppm.

The NMR spectroscopic data is in agreement with the literature.[96–98]

5.5.4 Intramolecular Hydroamination of 2,2-diphenylhex-5-en-1-amine

*2,2-Diphenylhex-5-en-1-amine (**39**)*

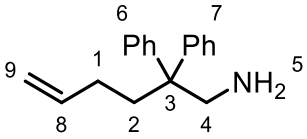

^{1}H NMR (600 MHz, Tol-d_8) : δ = 7.12 – 6.98 (m, 10H, aryl-H), 5.71 (ddt, *J* = 16.9, 10.2, 6.6 Hz, 1H, H-8), 4.97 – 4.88 (m, 2H, H-9), 3.09 (s, 2H, H-4), 2.19 – 2.15 (m, 2H, H-1), 1.75 (dtt, *J* = 10.5, 6.7, 1.4 Hz, 2H, H-2), 0.31 (s, 2H, NH_2) ppm.

^{13}C NMR (151 MHz, Tol-d_8): δ = 147.6, 139.7 (C-8), 129.0, 128.6, 126.5, 114.6 (C-9), 52.2 (C-4), 49.5 (C-3), 36.4 (C-2), 29.5 (C-1) ppm.

The NMR spectroscopic data is in agreement with the literature.[96]

*2-Methyl-5,5-diphenylpiperidine (**40**)*

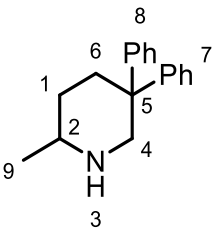

Full conversion of 2,2-diphenylhex-5-en-1-amine to 2-methyl-5,5-diphenylpiperidine was not achieved under any given reaction conditions, most certainly due to unknown (inorganic) impurities present in the substrate, that could not be removed, even after repeating the drying/purification step with stirring over CaH_2. Thus, no clean NMR spectrum was obtained.

5.5.5 Intramolecular Hydroamination of (1-allylcyclohexyl)methanamine

*(1-Allylcyclohexyl)methanamine (**37**)*

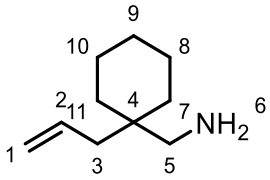

^{1}H NMR (700 MHz, Tol-d_8): δ = 5.73 (ddt, J = 16.3, 10.6, 7.5 Hz, 1H, H-2), 5.03 – 4.97 (m, 2H, H-1), 2.35 (s, 2H, H-5), 1.99 (d, J = 7.5 Hz, 2H, H-3), 1.34 (qd, J = 8.9, 4.0 Hz, 6H, Cy), 1.16 (q, J = 4.0 Hz, 4H, Cy), 0.40 (s, 1H, NH_2) ppm.

^{13}C NMR (176 MHz, Tol-d_8): δ = 136.1 (C-2), 116.9 (C-1), 49.2 (C-5), 40.5 (C-3), 37.7 (C-4), 33.8 (C-7, C-11), 27.3 (C-9), 27.2 (C-8, C-10) ppm.

The NMR spectroscopic data is in agreement with the literature.[96]

*3-Methyl-2-azaspiro[4.5]decane (**38**)*

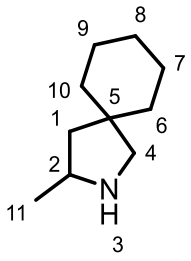

^{1}H NMR (400 MHz, Tol-d_8): δ = 2.98 (s, 1H, H-2), 2.70 (dd, *J* = 10.5, 4.7 Hz, 1H, H-4), 2.49 (t, *J* = 9.1 Hz, 1H, H-4), 1.55 (dd, *J* = 12.4, 6.7 Hz, 1H, H-1), 1.48 – 1.09 (m, 11H, Cy and NH), 1.05 (d, *J* = 6.3 Hz, 3H, H-11), 0.87 (dd, *J* = 12.3, 9.1 Hz, 1H, H-1) ppm.

^{13}C NMR (101 MHz, Tol-d_8) δ = 60.1 (C-4), 54.6 (C-2), 48.3 (C-1), 44.3 (C-5), 39.4 (Cy), 38.0 (Cy), 26.9 (Cy), 26.1 (Cy), 24.7 (Cy), 22.3 (C-11) ppm.

The NMR spectroscopic data is in agreement with the literature.[96,99]

6. References

(1) Reznichenko, A. L.; Nawara-Hultzsch, A. J.; Hultzsch, K. C. Asymmetric Hydroamination. In *Stereoselective Formation of Amines*; Li, W., Zhang, X., Eds.; Topics in Current Chemistry; Springer: Berlin, Heidelberg, 2014; pp 191–260. https://doi.org/10.1007/128_2013_500.

(2) Reznichenko, A. L.; Hultzsch, K. C. Early Transition Metal (Group 3–5, Lanthanides and Actinides) and Main Group Metal (Group 1, 2, and 13) Catalyzed Hydroamination. In *Hydrofunctionalization*; Ananikov, V. P., Tanaka, M., Eds.; Topics in Organometallic Chemistry; Springer: Berlin, Heidelberg, 2013; pp 51–114. https://doi.org/10.1007/3418_2011_22.

(3) Pohlki, F.; Doye, S. The Catalytic Hydroamination of Alkynes. *Chem. Soc. Rev.* **2003**, *32*, 104–114. https://doi.org/10.1039/b200386b.

(4) Ricci, A. *Amino Group Chemistry: From Synthesis to the Life Sciences*; Wiley-VCH: Weinheim, 2008.

(5) O´Neil, M. J. *The Merck Index: An Encyclopedia of Chemicals, Drugs, and Biologicals*, 15th ed.; Royal Society Of Chemistry, 2013.

(6) Müller, T. E.; Hultzsch, K. C.; Yus, M.; Foubelo, F.; Tada, M. Hydroamination: Direct Addition of Amines to Alkenes and Alkynes. *Chem. Rev.* **2008**, *108*, 3795–3892. https://doi.org/10.1021/cr0306788.

(7) Streiff, S.; Jérôme, F. Hydroamination of Non-Activated Alkenes with Ammonia: A Holy Grail in Catalysis. *Chem. Soc. Rev.* **2021**, *50*, 1512–1521. https://doi.org/10.1039/C9CS00873J.

(8) Amines Market Size, Share | Global Industry Analysis Report, 2025 https://www.grandviewresearch.com/industry-analysis/amines-industry (accessed 2021 -07 -06).

(9) Scriven, E. F. V.; Turnbull, K. Azides: Their Preparation and Synthetic Uses. *Chem. Rev.* **1988**, *88*, 297–368. https://doi.org/10.1021/cr00084a001.

(10) Blažević, N.; Kolbah, D.; Belin, B.; Šunjić, V.; Kajfež, F. Hexamethylenetetramine, A Versatile Reagent in Organic Synthesis. *Synthesis* **1979**, 161–176. https://doi.org/10.1055/s-1979-28602.

(11) Lapina, I. M.; Pevzner, L. M.; Potekhin, A. A. Reactions of Alkyl (Halomethyl)Furancarboxylates with Hexamethylenetetramine. *Russ. J. Gen. Chem.* **2006**, *76*, 1304–1309. https://doi.org/10.1134/S1070363206080251.

(12) Le, Z.-G.; Chen, Z.-C.; Hu, Y.; Zheng, Q.-G. Organic Reactions in Ionic Liquids: N-Alkylation of Phthalimide and Several Nitrogen Heterocycles. *Synthesis* **2004**, 208–212. https://doi.org/10.1055/s-2003-44383.

(13) Fletcher, S. The Mitsunobu Reaction in the 21 st Century. *Org. Chem. Front.* **2015**, *2*, 739–752. https://doi.org/10.1039/C5QO00016E.

(14) Gololobov, Y. G.; Kasukhin, L. F. Recent Advances in the Staudinger Reaction. *Tetrahedron* **1992**, *48*, 1353–1406. https://doi.org/10.1016/S0040-4020(01)92229-X.

(15) Wallace, K. J.; Hanes, R.; Anslyn, E.; Morey, J.; Kilway, K. V.; Siegel, J. Preparation of 1,3,5-Tris(Aminomethyl)-2,4,6-Triethylbenzene from Two Versatile 1,3,5-Tri(Halosubstituted) 2,4,6-Triethylbenzene Derivatives. *Synthesis* **2005**, 2080–2083. https://doi.org/10.1055/s-2005-869963.

(16) Podyacheva, E.; Afanasyev, O. I.; Tsygankov, A. A.; Makarova, M.; Chusov, D. Hitchhiker's Guide to Reductive Amination. *Synthesis* **2019**, *51*, 2667–2677. https://doi.org/10.1055/s-0037-1611788.

(17) Green, J. E.; Bender, D. M.; Jackson, S.; O'Donnell, M. J.; McCarthy, J. R. Mitsunobu Approach to the Synthesis of Optically Active α,α-Disubstituted Amino Acids. *Org. Lett.* **2009**, *11*, 807–810. https://doi.org/10.1021/ol802325h.

(18) Li, Y.; Marks, T. J. Organolanthanide-Catalyzed Intra- and Intermolecular Tandem C−N and C−C Bond-Forming Processes of Aminodialkenes, Aminodialkynes, Aminoalkeneynes, and Aminoalkynes. New Regiospecific Approaches to Pyrrolizidine, Indolizidine, Pyrrole, and Pyrazine Skeletons. *J. Am. Chem. Soc.* **1998**, *120*, 1757–1771. https://doi.org/10.1021/ja972643t.
(19) Gagné, M. R.; Stern, C. L.; Marks, T. J. Organolanthanide-Catalyzed Hydroamination. A Kinetic, Mechanistic, and Diastereoselectivity Study of the Cyclization of N-Unprotected Amino Olefins. *J. Am. Chem. Soc.* **1992**, *114*, 275–294. https://doi.org/10.1021/ja00027a036.
(20) Hong, S.; Marks, T. J. Organolanthanide-Catalyzed Hydroamination. *Acc. Chem. Res.* **2004**, *37*, 673–686. https://doi.org/10.1021/ar040051r.
(21) Johns, A. M.; Sakai, N.; Ridder, A.; Hartwig, J. F. Direct Measurement of the Thermodynamics of Vinylarene Hydroamination. *J. Am. Chem. Soc.* **2006**, *128*, 9306–9307. https://doi.org/10.1021/ja062773e.
(22) Müller, T. E.; Beller, M. Metal-Initiated Amination of Alkenes and Alkynes. *Chem. Rev.* **1998**, *98*, 675–704. https://doi.org/10.1021/cr960433d.
(23) Gagné, M. R.; Nolan, S. P.; Marks, T. J. Organolanthanide-Centered Hydroamination/Cyclization of Aminoolefins. Expedient Oxidative Access to Catalytic Cycles. *Organometallics* **1990**, *9*, 1716–1718. https://doi.org/10.1021/om00156a005.
(24) Gagné, M. R.; Marks, T. J. Organolanthanide-Catalyzed Hydroamination. Facile, Regiospecific Cyclization of Unprotected Amino Olefins. *J. Am. Chem. Soc.* **1989**, *111*, 4108–4109. https://doi.org/10.1021/ja00193a056.
(25) Li, Y.; Marks, T. J. Organolanthanide-Catalyzed Intramolecular Hydroamination/Cyclization of Aminoalkynes. *J. Am. Chem. Soc.* **1996**, *118*, 9295–9306. https://doi.org/10.1021/ja9612413.
(26) Ryu, J.-S.; Li, G. Y.; Marks, T. J. Organolathanide-Catalyzed Regioselective Intermolecular Hydroamination of Alkenes, Alkynes, Vinylarenes, Di- and Trivinylarenes, and Methylenecyclopropanes. Scope and Mechanistic Comparison to Intramolecular Cyclohydroaminations. *J. Am. Chem. Soc.* **2003**, *125*, 12584–12605. https://doi.org/10.1021/ja035867m.
(27) Haggin, J. Chemists Seek Greater Recognition for Catalysis. *Chem. Eng. News* **1993**, *71* (22), 23–27. https://doi.org/10.1021/cen-v071n022.p023.
(28) Reznichenko, A. L.; Hultzsch, K. C. Hydroamination of Alkenes. In *Organic Reactions*; John Wiley & Sons, Inc., Ed.; John Wiley & Sons, Inc.: Hoboken, NJ, USA, 2015; pp 1–554. https://doi.org/10.1002/0471264180.or088.01.
(29) Beller, M.; Breindl, C. Base-Catalyzed Hydroamination of Aromatic Olefins-an Efficient Route to 1-Aryl-4-(Arylethyl)Piperazines. *Tetrahedron* **1998**, *54*, 6359–6368. https://doi.org/10.1016/S0040-4020(98)00295-6.
(30) Giardello, M. A.; Conticello, V. P.; Brard, L.; Gagné, M. R.; Marks, T. J. Chiral Organolanthanides Designed for Asymmetric Catalysis. A Kinetic and Mechanistic Study of Enantioselective Olefin Hydroamination/Cyclization and Hydrogenation by C1-Symmetric Me2Si(Me4C5)(C5H3R*)Ln Complexes Where R* = Chiral Auxiliary. *J. Am. Chem. Soc.* **1994**, *116*, 10241–10254. https://doi.org/10.1021/ja00101a048.
(31) Bytschkov, I.; Doye, S. Group-IV Metal Complexes as Hydroamination Catalysts. *Eur. J. Org. Chem.* **2003**, 935–946. https://doi.org/10.1002/ejoc.200390149.
(32) Gribkov, D. V.; Hultzsch, K. C. Hydroamination/Cyclization of Aminoalkenes Using Cationic Zirconocene and Titanocene Catalysts. *Angew. Chem. Int. Ed.* **2004**, *43*, 5542–5546. https://doi.org/10.1002/anie.200460880.
(33) Hesp, K. D.; Stradiotto, M. Rhodium- and Iridium-Catalyzed Hydroamination of Alkenes. *ChemCatChem* **2010**, *2*, 1192–1207. https://doi.org/10.1002/cctc.201000102.
(34) Roesky, P. W.; Müller, T. E. Enantioselective Catalytic Hydroamination of Alkenes. *Angew. Chem. Int. Ed.* **2003**, *42*, 2708–2710. https://doi.org/10.1002/anie.200301637.

(35) Hong, S.; Kawaoka, A. M.; Marks, T. J. Intramolecular Hydroamination/Cyclization of Conjugated Aminodienes Catalyzed by Organolanthanide Complexes. Scope, Diastereo- and Enantioselectivity, and Reaction Mechanism. *J. Am. Chem. Soc.* **2003**, *125*, 15878–15892. https://doi.org/10.1021/ja036266y.
(36) Noyori, R. Asymmetric Catalysis: Science and Opportunities (Nobel Lecture). *Angew. Chem. Int. Ed.* **2002**, *41*, 2008–2022. https://doi.org/10.1002/1521-3773(20020617)41:12<2008::AID-ANIE2008>3.0.CO;2-4.
(37) Ananikov, V. P.; Beletskaya, I. P. Alkyne and Alkene Insertion into Metal–Heteroatom and Metal–Hydrogen Bonds: The Key Stages of Hydrofunctionalization Process. In *Hydrofunctionalization*; Ananikov, V. P., Tanaka, M., Eds.; Topics in Organometallic Chemistry; Springer: Berlin, Heidelberg, 2013; pp 1–19. https://doi.org/10.1007/3418_2012_54.
(38) Kim, H.-S.; Livinghouse, T.; SeoMoon, D.; Lee, P.-H. Intramolecular Hydroaminations of Aminoalkynes Catalyzed by Yttrium Complexes and Aminoallenes Catalyzed by Zirconium Complexes. *Bull. Korean Chem. Soc.* **2007**, *28*, 1127–1134. https://doi.org/10.5012/bkcs.2007.28.7.1127.
(39) Kim, H.; Livinghouse, T.; Lee, P. H. Efficient Intramolecular Hydroamination of Aminoalkynes Catalyzed by a Zirconium(IV) Complex. *Tetrahedron* **2008**, *64*, 2525–2529. https://doi.org/10.1016/j.tet.2008.01.031.
(40) Majumder, S.; Odom, A. L. Group-4 Dipyrrolylmethane Complexes in Intramolecular Olefin Hydroamination. *Organometallics* **2008**, *27*, 1174–1177. https://doi.org/10.1021/om700883a.
(41) Bexrud, J. A.; Beard, J. D.; Leitch, D. C.; Schafer, L. L. Intramolecular Hydroamination of Unactived Olefins with Ti(NMe2)4 as a Precatalyst. *Org. Lett.* **2005**, *7*, 1959–1962. https://doi.org/10.1021/ol0503992.
(42) Manna, K.; Ellern, A.; Sadow, A. D. A Zwitterionic Zirconium Complex That Catalyzes Hydroamination of Aminoalkenes at Room Temperature. *Chem. Commun.* **2009**, *46*, 339–341. https://doi.org/10.1039/B918989K.
(43) Manna, K.; Xu, S.; Sadow, A. D. A Highly Enantioselective Zirconium Catalyst for Intramolecular Alkene Hydroamination: Significant Isotope Effects on Rate and Stereoselectivity. *Angew. Chem. Int. Ed.* **2011**, *50*, 1865–1868. https://doi.org/10.1002/anie.201006163.
(44) Gribkov, D. V.; Hultzsch, K. C.; Hampel, F. 3,3‘-Bis(Trisarylsilyl)-Substituted Binaphtholate Rare Earth Metal Catalysts for Asymmetric Hydroamination. *J. Am. Chem. Soc.* **2006**, *128*, 3748–3759. https://doi.org/10.1021/ja058287t.
(45) Reznichenko, A. L.; Nguyen, H. N.; Hultzsch, K. C. Asymmetric Intermolecular Hydroamination of Unactivated Alkenes with Simple Amines. *Angew. Chem. Int. Ed.* **2010**, *49*, 8984–8987. https://doi.org/10.1002/anie.201004570.
(46) Reznichenko, A. L.; Hultzsch, K. C. C1-Symmetric Rare-Earth-Metal Aminodiolate Complexes for Intra- and Intermolecular Asymmetric Hydroamination of Alkenes. *Organometallics* **2013**, *32*, 1394–1408. https://doi.org/10.1021/om3010614.
(47) Tokunaga, M.; Eckert, M.; Wakatsuki, Y. Ruthenium-Catalyzed Intermolecular Hydroamination of Terminal Alkynes with Anilines: A Practical Synthesis of Aromatic Ketimines. *Angew. Chem. Int. Ed.* **1999**, *38*, 3222–3225. https://doi.org/10.1002/(SICI)1521-3773(19991102)38:21<3222::AID-ANIE3222>3.0.CO;2-7.
(48) Kawatsura, M.; Hartwig, J. F. Palladium-Catalyzed Intermolecular Hydroamination of Vinylarenes Using Arylamines. *J. Am. Chem. Soc.* **2000**, *122*, 9546–9547. https://doi.org/10.1021/ja002284t.
(49) Julian, L. D.; Hartwig, J. F. Intramolecular Hydroamination of Unbiased and Functionalized Primary Aminoalkenes Catalyzed by a Rhodium Aminophosphine Complex. *J. Am. Chem. Soc.* **2010**, *132*, 13813–13822. https://doi.org/10.1021/ja1052126.

(50) Liu, Z.; Hartwig, J. F. Mild, Rhodium-Catalyzed Intramolecular Hydroamination of Unactivated Terminal and Internal Alkenes with Primary and Secondary Amines. *J. Am. Chem. Soc.* **2008**, *130*, 1570–1571. https://doi.org/10.1021/ja710126x.
(51) Hong, S.; Marks, T. J. Highly Stereoselective Intramolecular Hydroamination/Cyclization of Conjugated Aminodienes Catalyzed by Organolanthanides. *J. Am. Chem. Soc.* **2002**, *124*, 7886–7887. https://doi.org/10.1021/ja020226x.
(52) Arredondo, V. M.; Tian, S.; McDonald, F. E.; Marks, T. J. Organolanthanide-Catalyzed Hydroamination/Cyclization. Efficient Allene-Based Transformations for the Syntheses of Naturally Occurring Alkaloids. *J. Am. Chem. Soc.* **1999**, *121*, 3633–3639. https://doi.org/10.1021/ja984305d.
(53) Gagné, M. R.; Brard, L.; Conticello, V. P.; Giardello, M. A.; Stern, C. L.; Marks, T. J. Stereoselection Effects in the Catalytic Hydroamination/Cyclization of Amino Olefins at Chiral Organolanthanide Centers. *Organometallics* **1992**, *11*, 2003–2005. https://doi.org/10.1021/om00042a012.
(54) Tian, S.; Arredondo, V. M.; Stern, C. L.; Marks, T. J. Constrained Geometry Organolanthanide Catalysts. Synthesis, Structural Characterization, and Enhanced Aminoalkene Hydroamination/Cyclization Activity. *Organometallics* **1999**, *18*, 2568–2570. https://doi.org/10.1021/om990146a.
(55) Bürgstein, M. R.; Berberich, H.; Roesky, P. W. (Aminotroponiminato)Yttrium Amides as Catalysts in Alkyne Hydroamination. *Organometallics* **1998**, *17*, 1452–1454. https://doi.org/10.1021/om9711077.
(56) Roesky, P. W. The Co-Ordination Chemistry of Aminotroponiminates. *Chem. Soc. Rev.* **2000**, *29*, 335–345. https://doi.org/10.1039/A906763I.
(57) Bürgstein, M. R.; Berberich, H.; Roesky, P. W. Homoleptic Lanthanide Amides as Homogeneous Catalysts for Alkyne Hydroamination and the Tishchenko Reaction. *Chem. – Eur. J.* **2001**, *7*, 3078–3085. https://doi.org/10.1002/1521-3765(20010716)7:14<3078::AID-CHEM3078>3.0.CO;2-E.
(58) Li, Y.; Marks, T. J. Diverse Mechanistic Pathways and Selectivities in Organo-f-Element-Catalyzed Hydroamination. Intermolecular Organolanthanide-Catalyzed Alkyne and Alkene Hydroamination. *Organometallics* **1996**, *15*, 3770–3772. https://doi.org/10.1021/om960293y.
(59) Giardello, M. A.; Conticello, V. P.; Brard, L.; Sabat, M.; Rheingold, A. L.; Stern, C. L.; Marks, T. J. Chiral Organolanthanides Designed for Asymmetric Catalysis. Synthesis, Characterization, and Configurational Interconversions of Chiral, C1-Symmetric Organolanthanide Halides, Amides, and Hydrocarbyls. *J. Am. Chem. Soc.* **1994**, *116*, 10212–10240. https://doi.org/10.1021/ja00101a047.
(60) O'Shaughnessy, P. N.; Scott, P. Biaryl Amine Ligands for Lanthanide Catalysed Enantioselective Hydroamination/Cyclisation of Aminoalkenes. *Tetrahedron Asymmetry* **2003**, *14*, 1979–1983. https://doi.org/10.1016/S0957-4166(03)00429-4.
(61) Hultzsch, K. C.; Hampel, F.; Wagner, T. New Yttrium Complexes Bearing Diamidoamine Ligands as Efficient and Diastereoselective Catalysts for the Intramolecular Hydroamination of Alkenes and Alkynes. *Organometallics* **2004**, *23*, 2601–2612. https://doi.org/10.1021/om030679q.
(62) Nguyen, H. N.; Lee, H.; Audörsch, S.; Reznichenko, A. L.; Nawara-Hultzsch, A. J.; Schmidt, B.; Hultzsch, K. C. Asymmetric Intra- and Intermolecular Hydroamination Catalyzed by 3,3′-Bis(Trisarylsilyl)- and 3,3′-Bis(Arylalkylsilyl)-Substituted Binaphtholate Rare-Earth-Metal Complexes. *Organometallics* **2018**, *37*, 4358–4379. https://doi.org/10.1021/acs.organomet.8b00510.
(63) Hua, Z.; Vassar, V. C.; Ojima, I. Synthesis of New Chiral Monodentate Phosphite Ligands and Their Use in Catalytic Asymmetric Hydrogenation. *Org. Lett.* **2003**, *5* (21), 3831–3834. https://doi.org/10.1021/ol035343r.
(64) Reznichenko, A. L.; Emge, T. J.; Audörsch, S.; Klauber, E. G.; Hultzsch, K. C.; Schmidt, B. Group 5 Metal Binaphtholate Complexes for Catalytic Asymmetric Hydroaminoalkylation and Hydroamination/Cyclization. *Organometallics* **2011**, *30*, 921–924. https://doi.org/10.1021/om1011006.

(65) Nádvornik, M.; Handliř, K.; Holeček, J.; Klikorka, J.; Lyčka, A. Synthese von Einigen Alkyldiphenylchlorsilanen Und Alkyldiphenylsilanolen. *Z. Für Chem.* **1980**, *20*, 343–343. https://doi.org/10.1002/zfch.19800200913.
(66) Gilli, G.; Gilli, P. *The Nature of the Hydrogen Bond: Outline of a Comprehensive Hydrogen Bond Theory*; International Union of Crystallography Monographs on Crystallography; Oxford University Press: Oxford, 2009. https://doi.org/10.1093/acprof:oso/9780199558964.001.0001.
(67) Kochnev, A. I.; Oleynik, I. I.; Oleynik, I. V.; Ivanchev, S. S.; Tolstikov, G. A. Synthesis of Salicylaldehydes Bearing Bulky Substituents in the Positions 3 and 5. *Russ. Chem. Bull.* **2007**, *56*, 1125–1129. https://doi.org/10.1007/s11172-007-0170-5.
(68) Zhu, J.; Chen, E. Y. -X. Catalyst-Sidearm-Induced Stereoselectivity Switching in Polymerization of a Racemic Lactone for Stereocomplexed Crystalline Polymer with a Circular Life Cycle. *Angew. Chem. Int. Ed.* **2019**, *58*, 1178–1182. https://doi.org/10.1002/anie.201813006.
(69) Okuda, J.; Fokken, S.; Kleinhenn, T.; Spaniol, T. P. Titanium Complexes Containing a Disulfide-Bridged Bis(Phenolato) Ligand: Synthesis and Structural Characterization of Three Different Bonding Modes. *Eur. J. Inorg. Chem.* **2000**, 1321–1326. https://doi.org/10.1002/(SICI)1099-0682(200006)2000:6<1321::AID-EJIC1321>3.0.CO;2-U.
(70) Hultzsch, K. C.; Gribkov, D. V.; Hampel, F. Non-Metallocene Rare Earth Metal Catalysts for the Diastereoselective and Enantioselective Hydroamination of Aminoalkenes. *J. Organomet. Chem.* **2005**, *690*, 4441–4452. https://doi.org/10.1016/j.jorganchem.2004.11.058.
(71) Alonso, J. A.; Martínez-Lope, M. J.; Casais, M. T.; Fernández-Díaz, M. T. Evolution of the Jahn−Teller Distortion of MnO_6 Octahedra in $RMnO_3$ Perovskites (R = Pr, Nd, Dy, Tb, Ho, Er, Y): A Neutron Diffraction Study. *Inorg. Chem.* **2000**, *39*, 917–923. https://doi.org/10.1021/ic990921e.
(72) Ketkaew, R.; Tantirungrotechai, Y.; Harding, P.; Chastanet, G.; Guionneau, P.; Marchivie, M.; Harding, D. J. OctaDist: A Tool for Calculating Distortion Parameters in Spin Crossover and Coordination Complexes. *Dalton Trans.* **2021**, *50*, 1086–1096. https://doi.org/10.1039/D0DT03988H.
(73) Eppinger, J.; Spiegler, M.; Hieringer, W.; Herrmann, W. A.; Anwander, R. C2-Symmetric Ansa-Lanthanidocene Complexes. Synthesis via Silylamine Elimination and β-SiH Agostic Rigidity. *J. Am. Chem. Soc.* **2000**, *122*, 3080–3096. https://doi.org/10.1021/ja992786a.
(74) Lian, B.; Spaniol, T. P.; Horrillo-Martínez, P.; Hultzsch, K. C.; Okuda, J. Imido and Amido Titanium Complexes That Contain a [OSSO]-Type Bis(Phenolato) Ligand: Synthesis, Structures, and Hydroamination Catalysis. *Eur. J. Inorg. Chem.* **2009**, *2009*, 429–434. https://doi.org/10.1002/ejic.200800977.
(75) Takashima, Y.; Nakayama, Y.; Hirao, T.; Yasuda, H.; Harada, A. Bis(Amido)Titanium Complexes Having Chelating Diaryloxo Ligands Bridged by Sulfur or Methylene and Their Catalytic Behaviors for Ring-Opening Polymerization of Cyclic Esters. *J. Organomet. Chem.* **2004**, *689*, 612–619. https://doi.org/10.1016/j.jorganchem.2003.10.042.
(76) Reznichenko, A. L. Stereoselective Addition of Simple Amines to Unactivated Alkenes. PhD Thesis, Graduate School-New Brunswick, Rutgers, The State University of New Jersey, 2012.
(77) Thorn, M. G.; Moses, J. E.; Fanwick, P. E.; Rothwell, I. P. New Tantalum Compounds Supported by 3,3′-Disubstituted-1,1′-Bi-2-Naphthoxide Ligation. *J. Chem. Soc. Dalton Trans.* **2000**, 2659–2660. https://doi.org/10.1039/B005681M.
(78) Son, A. J. R.; Schweiger, S. W.; Thorn, M. G.; Moses, J. E.; Fanwick, P. E.; Rothwell, I. P. The Isolation and Chemistry of Tantalum Dimethylamides Containing Resolved 3,3′-Disubstituted-1,1′-Bi-2,2′-Naphthoxide Ligands. *Dalton Trans.* **2003**, 1620–1627. https://doi.org/10.1039/B212910H.

(79) Weinert, C. S.; Fanwick, P. E.; Rothwell, I. P. Isolation and Chemistry of Tantalum(V) Compounds Containing Two Resolved 3,3‘-Disubstituted-1,1‘-Bi-2,2‘-Naphthoxide Ligands. *Organometallics* **2002**, *21*, 484–490. https://doi.org/10.1021/om0108200.
(80) Weinert, C. S.; Fanwick, P. E.; Rothwell, I. P. Synthesis of the Tantalum Hydride Complex (R,R)-[Ta(O2C20H10{SiMe3}2-3,3‘)2(H)] and Reactivity with Aldehydes, Ketones, Acetylenes, and Related Substrates: A Reagent for the Asymmetric Hydrogenation of Prochiral Carbonyl Species. *Organometallics* **2005**, *24*, 5759–5766. https://doi.org/10.1021/om050633s.
(81) Addison, A. W.; Rao, T. N.; Reedijk, J.; Rijn, J. van; Verschoor, G. C. Synthesis, Structure, and Spectroscopic Properties of Copper(II) Compounds Containing Nitrogen–Sulphur Donor Ligands; the Crystal and Molecular Structure of Aqua[1,7-Bis(N-Methylbenzimidazol-2′-Yl)-2,6-Dithiaheptane]Copper(II) Perchlorate. *J. Chem. Soc. Dalton Trans.* **1984**, 1349–1356. https://doi.org/10.1039/DT9840001349.
(82) Hultzsch, K. C.; Soltys, J.; Wolff, M.; Nawara-Hultzsch, A. J. Unpublished Results.
(83) Farrugia, L. J. WinGX and ORTEP for Windows: An Update. *J. Appl. Crystallogr.* **2012**, *45*, 849–854. https://doi.org/10.1107/S0021889812029111.
(84) Sartori, G.; Bigi, F.; Maggi, R.; Porta, C. Metal-Template Ortho-Regioselective Mono- and Bis-de-Tert-Butylation of Poly-Tert-Butylated Phenols. *Tetrahedron Lett.* **1994**, *35*, 7073–7076. https://doi.org/10.1016/0040-4039(94)88229-0.
(85) Ingenfeld, B.; Straub, S.; Frömbgen, C.; Lützen, A. Synthesis of Monofunctionalized Calix[5]Arenes. *Synthesis* **2018**, *50*, 676–684. https://doi.org/10.1055/s-0036-1589127.
(86) Weller, D. D.; Stirchak, E. P. Quassinoid Synthesis via O-Quinone Diels-Alder Reactions. *J. Org. Chem.* **1983**, *48*, 4873–4879. https://doi.org/10.1021/jo00173a018.
(87) Lyčka, A.; Šnobl, D.; Handlíř, K.; Holeček, J.; Nádvorník, M. ^{29}Si and ^{13}C NMR Spectra of Some Alkyldiphenylchlorosilanes, Alkyldiphenylsilanoles and Bis(Alkyldiphenylsilyl)Chromates. *Collect. Czechoslov. Chem. Commun.* **1982**, *47*, 603–612. https://doi.org/10.1135/cccc19820603.
(88) Anwander, R.; Runte, O.; Eppinger, J.; Gerstberger, G.; Herdtweck, E.; Spiegler, M. Synthesis and Structural Characterisation of Rare-Earth Bis(Dimethylsilyl)Amides and Their Surface Organometallic Chemistry on Mesoporous MCM-41. *J. Chem. Soc. Dalton Trans.* **1998**, 847–858. https://doi.org/10.1039/A705608G.
(89) Booij, M.; Kiers, N. H.; Heeres, H. J.; Teuben, J. H. On the Synthesis of Monopentamethylcyclopentadienyl Derivatives of Yttrium, Lanthanum, and Cerium. *J. Organomet. Chem.* **1989**, *364*, 79–86. https://doi.org/10.1016/0022-328X(89)85333-1.
(90) Gribkov, D. V. Novel Catalysts for Stereoselective Hydroamination of Olefins Based on Rare Earth and Group IV Metals. PhD Thesis, Universität Erlangen-Nürnberg, 2005.
(91) Dolomanov, O. V.; Bourhis, L. J.; Gildea, R. J.; Howard, J. a. K.; Puschmann, H. OLEX2: A Complete Structure Solution, Refinement and Analysis Program. *J. Appl. Crystallogr.* **2009**, *42*, 339–341. https://doi.org/10.1107/S0021889808042726.
(92) Hübschle, C. B.; Sheldrick, G. M.; Dittrich, B. ShelXle: A Qt Graphical User Interface for SHELXL. *J. Appl. Crystallogr.* **2011**, *44*, 1281–1284. https://doi.org/10.1107/S0021889811043202.
(93) Spek, A. L. Structure Validation in Chemical Crystallography. *Acta Crystallogr. D Biol. Crystallogr.* **2009**, *65*, 148–155. https://doi.org/10.1107/S090744490804362X.
(94) Kondo, T.; Okada, T.; Mitsudo, T. Ruthenium-Catalyzed Intramolecular Oxidative Amination of Aminoalkenes Enables Rapid Synthesis of Cyclic Imines. *J. Am. Chem. Soc.* **2002**, *124*, 186–187. https://doi.org/10.1021/ja017012k.
(95) Bender, C. F.; Widenhoefer, R. A. Platinum-Catalyzed Intramolecular Hydroamination of Unactivated Olefins with Secondary Alkylamines. *J. Am. Chem. Soc.* **2005**, *127*, 1070–1071. https://doi.org/10.1021/ja043278q.
(96) Crimmin, M. R.; Arrowsmith, M.; Barrett, A. G. M.; Casely, I. J.; Hill, M. S.; Procopiou, P. A. Intramolecular Hydroamination of Aminoalkenes by Calcium and Magnesium Complexes: A Synthetic and Mechanistic Study. *J. Am. Chem. Soc.* **2009**, *131*, 9670–9685. https://doi.org/10.1021/ja9003377.

(97) Crimmin, M. R.; Casely, I. J.; Hill, M. S. Calcium-Mediated Intramolecular Hydroamination Catalysis. *J. Am. Chem. Soc.* **2005**, *127*, 2042–2043. https://doi.org/10.1021/ja043576n.
(98) Hesp, K. D.; Tobisch, S.; Stradiotto, M. $[Ir(COD)Cl]_2$ as a Catalyst Precursor for the Intramolecular Hydroamination of Unactivated Alkenes with Primary Amines and Secondary Alkyl- or Arylamines: A Combined Catalytic, Mechanistic, and Computational Investigation. *J. Am. Chem. Soc.* **2010**, *132*, 413–426. https://doi.org/10.1021/ja908316n.
(99) Arrowsmith, M.; Crimmin, M. R.; Barrett, A. G. M.; Hill, M. S.; Kociok-Köhn, G.; Procopiou, P. A. Cation Charge Density and Precatalyst Selection in Group 2-Catalyzed Aminoalkene Hydroamination. *Organometallics* **2011**, *30*, 1493–1506. https://doi.org/10.1021/om101063m.

7. Appendix

7.1 List of Figures

7.2 List of Schemes

7.3 List of Tables

7.4 Supplementary information

7.4.1 Overview Substrates, Products, Ligands and Metal Complexes

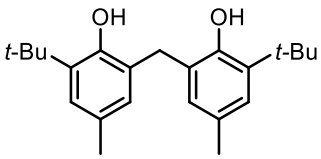

1

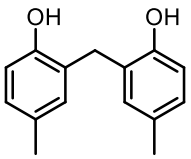

2

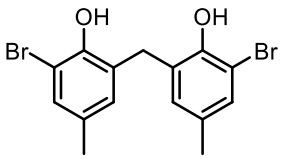

3

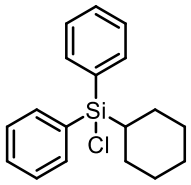

5

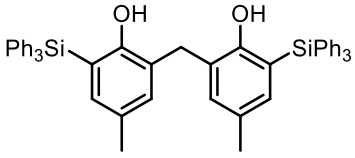

6

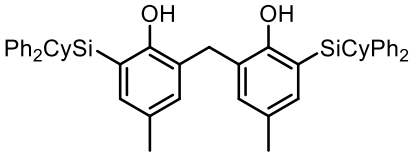

7

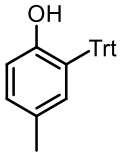

9

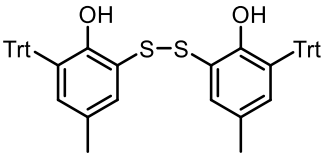

10

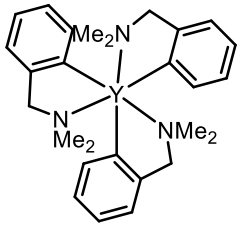

11-Y

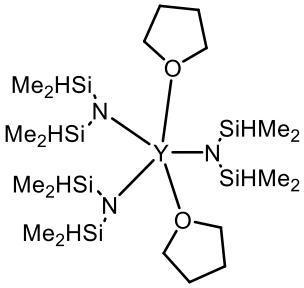

16-Y

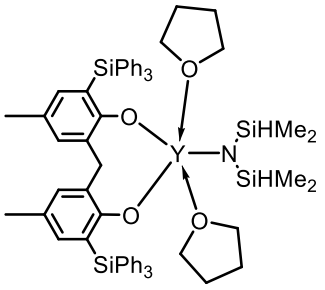

17-Y

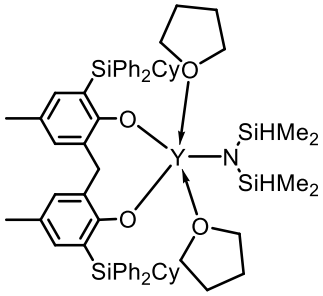

18-Y

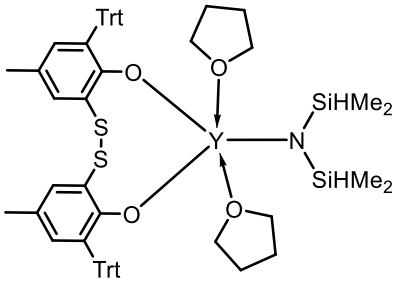

19-Y

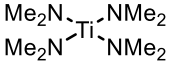

20-Ti

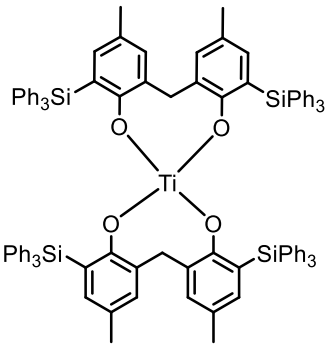

22-Ti

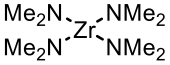

25-Zr

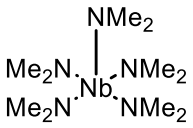

28-Nb

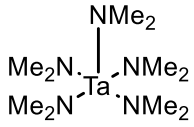

30-Ta

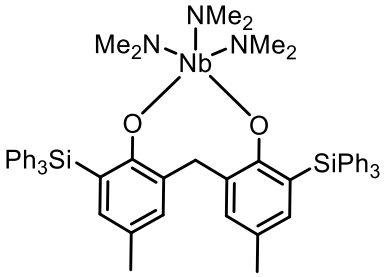

29-Nb

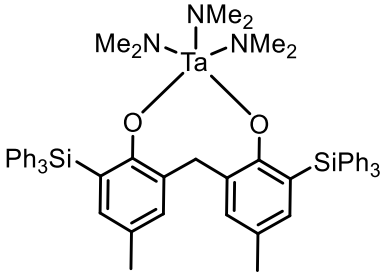

31-Ta

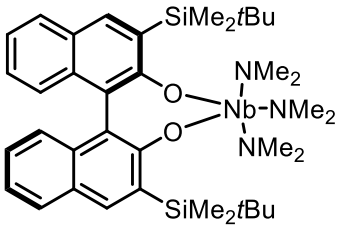

32-Nb

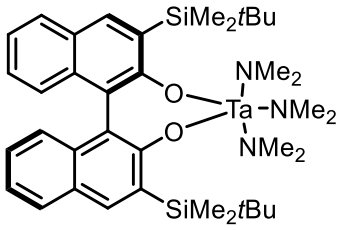

33-Ta

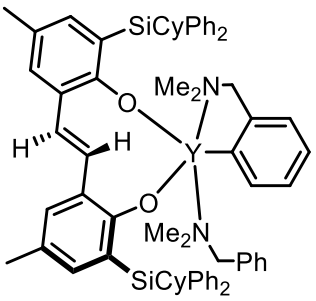

36-Y

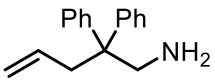

34

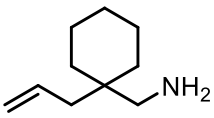

37

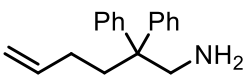

39

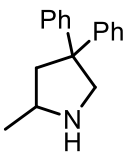

35

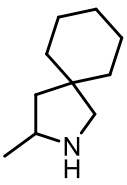

38

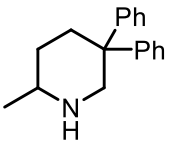

40

7.4.2 NMR Spectra

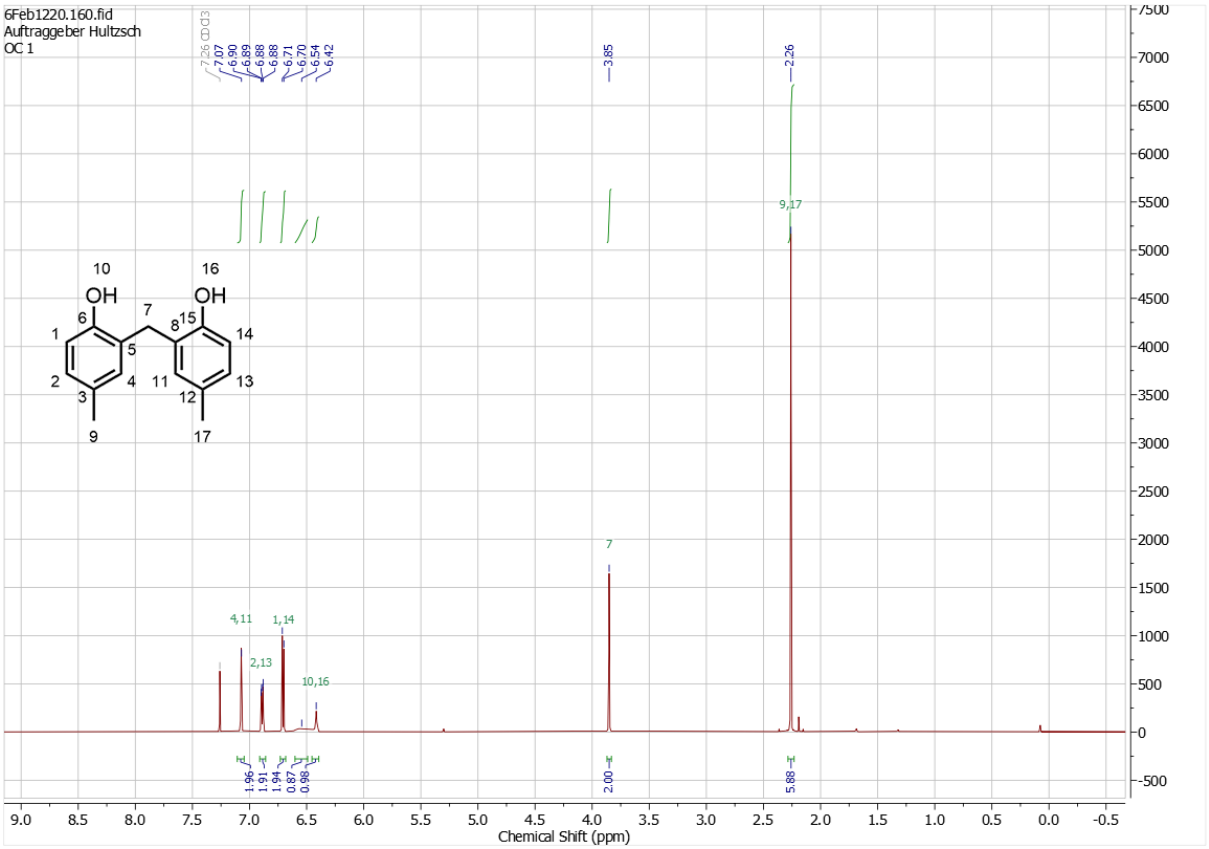

Supp. 1. ^{1}H-NMR spectrum of 2,2'-methylenebis(4-methylphenol) (**2**); solvent: $CDCl_3$, 600 MHz.

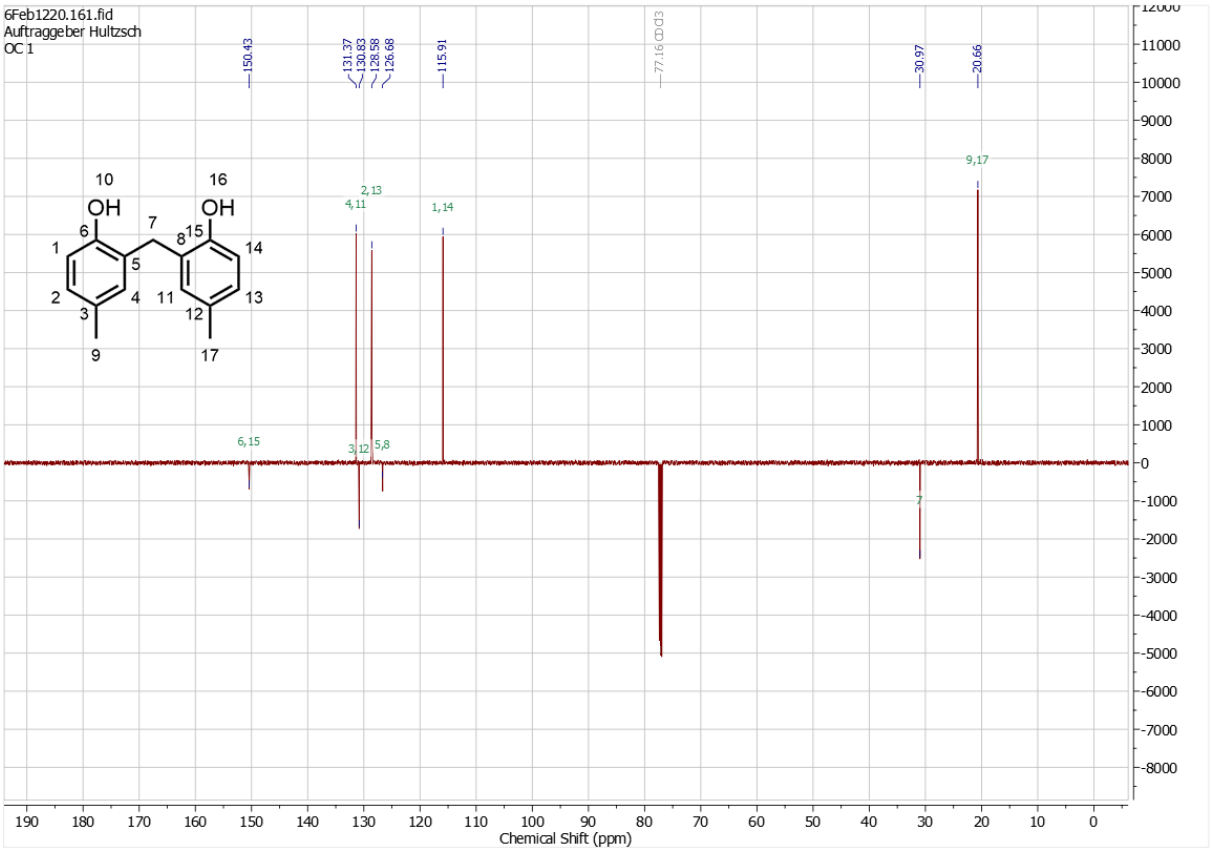

Supp. 2. ^{13}C-NMR spectrum of 2,2'-methylenebis(4-methylphenol) (**2**); solvent: $CDCl_3$, 151 MHz.

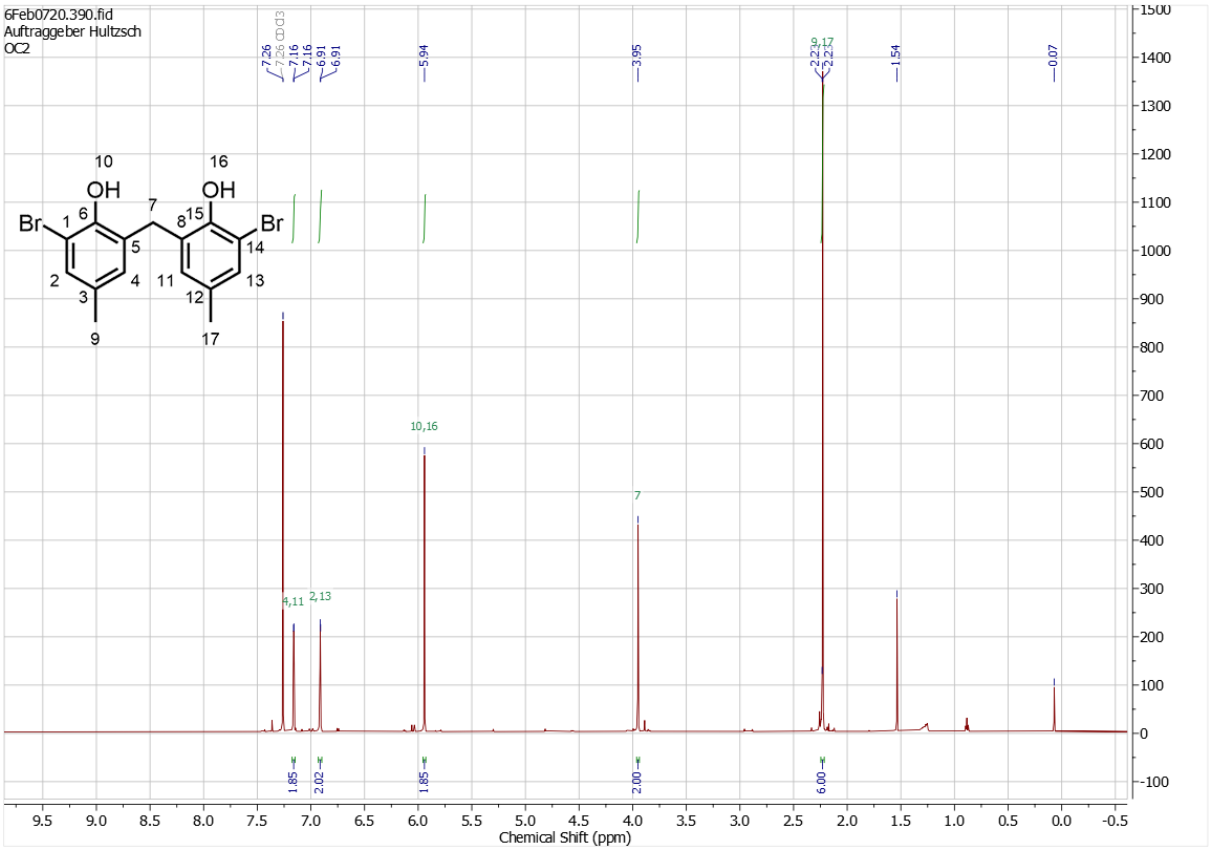

Supp. 3. ^{1}H-NMR spectrum of 6,6'-methylenebis(2-bromo-4-methylphenol) (**3**); solvent: $CDCl_3$, 600 MHz.

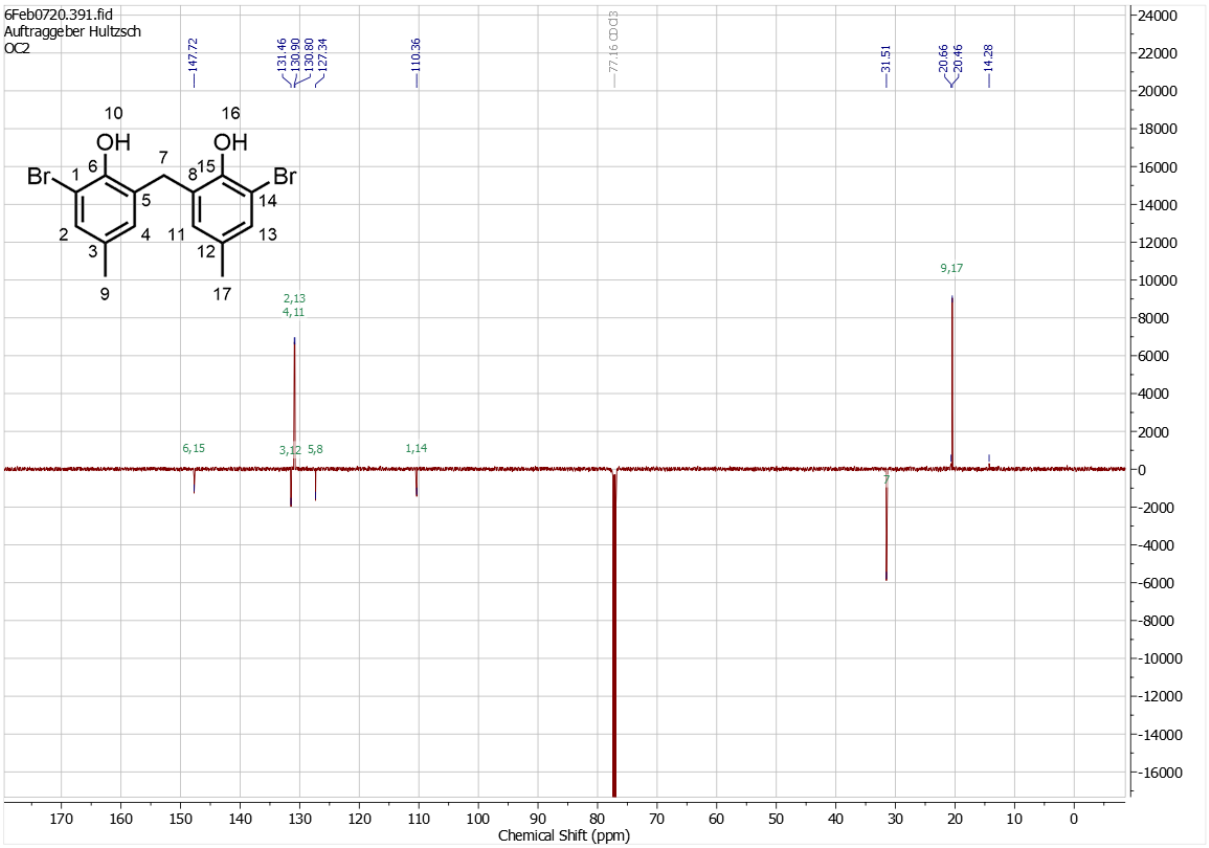

Supp. 4. ^{13}C-NMR spectrum of 6,6'-methylenebis(2-bromo-4-methylphenol) (**3**); solvent: $CDCl_3$, 151 MHz.

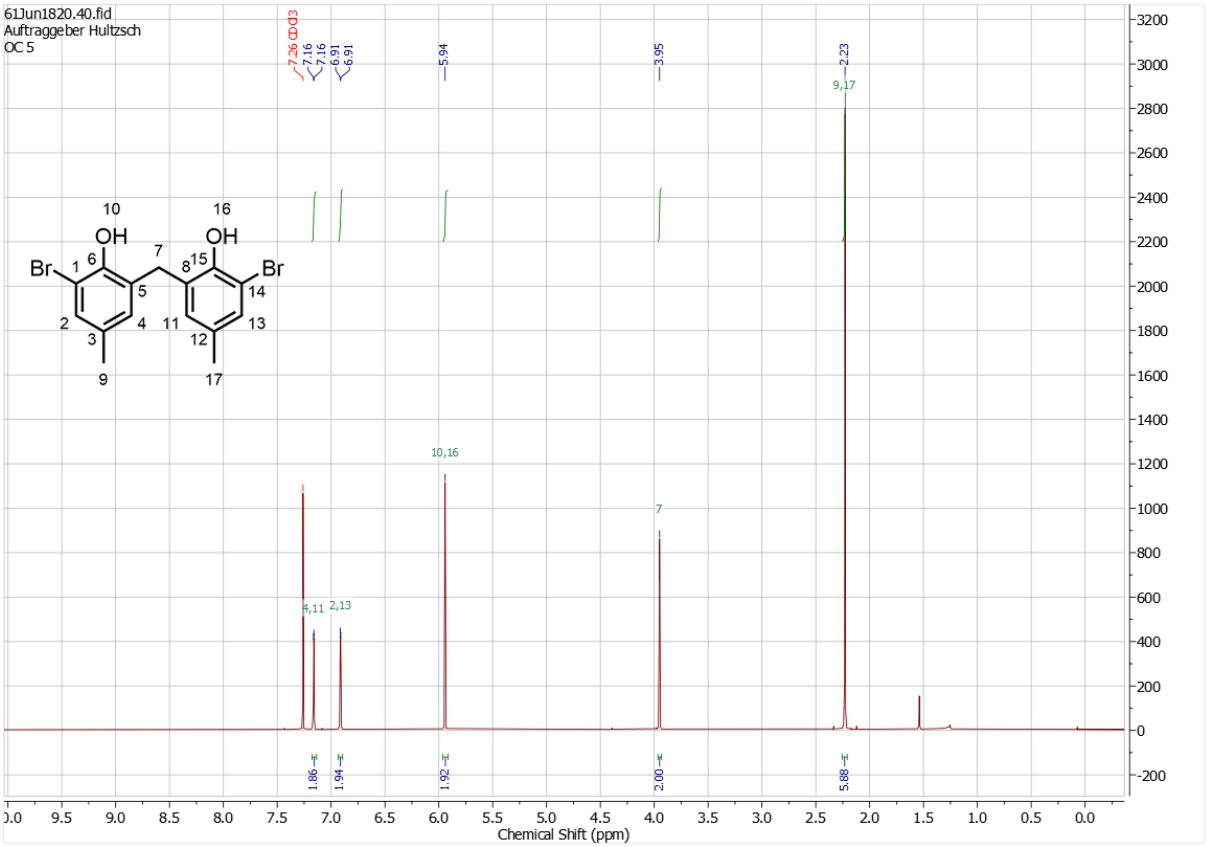

Supp. 5. ^{1}H-NMR spectrum of 6,6'-methylenebis(2-bromo-4-methylphenol) (**3**); solvent: $CDCl_3$, 600 MHz.

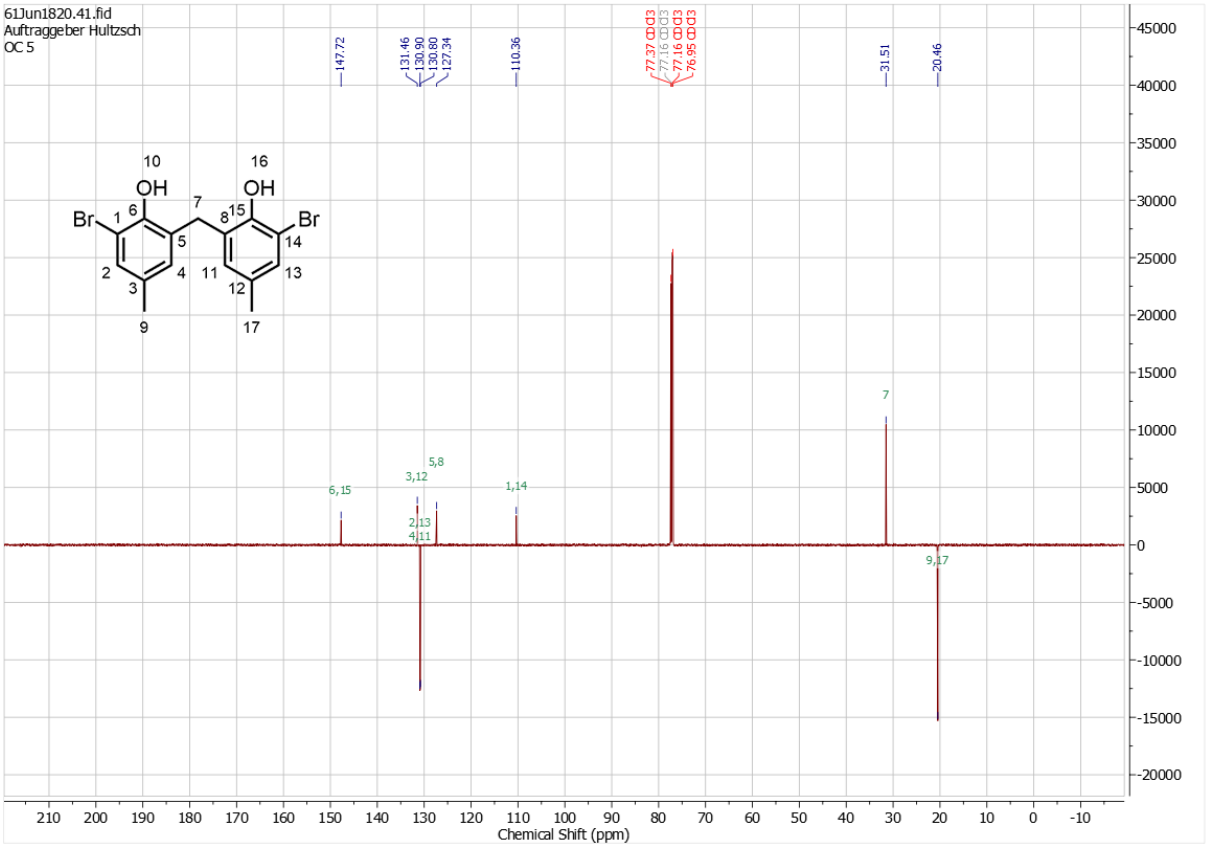

Supp. 6. ^{13}C-NMR spectrum of 6,6'-methylenebis(2-bromo-4-methylphenol) (**3**); solvent: $CDCl_3$, 151 MHz.

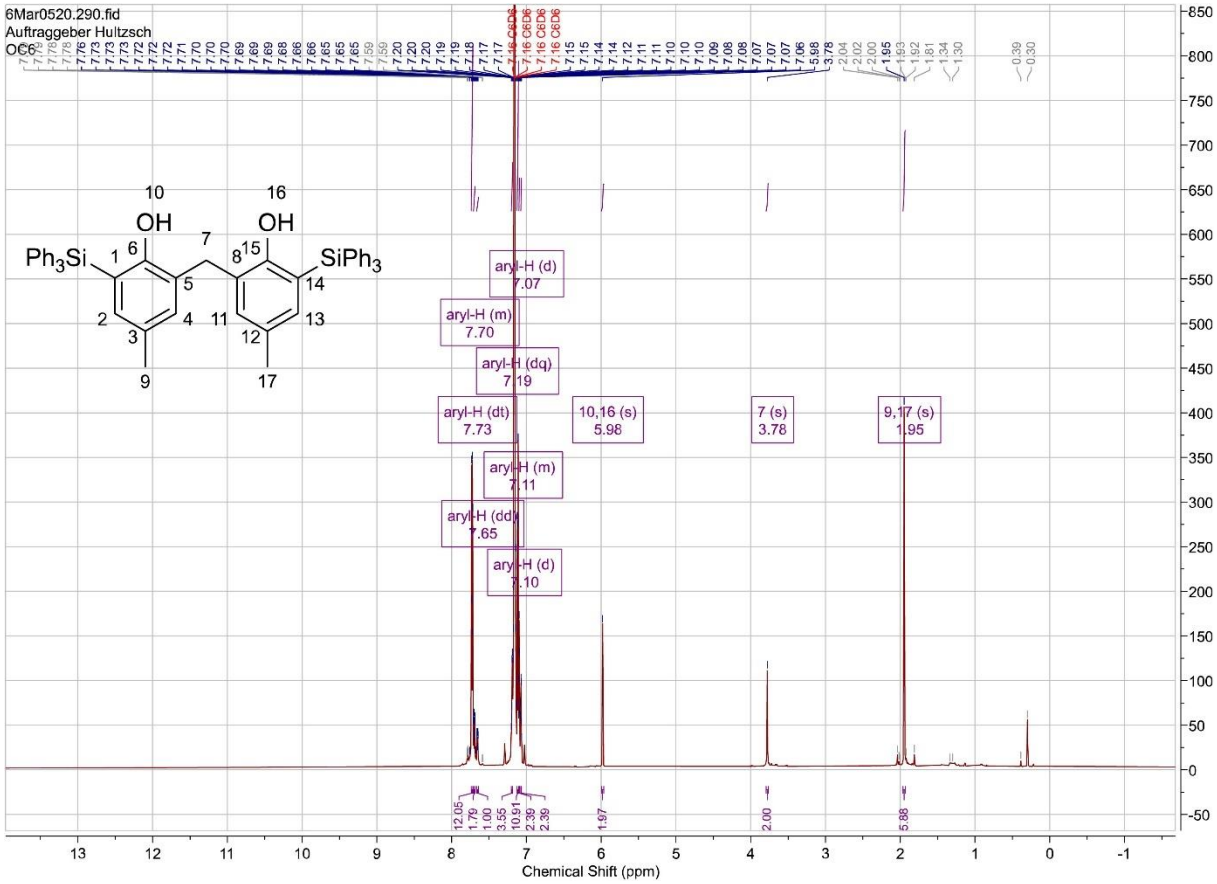

Supp. 7. ^{1}H-NMR spectrum of 6,6'-methylenebis(4-methyl-2-(triphenylsilyl)phenol) (**6**); solvent: C_6D_6, 600 MHz.

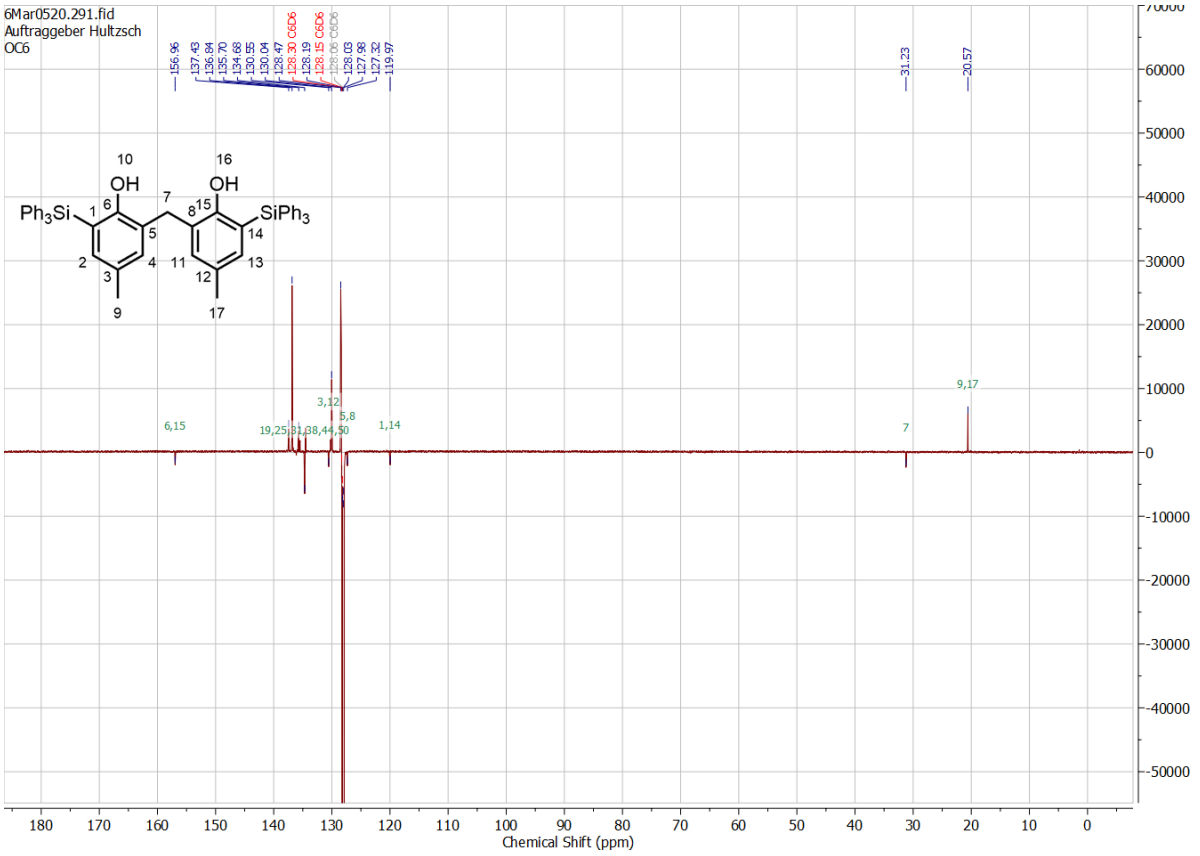

Supp. 8. ^{13}C-NMR spectrum of 6,6'-methylenebis(4-methyl-2-(triphenylsilyl)phenol) (**6**); solvent: C_6D_6, 151 MHz.

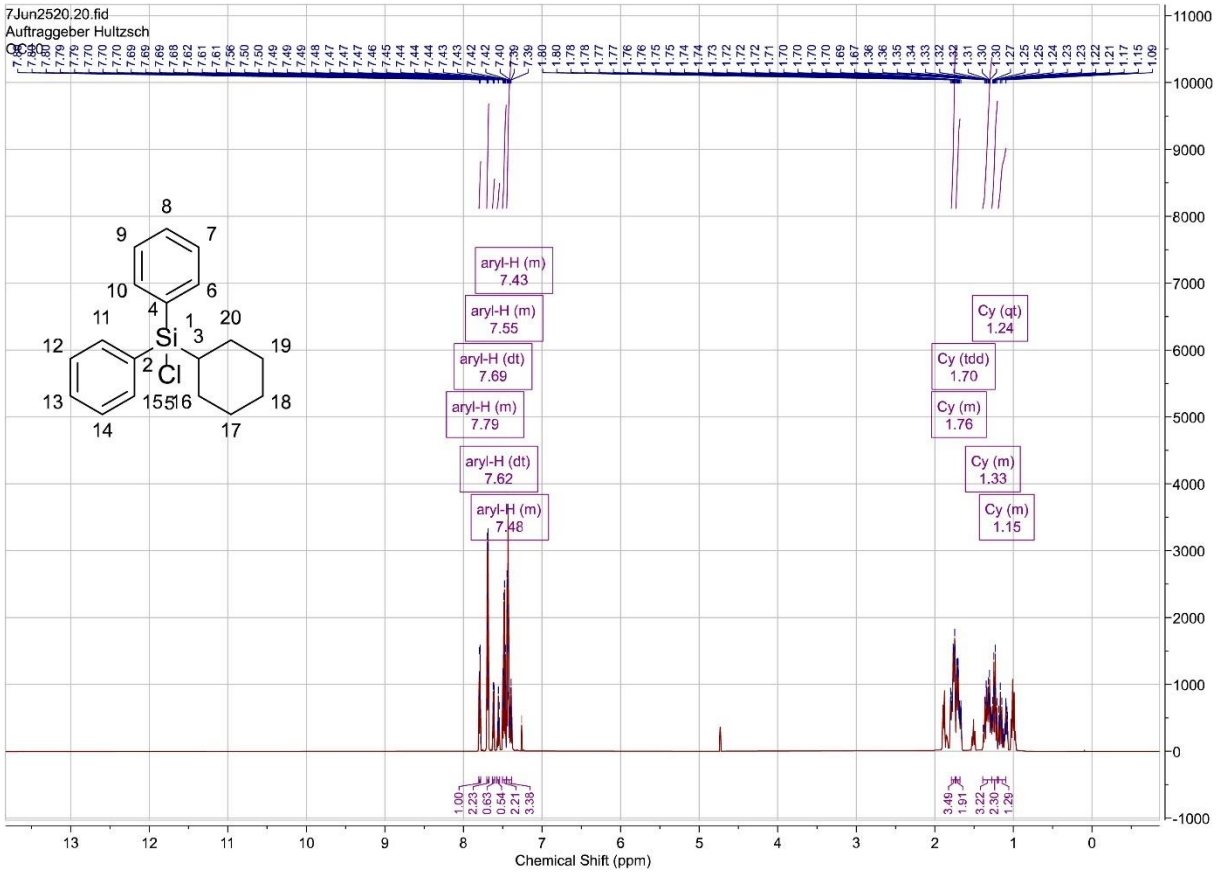

Supp. 9. ^{1}H-NMR spectrum of chloro(cyclohexyl)diphenylsilane (**5**); solvent: $CDCl_3$, 700 MHz.

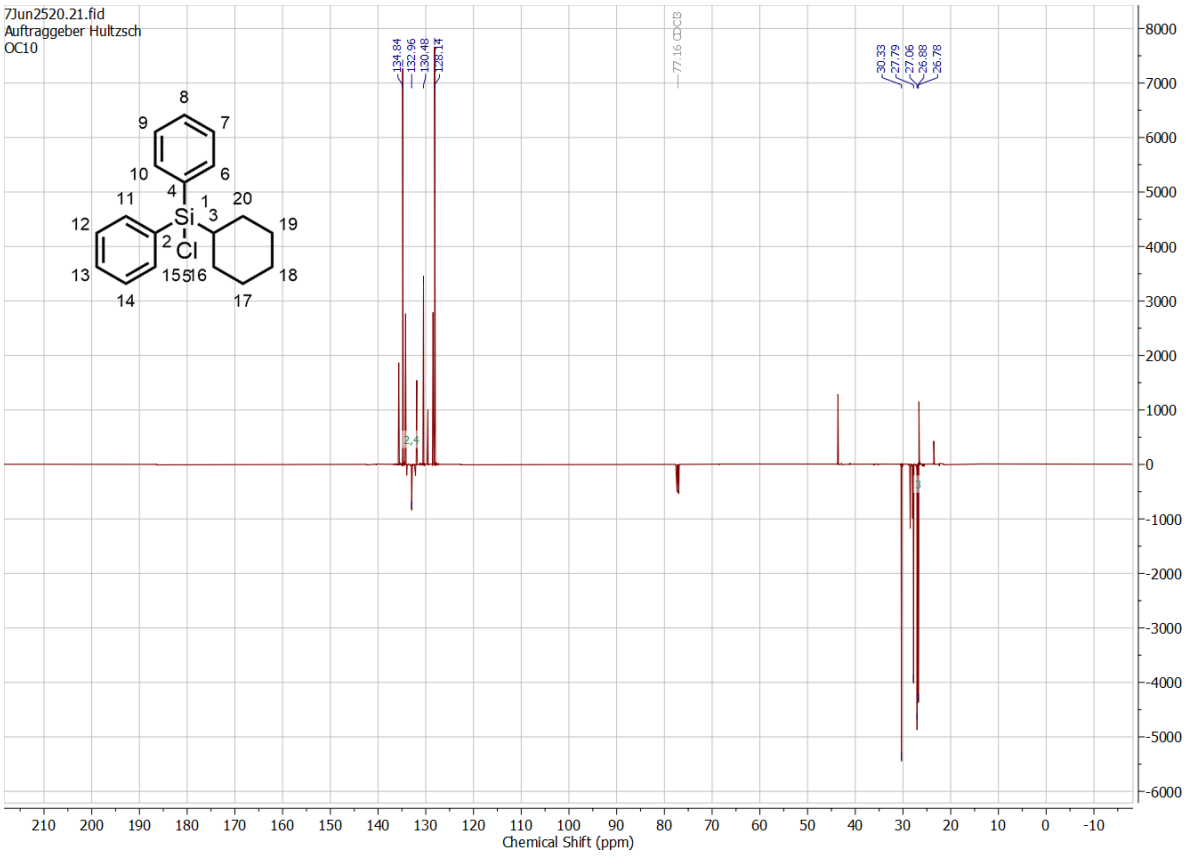

Supp. 10. ^{13}C-NMR spectrum of chloro(cyclohexyl)diphenylsilane (**5**); solvent: $CDCl_3$, 176 MHz.

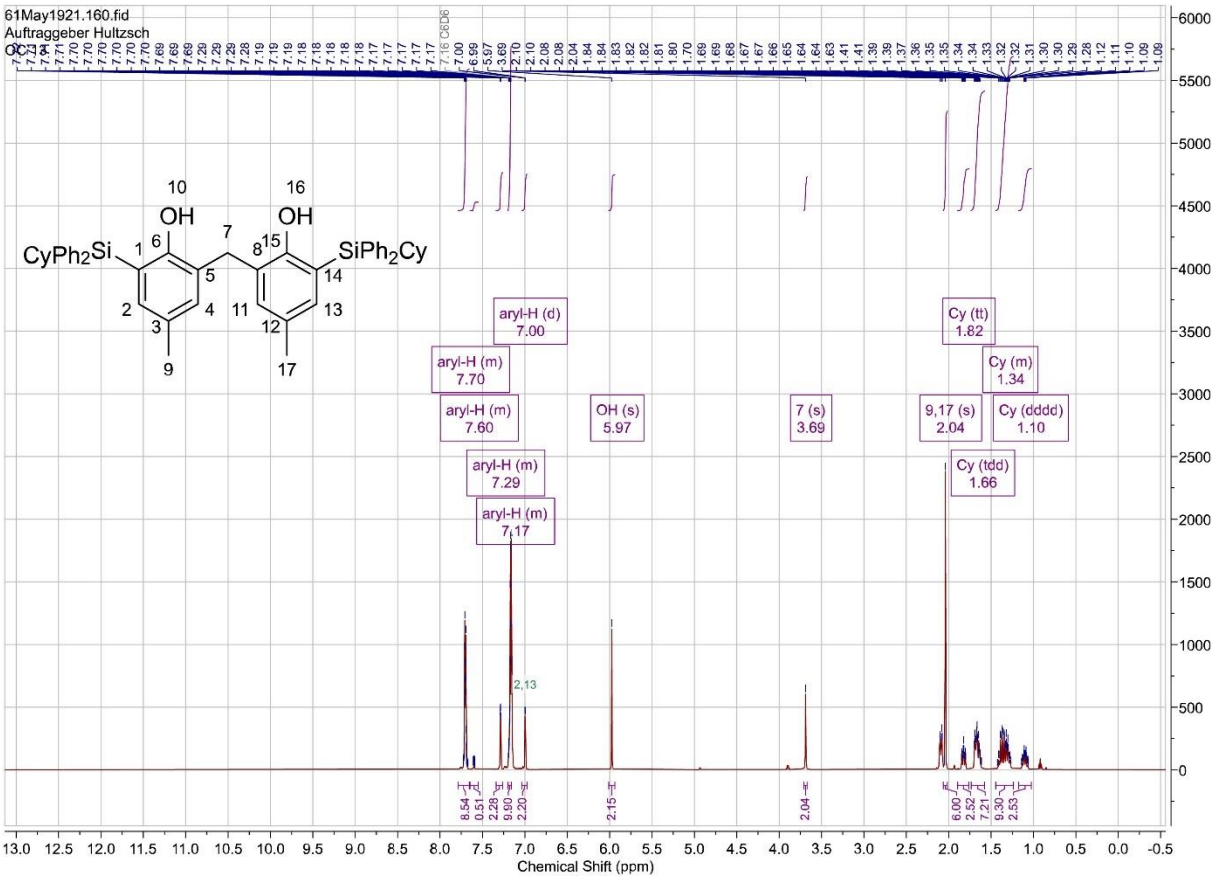

Supp. 11. ^{1}H-NMR spectrum of 6,6'-methylenebis(2-(cyclohexyldiphenylsilyl)-4-methylphenol) (**7**); solvent: C_6D_6, 600 MHz.

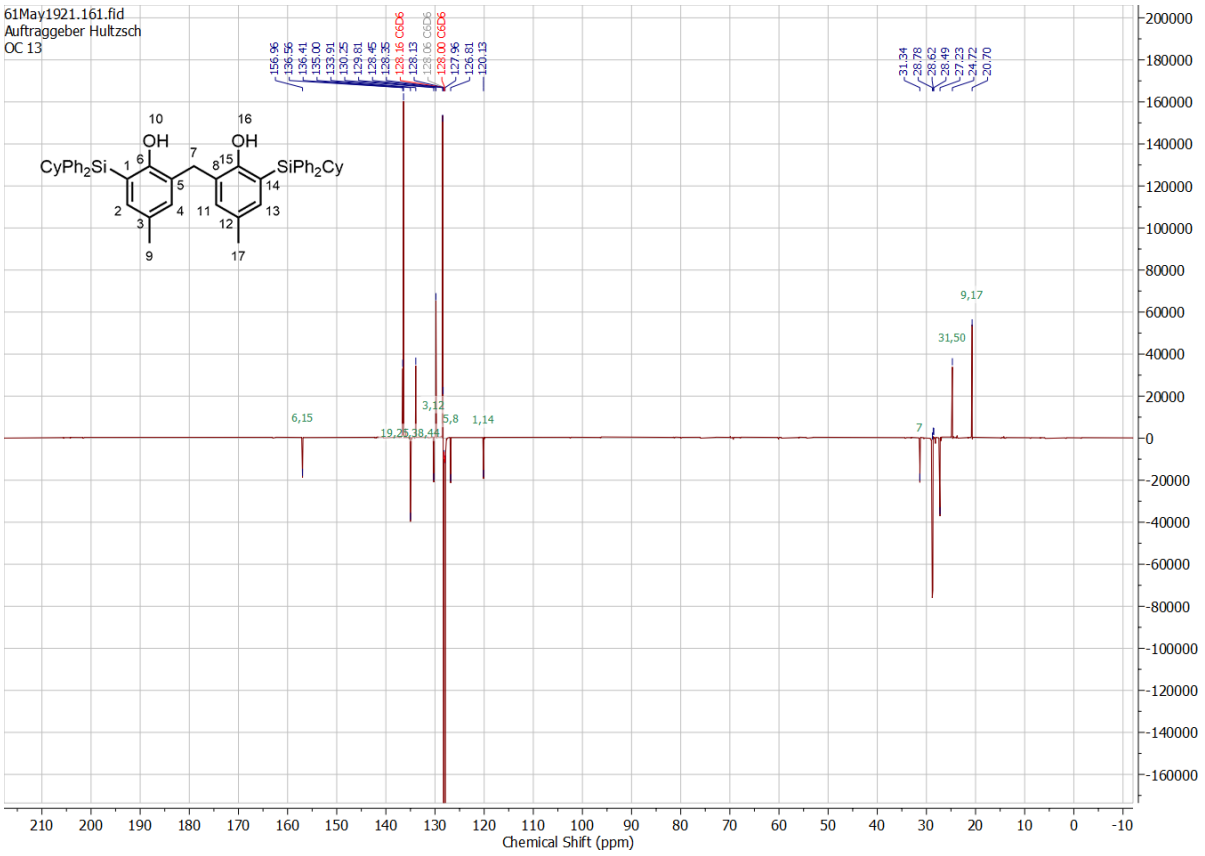

Supp. 12. ^{13}C-NMR spectrum of 6,6'-methylenebis(2-(cyclohexyldiphenylsilyl)-4-methylphenol) (**7**); solvent: C_6D_6, 151 MHz.

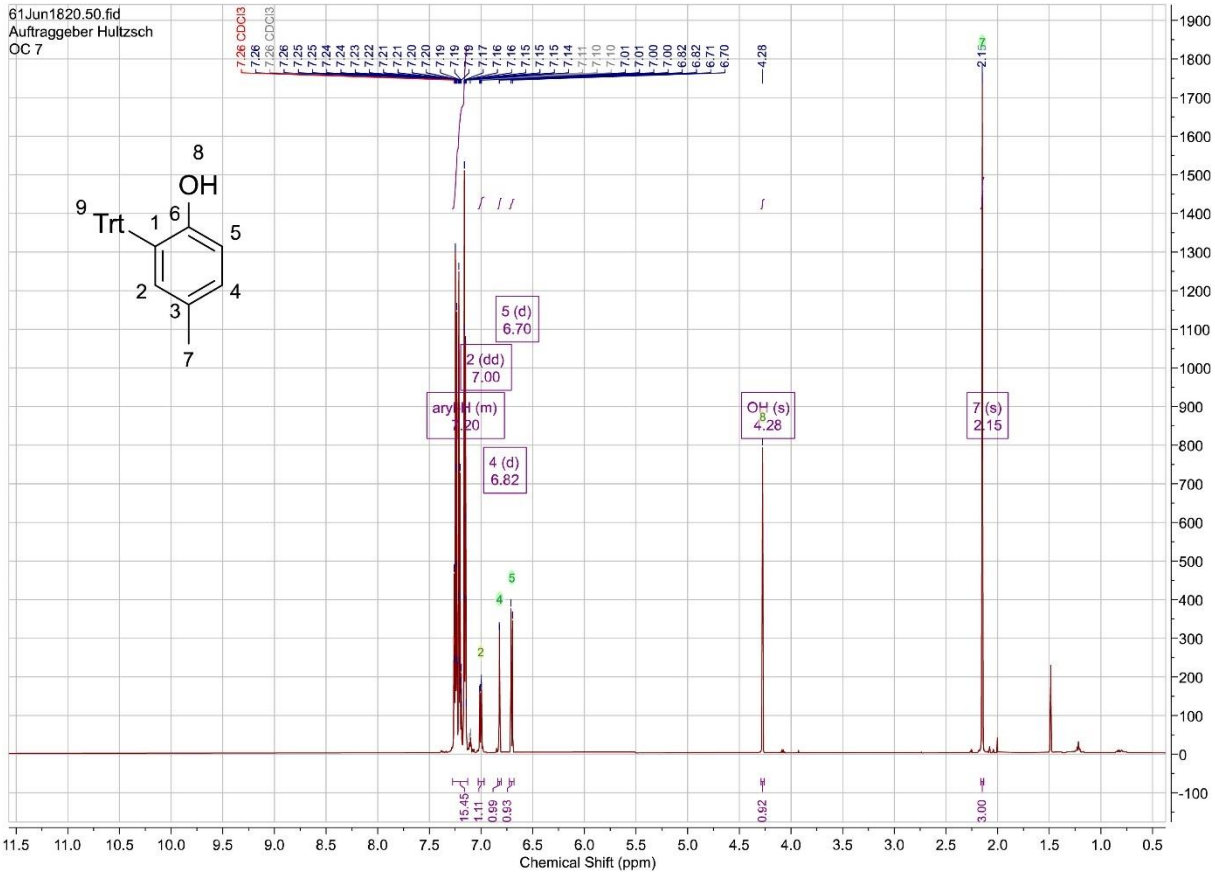

Supp. 13. ^{1}H-NMR spectrum of 4-methyl-2-tritylphenol (**9**); solvent: $CDCl_3$, 600 MHz.

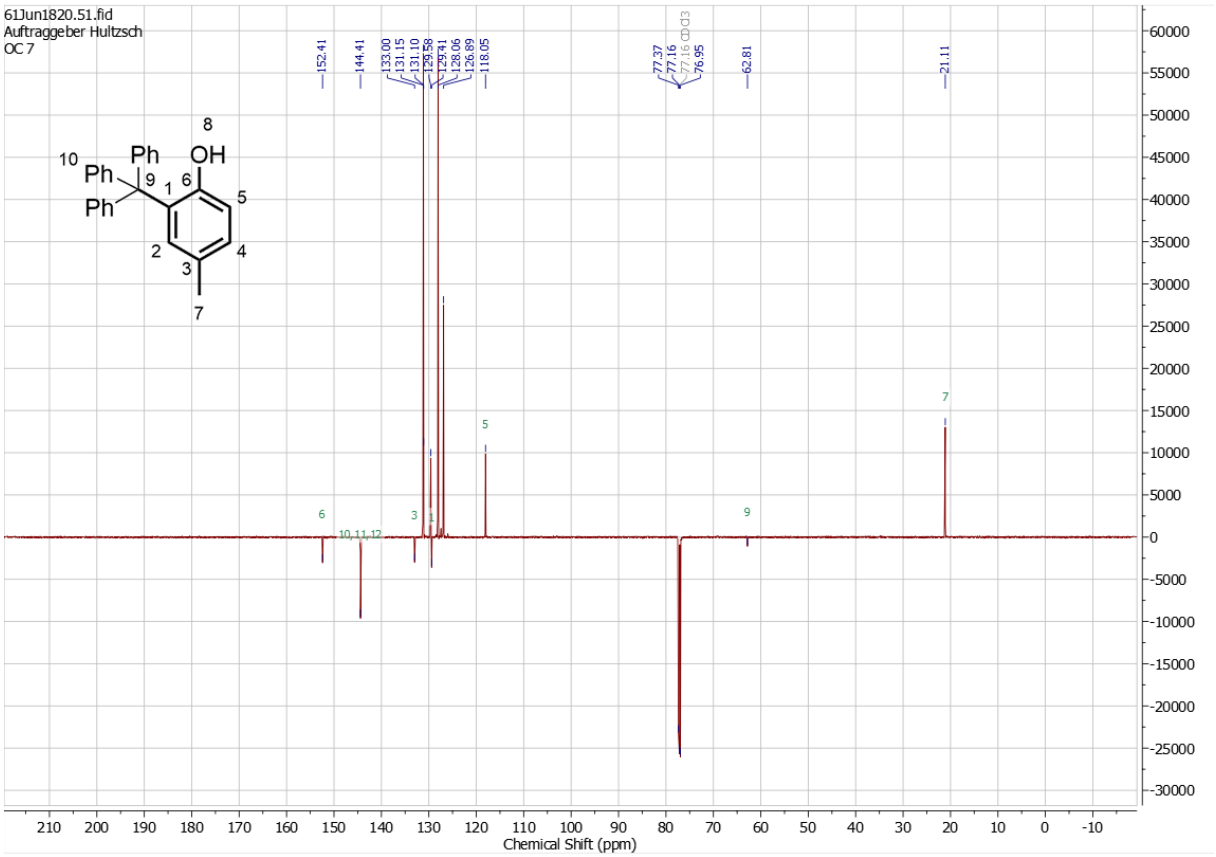

Supp. 14. ^{13}C-NMR spectrum of 4-methyl-2-tritylphenol (**9**); solvent: $CDCl_3$, 151 MHz.

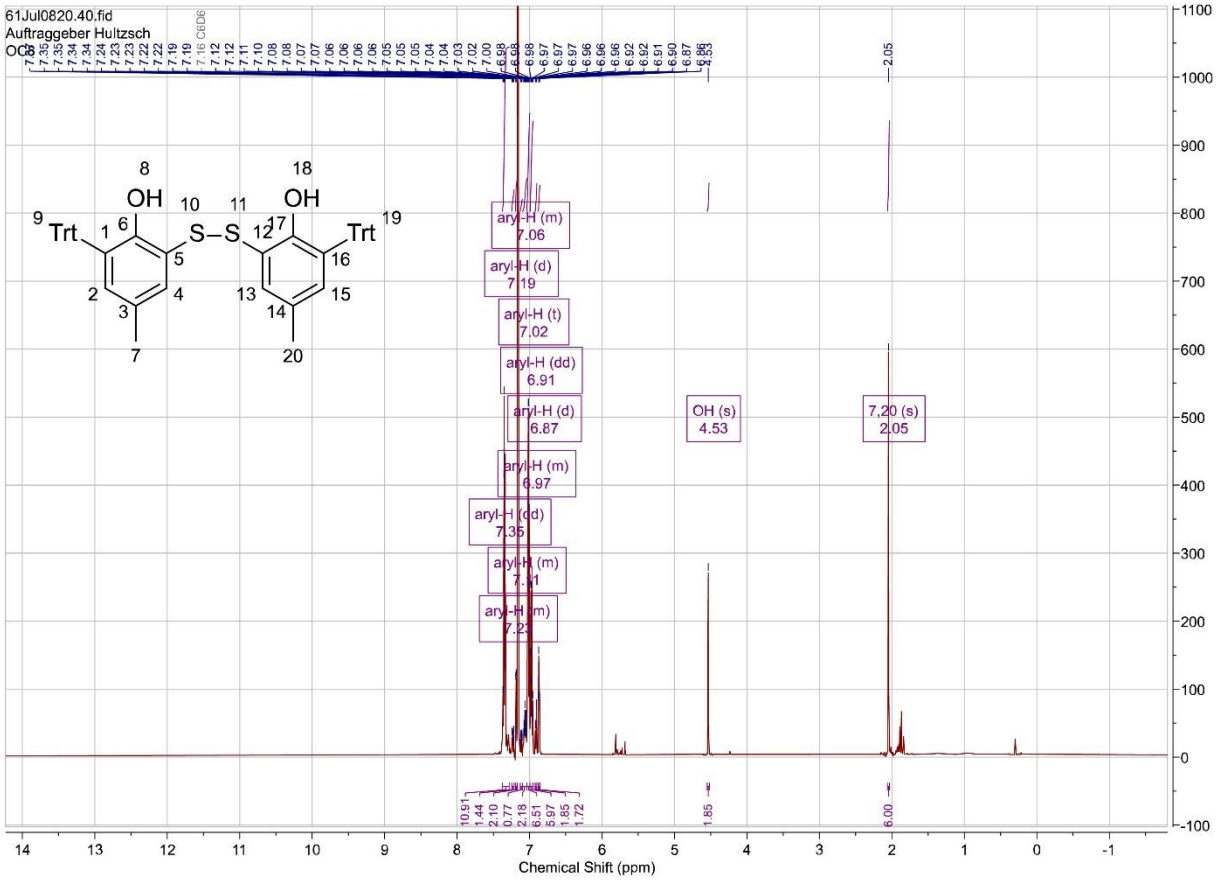

Supp. 15. ^{1}H-NMR spectrum of 6,6'-disulfanediylbis(4-methyl-2-tritylphenol) (**10**); solvent: C_6D_6, 600 MHz.

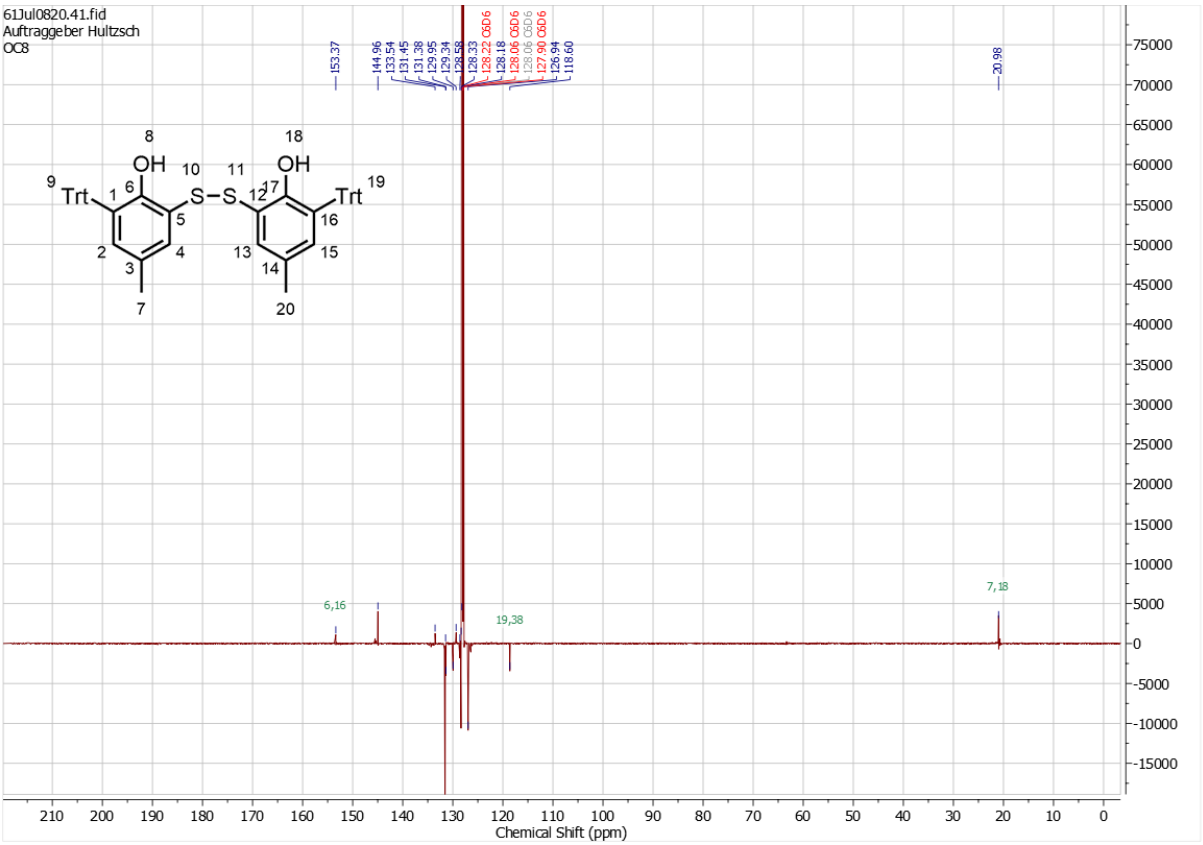

Supp. 16. ^{13}C-NMR spectrum of 6,6'-disulfanediylbis(4-methyl-2-tritylphenol) (**10**); solvent: C_6D_6, 151 MHz.

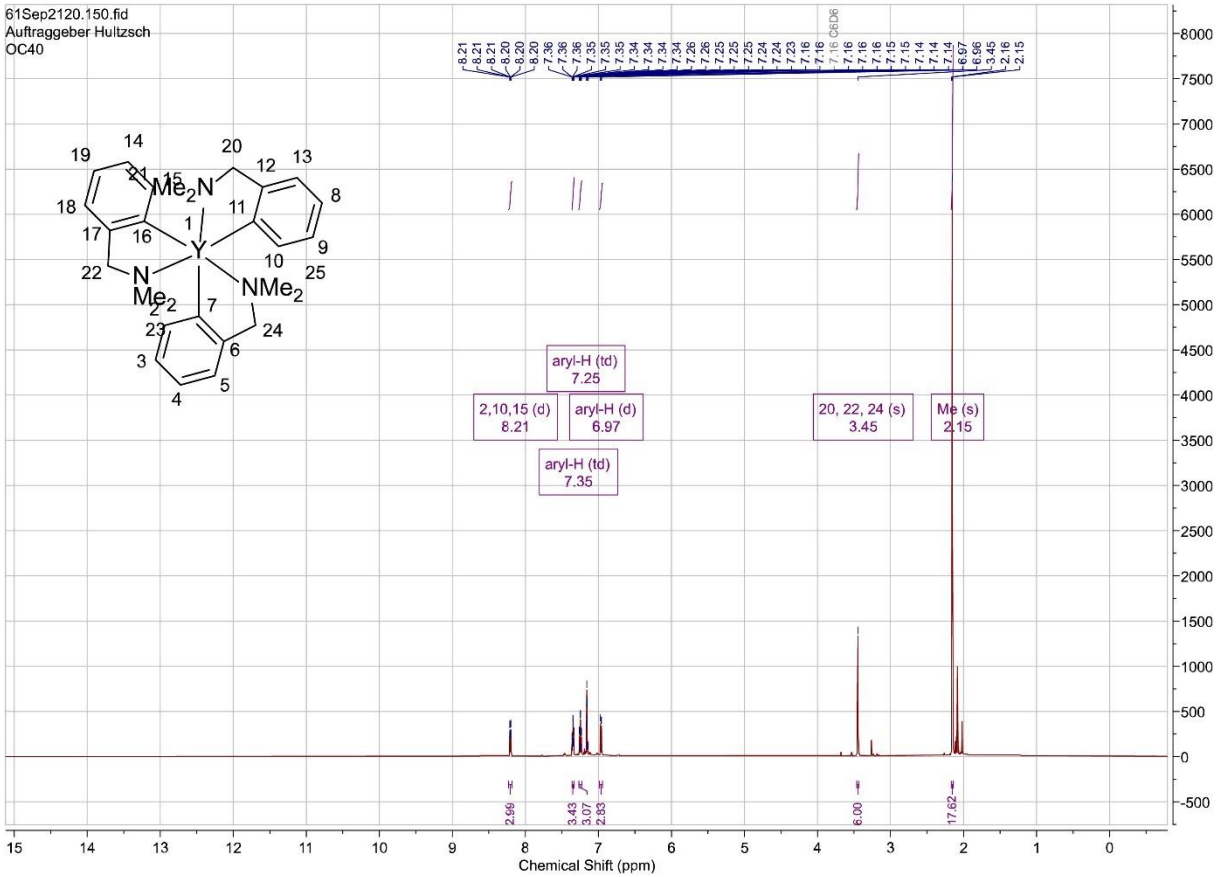

Supp. 17. ^{1}H-NMR spectrum of [Y(*o*-$C_6H_4CH_2NMe_2$)$_3$] (**11-Y**); solvent: C_6D_6, 600 MHz.

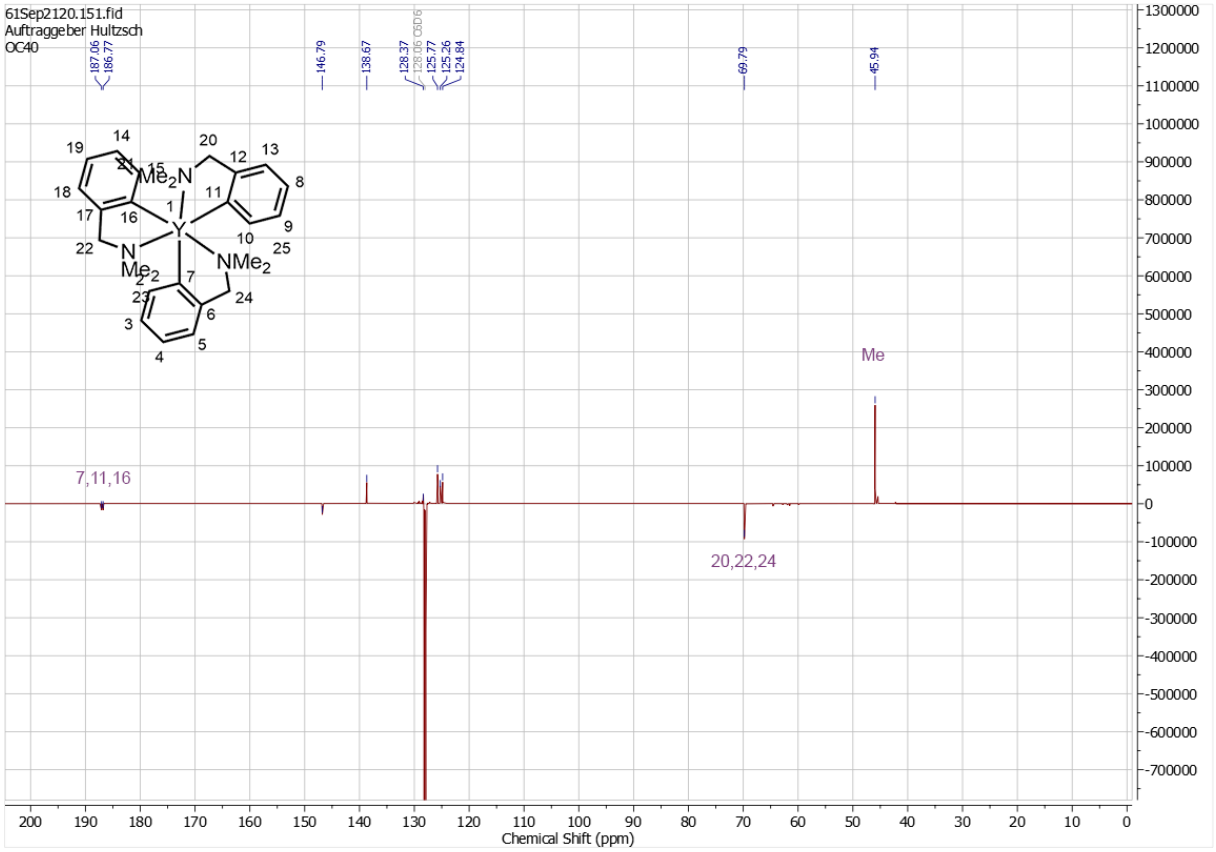

Supp. 18. ^{13}C-NMR spectrum of [Y(*o*-$C_6H_4CH_2NMe_2$)$_3$] (**11-Y**); solvent: C_6D_6, 151 MHz.

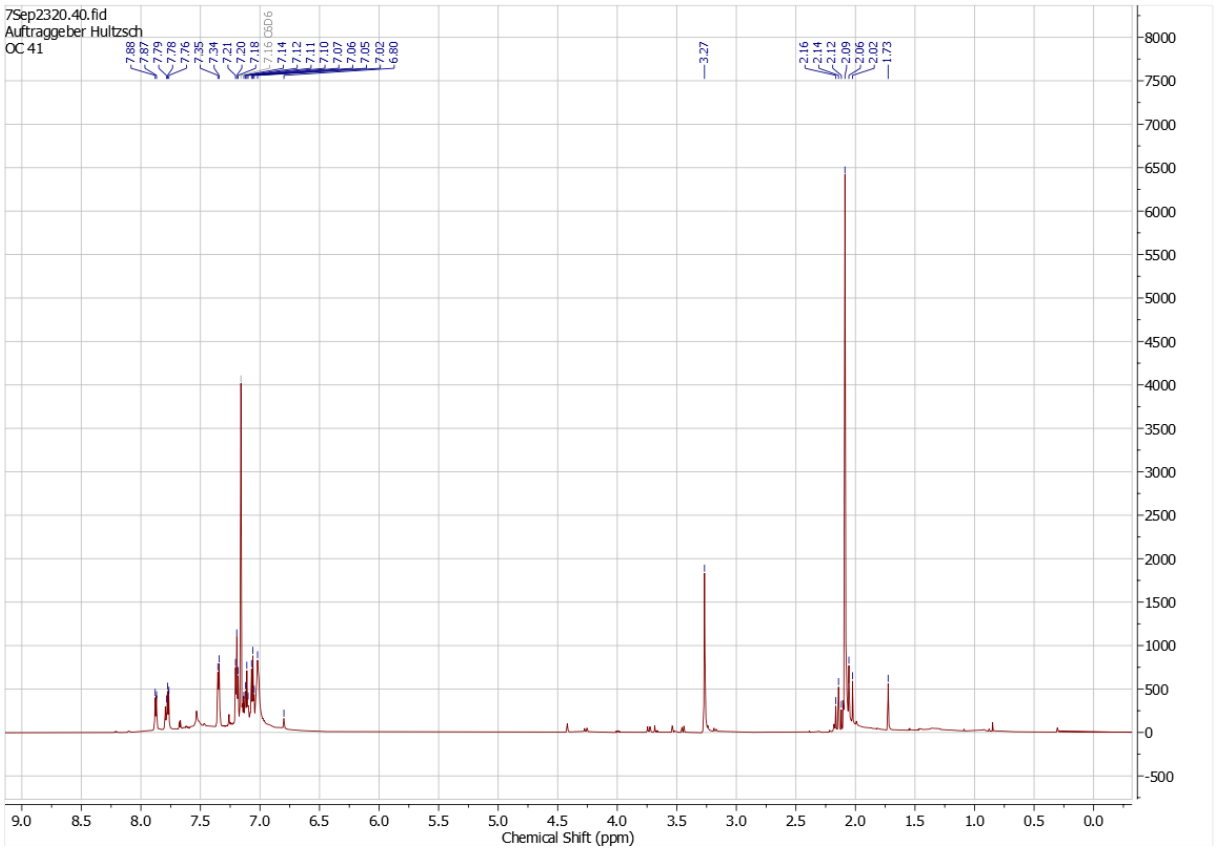

Supp. 19. ^{1}H-NMR spectrum of the attempted complexation of [Y(o-$C_6H_4CH_2NMe_2)_3$] with 6,6'-methylenebis(4-methyl-2-(triphenylsilyl)phenol) at room temperature; solvent: C_6D_6, 700 MHz.

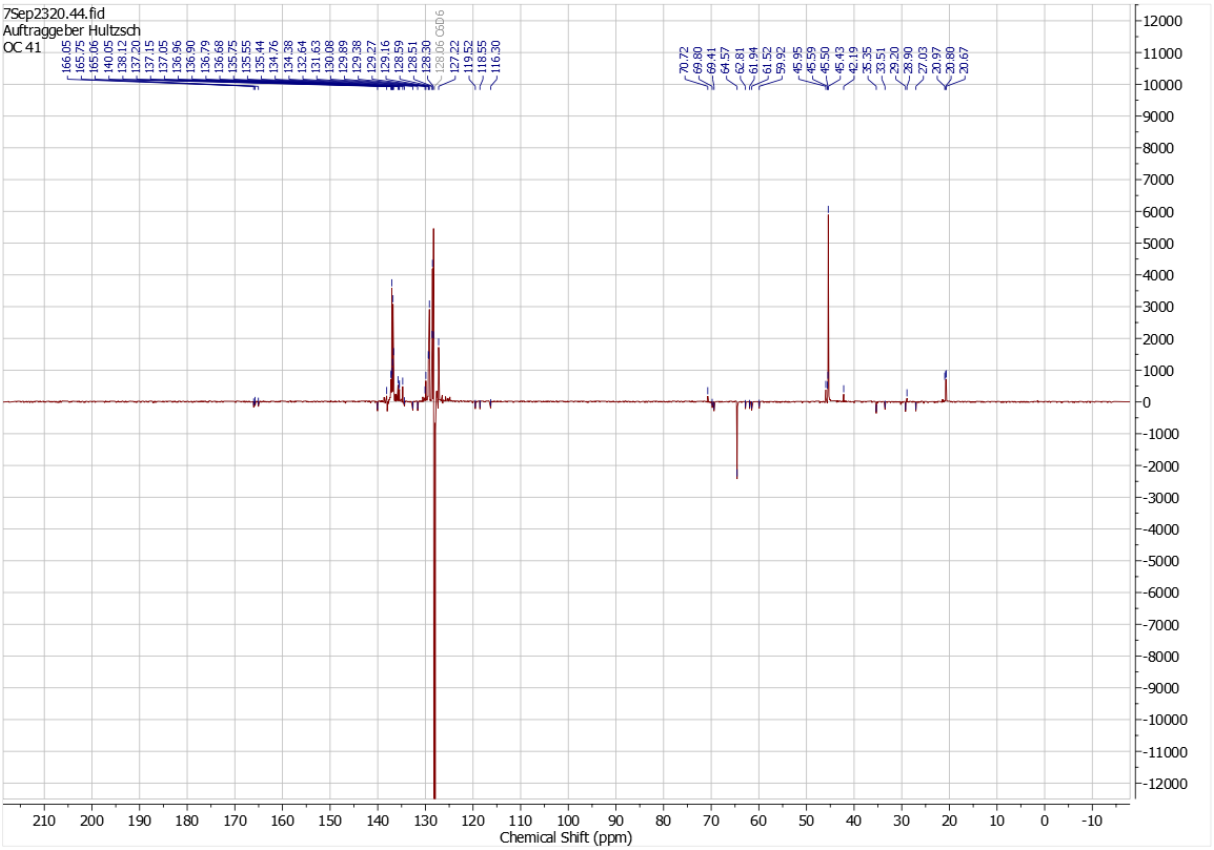

Supp. 20. ^{13}C-NMR spectrum of the attempted complexation of [Y(o-$C_6H_4CH_2NMe_2)_3$] with 6,6'-methylenebis(4-methyl-2-(triphenylsilyl)phenol) at room temperature; solvent: C_6D_6, 176 MHz.

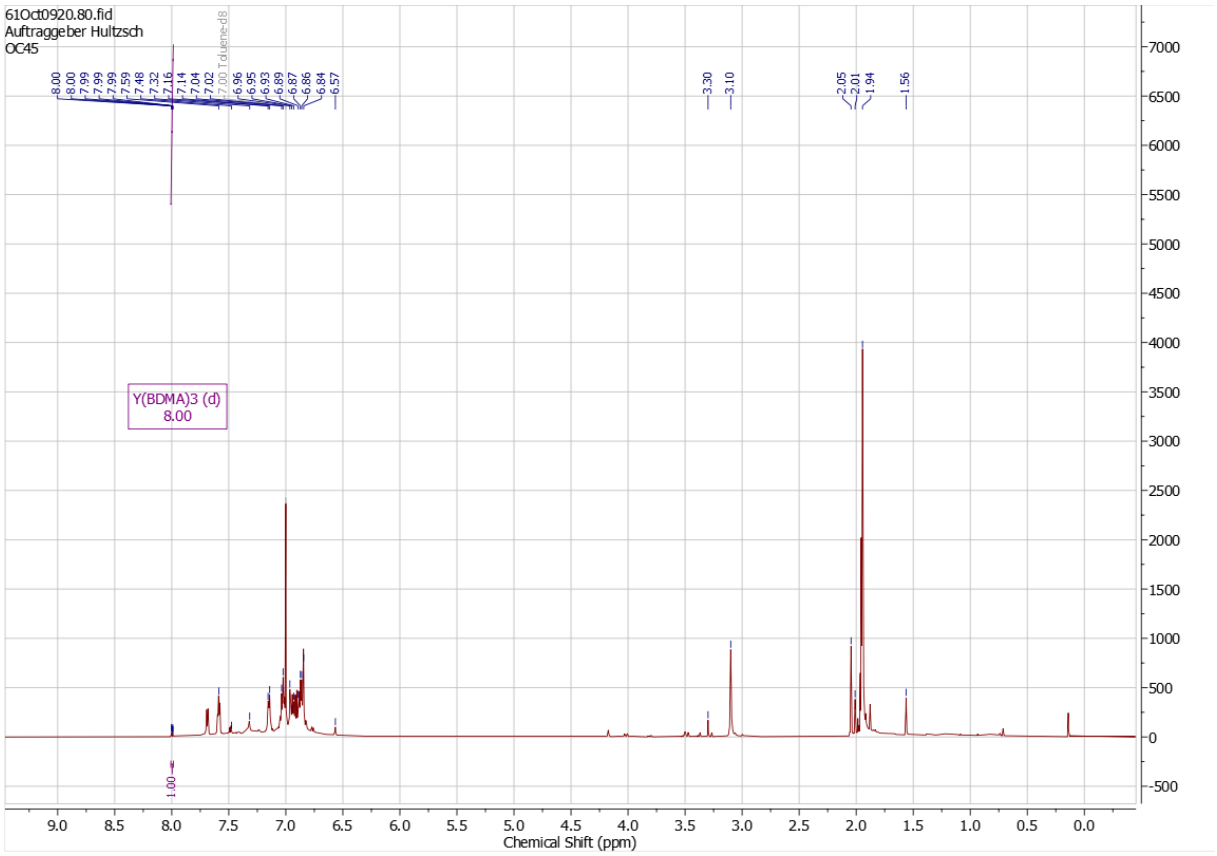

Supp. 21. ^{1}H-NMR spectrum of the attempted complexation of [Y(o-$C_6H_4CH_2NMe_2$)$_3$] with 6,6'-methylenebis(4-methyl-2-(triphenylsilyl)phenol) at –20 °C; solvent: toluene-d_8, 600 MHz.

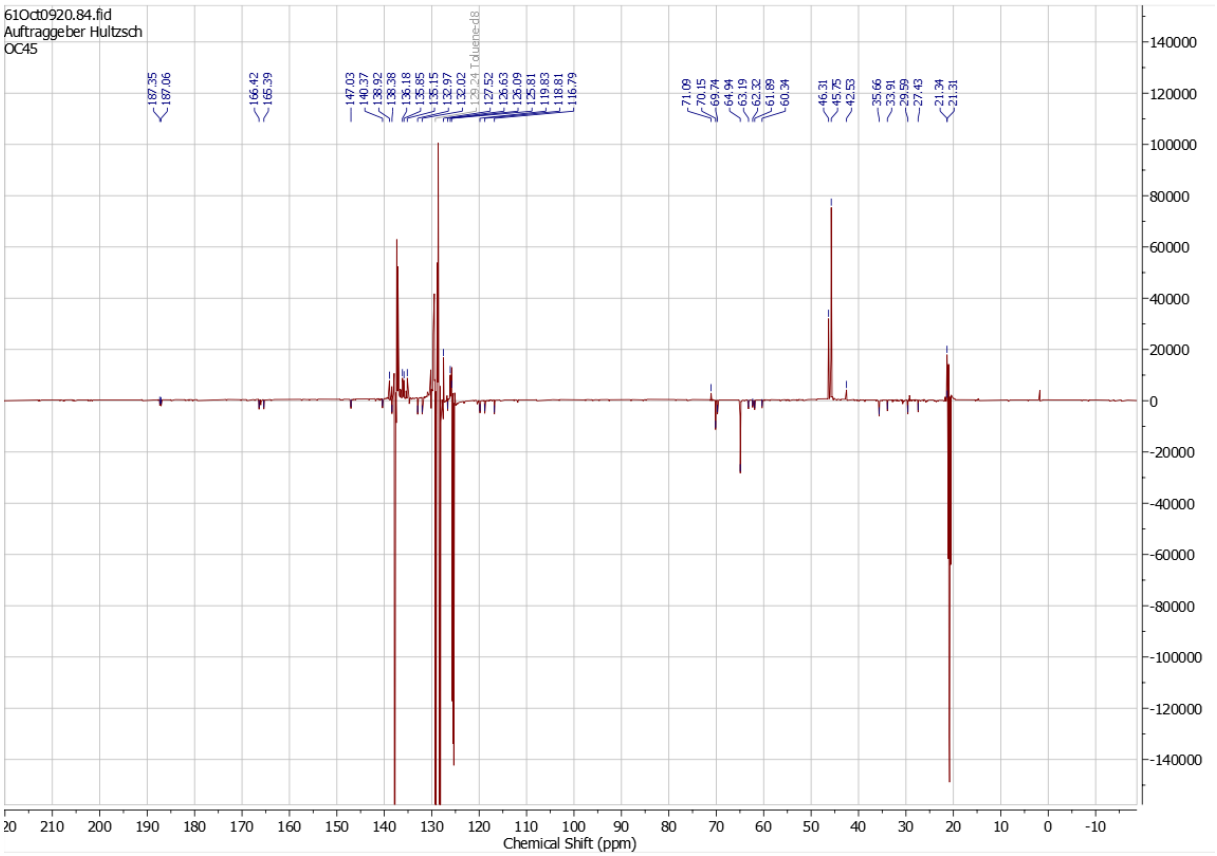

Supp. 22. ^{1}H-NMR spectrum of the attempted complexation of [Y(o-$C_6H_4CH_2NMe_2)_3$] with 6,6'-methylenebis(4-methyl-2-(triphenylsilyl)phenol) at –20 °C; solvent: toluene-d_8, 151 MHz.

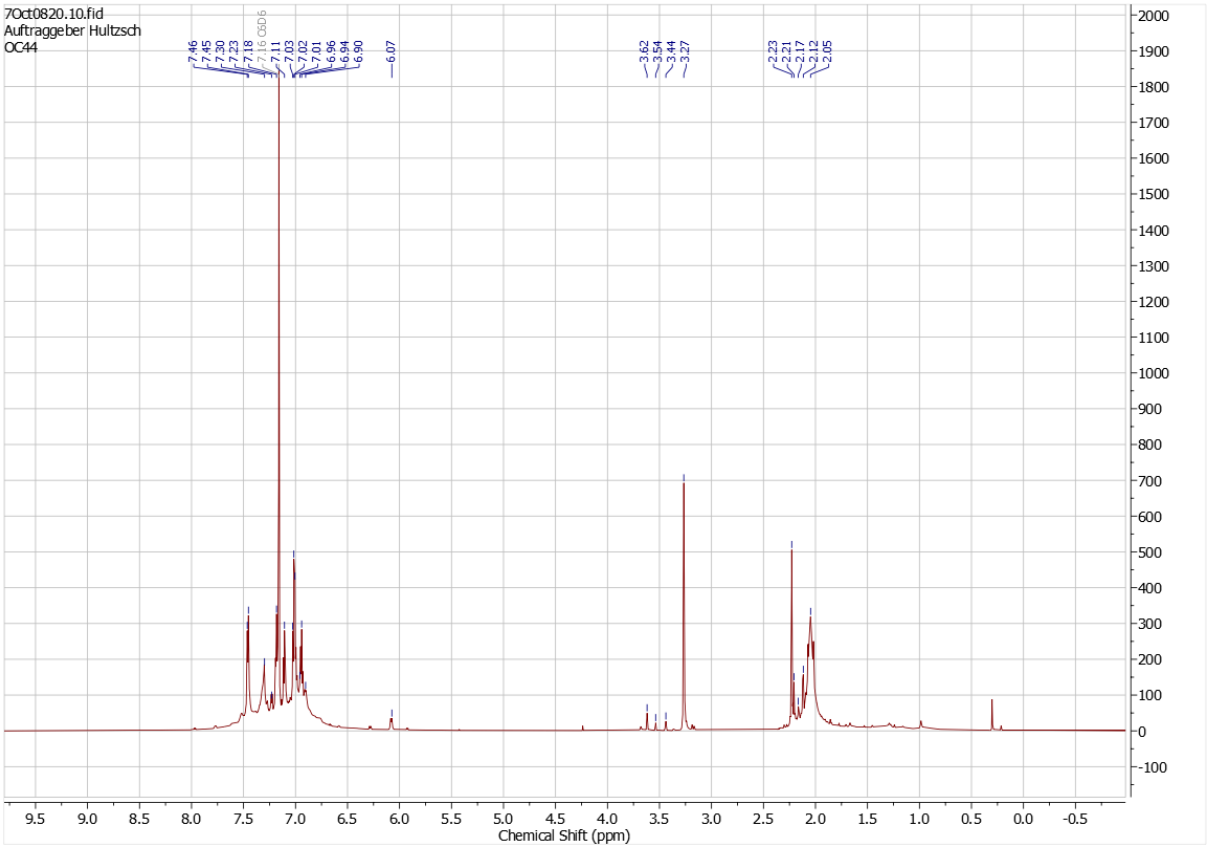

Supp. 23. ^{1}H-NMR spectrum of the attempted complexation of [Y(o-$C_6H_4CH_2NMe_2$)$_3$] with 6,6'-disulfanediylbis(4-methyl-2-tritylphenol) at room temperature; solvent: C_6D_6, 700 MHz.

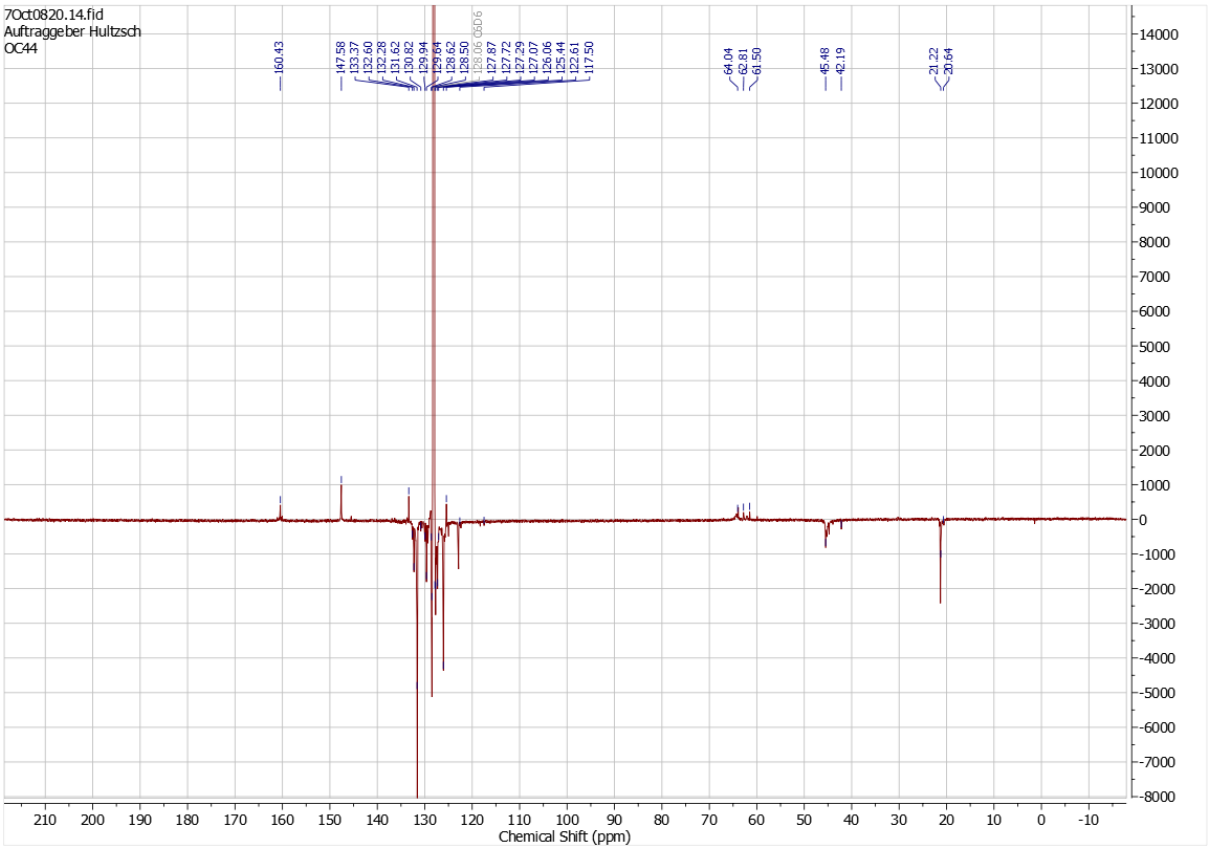

Supp. 24. ^{1}H-NMR spectrum of the attempted complexation of [Y(o-$C_6H_4CH_2NMe_2)_3$] with 6,6'-disulfanediylbis(4-methyl-2-tritylphenol) at room temperature; solvent: C_6D_6, 176 MHz.

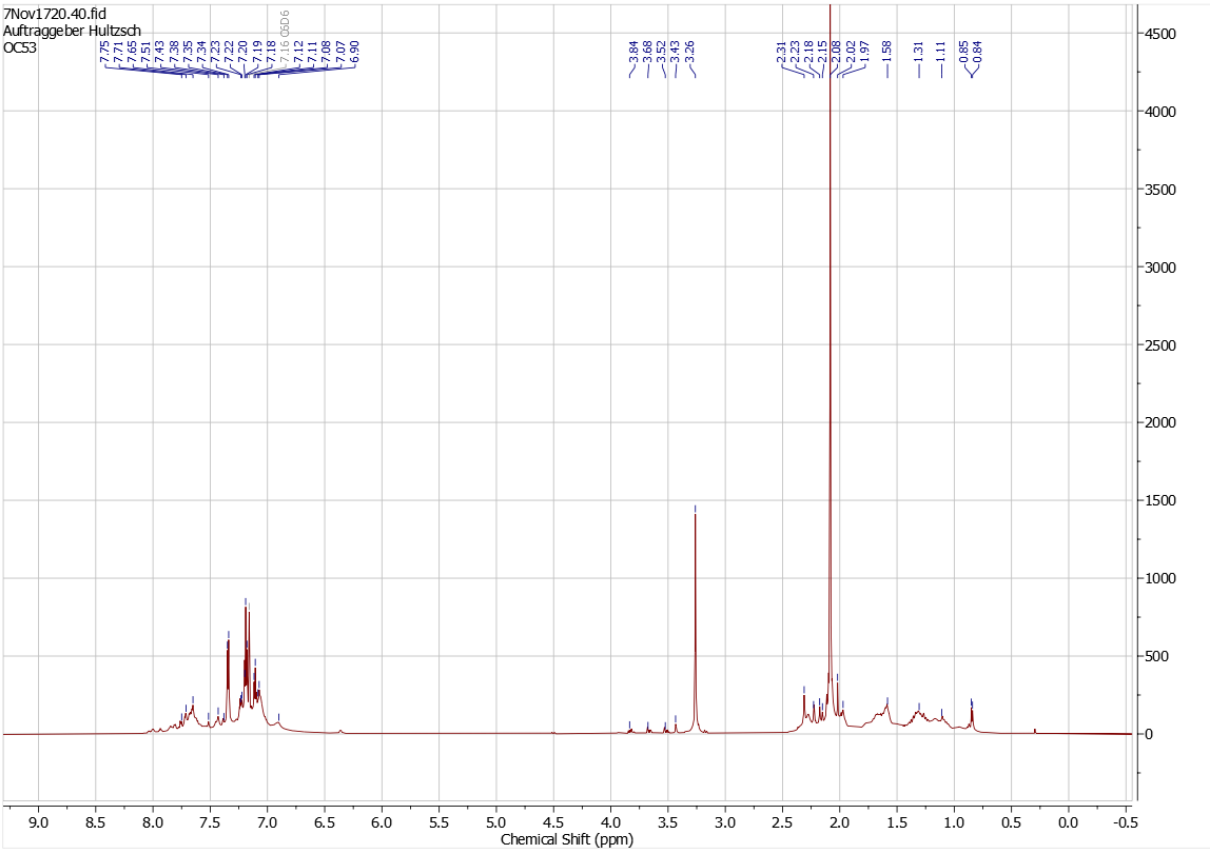

Supp. 25. ^{1}H-NMR spectrum of the attempted complexation of [Y(o-$C_6H_4CH_2NMe_2)_3$] with 6,6'-methylenebis(2-(cyclohexyldiphenylsilyl)-4-methylphenol) at room temperature; solvent: C_6D_6, 700 MHz.

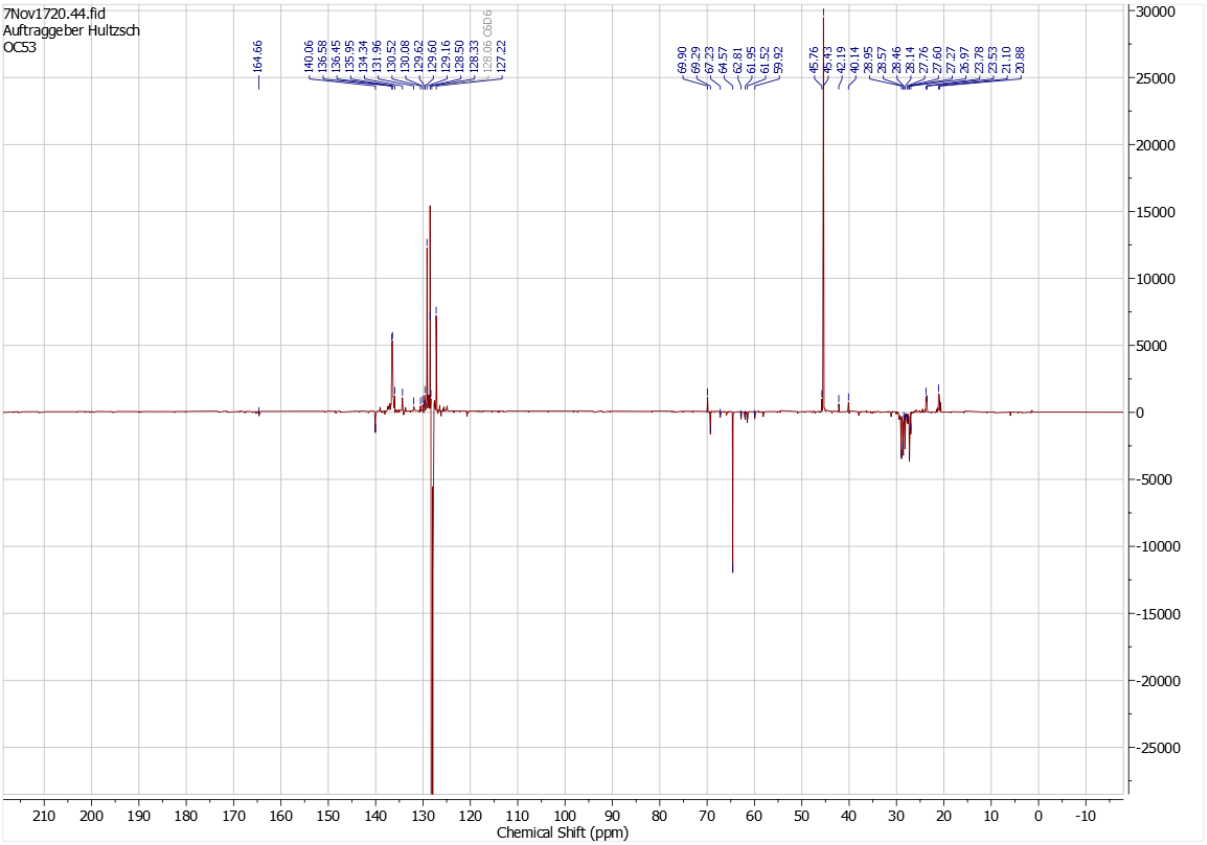

Supp. 26. ^{13}C-NMR spectrum of the attempted complexation of [Y(o-$C_6H_4CH_2NMe_2)_3$] with 6,6'-methylenebis(2-(cyclohexyldiphenylsilyl)-4-methylphenol) at room temperature; solvent: C_6D_6, 176 MHz.

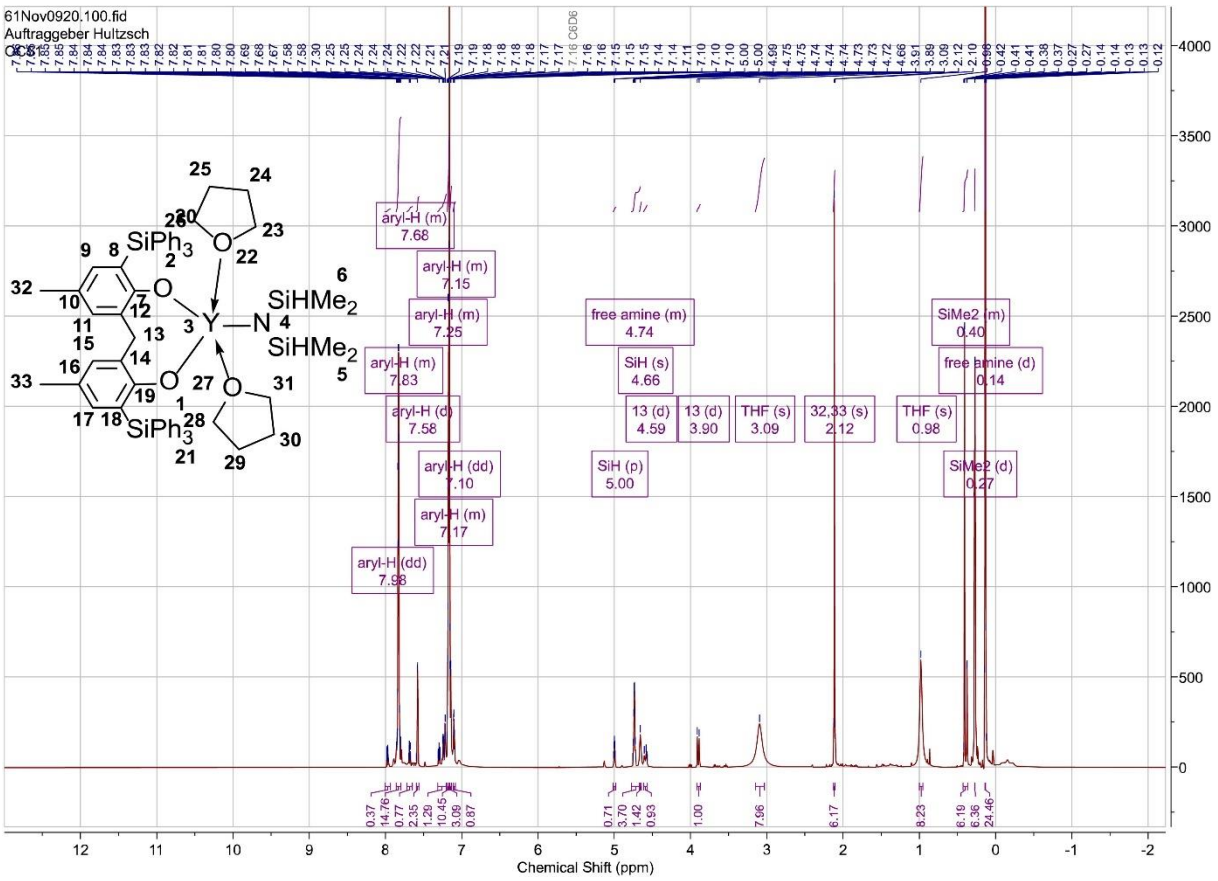

Supp. 27. ^{1}H-NMR spectrum of the complex **17-Y**; solvent: C_6D_6, 600 MHz.

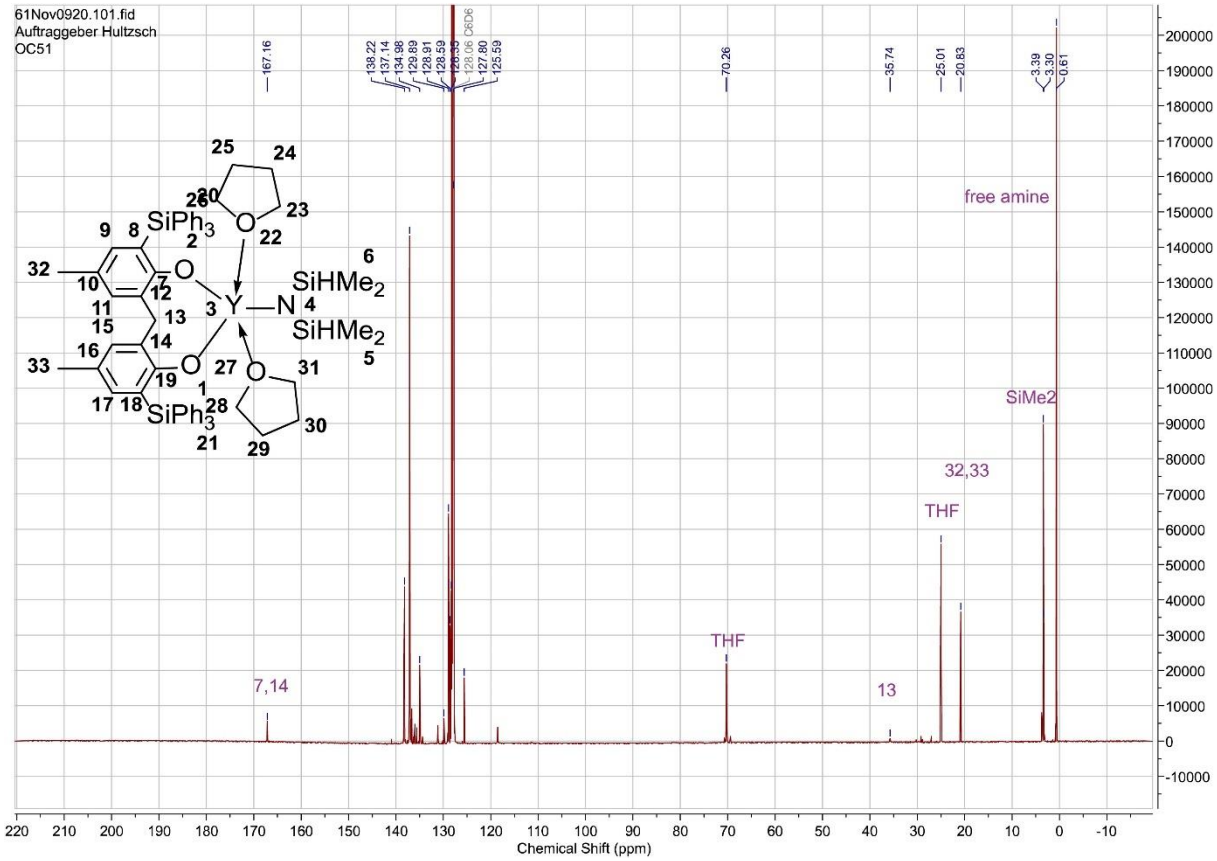

Supp. 28. ^{13}C-NMR spectrum of the complex **17-Y**; solvent: C_6D_6, 151 MHz.

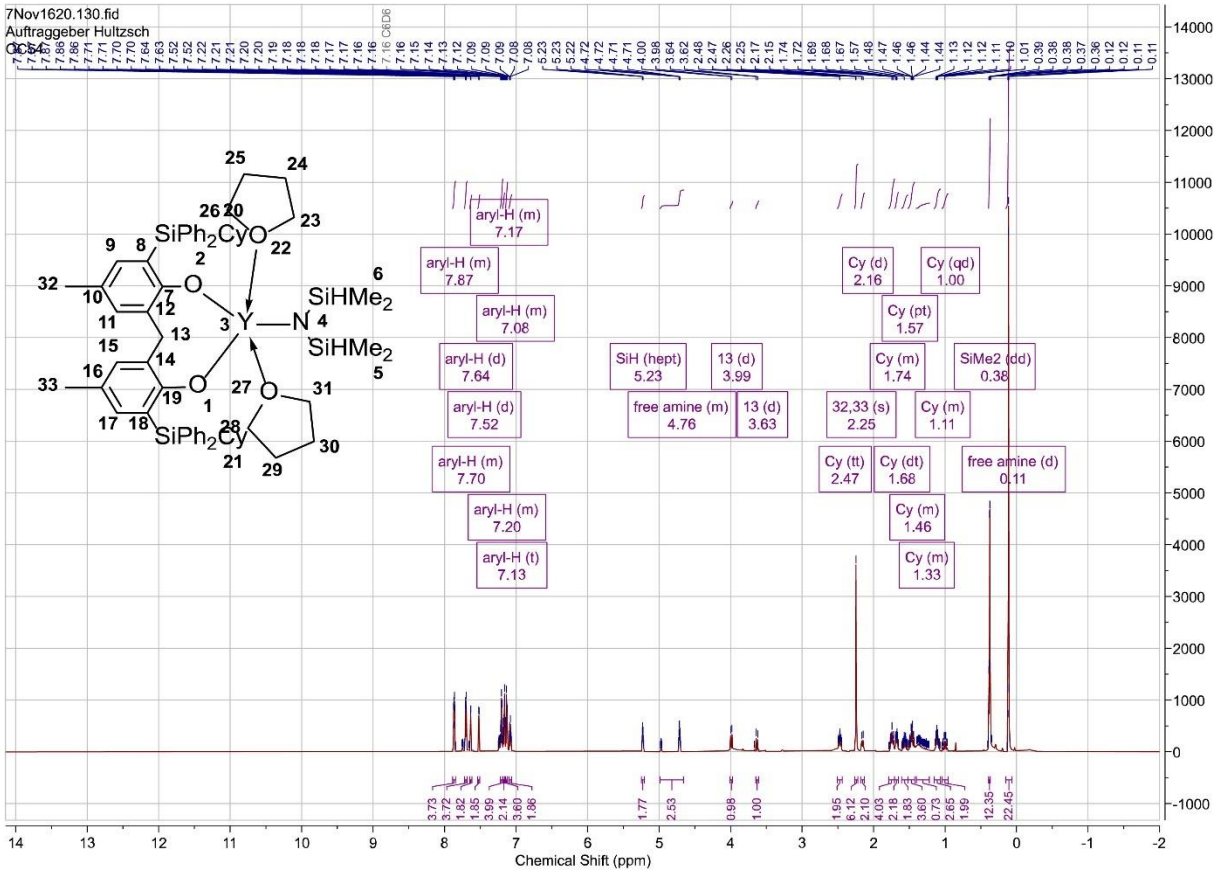

Supp. 29. ^{1}H-NMR spectrum of the complex **18-Y**; solvent: C_6D_6, 700 MHz.

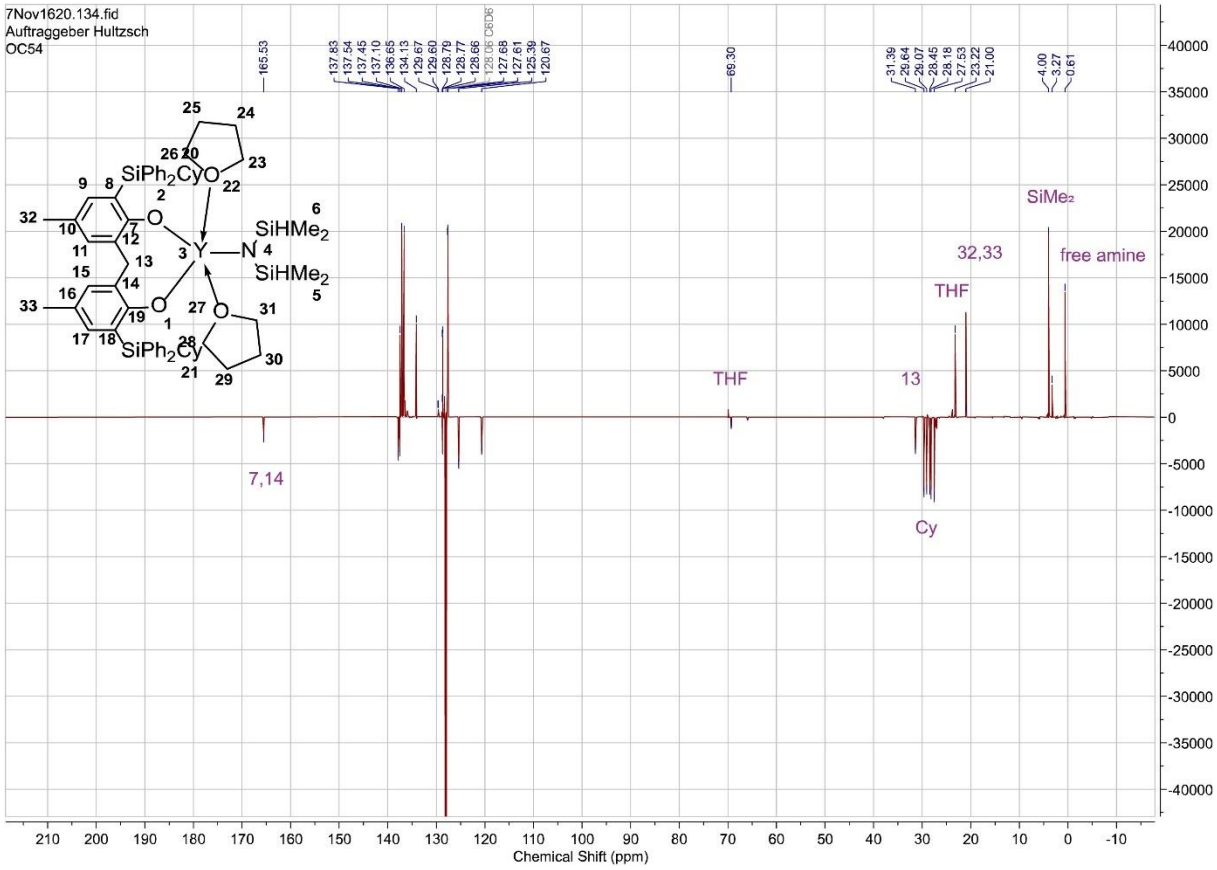

Supp. 30. ^{13}C-NMR spectrum of the complex **18-Y**; solvent: C_6D_6, 176 MHz.

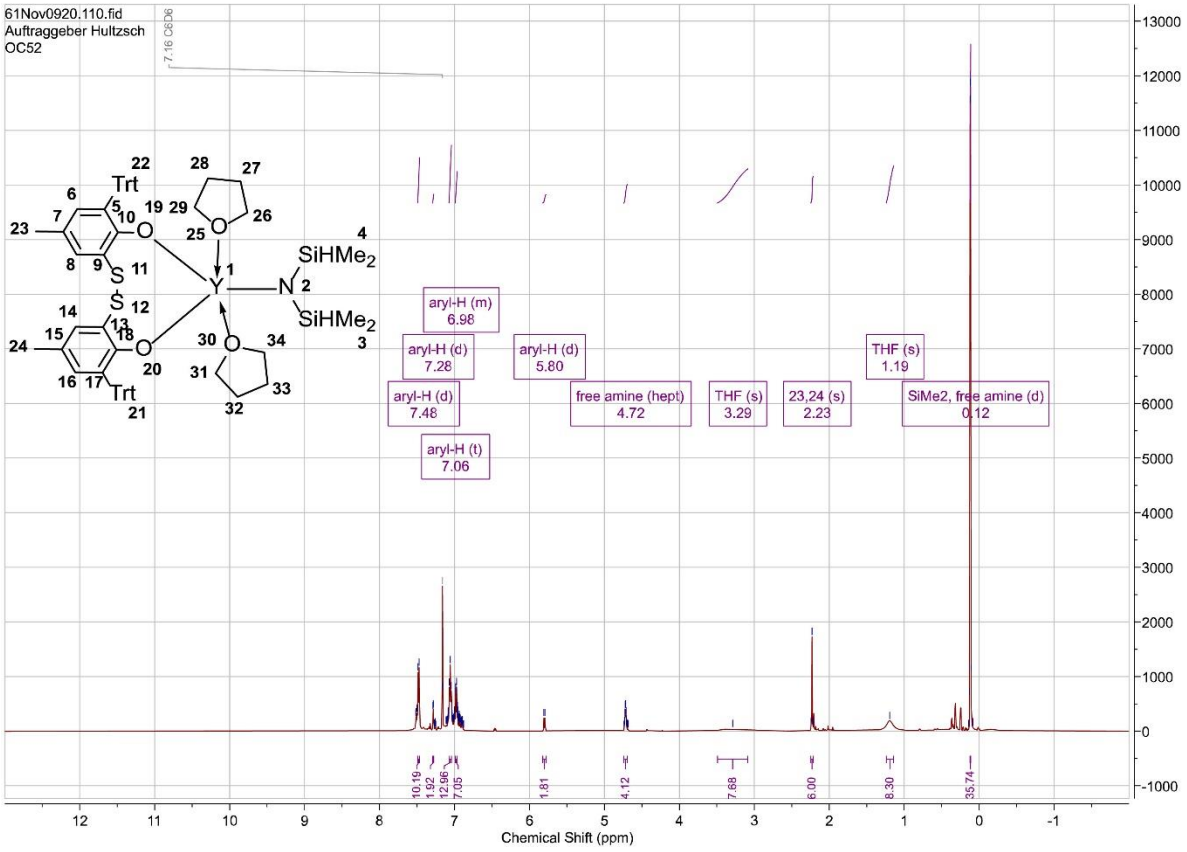

Supp. 31. ^{1}H-NMR spectrum of the complex **19-Y**; solvent: C_6D_6, 600 MHz.

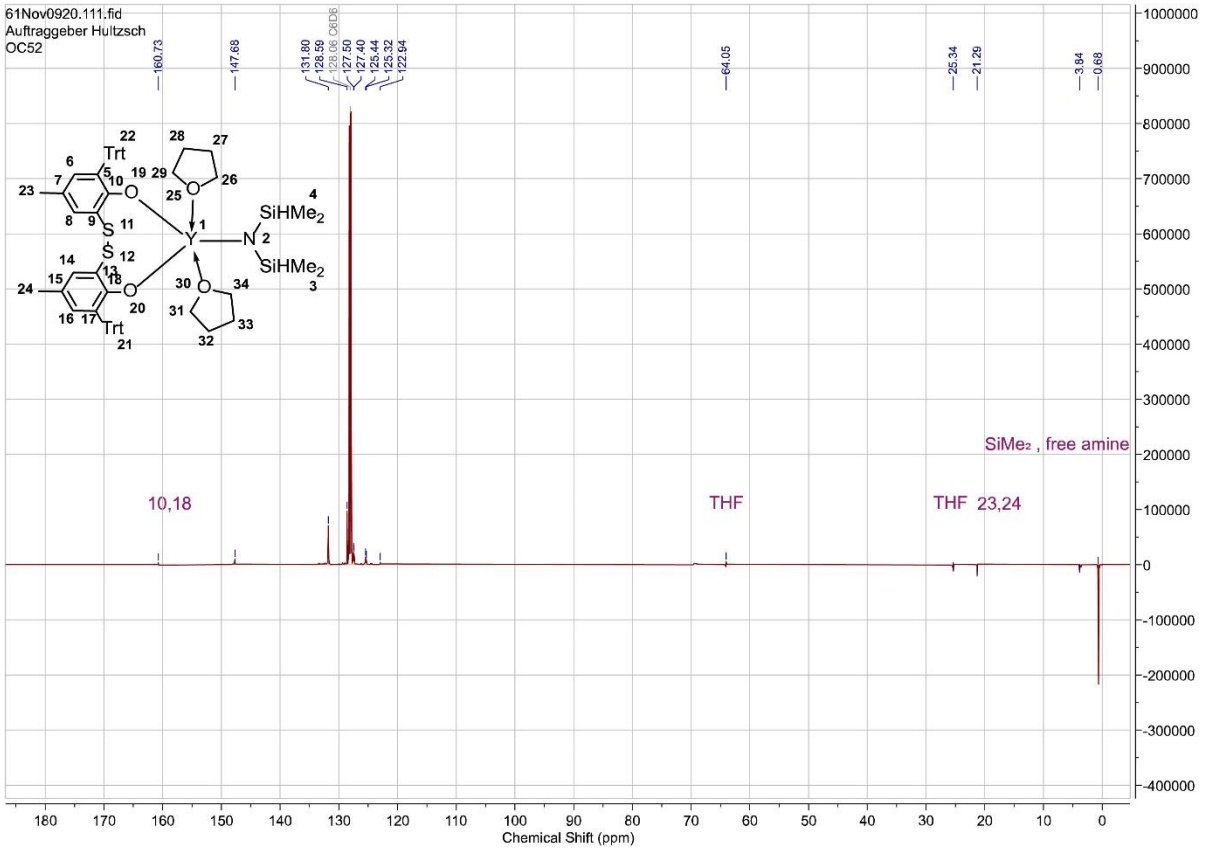

Supp. 32. ^{13}C-NMR spectrum of the complex **19-Y**; solvent: C_6D_6, 151 MHz.

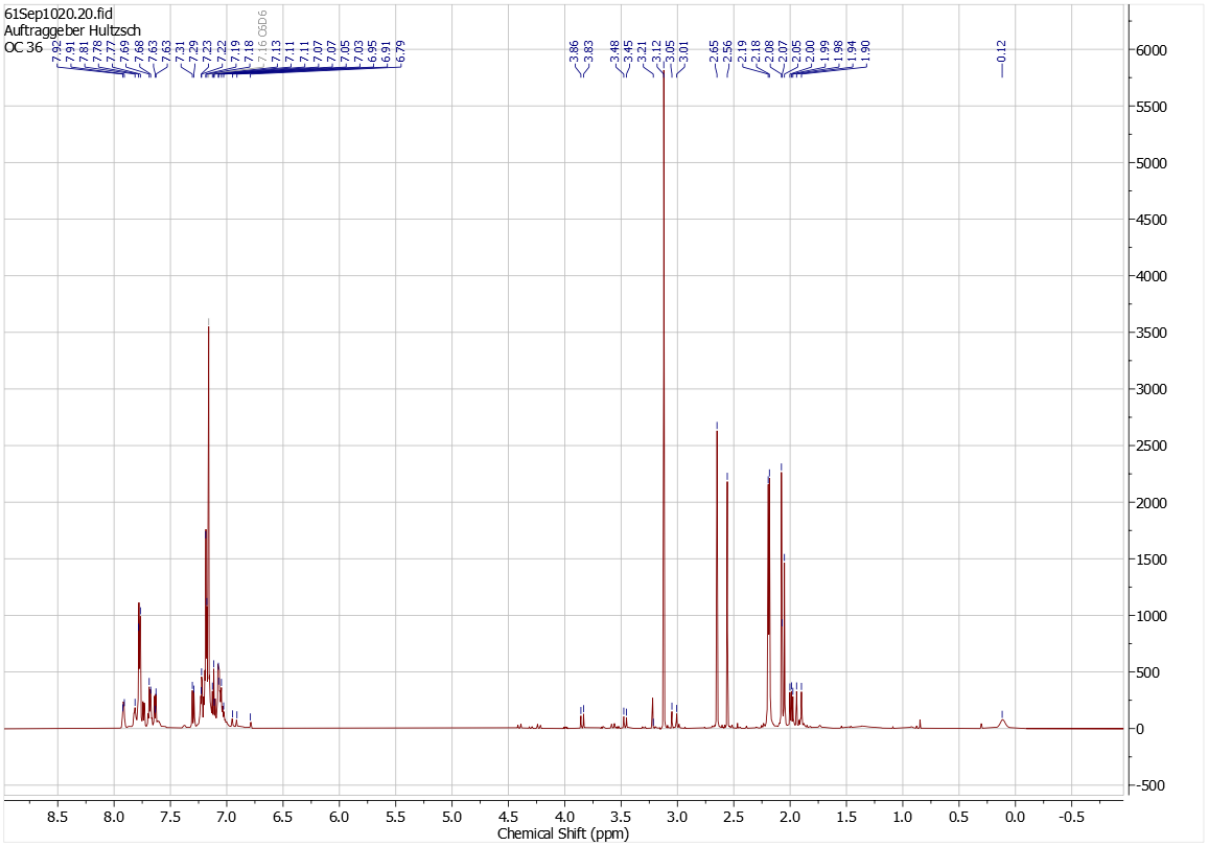

Supp. 33. ^{1}H-NMR spectrum of the attempted complexation of $Ti(NMe_2)_4$ with 6,6'-methylenebis(4-methyl-2-(triphenylsilyl)phenol) at room temperature; solvent: C_6D_6, 600 MHz.

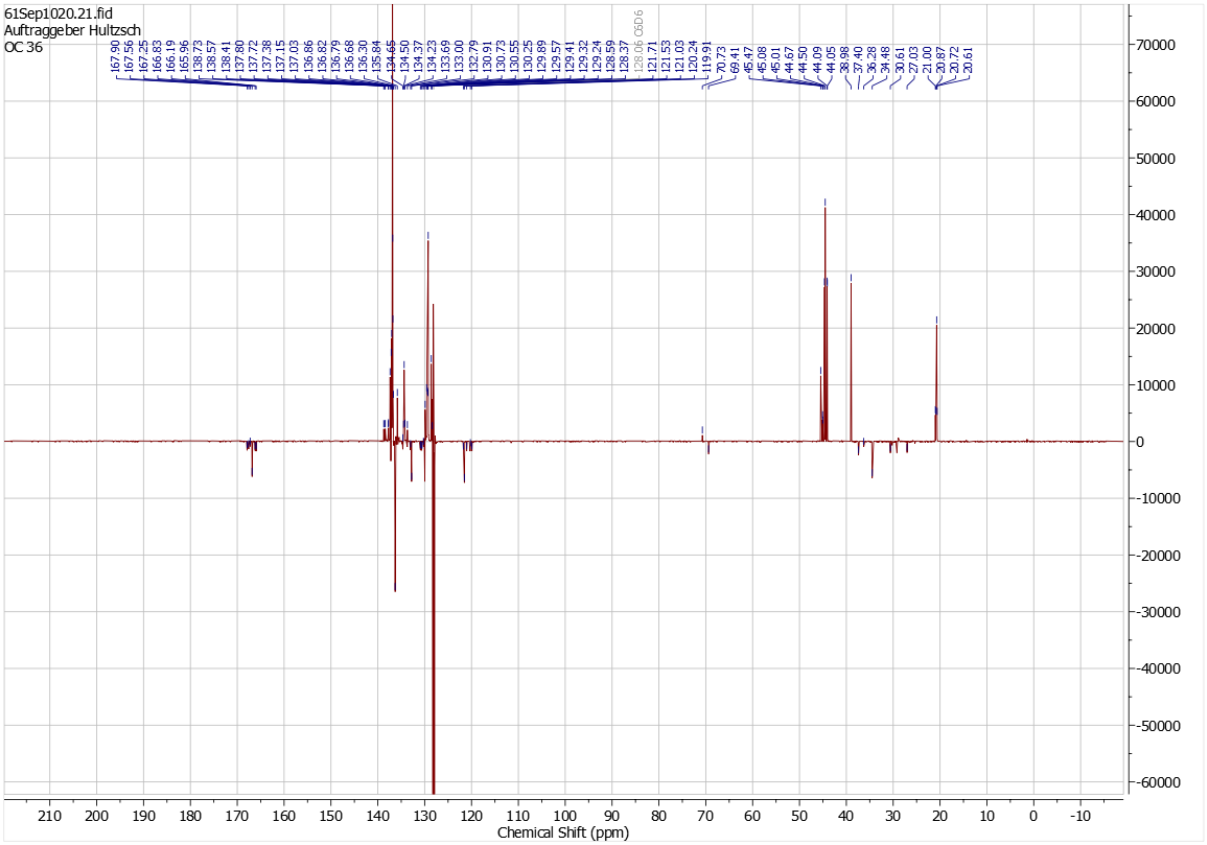

Supp. 34. ^{13}C-NMR spectrum of the attempted complexation of $Ti(NMe_2)_4$ with 6,6'-methylenebis(4-methyl-2-(triphenylsilyl)phenol) at room temperature; solvent: C_6D_6, 151 MHz.

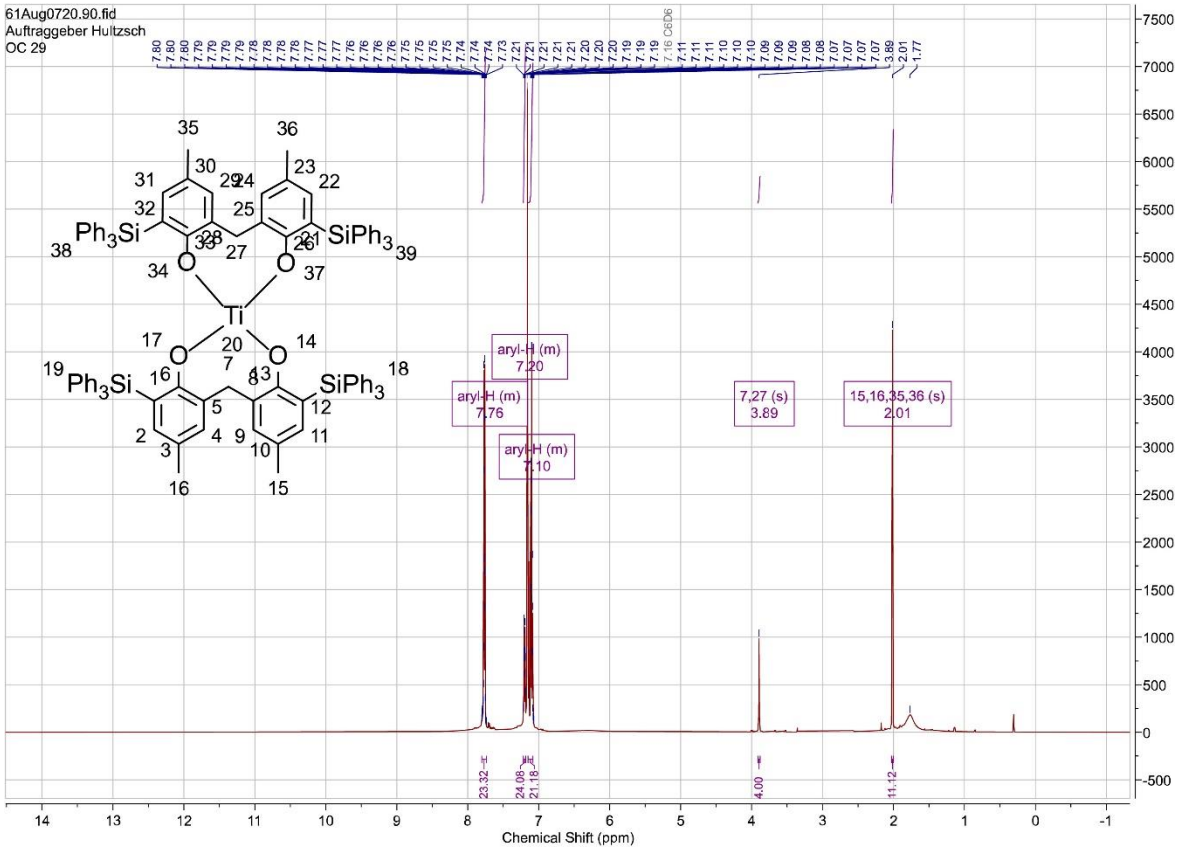

Supp. 35. ^{1}H-NMR spectrum of the complex **22-Ti**; solvent: C_6D_6, 600 MHz.

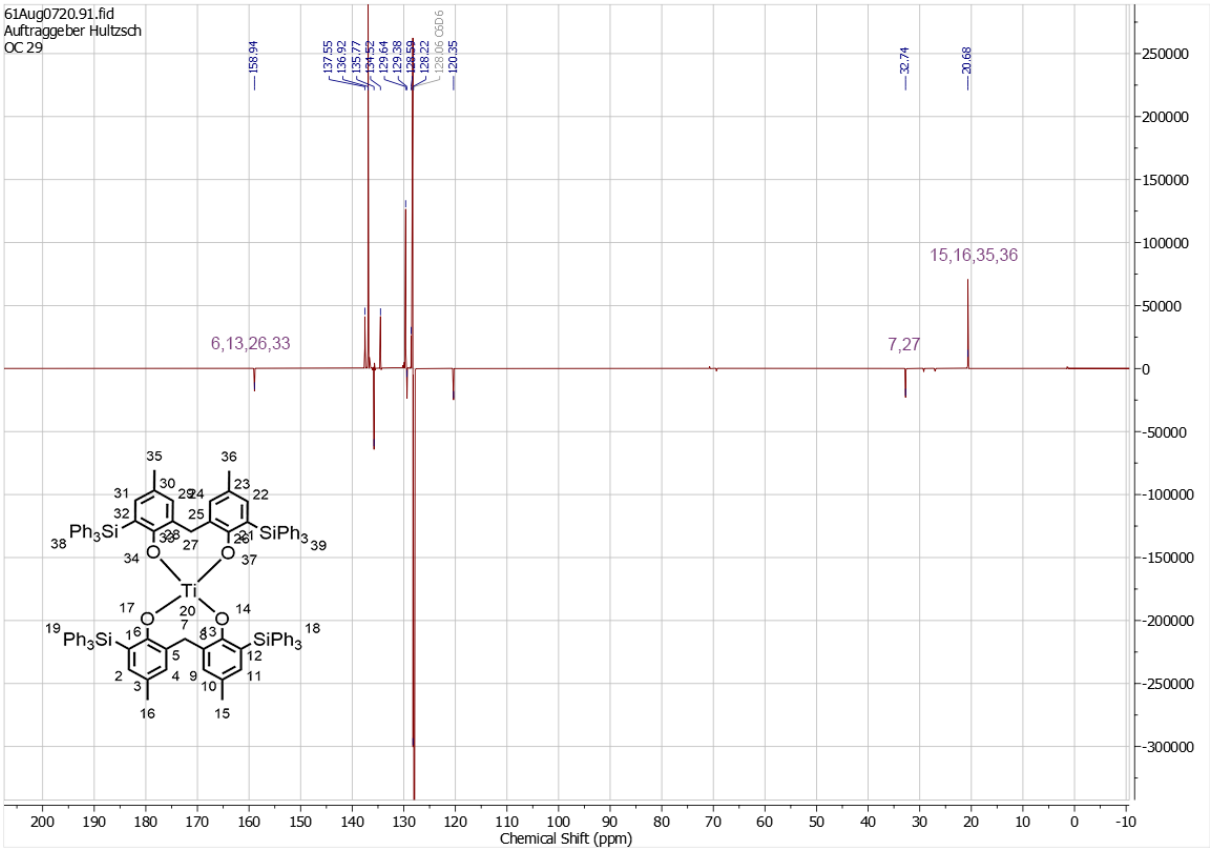

Supp. 36. ^{13}C-NMR spectrum of the complex **22-Ti**; solvent: C_6D_6, 151 MHz.

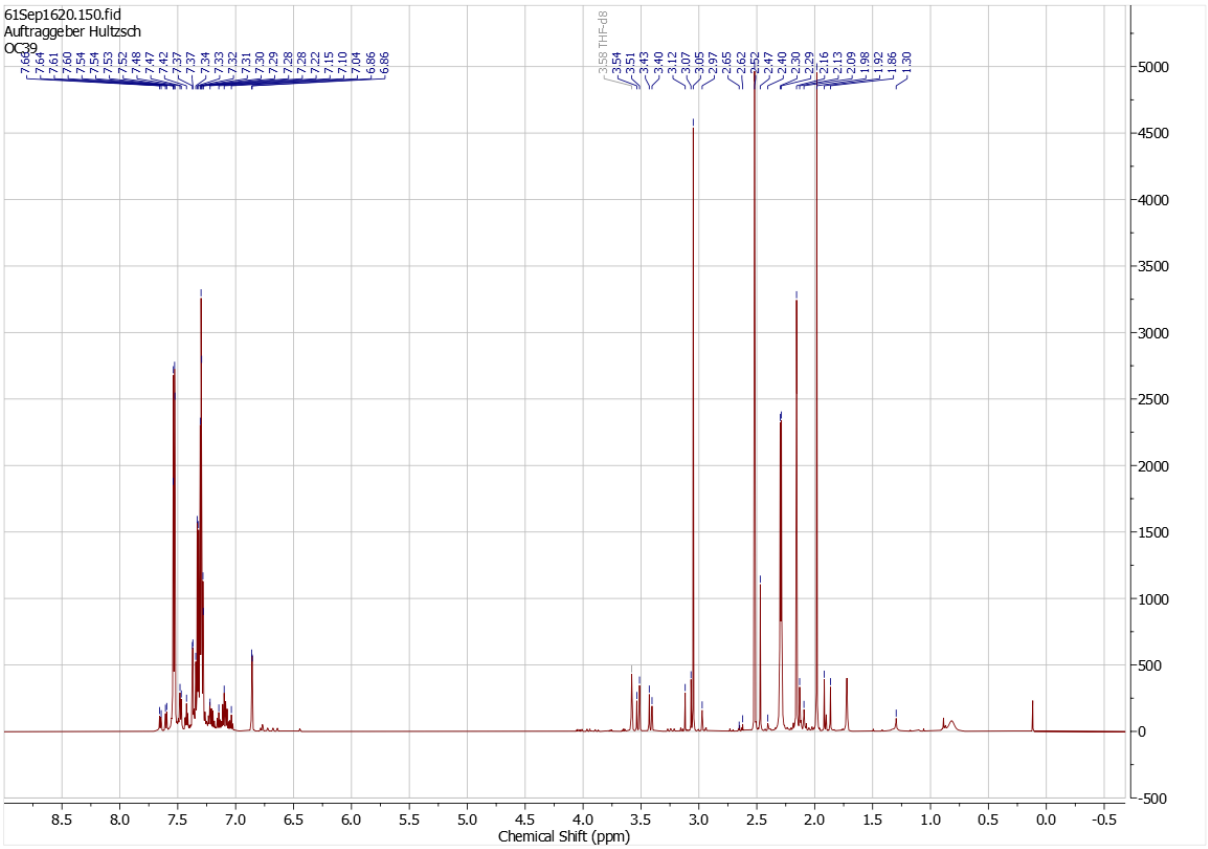

Supp. 37. ^{1}H-NMR spectrum of the attempted complexation of $Ti(NMe_2)_4$ with 6,6'-methylenebis(4-methyl-2-(triphenylsilyl)phenol) at –20 °C; solvent: THF-d_8, 600 MHz.

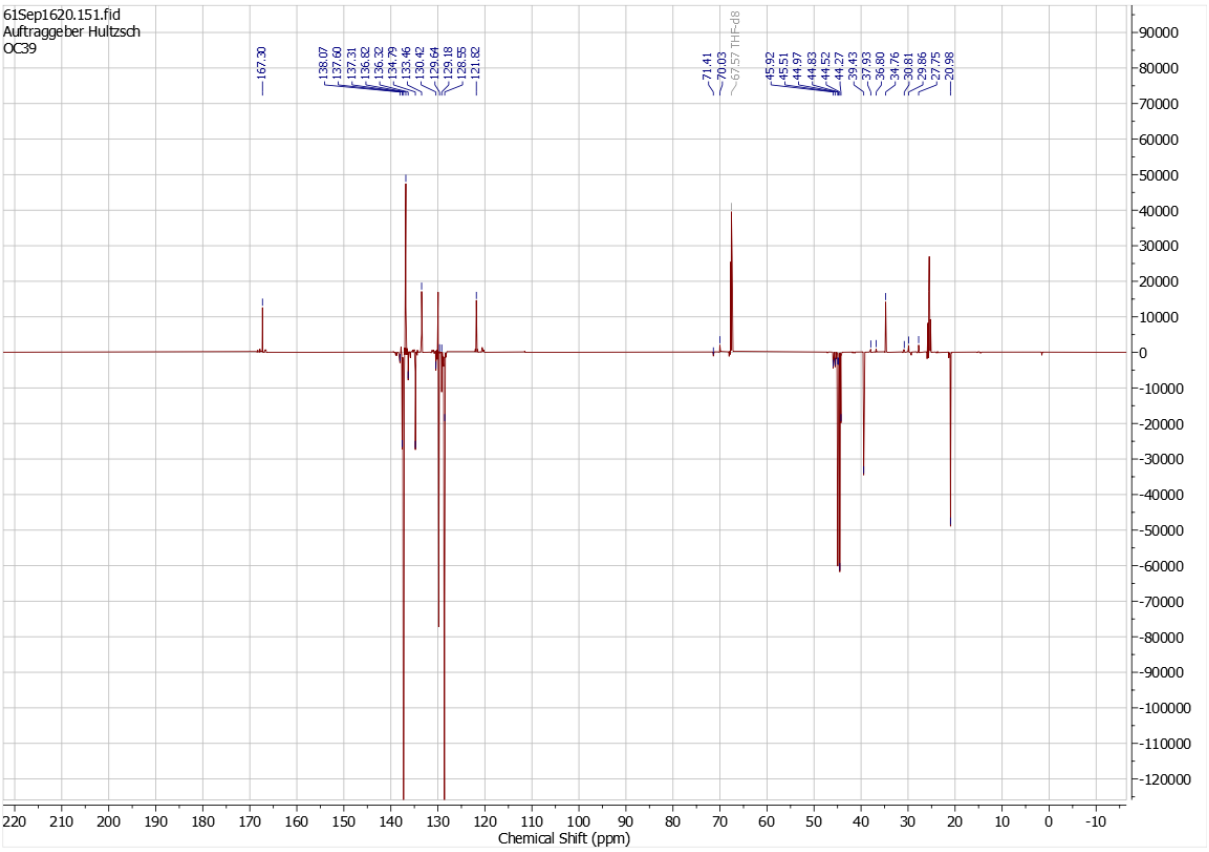

Supp. 38. ^{13}C-NMR spectrum of the complexation of $Ti(NMe_2)_4$ with 6,6'-methylenebis(4-methyl-2-(triphenylsilyl)phenol) at –20 °C; solvent: THF-d_8, 151 MHz.

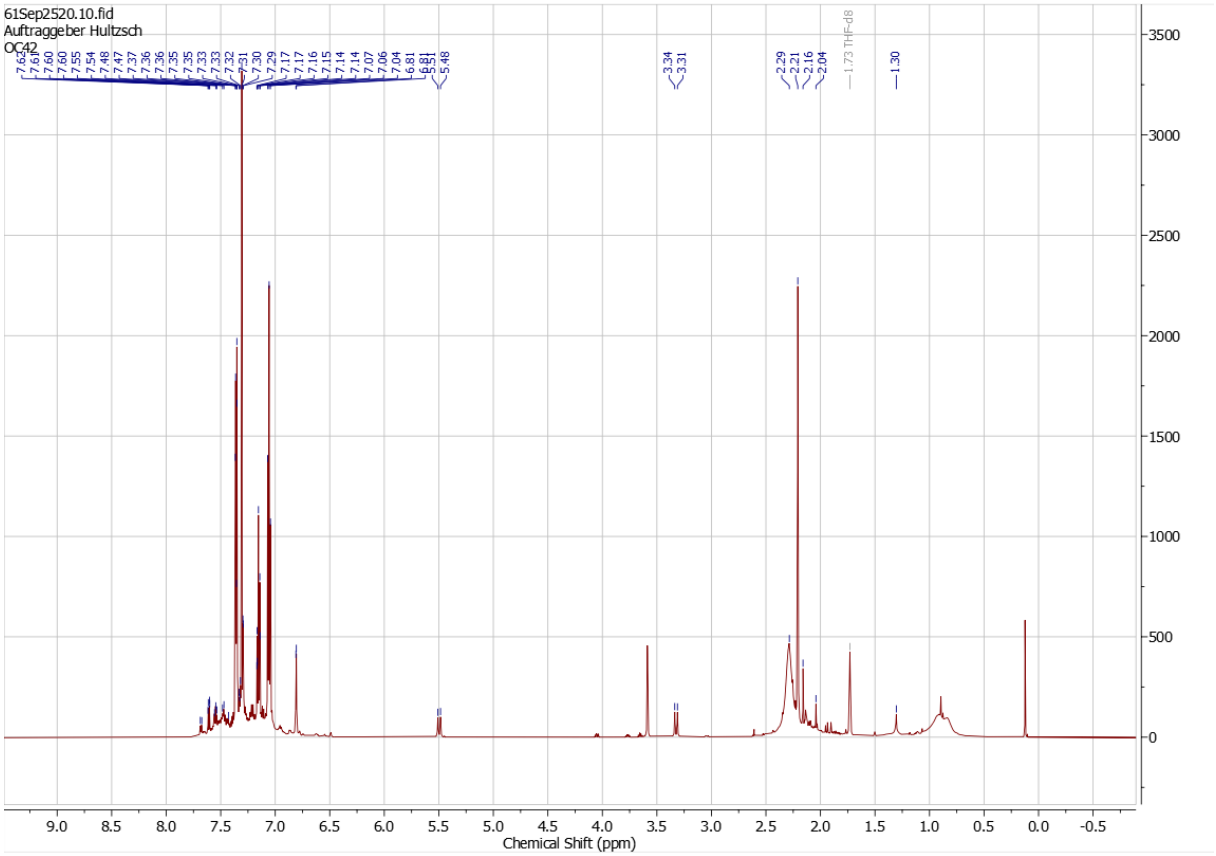

Supp. 39. ^{1}H-NMR spectrum of the attempted complexation of $Ti(NMe_2)_4$ with 6,6'-methylenebis(4-methyl-2-(triphenylsilyl)phenol) at –78 °C; solvent: THF-d_8, 600 MHz.

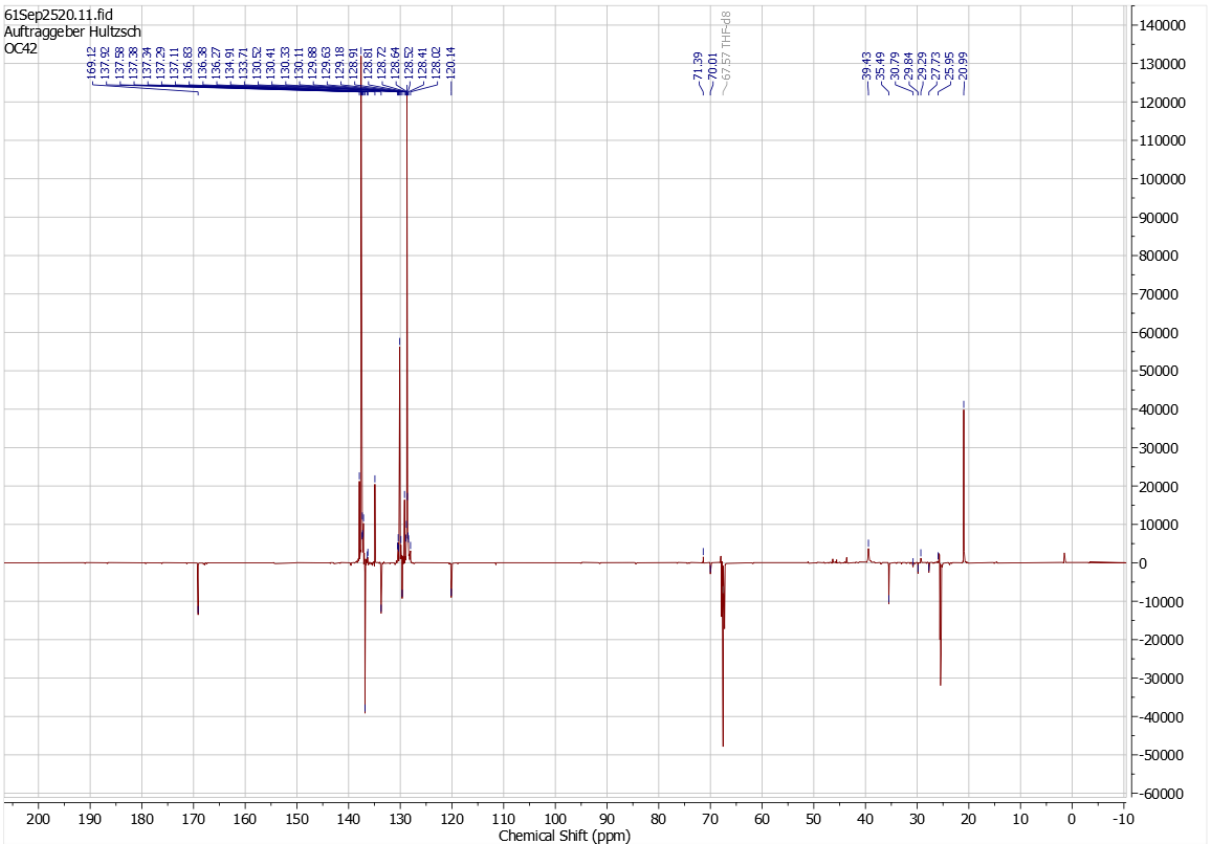

Supp. 40. ^{13}C-NMR spectrum of the attempted complexation of $Ti(NMe_2)_4$ with 6,6'-methylenebis(4-methyl-2-(triphenylsilyl)phenol) at –78 °C; solvent: THF-d_8, 151 MHz.

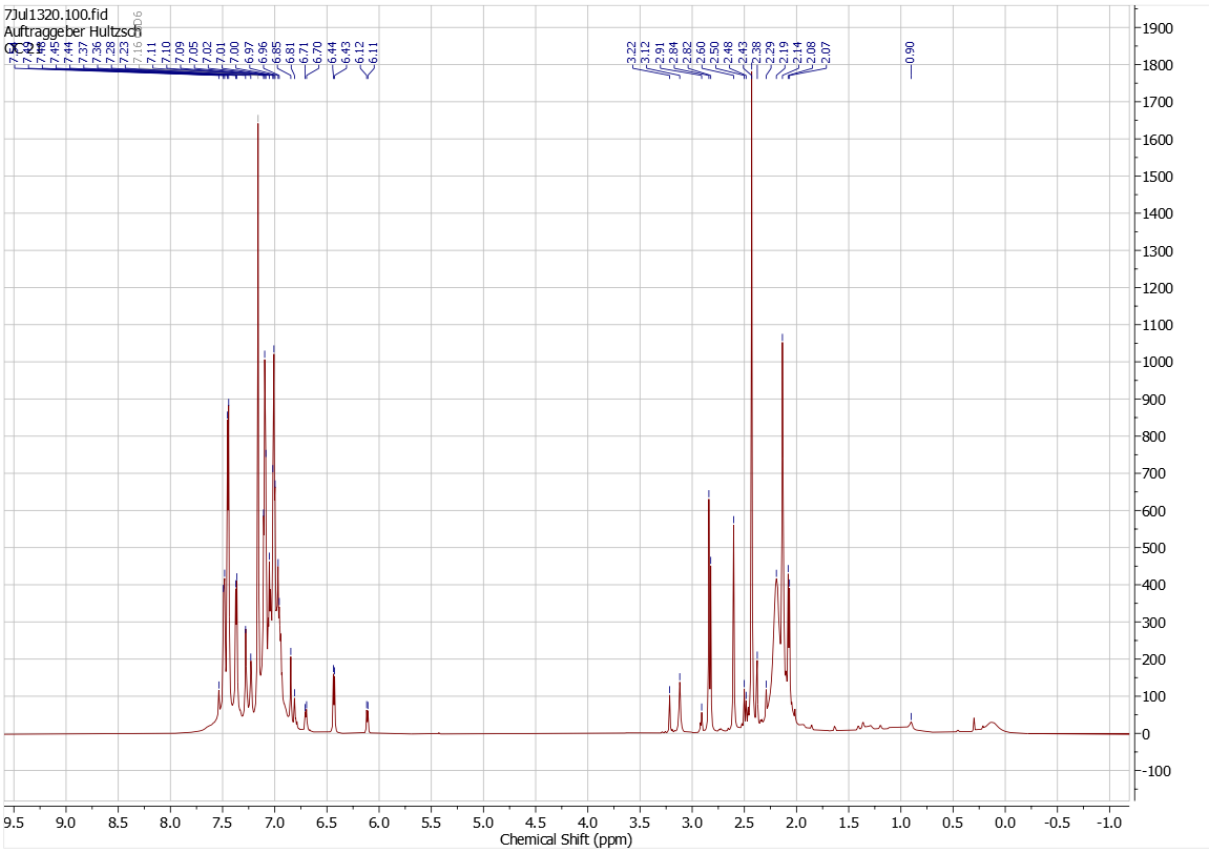

Supp. 41. ^{1}H-NMR spectrum of the attempted complexation of $Ti(NMe_2)_4$ with 6,6'-disulfanediylbis(4-methyl-2-tritylphenol) at room temperature; solvent: C_6D_6, 700 MHz.

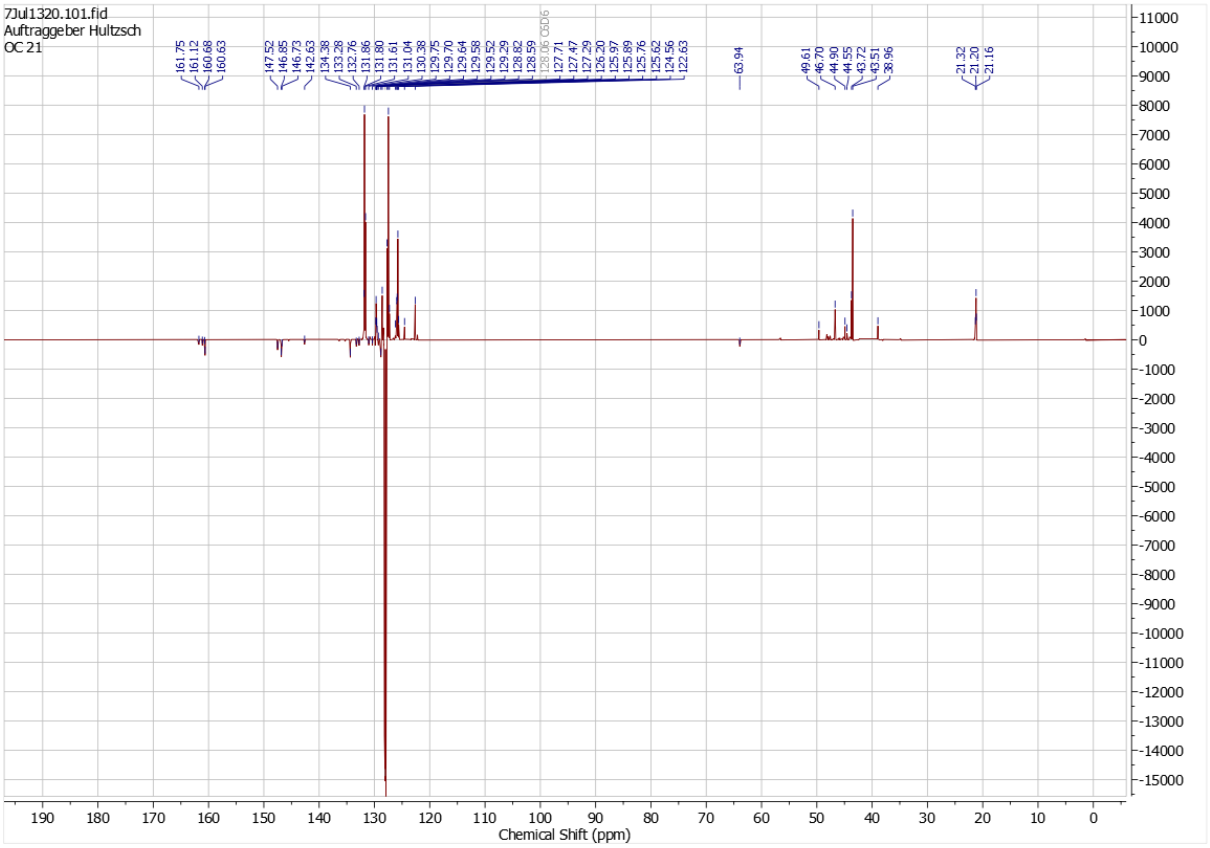

Supp. 42. ^{13}C-NMR spectrum of the attempted complexation of $Ti(NMe_2)_4$ with 6,6'-disulfanediylbis(4-methyl-2-tritylphenol) at room temperature; solvent: C_6D_6, 176 MHz.

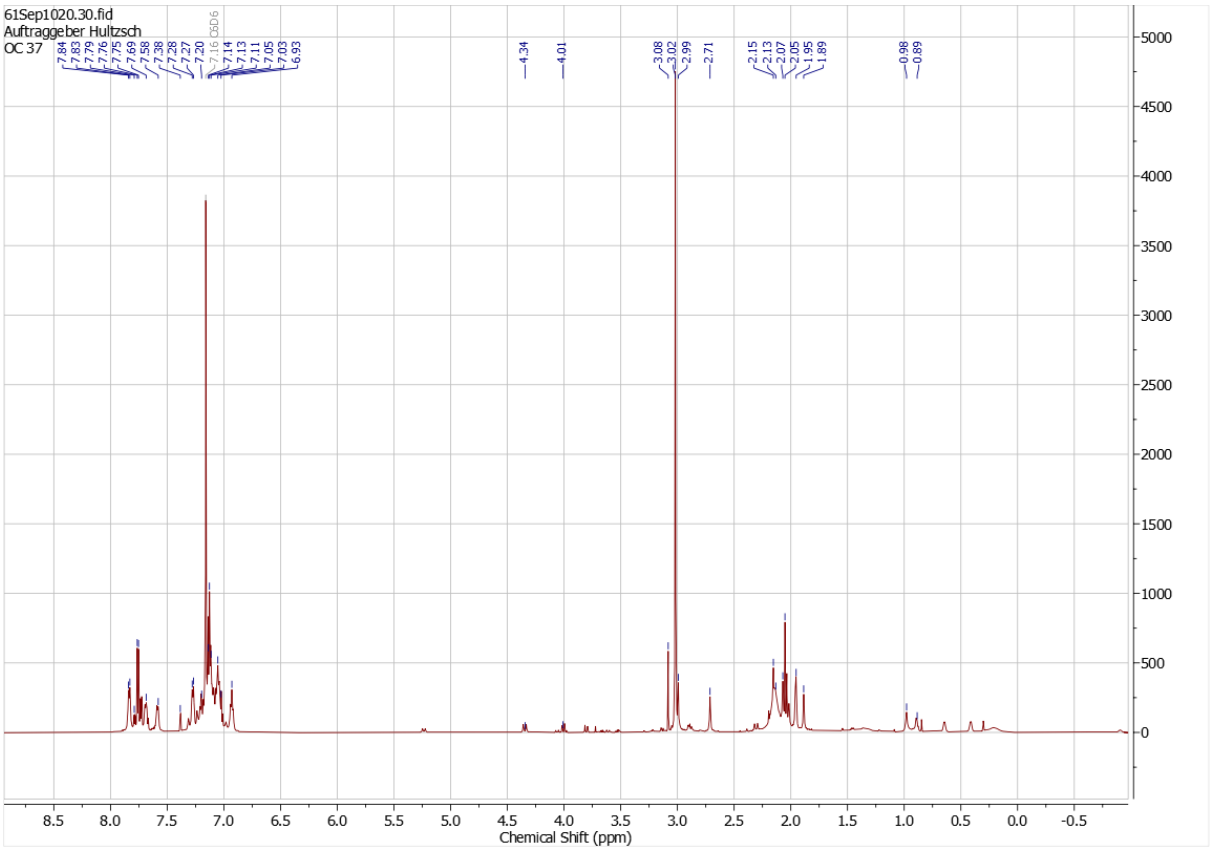

Supp. 43. ^{1}H-NMR spectrum of the attempted complexation of $Zr(NMe_2)_4$ with 6,6'-methylenebis(4-methyl-2-(triphenylsilyl)phenol) at room temperature; solvent: C_6D_6, 600 MHz.

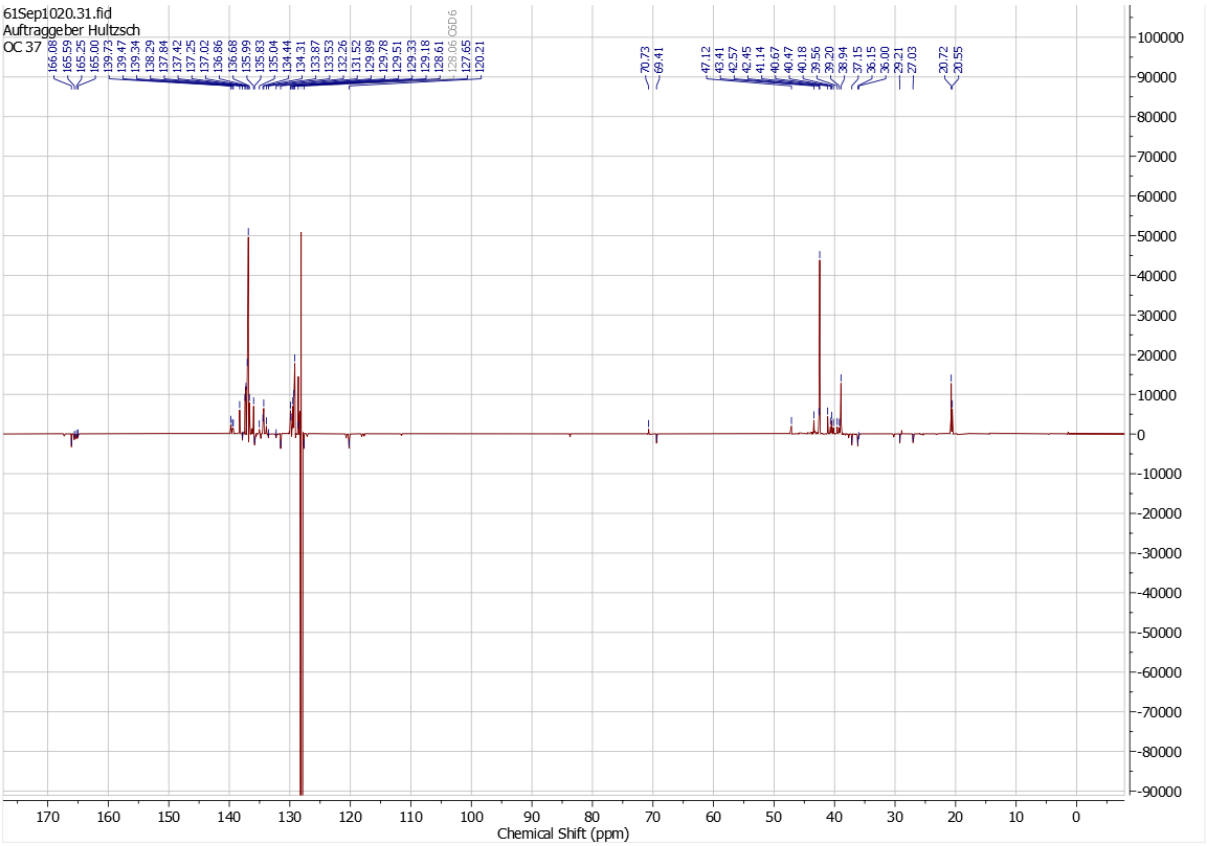

Supp. 44. ^{13}C-NMR spectrum of the attempted complexation of $Zr(NMe_2)_4$ with 6,6'-methylenebis(4-methyl-2-(triphenylsilyl)phenol) at room temperature; solvent: C_6D_6, 151 MHz.

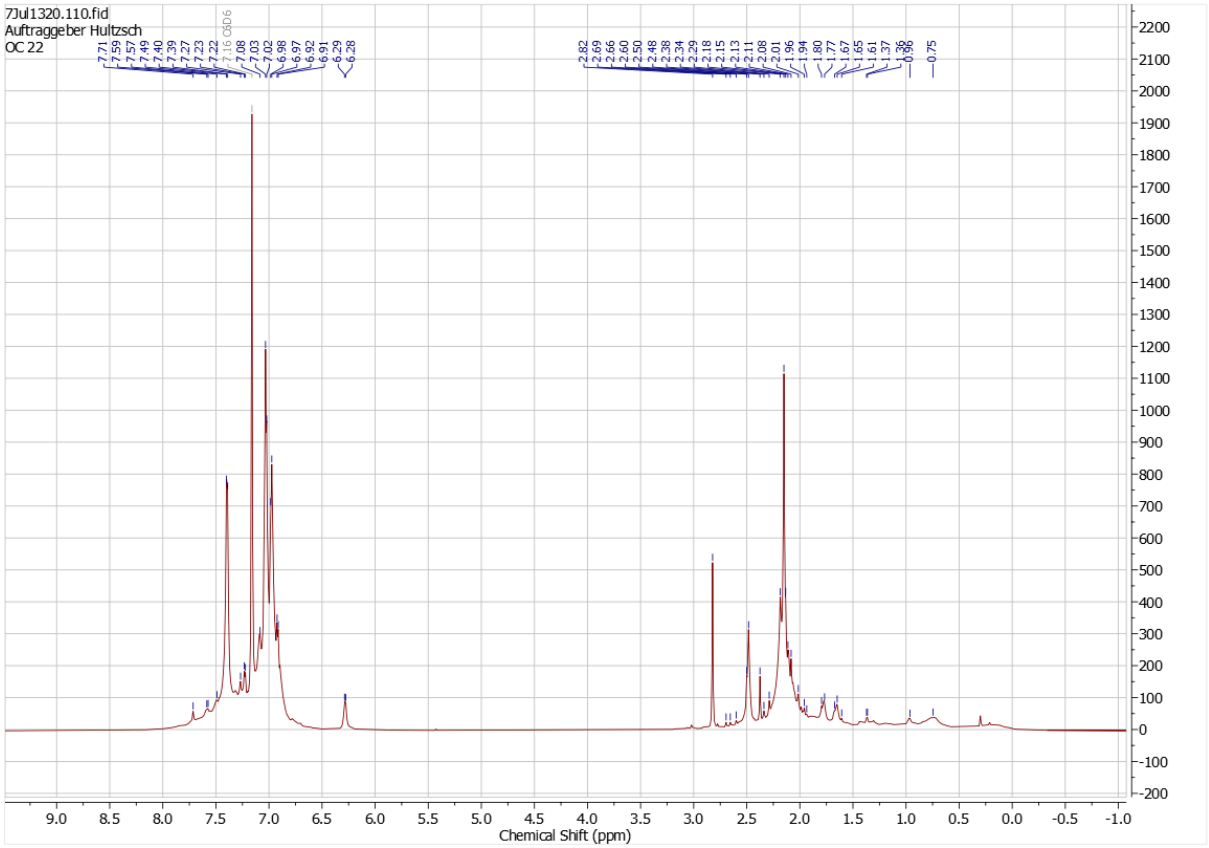

Supp. 45. ^{1}H-NMR spectrum of the attempted complexation of $Zr(NMe_2)_4$ with 6,6'-disulfanediylbis(4-methyl-2-tritylphenol) at room temperature; solvent: C_6D_6, 700 MHz.

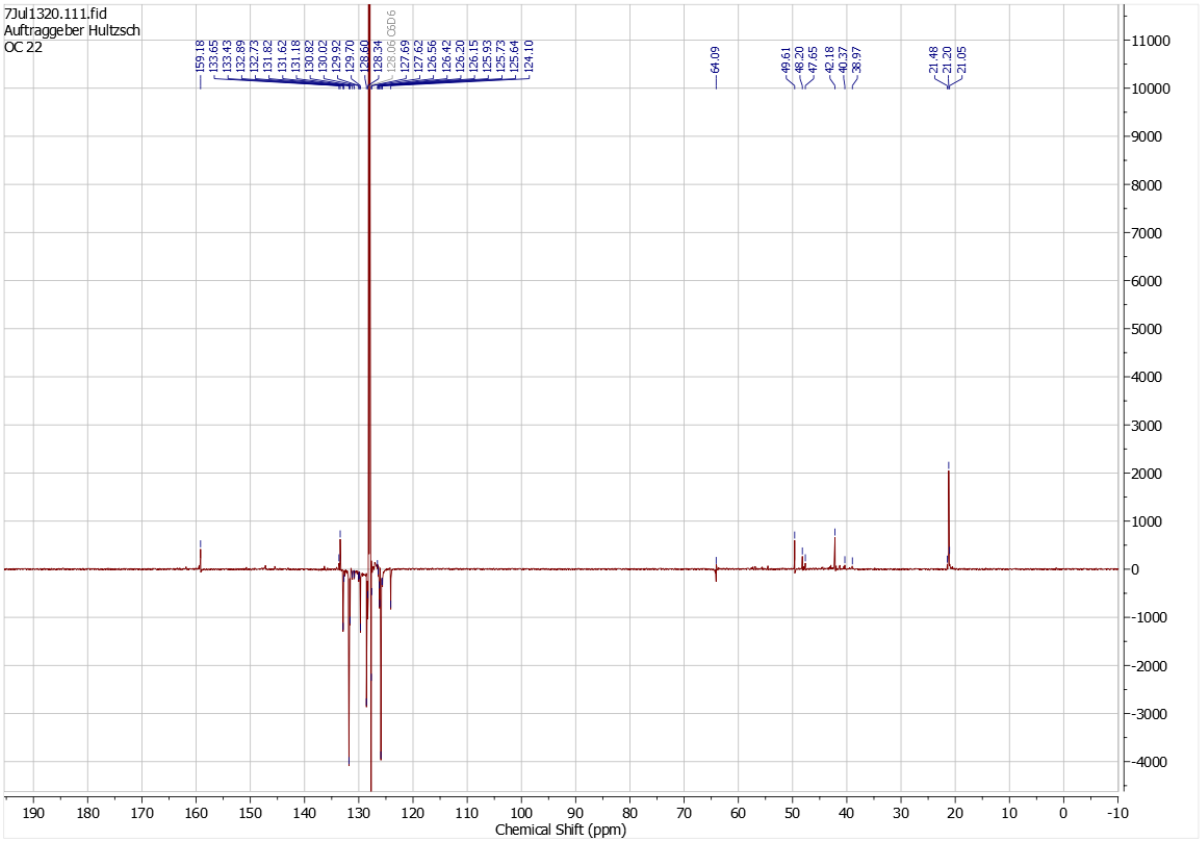

Supp. 46. ^{13}C-NMR spectrum of the attempted complexation of $Zr(NMe_2)_4$ with 6,6'-disulfanediylbis(4-methyl-2-tritylphenol) at room temperature; solvent: C_6D_6, 176 MHz.

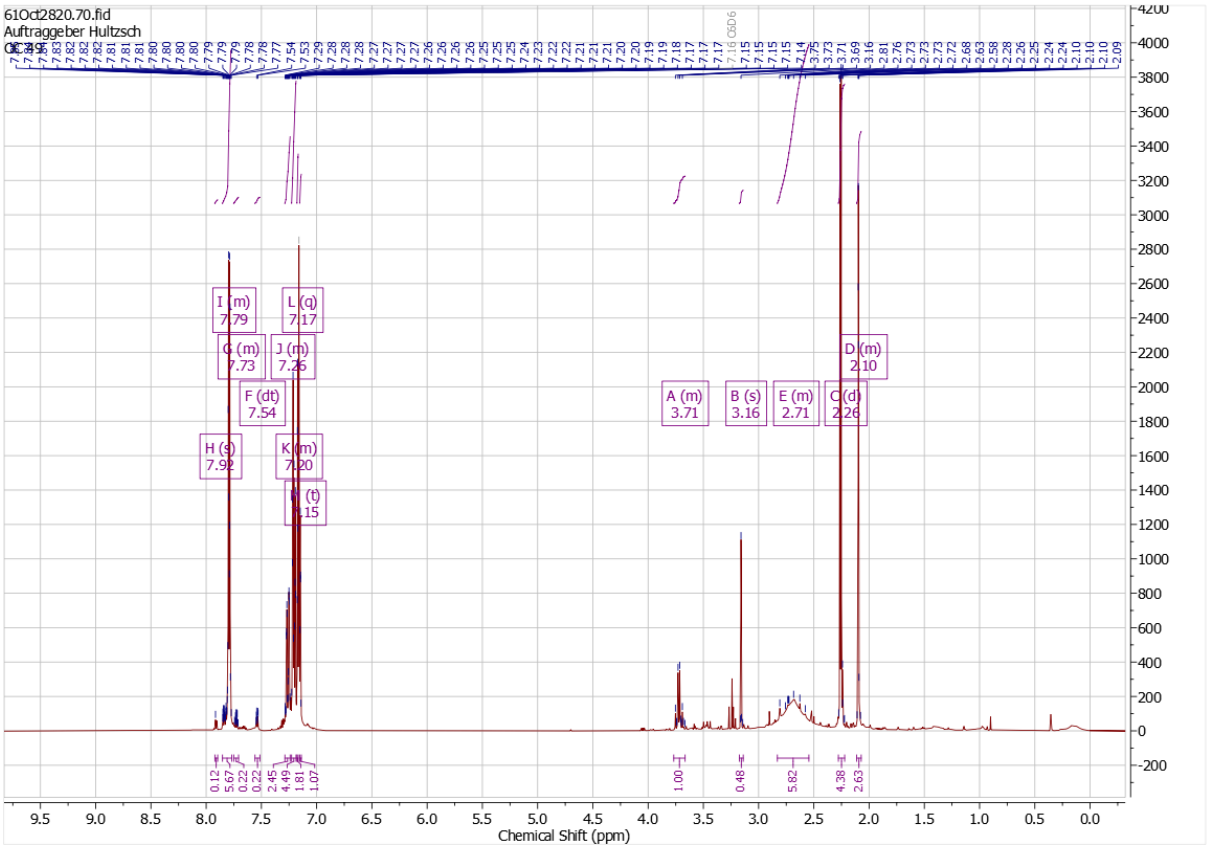

Supp. 47. ^{1}H-NMR spectrum of the complexation of $Nb(NMe_2)_5$ with 6,6'-methylenebis(4-methyl-2-(triphenylsilyl)phenol) at room temperature; solvent: C_6D_6, 600 MHz.

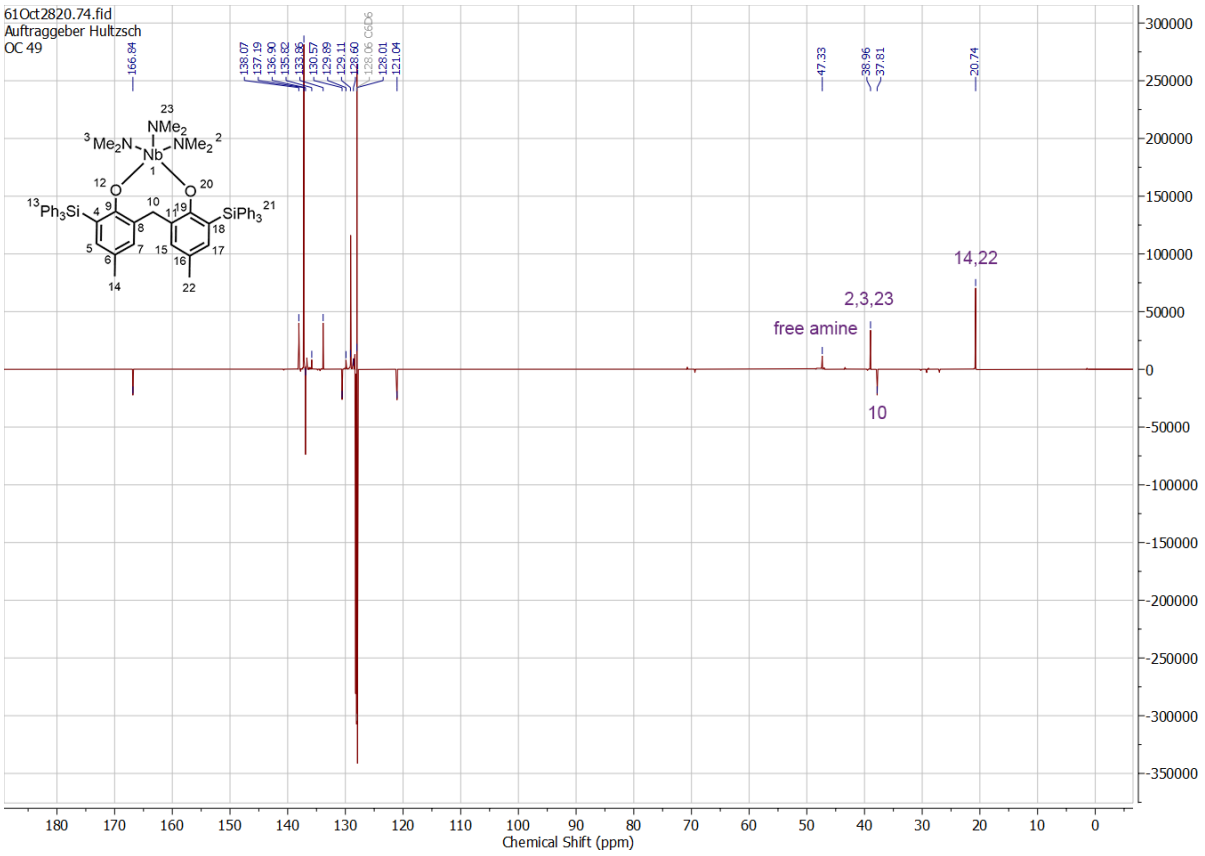

Supp. 48. ^{13}C-NMR spectrum of the complexation of $Nb(NMe_2)_5$ with 6,6'-methylenebis(4-methyl-2-(triphenylsilyl)phenol) at room temperature; solvent: C_6D_6, 600 MHz.

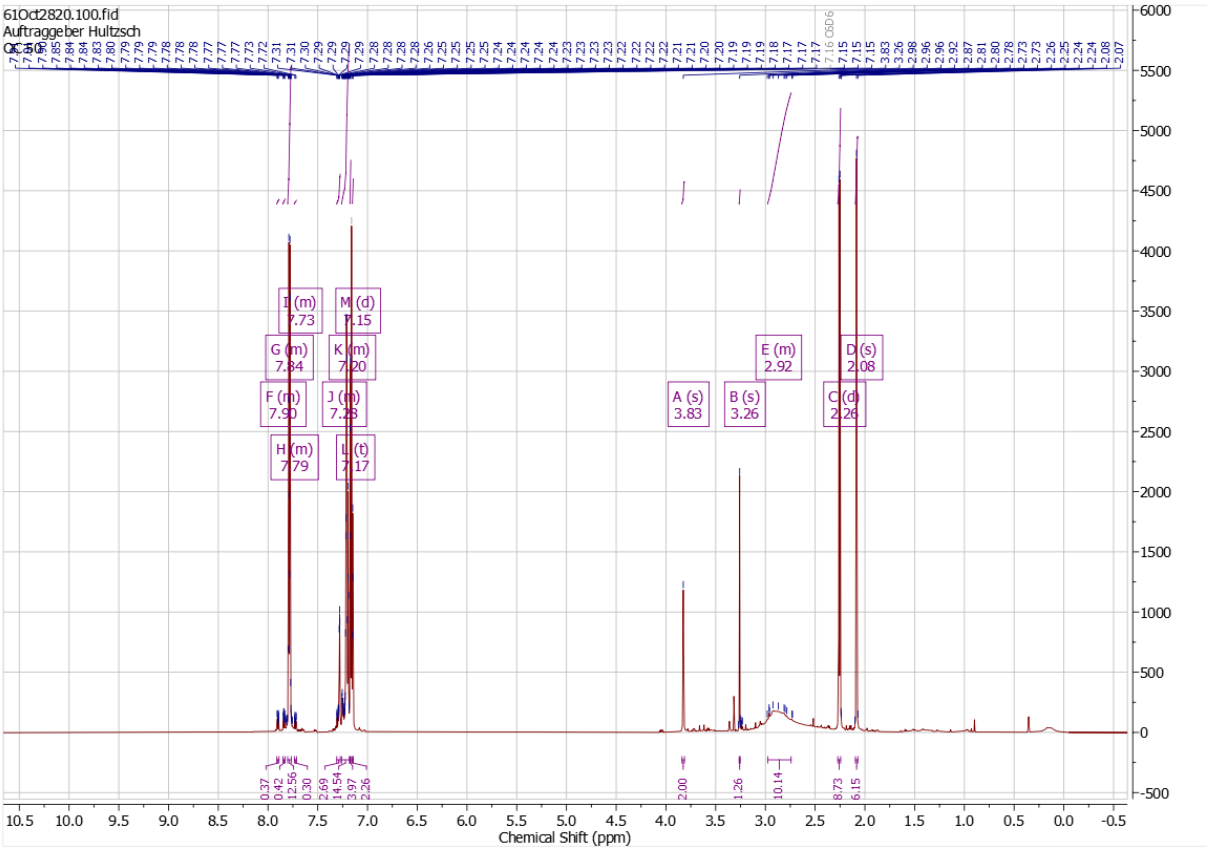

Supp. 49. ^{1}H-NMR spectrum of the complexation of $Ta(NMe_2)_5$ with 6,6'-methylenebis(4-methyl-2-(triphenylsilyl)phenol) at room temperature; solvent: C_6D_6, 600 MHz.

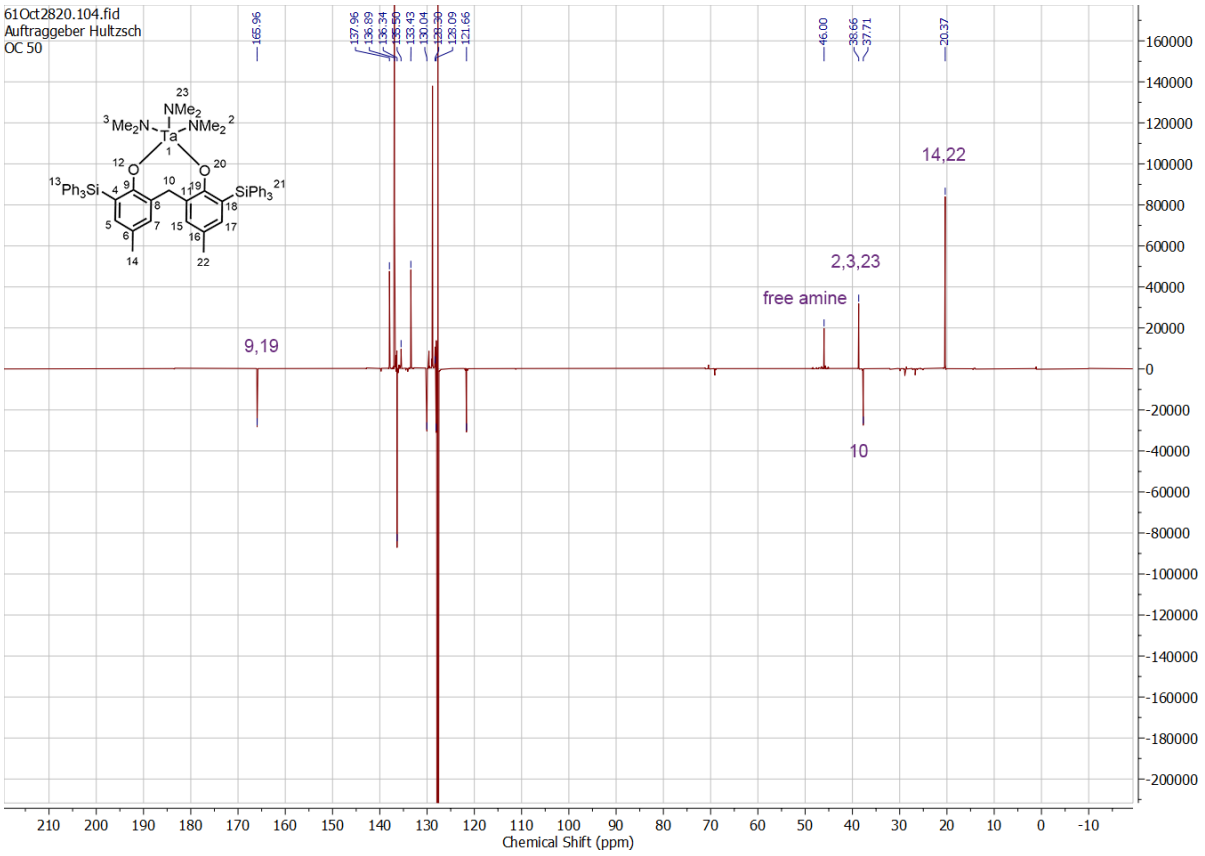

Supp. 50. ^{13}C-NMR spectrum of the complexation of $Ta(NMe_2)_5$ with 6,6'-methylenebis(4-methyl-2-(triphenylsilyl)phenol) at room temperature; solvent: C_6D_6, 151 MHz.

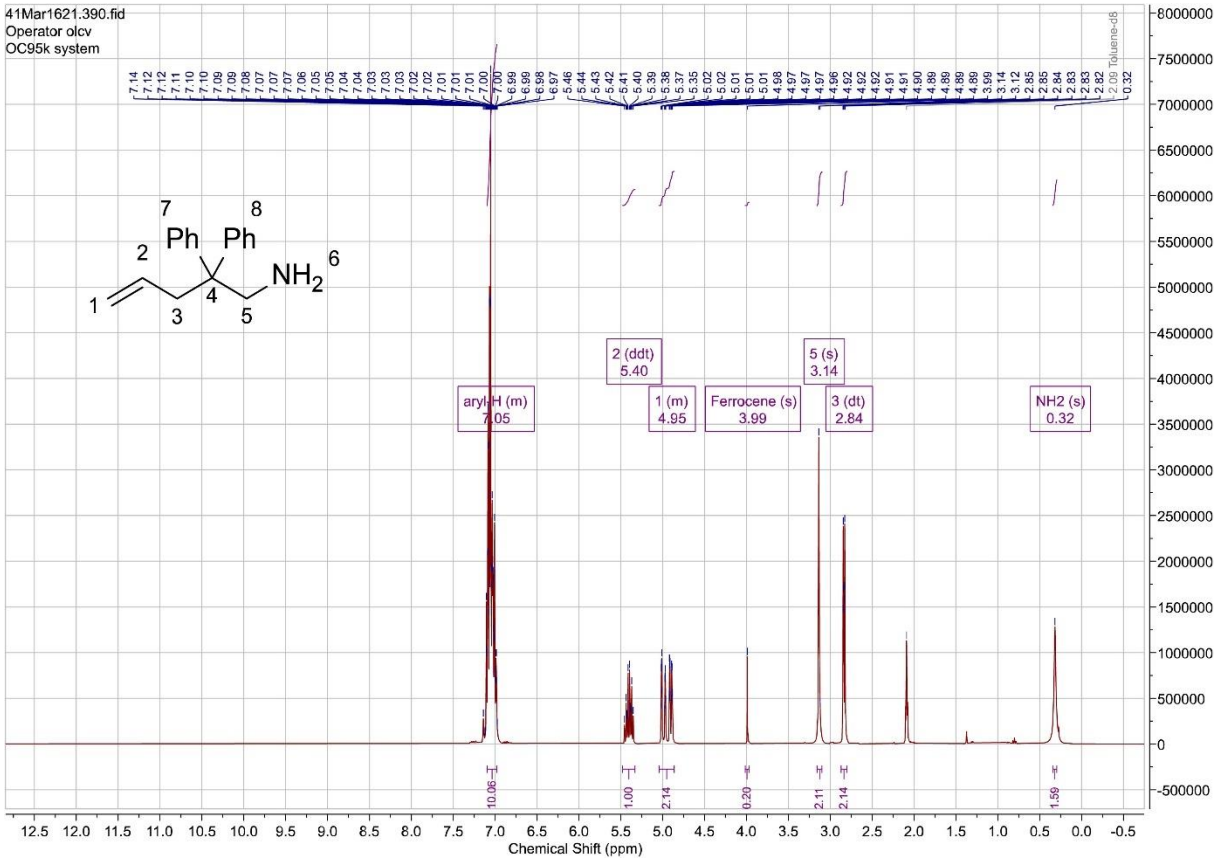

Supp. 51. ^{1}H-NMR spectrum of 2,2-diphenylpent-4-en-1-amine (**34**); solvent: toluene-d_8, 400 MHz.

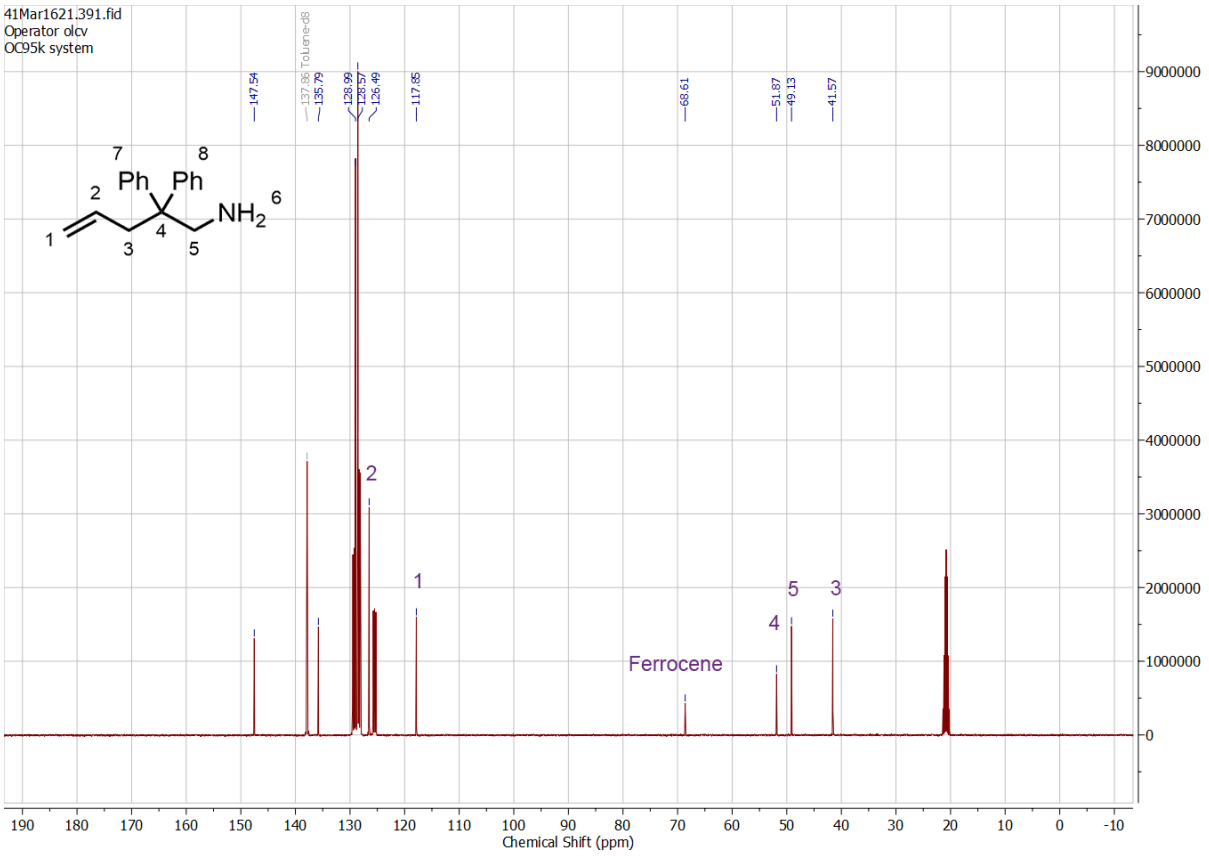

Supp. 52. ^{13}C-NMR spectrum of 2,2-diphenylpent-4-en-1-amine (**34**); solvent: toluene-d_8, 101 MHz.

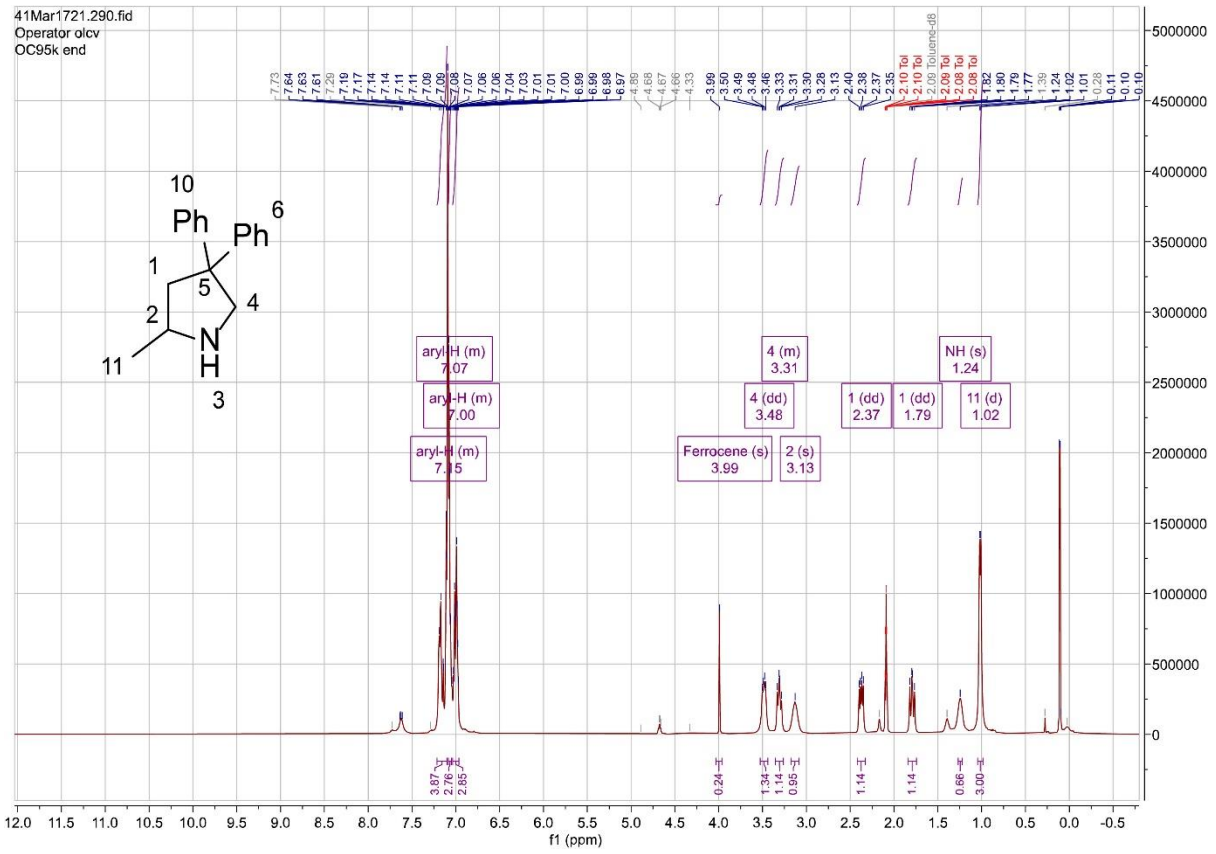

Supp. 53. ^{1}H-NMR spectrum of 2-methyl-4,4-diphenylpyrrolidine (**35**); solvent: toluene-d_8, 400 MHz.

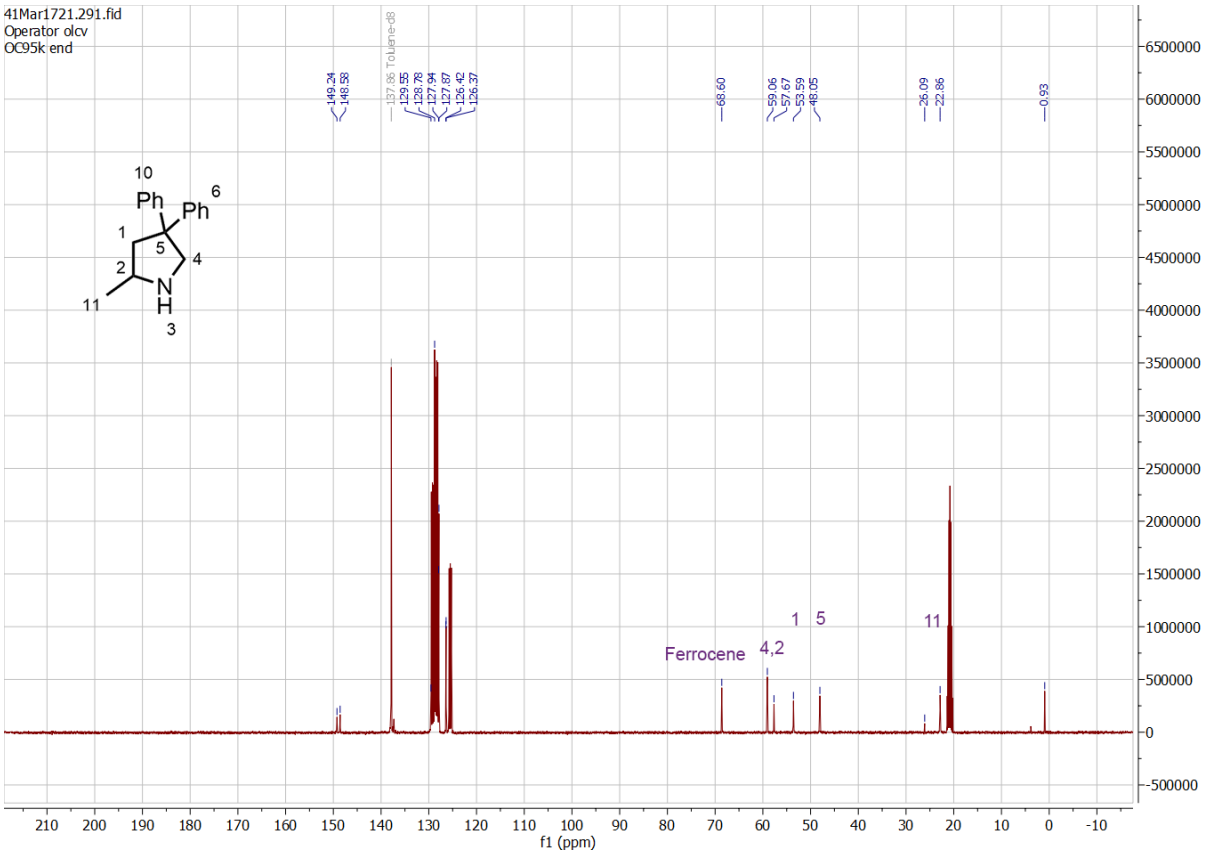

Supp. 54. ^{13}C-NMR spectrum of 2-methyl-4,4-diphenylpyrrolidine (**35**); solvent: toluene-d_8, 101 MHz.

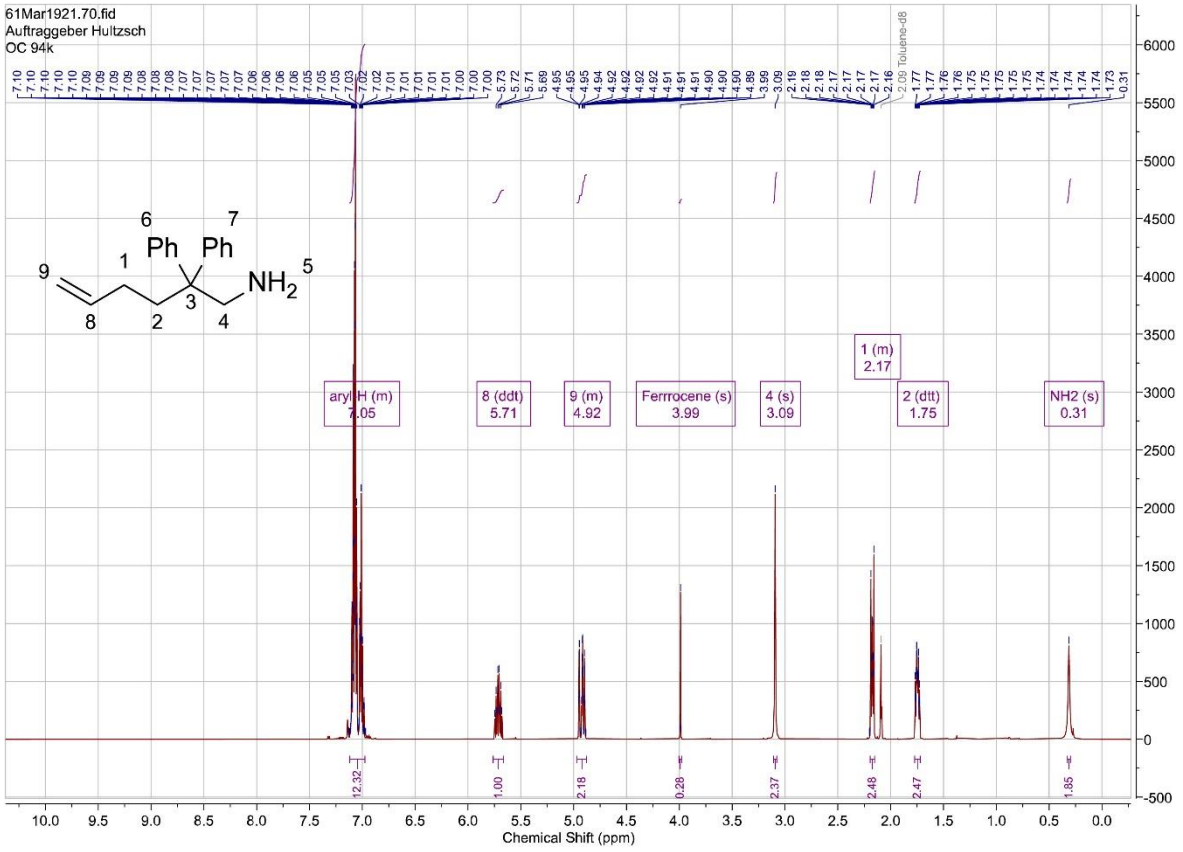

Supp. 55. ^{1}H-NMR spectrum of 2,2-diphenylhex-5-en-1-amine (**39**); solvent: toluene-d_8, 600 MHz.

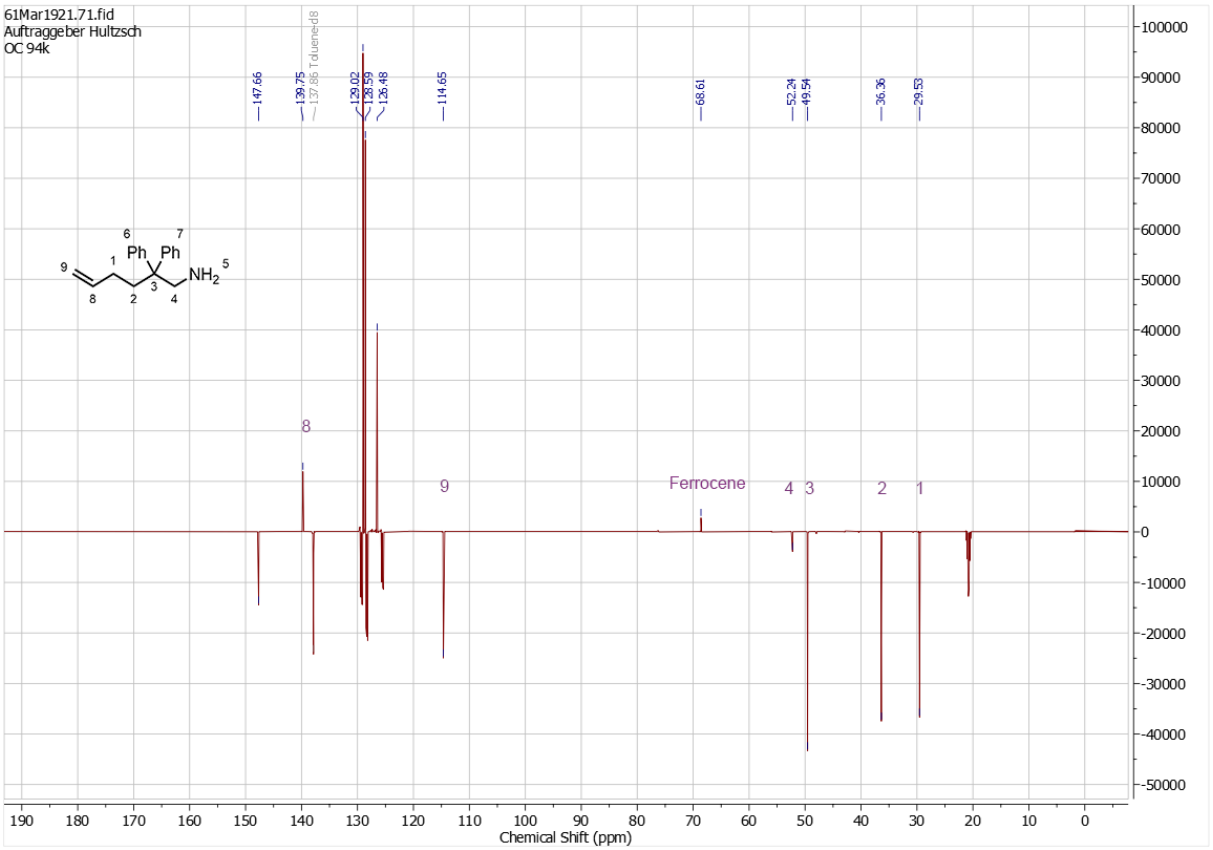

Supp. 56. ^{13}C-NMR spectrum of 2,2-diphenylhex-5-en-1-amine (**39**); solvent: toluene-d_8, 151 MHz.

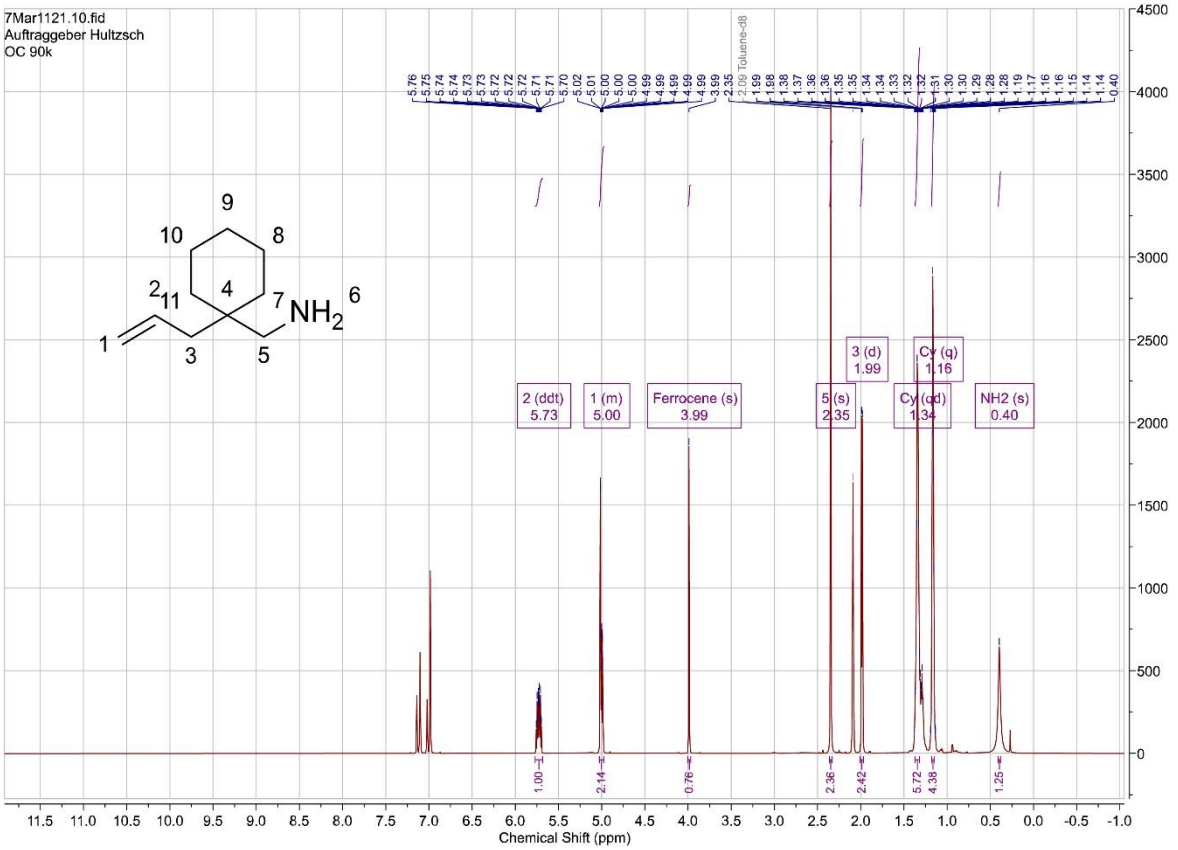

Supp. 57. ^{1}H-NMR spectrum of (1-allylcyclohexyl)methanamine (**37**); solvent: toluene-d_8, 700 MHz.

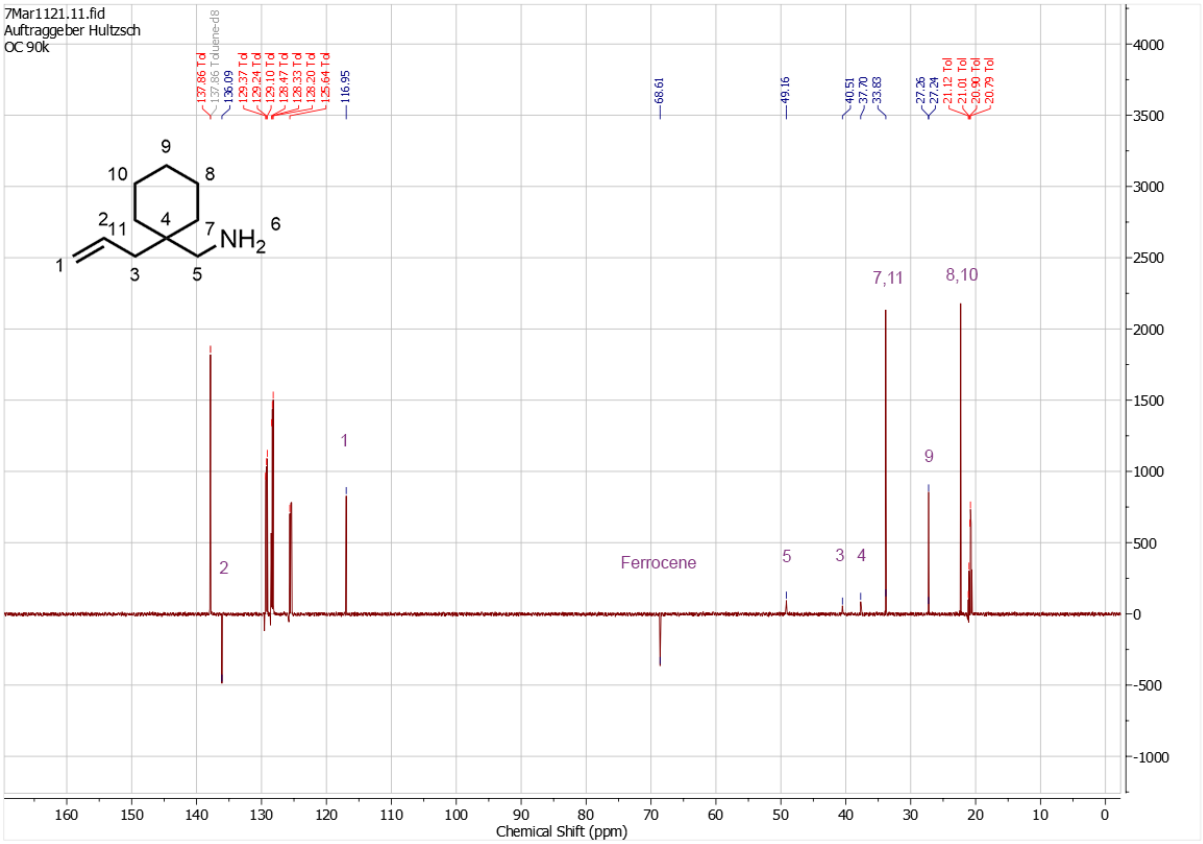

Supp. 58. ^{13}C-NMR spectrum of (1-allylcyclohexyl)methanamine (**37**); solvent: toluene-d_8, 176 MHz.

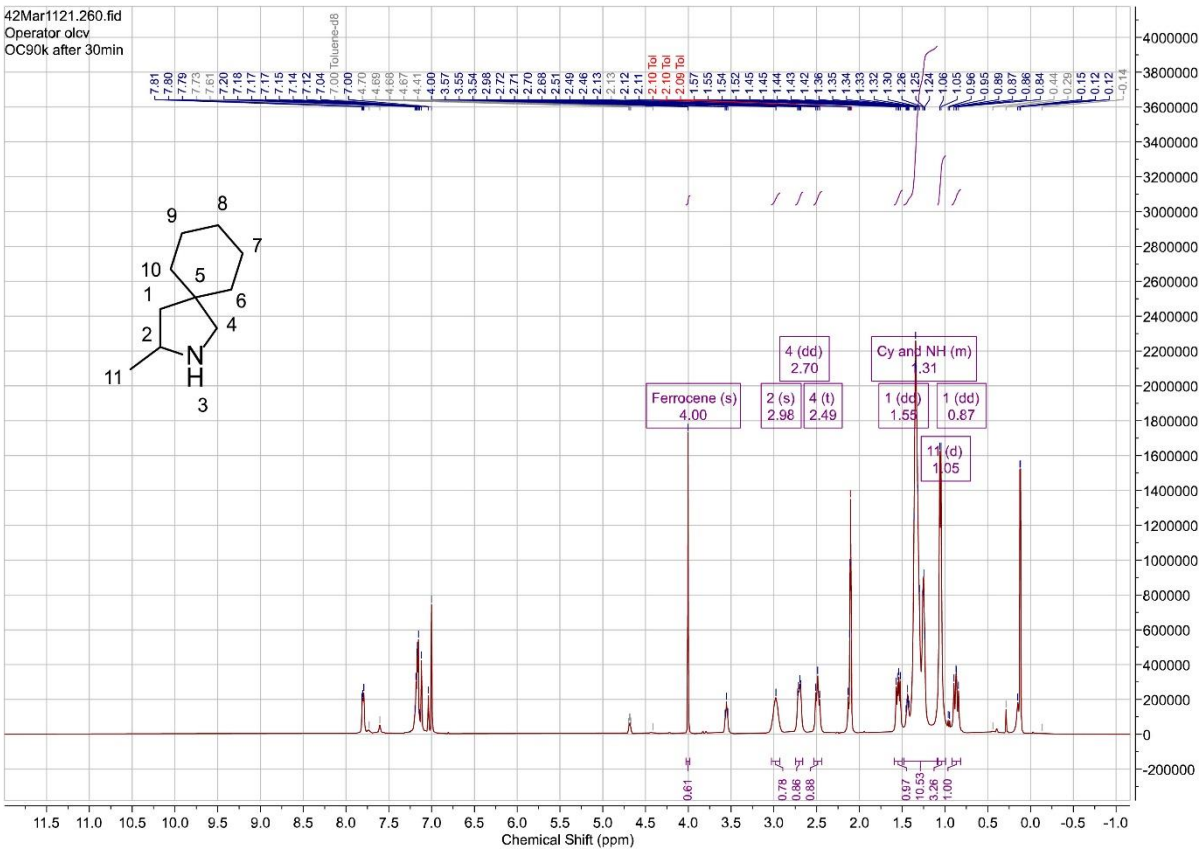

Supp. 59. ^{1}H-NMR spectrum of 3-methyl-2-azaspiro[4.5]decane (**38**); solvent: toluene-d_8, 400 MHz.

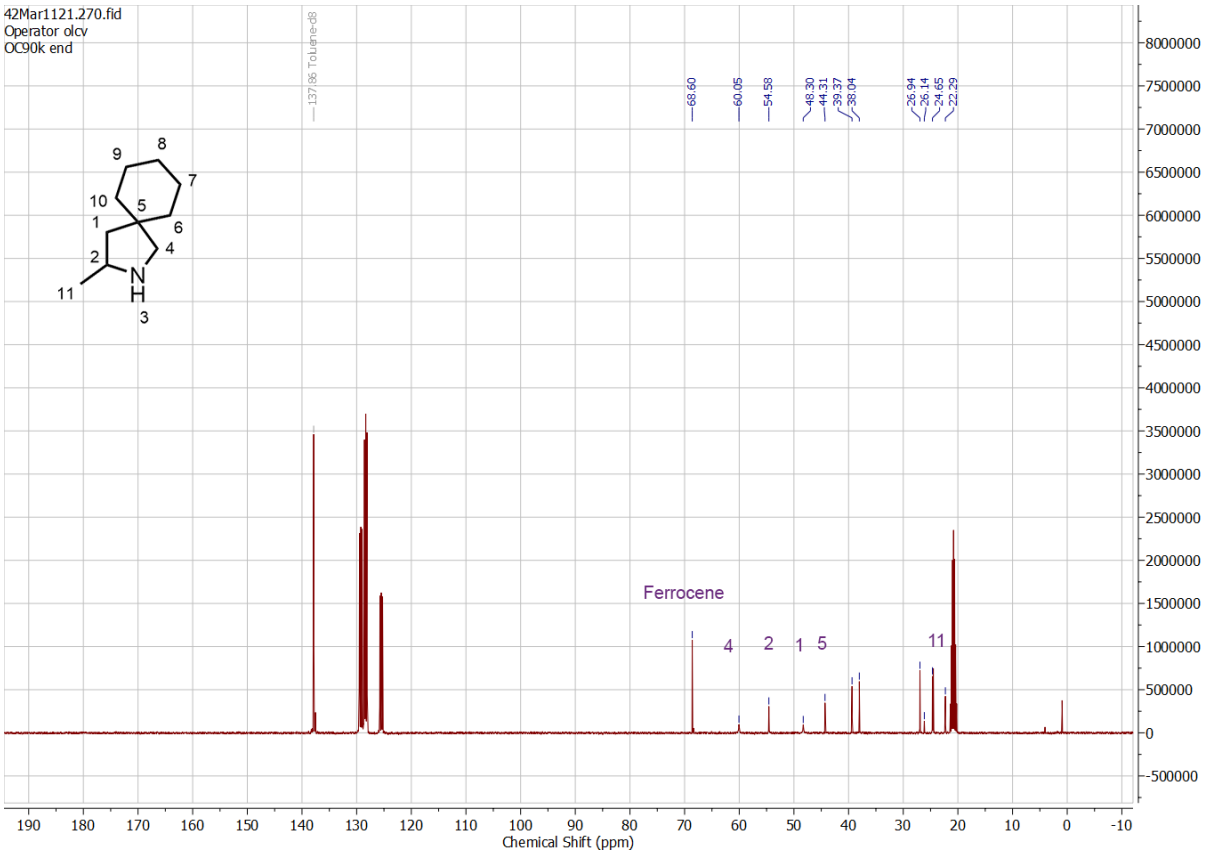

Supp. 60. ^{13}C-NMR spectrum of 3-methyl-2-azaspiro[4.5]decane (**38**); solvent: toluene-d_8, 101 MHz.